NPL

NPL REPORT OP3

CEOS comparison of IR brightness temperature measurements in support of satellite validation. Part I: Laboratory and ocean surface temperature comparison of radiation thermometers.

E. Theocharous, E. Usadi and N. P. Fox

July 2010

CEOS comparison of IR brightness temperature measurements in support of satellite validation. Part I: Laboratory and ocean surface temperature comparison of radiation thermometers

E. Theocharous, E. Usadi and N. P. Fox
Engineering Measurement Division

Abstract

A comparison of terrestrial based infrared (IR) radiometric instrumentation used to support calibration and validation of satellite borne sensors with emphasis on sea/water surface temperature was completed at NPL and at the University of Miami during April and May 2009. The objectives of the 2009 comparison were to establish the "degree of equivalence" between terrestrially based IR Cal/Val measurements made in support of satellite observations of the Earth's surface temperature and to establish their traceability to SI units through the participation of National Metrology Institutes (NMIs). During the 2009 comparison, NPL acted as the pilot laboratory and provided traceability to SI units during laboratory comparisons in Europe. NPL was supported by the Rosenstiel School of Marine and Atmospheric Science (RSMAS), University of Miami, acting as hosts, and by NIST providing traceability to SI units during laboratory measurements at RSMAS. The 2009 comparison consisted of two stages in order to allow maximum participation and enable the traceability chain to be established to both NPL and NIST scales. Stage 1 took place at NPL in April 2009 and involved laboratory measurements of participants' blackbodies calibrated using the NPL reference transfer radiometer (AMBER), while participants' radiometers were calibrated using the NPL variable temperature blackbody. Stage 2 took place at RSMAS in May 2009 and involved laboratory measurements of participants' blackbodies calibrated using the NIST Thermal-Infrared Transfer Radiometer (TXR), while participants' radiometers were calibrated using the RSMAS and NIST water bath blackbodies. Stage 2 also included the testing of the same radiometers alongside each other, completing direct daytime and nighttime measurements of the surface temperature of the ocean. This report provides the results, together with uncertainties as provided by the participants, for the comparison of the participants' radiometers, when they were monitoring the radiance temperature of the NPL variable temperature blackbody, the RSMAS water bath blackbody and NIST water bath blackbody. It also provides results of the measurement of the ocean surface temperature completed at the University of Miami. During the 2009 comparison, all participants were encouraged to develop uncertainty budgets for all measurements they reported. All measurements reported by the participants, along with their associated uncertainties, were analysed by the pilot laboratory and are presented in this report.

ISSN: 1754-2944

National Physical Laboratory
Hampton Road, Teddington, Middlesex, TW11 0LW

Approved on behalf of NPLML by Dr Ian Severn, Head, Engineering Measurement Division.

CONTENTS

1. INTRODUCTION

The measurement of the Earth's surface temperature and more fundamentally, its temporal and spatial variation, is a critical operational product for meteorology and an essential parameter for climate monitoring. Satellites have been monitoring global surface temperature for some time. However, it is essential for long-term records that such measurements are fully anchored to SI units.

Field-deployed infrared radiometers1 currently provide the most accurate surface-based measurements which are used for Cal/Val. These radiometers are in principle calibrated traceably to SI units, generally through a blackbody radiator. However, they are of varying design and are operated by different teams in different parts of the globe. It is essential for the integrity of their use, that any differences in their measurements are understood, so that any potential biases are removed and are not transferred to satellite sensors.

A comparison of terrestrial based infrared (IR) radiometric instrumentation used to support calibration and validation of satellite borne sensors with emphasis on sea/water surface temperature was completed in Miami in 2001 (Barton et al., 2004) (Rice et al., 2004). However, eight years had passed, and as many of the satellite sensors originally supported were nearing the end of their life, a similar comparison was repeated in 2009. The objectives of the 2009 comparison were to establish the "degree of equivalence" between terrestrially based IR Cal/Val measurements made in support of satellite observations of the Earth's surface temperature and to establish their traceability to SI units through the participation of NMIs.

2. ORGANISATION OF THE COMPARISON

During the 2009 comparison, NPL acted as the pilot laboratory and provided traceability to SI units during laboratory comparisons in Europe. NPL was supported by the Rosenstiel School of Marine and Atmospheric Science (RSMAS), University of Miami, acting as hosts, and by NIST providing traceability to SI units during laboratory measurements at RSMAS. The 2009 comparison consisted of two stages in order to allow maximum participation and enable the traceability chain to be established to both NPL and NIST. Stage 1 took place at NPL in April 2009 and involved laboratory measurements of participants' blackbodies calibrated using the NPL reference transfer radiometer (AMBER) (Theocharous et al., 1998), while the performance of the participants' radiometers was compared using the NPL variable temperature blackbody. The performance of 4 blackbodies and 8 radiometers operating on 24 measurement channels was compared during Stage 1. Stage 2 took place at RSMAS in May 2009 and involved laboratory measurements of participants' blackbodies calibrated using the NIST Thermal-Infrared Transfer radiometer (TXR) (Rice and Johnson, 1998), while the performance of the participants' radiometers was compared using the RSMAS water bath blackbody and the NIST water bath blackbody (Fowler, 1995). The performance of 9 radiometers operating on 14 measurement channels was compared during Stage 2. Stage 2 also included the testing of the same radiometers alongside each other, completing direct daytime and night time measurements of the skin temperature of the ocean. Because AMBER and the NPL variable temperature blackbody were not readily portable, linkage between the two stages was established though participants radiometers used in both stages, serving as transfer standards.

This report provides the results, together with uncertainties as provided by the participants, for the comparison of the participant's radiometers, when they were monitoring the radiance temperature of the NPL variable temperature blackbody, the RSMAS water bath blackbody and NIST water bath blackbody. It also provides results of the measurement of the ocean surface temperature completed at

1 This report describes the comparison of instruments which are referred to by participants as "radiometers". However, radiometers generally measure and report radiometric parameters in radiometric units (W, Wm^{-2}, etc.). The instruments we are dealing with measure temperature (in units of degrees C units or K) so they are thermometers or "radiation thermometers". However, in view of the common usage of the terminology for this application, the report will continue to use the term "radiometer".

the University of Miami. The comparison of the participants' blackbodies, as measured by the NPL AMBER radiometer and the NIST TXR radiometer will be presented in a second report which will be issued shortly.

During the 2009 comparison, all participants were encouraged to develop uncertainty budgets for all measurements they reported. In order to achieve optimum comparability, lists containing the principal influence parameters for the measurements were provided to all participants. All measurements reported by the participants, along with their associated uncertainties, were analysed by the pilot laboratory and are presented in this report.

3. PARTICIPANTS' MEASUREMENTS AND RESULTS

Section 3 provides the results of the comparison of the participants' radiometers, when they were monitoring the radiance temperature of the NPL variable temperature blackbody, the RSMAS water bath blackbody and NIST water bath blackbody. It also provides the results of the measurement of the ocean surface temperature completed at the University of Miami.

Section 3 also provides the uncertainties (and where available the uncertainty budgets) of the radiometers which took part in the comparisons, as provided by the participants. In some cases the level of detail provided by participants in the uncertainty budgets of their measurements is fairly limited and not ideal. However, whatever was provided by the participants is included in this report, along with a summary of the results for each participant for each stage of the comparison.

3.1 Mediterranean Centre for Environmental Studies (Fundación Centro de Estudios Ambientales del Mediterraneo, CEAM) www.ceam.es

3.1.1 Contact information

CEAM contact for the comparison: Dr Raquel Niclos
Address: 14 Charles Darwin (Parc Tecnologic), 46980 PATERNA, Valencia, Spain
Email: niclos@ceam.es

3.1.2 Radiometers used in the comparisons

CEAM only took part in the Miami comparison (laboratory and ocean surface temperature measurements). CEAM used a number of radiometers during the Miami comparisons from two different manufacturers, Apogee and Everest.
The following radiometers manufactured by APOGEE Instruments took part in the Miami comparison:

Type-APOGEE model	IRTS-P5-A (SI-322) (CEAM RA4)	IRR-P (SI-111) CEAM RA2 and CEAM RA3	IRR-PN (SI-112) CEAM RA1
FOV	4° half angle	22° half angle	18° half angle
Spectral band (µm)	6.5-14	8-14	8-14

Full on information on these radiometers can be found at:
http://www.apogeeinstruments.com/infrared_temperature_sensors.htm

The CEAM RA1, RA2 and RA3 radiometers took part in both Laboratory and Ocean comparisons and their measurements are described below. The CEAM RA4 radiometer was only used in the Miami Laboratory comparison due to time constraints and its measurements are also described in this Section.

N.B. The radiometer numbering has changed slightly from the pre-draft A report to ensure consistency between Laboratory and Ocean view measurements.

3.1.2.1 Outline technical description of the CEAM RA1, RA2 and RA3 radiometers:

These radiometers use a thermopile detector to provide a millivolt output which is dependent on the temperature difference between the target being viewed and the radiometer body temperature. A thermistor is used to measure the temperature of the sensor body, which is used to reference the target temperature. These radiometers operate in the 8 µm to 14 µm spectral band. The instruments use a germanium lens and have a field of view of 22º half angle (IRR-P model, Radiometers 1-2) and 18º half angle (IRR-PN model, Radiometer 3).

References:

Campbell Scientific and Apogee Instruments. 2007. IRR-P Precision Infrared Temperature Sensor. Instruction manual. 10pp.

Bugbee, B., Blonquist, M., Lewis, N. Design and Calibration of a New Infra-red Radiometer.(website)

Establishment of traceability route for primary calibration including date of last realisation and uncertainty budget.

According to Apogee Instruments Inc., the radiometers were calibrated using a blackbody cone, obtaining the following values:

Absolute accuracy: ±0.2K @ 263K to 338K and ±0.5K @ 233K to 343K

Uniformity: ±0.1K @ 263K to 338K and ±0.3K @ 233K to 343K

Repeatability: ±0.05K @ 263K to 338K and ±0.1K @ 233K to 343K

Each of the radiometers was provided with different calibration coefficients, which were obtained by means of custom calibrations by the manufacturer (calibration date: February 2008).

Because of the limited detail about the traceability of this primary calibration, CEAM carried out the following error analysis based on laboratory measurements using a Landcal Blackbody Source P80P

http://landinstruments.net/infrared/products/calibration_sources/p80p.htm (April,009).

The basis for the uncertainty estimates in the following tables are:

- **Repeatability**: Typical value of the standard deviation of 180 measurements (1 per second, since the radiometer response time is shorter than 1s) at a fixed black body temperature without radiometer re-alignment.
- **Reproducibility**: Typical value of difference between runs (run to run) of radiometer measurements at the same black body temperature including re-alignment.
- **Linearity** of radiometer: uncertainty of a linear regression between Landcal Blackbody Source P80P temperatures and radiometer brightness temperatures.
- **Primary calibration**: Typical value of difference between radiometer brightness temperatures and Landcal Blackbody Source P80P temperatures (K). N.B. This is the wrong definition of the uncertainty associated with the "Primary calibration".
- **Drift since calibration**: 0.0 K (as expected since very recent calibration measurements).

CEAM Radiometer 1 (CEAM RA1): IRR-PN (SI-112) - APOGEE Instruments

Parameter	Type A Uncertainty in Value / %	Type B Uncertainty in Value / K	Uncertainty in Brightness temperature K
Repeatability of measurement(1)	0.009K / 0.003%		0.009
Reproducibility of measurement(2)	0.06K / 0.019%		0.06
Linearity of radiometer(3)		0.04 K	0.04
Primary calibration(4)		0.15 K	0.15
Drift since calibration		-	-
RMS total	0.06K / 0.019%	0.16 K	0.17

CEAM Radiometer 2 (CEAM RA2): IRR-P (SI-111) - APOGEE instruments (Unit 1)

Parameter	Type A Uncertainty in Value / %	Type B Uncertainty in Value / (appropriate units)	Uncertainty in Brightness temperature K
Repeatability of measurement(1)	0.009K / 0.003%		0.009
Reproducibility of measurement(2)	0.03K / 0.010%		0.03
Linearity of radiometer(3)		0.02 K	0.02
Primary calibration(4)		0.06 K	0.06
Drift since calibration		-	-
RMS total	0.03K / 0.011%	0.06 K	0.07

CEAM Radiometer 3 (CEAM RA3): IRR-P (SI-111) - APOGEE instruments (Unit 2)

Parameter	Type A Uncertainty in Value / %	Type B Uncertainty in Value / (appropriate units)	Uncertainty in Brightness temperature K
Repeatability of measurement(1)	0.008K / 0.003%		0.008
Reproducibility of measurement(2)	0.06K / 0.02%		0.06
Linearity of radiometer(3)		0.08 K	0.08
Primary calibration(4)		0.17 K	0.17
Drift since calibration		-	-
RMS total	0.06K / 0.02%	0.18 K	0.19

(1) Typical value of the standard deviation of 180 measurements at fixed black body temperature without re-alignment of radiometer.
(2) Typical value of difference between two runs of radiometer measurements at the same black body temperature including re-alignment.
(3) Uncertainty of the lineal regression between the Landcal Blackbody Source P80P temperatures and the radiometer brightness temperatures.
(4) Typical value of difference between radiometer brightness temperature and Landcal Blackbody Source P80P temperature.

Operational methodology during measurement campaign:

Calibration measurements were performed in the laboratory following, as closely as possible, the procedures described in the Draft Protocol. The Landcal Blackbody Source P80P was set at 4 temperatures (278, 283, 293 and 303 K) in 3 different runs. Enough time was allowed for the black body to reach equilibrium at each temperature. Radiometers were aligned with the black body cavity, and placed at a distance so that the field of view was smaller than the cavity diameter. The measured values reported above are typical values for all blackbody temperatures considered for each radiometer.

Radiometer usage (deployment)

Currently, these radiometers are being used for field measurements (hand held and mounted in meteorological towers) of surface temperature and emissivity, both for research on surface thermal emission properties and heat fluxes and for testing thermal infrared products from satellite sensors (MSG/SEVIRI, Terra/MODIS, Aqua/MODIS, Landsat/ETM+).

Sea surface temperature measurements

The uncertainty of these radiometers in measuring the sea surface temperature aspect of this comparison is as follows:

	Wavelength	**Uncertainty**	**Uncertainty**
	μm	**Type A**	**Type B**
		K	**K**
CEAM RA1			
Apogee IRR-PN	11.5 μm	0.02 to 0.18	0.18
CEAM RA2			
Apogee IRR-P1	11.5 μm	0.02 to 0.15	0.07 to 0.09
CEAM RA3			
Apogee IRR-P2	11.5 μm	0.04 to 0.14	0.2

3.1.2.2 Outline technical description of instrument: CEAM RA4: APOGEE IRTS-P5-A

The sensor is calibrated so that the output signal when viewing the target temperature is the same output voltage as if a type K thermocouple were sensing the target temperature. A separate type K thermocouple is used to measure the temperature of the sensor body, which is used to correct the target temperature. Spectral band: 6-14 μm. Optics: Silicon lens. Field of view: 4º half angle.

References:

Campbell Scientific and Apogee Instruments. 2006. IRTS-P Precision Infrared Temperature Sensor. Instruction Manual. 12pp.

Establishment of traceability route for primary calibration including date of last realisation and breakdown of uncertainty:

According to Apogee Instruments Inc., the radiometer was calibrated with a blackbody cone, obtaining the following values:
Absolute accuracy: ±0.3K @ 263K to 328K (±0.1K when sensor body and target are at the same temperature).

Uniformity: ±0.2K @ 263K to 328K

Repeatability: ±0.05K @ 263K to 328K

Because of the limited detail about the traceability of this primary calibration, CEAM carried out the following error analysis based on laboratory measurements using a Landcal Blackbody Source P80P, (April 2009)

(http://landinstruments.net/infrared/products/calibration_sources/p80p.htm).

The basis for deriving these values is as per the descriptions earlier in section 3.1.2.1. The exception to this is the **primary calibration**. In this case the primary calibration value has been obtained using the radiometer brightness temperatures calculated with our own calibration function (obtained from CEAM calibration measurements), which differs from that provided by the manufacturer. In this case, the manufacturer only provided CEAM with general coefficients for the radiometer model, but no custom calibration coefficients.

Radiometer 4: IRTS-P5-A - APOGEE INSTRUMENTS

Parameter	Type A Uncertainty in Value / %	Type B Uncertainty in Value / (appropriate units)	Uncertainty in Brightness temperature K
Repeatability of measurement(1)	0.010K / 0.004%		0.010
Reproducibility of measurement(2)	0.07K / 0.02%		0.07
Linearity of radiometer(3)		0.09 K	0.09
Primary calibration(4)		0.3 K	0.3
Drift since calibration		-	-
RMS total	0.07K / 0.02%	0.3 K	0.3

(1) Typical value of the standard deviation of 180 measurements at fixed black body temperature without re-alignment of radiometer.
(2) Typical value of difference between two runs of radiometer measurements at the same black body temperature including re-alignment.
(3) Uncertainty of the lineal regression between the Landcal Blackbody Source P80P temperatures and the radiometer brightness temperatures.
(4) Typical value of difference between radiometer brightness temperature and Landcal Blackbody Source P80P temperature. N.B. This is the wrong definition of the uncertainty associated with the "Primary calibration".

Operational methodology during measurement campaign:

Calibration measurements were performed in the laboratory following, as closely as possible, the procedures described in the Draft Protocol. The Landcal Blackbody Source P80P was set at 4 temperatures (278, 283, 293 and 303 K) in 3 different runs. Enough time was allowed for the black body to reach equilibrium at each temperature. Radiometers were aligned with the black body cavity, and placed at a distance so that the field of view was smaller than the cavity diameter. The measured values reported above are typical values for all black body temperatures considered for each radiometer.

Radiometer usage (deployment)

Currently, this radiometer is not often used due to its wide spectral band. The new radiometers 1-3 (8-14 μm) are preferred. Nevertheless, depending on the results of this IR comparison, this model could be used for future field or laboratory measurements.

3.1.2.3 Outline technical description of radiometer: CEAM RA 5: EVEREST 6000.1ZL radiometer:

The fifth radiometer from this institute is manufactured by Everest Interscience Inc. **http://www.everestinterscience.com/products/productguide.htm** and is a Vario-Zoom Infrared Temperature Sensor with a variable FOV from 2º to 20º. Spectral band: 8-14 μm.

Type of detector: Thermopile with internal temperature compensation operating in the spectral band: 8-14 μm. Optics: Zinc Selenide with a 10º field of view (half angle). This radiometer has a system for varying the field of view from 2º to 20º. However, as this system is manually operated, we prefer to fix it at 20º, since it seems to be the most reliable configuration.

References:

Everest Interscience. 2008. Model 6000.1ZL Vario-Zooom infrared temperature sensor. Operating Manual. 8pp.

ASTM International. 2007. Standard Test Methods for Radiation Thermometers (single waveband type). 7pp.

Establishment of traceability route for primary calibration including date of last realisation and breakdown of uncertainty:

According to Everest Interscience Inc., the radiometer was calibrated with a reference temperature source, obtaining the following values:

Accuracy: ±0.5K. (Scale range: 233K to 373K)

Repeatability: ±0.1K

Noise Effective Temperature: ±0.2K

As we did not have more detail about the traceability of this primary calibration, we have carried out the following error analysis based on laboratory measurements using a Landcal Blackbody Source P80P (April 2009)

(http://landinstruments.net/infrared/products/calibration_sources/p80p.htm).

The basis for deriving these values is as per the descriptions earlier in section 3.1.2.1. The exception to this is the **primary calibration**. In this case the primary calibration value has been obtained using the radiometer brightness temperatures calculated with our own calibration function (obtained from our calibration measurements), which differs from that provided by the manufacturer. In this case, the manufacturer only provided us with general coefficients for the radiometer model, but no custom calibration coefficients.

CEAM RA5 : 6000.1ZL - EVEREST INTERSCIENCE

Parameter	Type A Uncertainty in Value / %	Type B Uncertainty in Value /	Uncertainty in Brightness temperature K
Repeatability of measurement(1)	0.06K / 0.019%		0.06
Reproducibility of measurement(2)	0.3K / 0.09%		0.3
Linearity of radiometer(3)		0.3 K	0.3
Primary calibration(4)		1.1 K	1.1
Drift since calibration		-	-
RMS total	0.3K / 0.09%	1.2 K	1.2

(1) Typical value of the standard deviation of 180 measurements at fixed black body temperature without re-alignment of radiometer.
(2) Typical value of difference between two runs of radiometer measurements at the same black body temperature including re-alignment.
(3) Uncertainty of the lineal regression between the Landcal Blackbody Source P80P temperatures and the radiometer brightness temperatures.
(4) Typical value of difference between radiometer brightness temperature and Landcal Blackbody Source P80P temperature.

Operational methodology during measurement campaign:

Calibration measurements were performed in the laboratory following, as closely as possible, the procedures described in the Draft Protocol. The Landcal Blackbody Source P80P was set at 4 temperatures (278, 283, 293 and 303 K) in 3 different runs. Enough time was allowed for the black body to reach equilibrium at each temperature. Radiometers were aligned with the black body cavity, and placed at a distance so that the field of view was smaller than the cavity diameter. The measured values reported above are typical values for all black body temperatures considered for each radiometer.

3.1.3 Results of the comparison of the CEAM radiometers

3.1.3.1 Comparison to the RSMAS reference blackbody

3.1.3.1.1 RA1 radiometer results viewing the RSMAS blackbody

Figures 3.1.1 to 3.1.5 show the temperature values measured by the CEAM RA1 radiometer when monitoring the RSMAS blackbody cavity. Figure 3.1.6 shows the corresponding measurements when the same radiometer was viewing the NIST blackbody cavity. Figures 3.1.7 to 3.1.11 show the temperature values measured by the CEAM RA2 radiometer when monitoring the RSMAS blackbody cavity. Figure 3.1.12 shows the corresponding measurements when the same radiometer was viewing the NIST blackbody cavity.

Figures 3.1.13 to 3.1.17 show the temperature values measured by the CEAM RA3 radiometer when monitoring the RSMAS blackbody cavity. Figure 3.1.18 shows the corresponding measurements when the same radiometer was viewing the NIST blackbody cavity. Figures 3.1.19 to 3.1.23 show the temperature values reported by the CEAM RA4 radiometer when monitoring the RSMAS blackbody

cavity. Figure 3.1.24 shows the corresponding measurements when the same radiometer was viewing the NIST blackbody cavity. Figures 3.1.25 to 3.1.29 show the temperature values measured by the CEAM RA5 radiometer when monitoring the RSMAS blackbody cavity. Figure 3.1.30 shows the corresponding measurements when the same radiometer was viewing the NIST blackbody cavity.

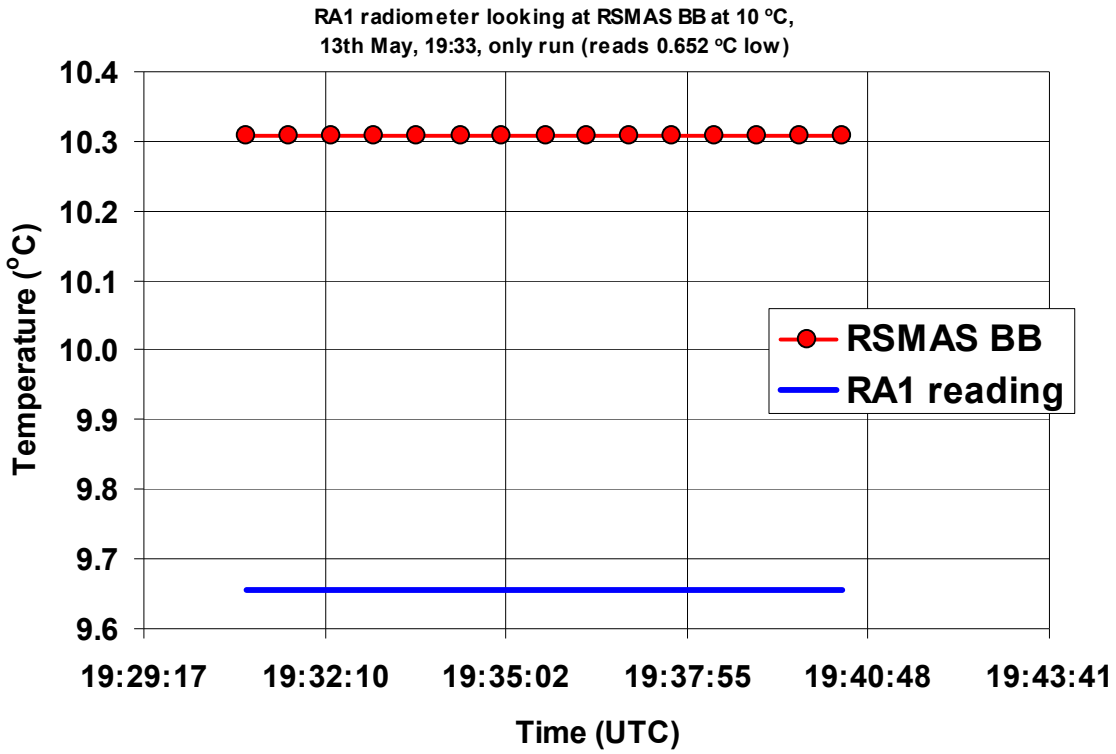

Figure 3.1.1: RA1 radiometer viewing the RSMAS blackbody at 10 °C.
<Radiometer measurement> – RSMAS blackbody temperature = -0.652 °C
(brackets indicate average over time interval shown).

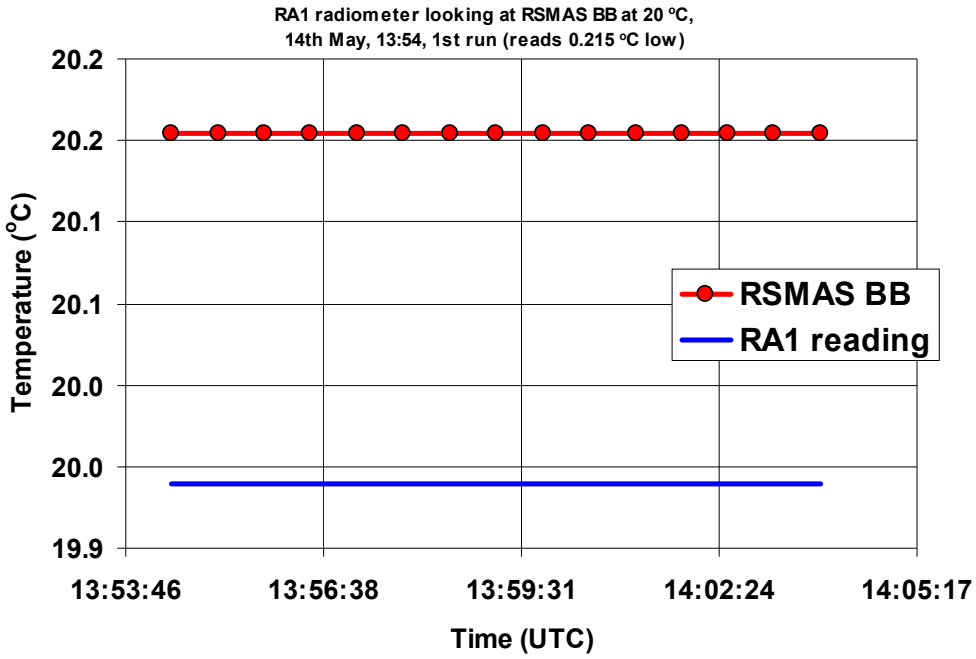

Figure 3.1.2: RA1 radiometer viewing the RSMAS blackbody at 20 °C, 1st measurement. <Radiometer measurement> – RSMAS blackbody temp. = -0.215 °C (brackets indicate average over time interval shown).

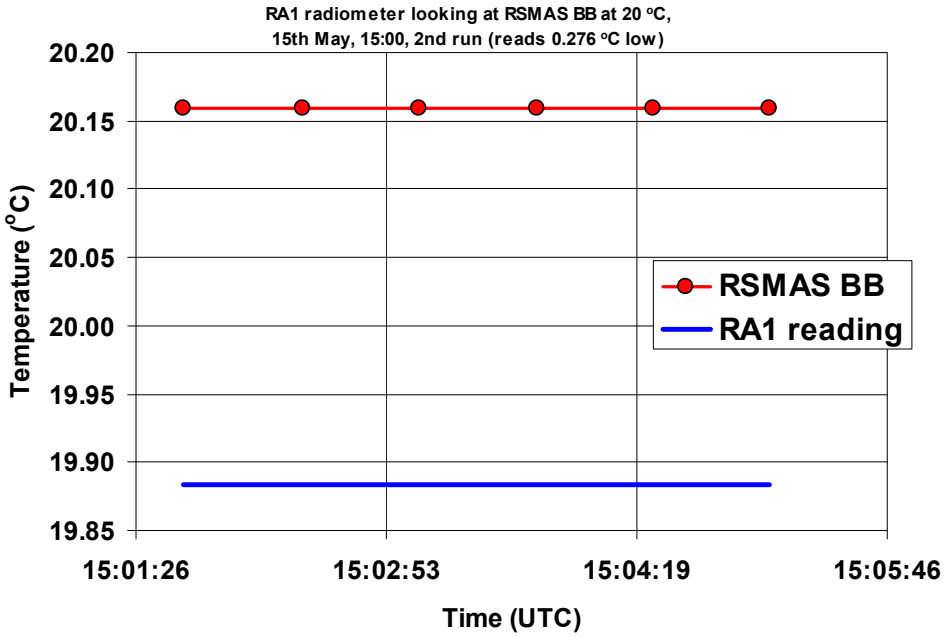

Figure 3.1.3: RA1 radiometer viewing the RSMAS blackbody at 20 °C, 2nd measurement. <Radiometer measurement> – RSMAS blackbody temp. = -0.276 °C (brackets indicate average over time interval shown).

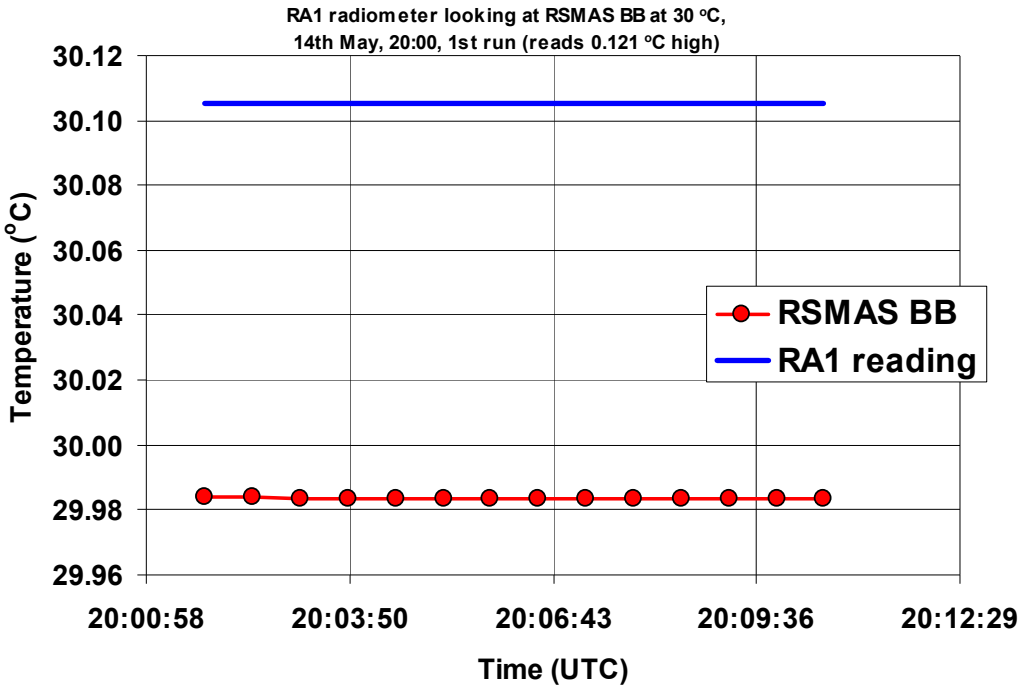

Figure 3.1.4: RA1 radiometer viewing the RSMAS blackbody at 30 °C,
1st measurement. <Radiometer measurement> – RSMAS blackbody temp. = +0.121 °C
(brackets indicate average over time interval shown).

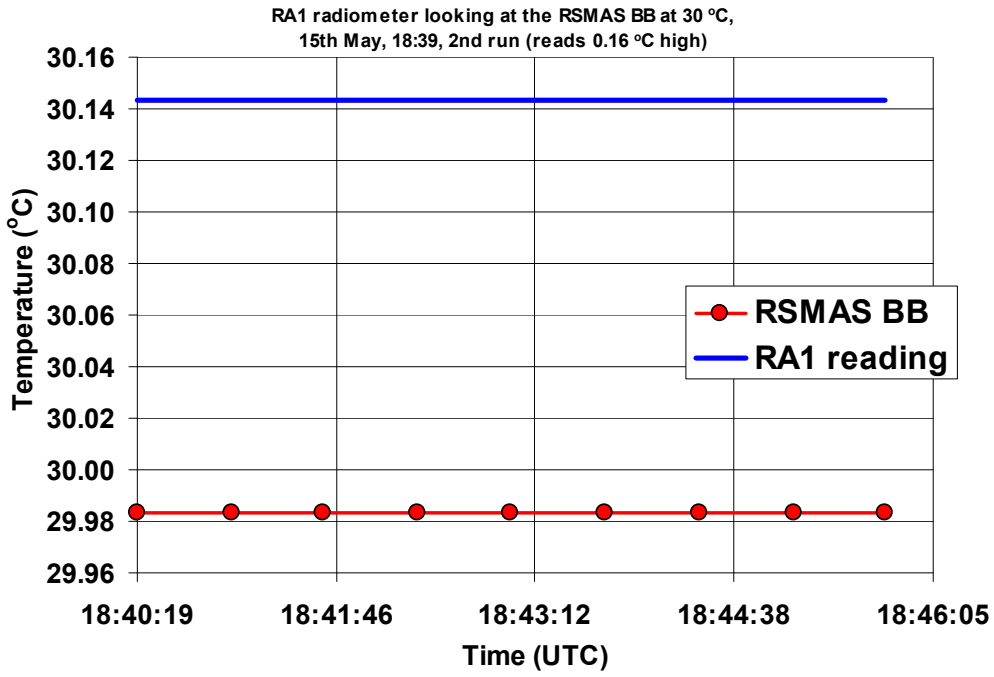

Figure 3.1.5: RA1 radiometer viewing the RSMAS blackbody at 30 °C,
2nd measurement. <Radiometer measurement> – RSMAS blackbody temp. = +0.16 °C
(brackets indicate average over time interval shown).

3.1.3.1.2 RA1 Radiometer viewing the NIST blackbody

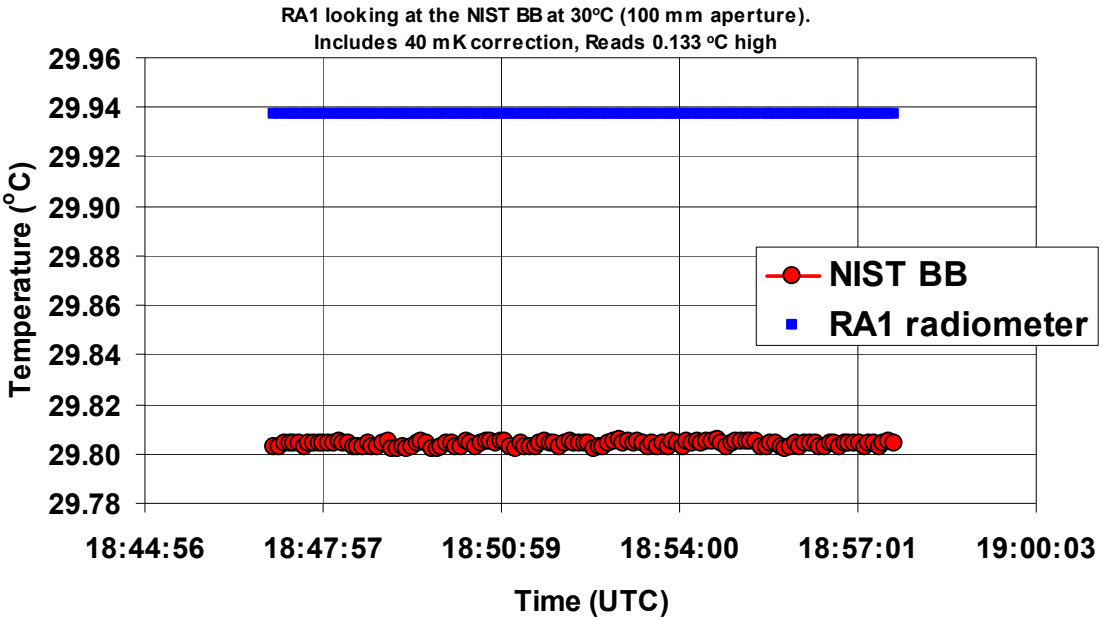

Figure 3.1.6: RA1 radiometer viewing the NIST blackbody at 30 °C.
<Radiometer measurement> – RSMAS blackbody temperature = +0.133 °C
(brackets indicate average over time interval shown).

3.1.3.1.3 RA2 radiometer results viewing the RSMAS blackbody

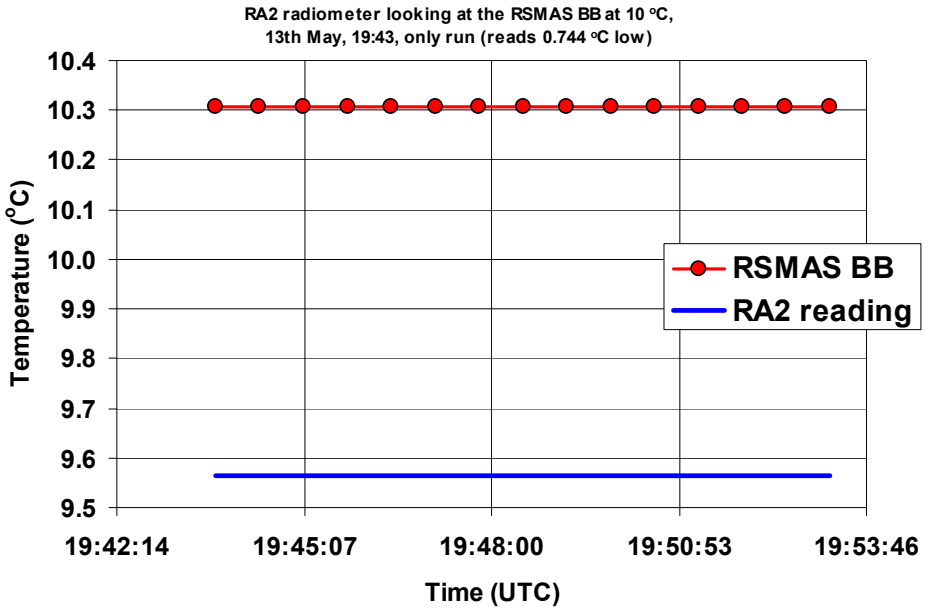

Figure 3.1.7: RA2 radiometer viewing the RSMAS blackbody at 10 °C.
<Radiometer measurement> – RSMAS blackbody temperature = -0.744 °C
(brackets indicate average over time interval shown).

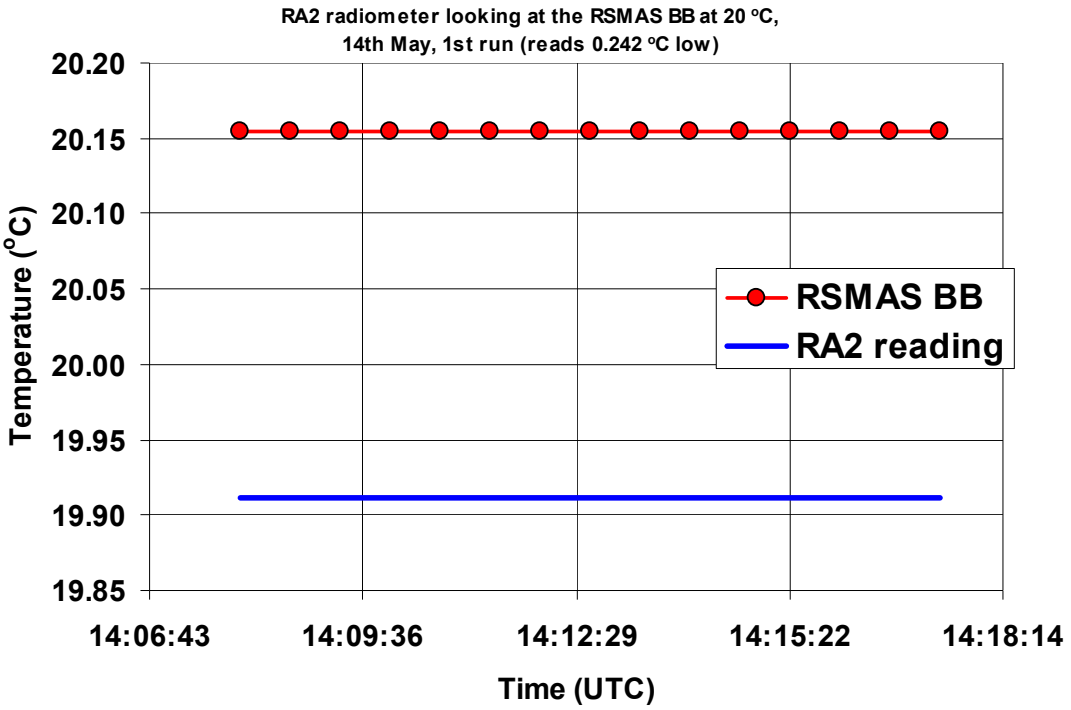

Figure 3.1.8: RA2 radiometer viewing the RSMAS BB at 20 °C, 1st measurement.
<Radiometer measurement> – RSMAS blackbody temperature = -0.242 °C
(brackets indicate average over time interval shown).

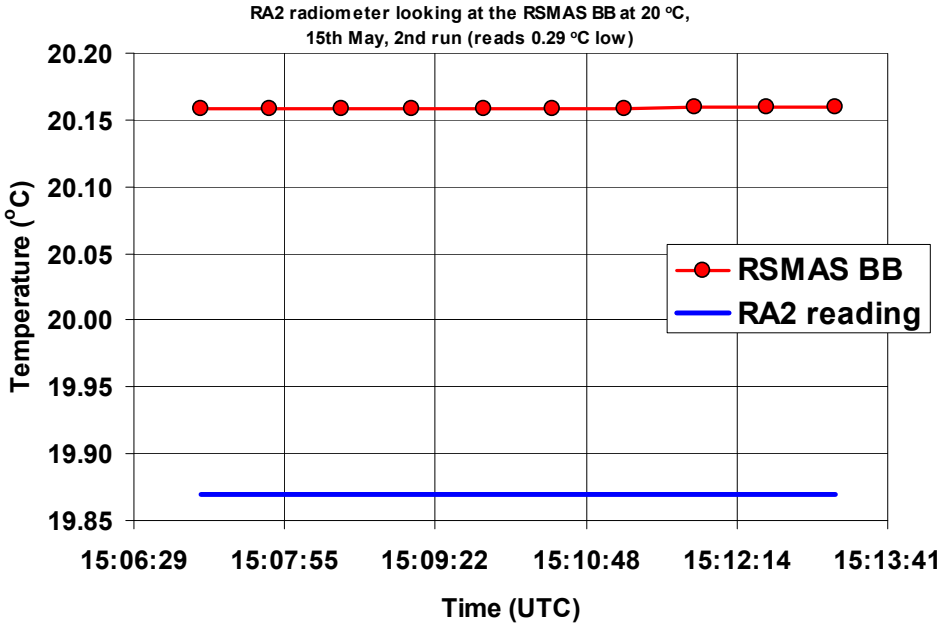

Figure 3.1.9: RA2 radiometer viewing the RSMAS BB at 20 °C, 2nd measurement.
<Radiometer measurement> – RSMAS blackbody temperature = -0.29 °C
(brackets indicate average over time interval shown).

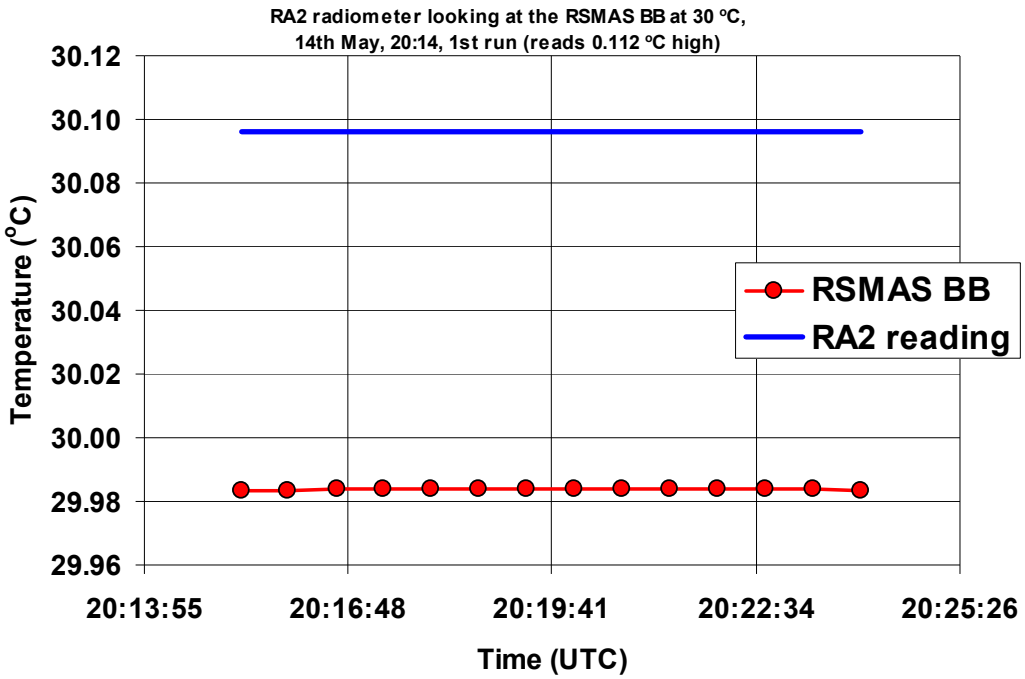

Figure 3.1.10: RA2 radiom. viewing the RSMAS BB at 30 °C, 1st measurement.
<Radiometer measurement> – RSMAS blackbody temperature = +0.112 °C
(brackets indicate average over time interval shown).

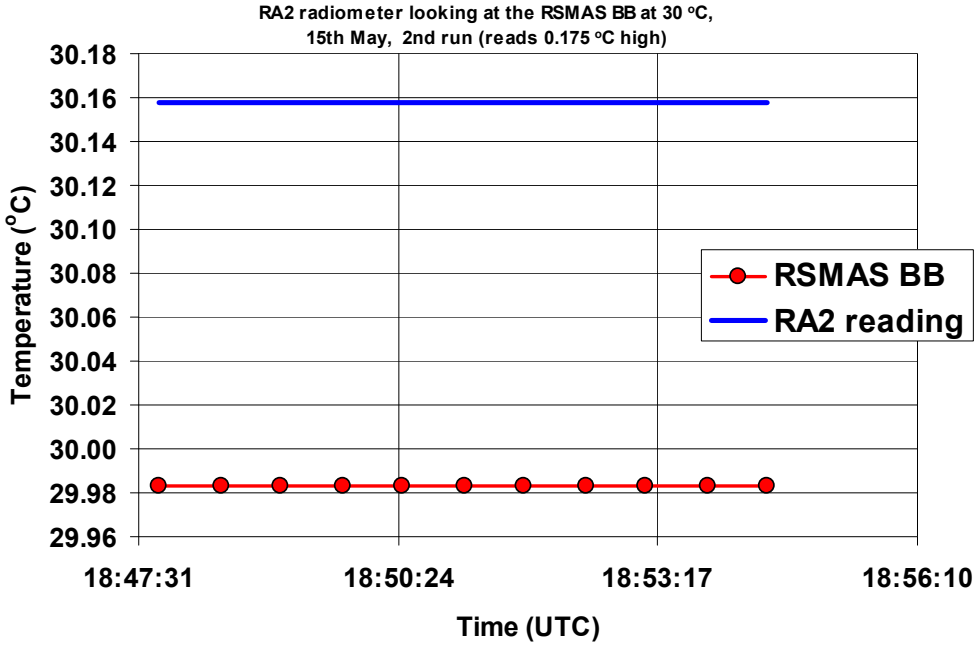

Figure 3.1.11: RA2 radiom. viewing the RSMAS BB at 30 °C, 2nd measurement.
<Radiometer measurement> – RSMAS blackbody temperature = +0.175 °C
(brackets indicate average over time interval shown).

3.1.3.1.4 RA2 radiometer viewing the NIST blackbody

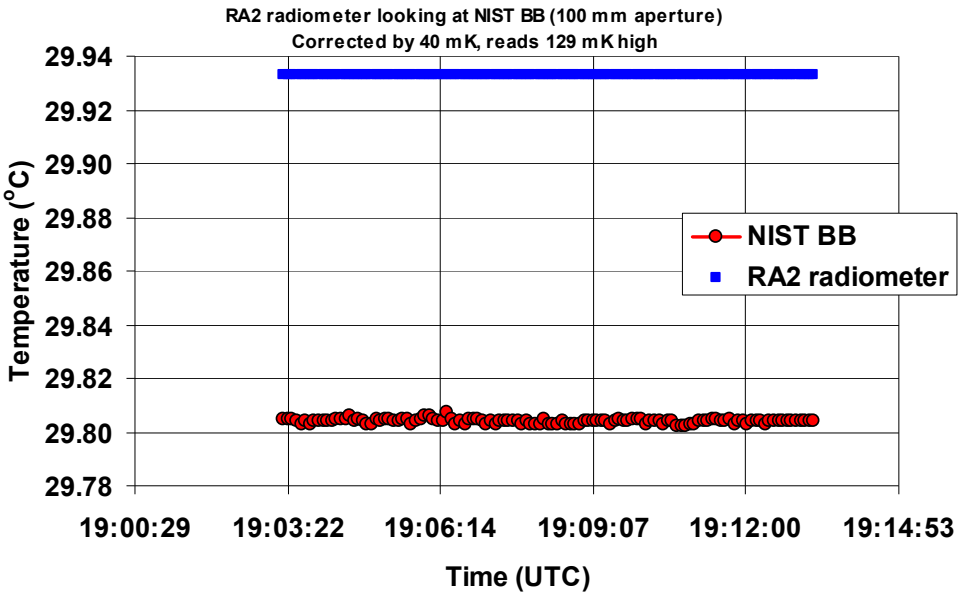

Figure 3.1.12: RA2 radiometer viewing the NIST blackbody at 30 °C.
<Radiometer measurement> – RSMAS blackbody temperature = +0.129 °C
(brackets indicate average over time interval shown).

3.1.3.1.5. RA3 radiometer viewing the RSMAS blackbody

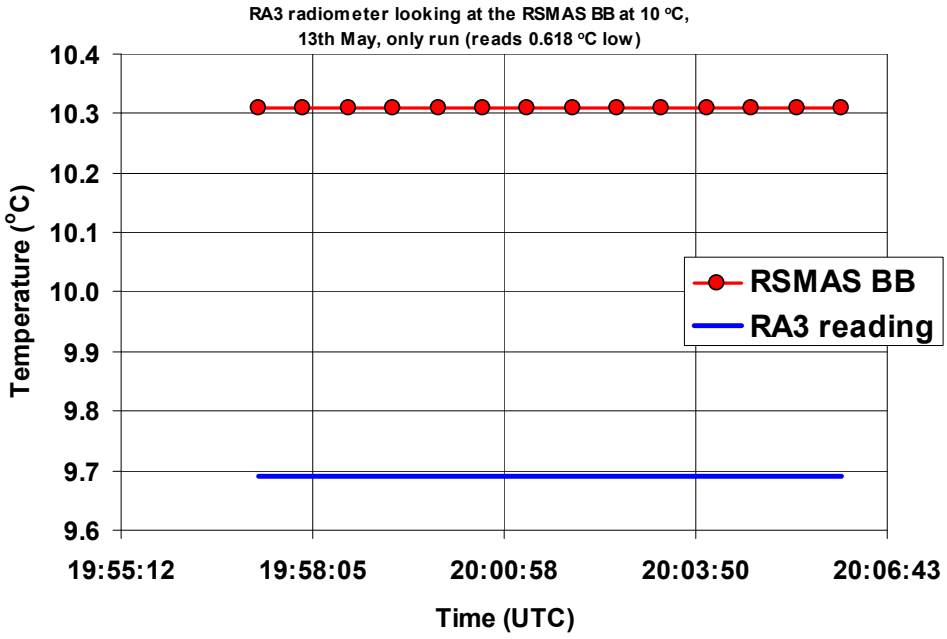

Figure 3.1.13: RA3 radiometer. viewing the RSMAS blackbody at 10 °C.
<Radiometer measurement> – RSMAS blackbody temperature = -0.618 °C
(brackets indicate average over time interval shown).

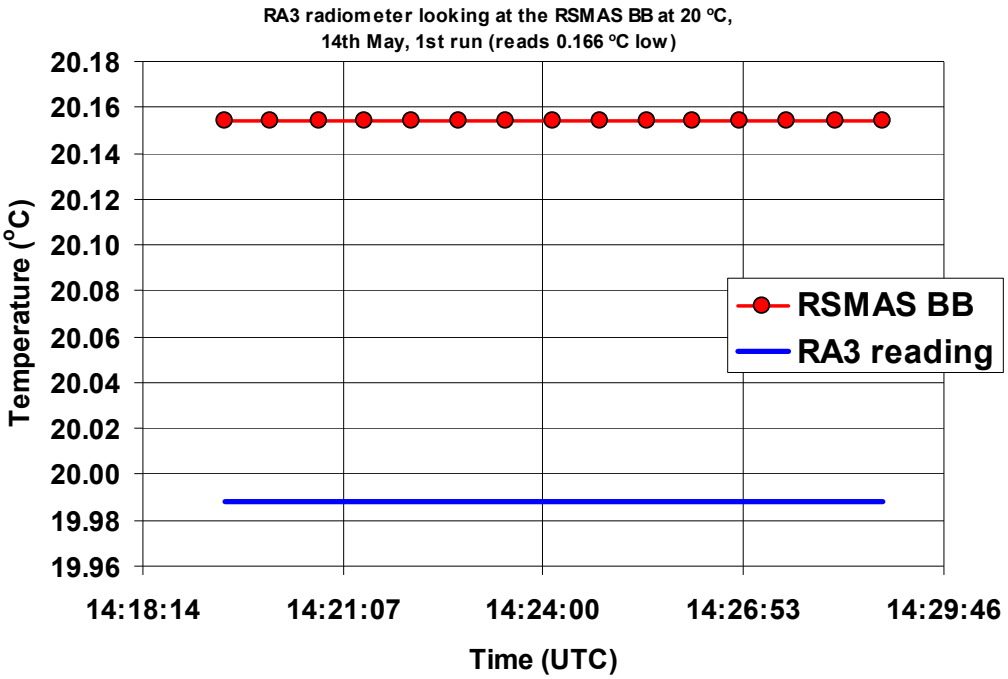

Figure 3.1.14: RA3 radiometer viewing the RSMAS blackbody at 20 °C, 1st run.
<Radiometer measurement> – RSMAS blackbody temperature = -0.166 °C
(brackets indicate average over time interval shown).

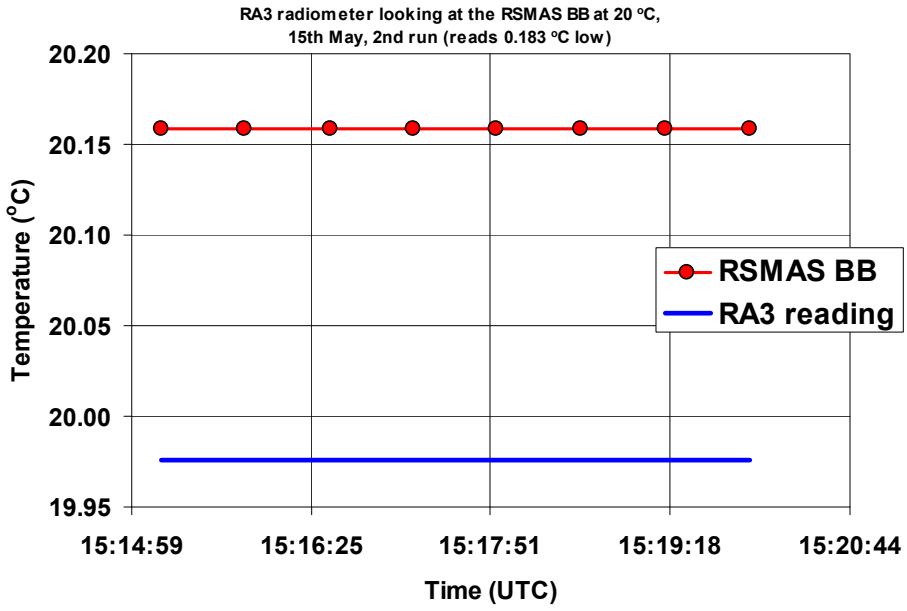

Figure 3.1.15: RA3 radiometer viewing the RSMAS blackbody at 20 °C, 2nd run.
<Radiometer measurement> – RSMAS blackbody temperature = -0.183 °C
(brackets indicate average over time interval shown).

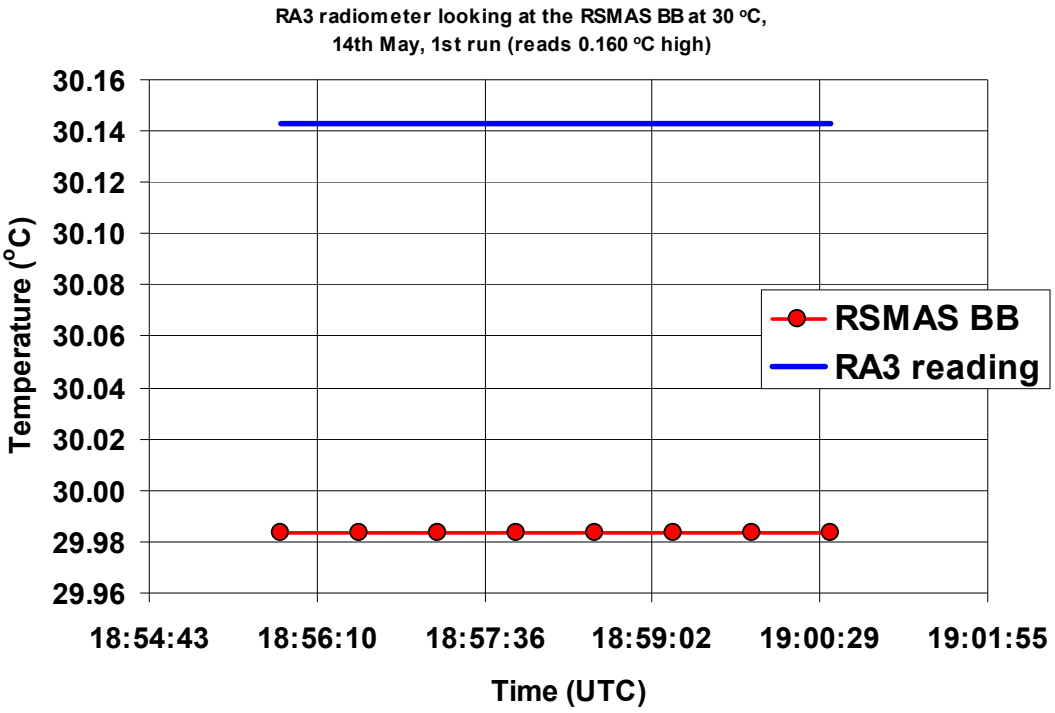

Figure 3.1.16: RA3 radiometer viewing the RSMAS blackbody at 30 °C, 1st run.
<Radiometer measurement> – RSMAS blackbody temperature = +0.16 °C
(brackets indicate average over time interval shown).

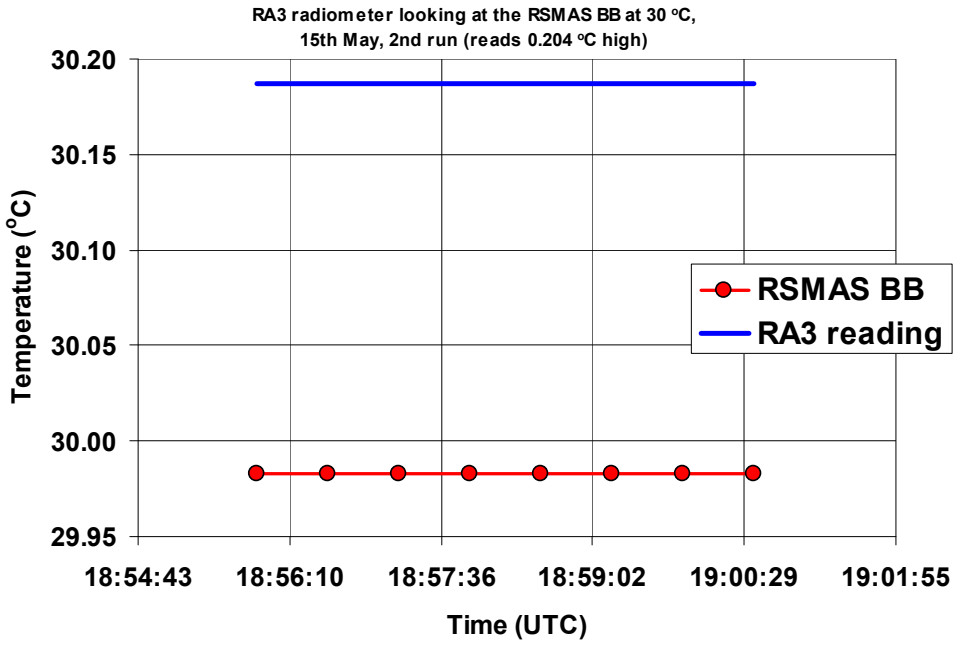

Figure 3.1.17: RA3 radiometer viewing the RSMAS blackbody at 30 °C, 2nd run.
<Radiometer measurement> – RSMAS blackbody temperature = +0.204 °C
(brackets indicate average over time interval shown).

3.1.3.1.6 RA3 radiometer viewing the NIST blackbody

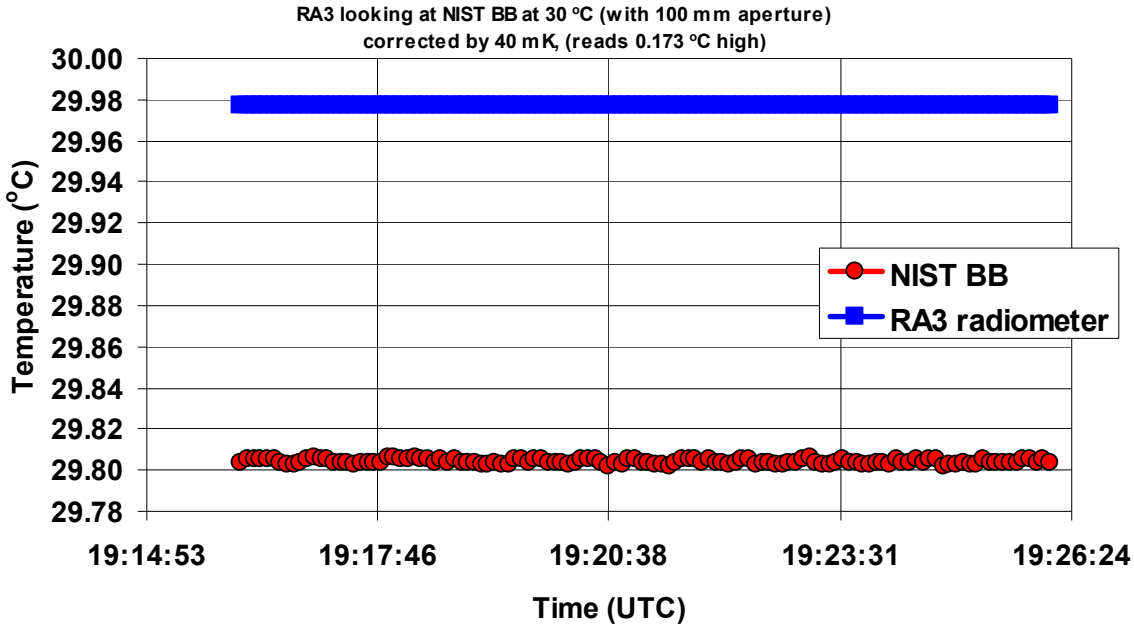

Figure 3.1.18: RA3 radiometer viewing the RSMAS blackbody at 30 °C.
<Radiometer measurement> – RSMAS blackbody temperature = +0.173 °C
(brackets indicate average over time interval shown).

3.1.3.1.7 RA4 radiometer viewing the RSMAS blackbody

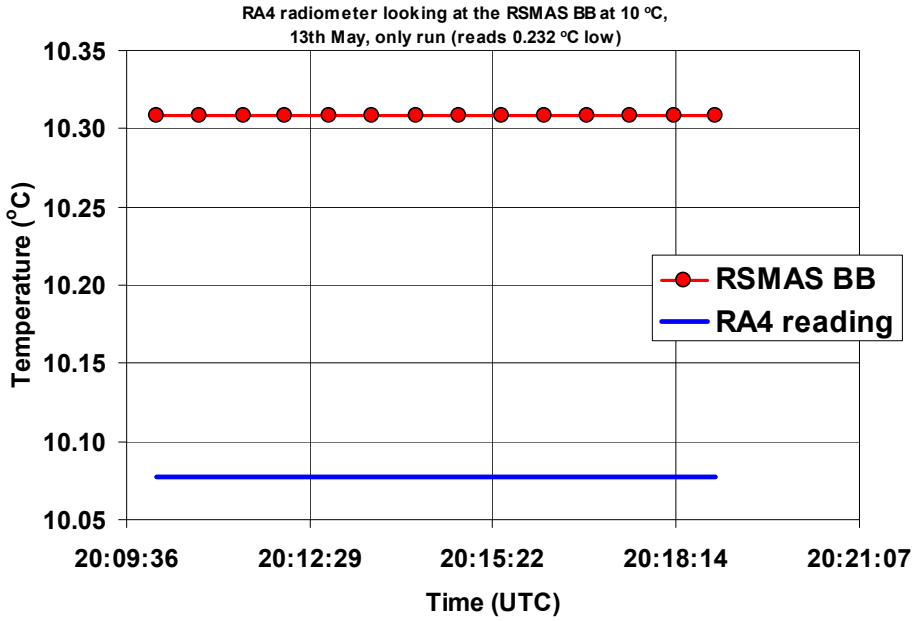

Figure 3.1.19: RA4 radiometer viewing the RSMAS blackbody at 10 °C.
<Radiometer measurement> – RSMAS blackbody temperature = -0.232 °C
(brackets indicate average over time interval shown).

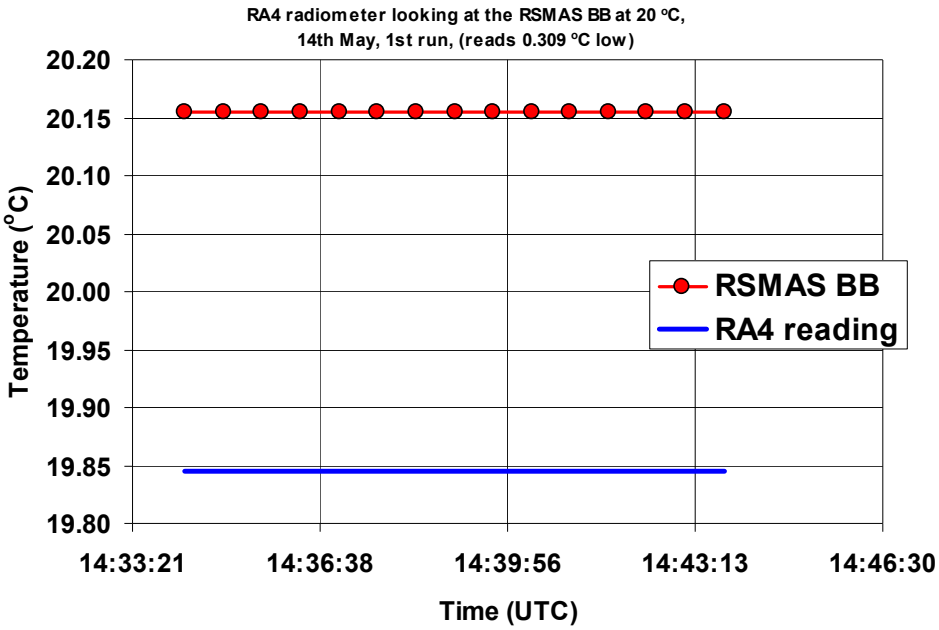

Figure 3.1.20: RA4 radiometer viewing the RSMAS blackbody at 20 °C, 1st run.
<Radiometer measurement> – RSMAS blackbody temperature = -0.309 °C
(brackets indicate average over time interval shown).

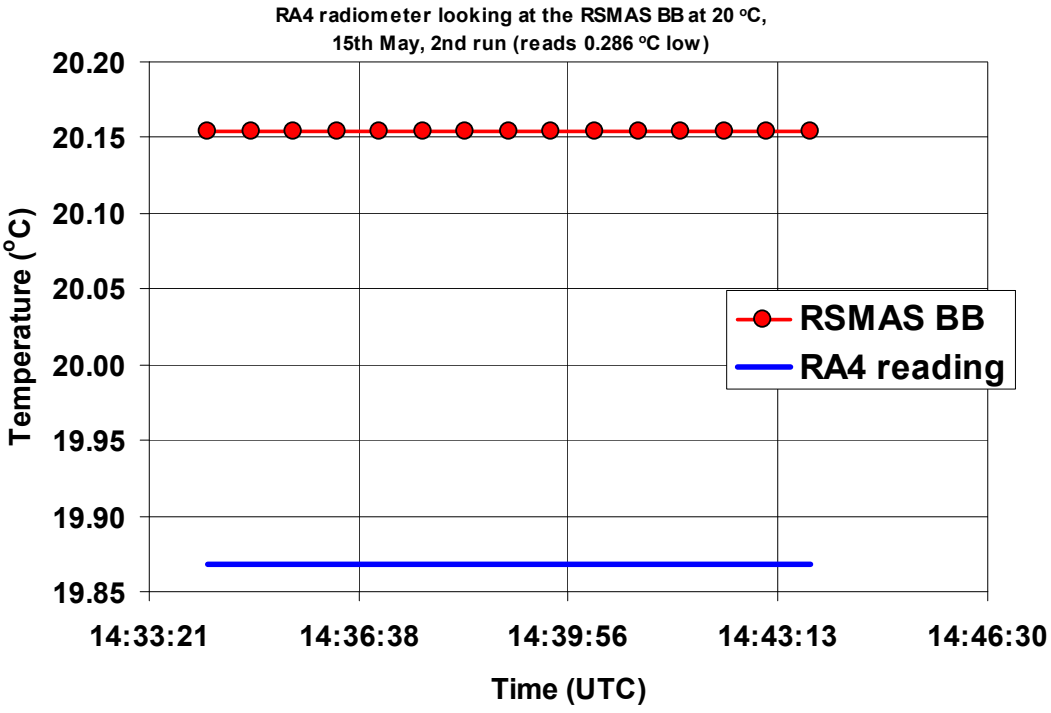

Figure 3.1.21: RA4 radiometer viewing the RSMAS blackbody at 20 °C, 2nd run.
<Radiometer measurement> – RSMAS blackbody temperature = -0.286 °C
(brackets indicate average over time interval shown).

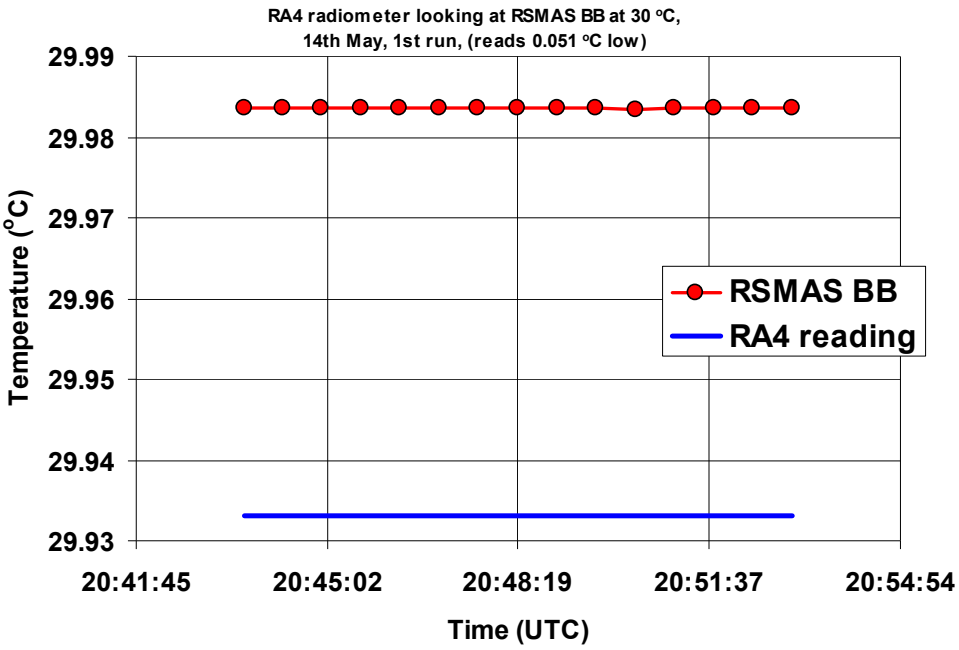

Fig 3.1.22: RA4 radiometer viewing the RSMAS blackbody at 30 °C, 1st run.
<Radiometer measurement> – RSMAS blackbody temperature = -0.051 °C
(brackets indicate average over time interval shown).

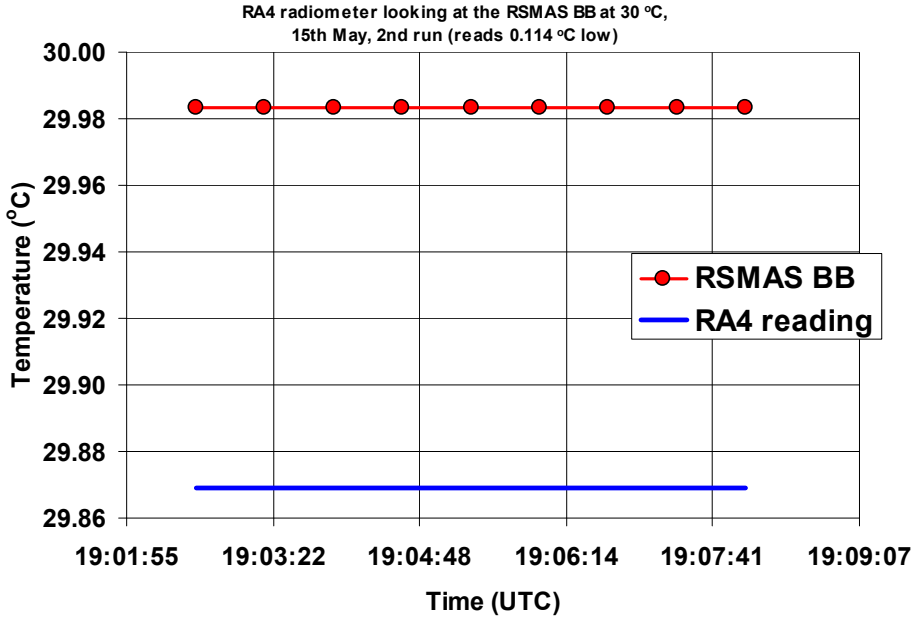

Figure 3.1.23: RA4 radiometer viewing the RSMAS blackbody at 30 °C.
<Radiometer measurement> – RSMAS blackbody temperature = -0.114 °C
(brackets indicate average over time interval shown).

3.1.3.1.8 RA4 radiometer viewing the NIST blackbody

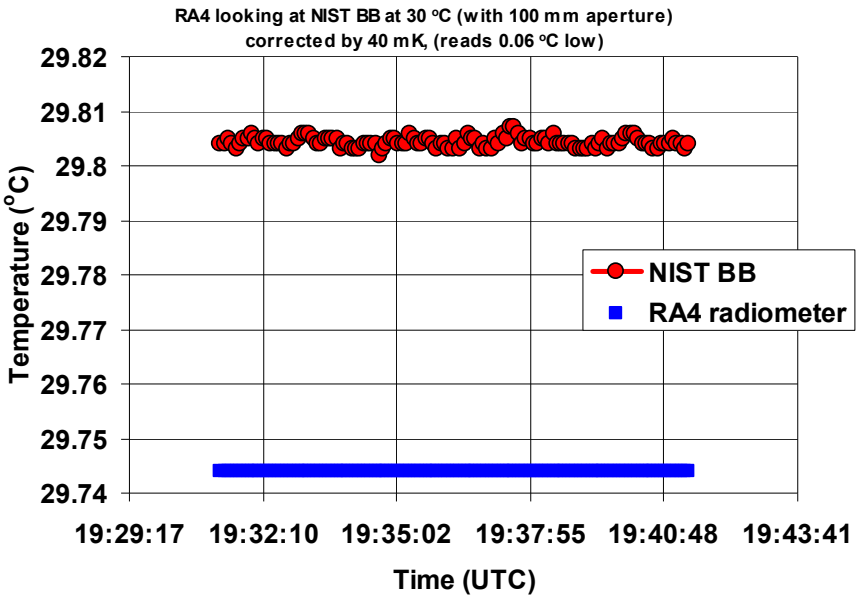

Figure 3.1.24: RA4 radiometer viewing the NIST blackbody at 30 °C.
<Radiometer measurement> – RSMAS blackbody temperature = -0.06 °C
(brackets indicate average over time interval shown).

3.1.3.1.9 RA5 radiometer viewing the RSMAS blackbody

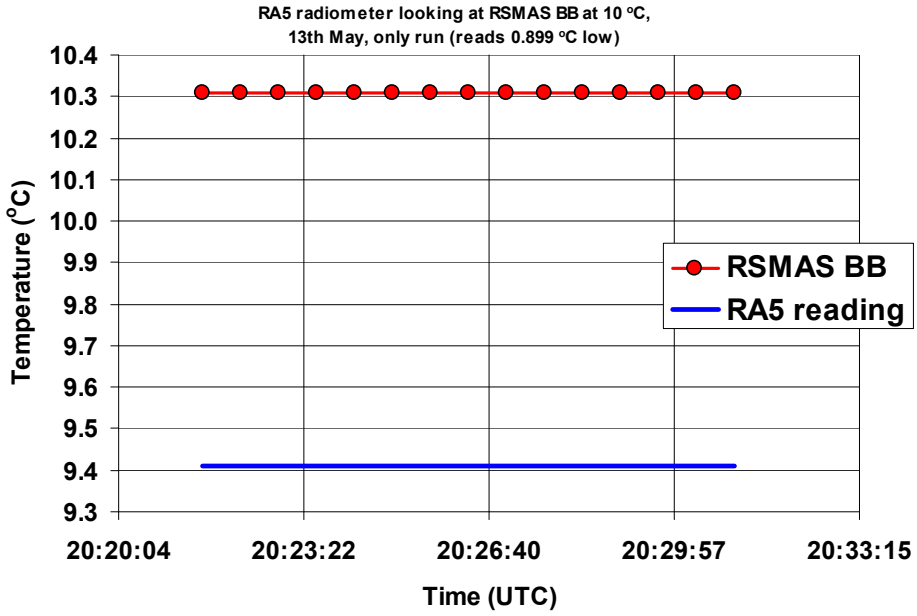

Figure 3.1.25: RA5 radiometer viewing the RSMAS blackbody at 10 °C.
<Radiometer measurement> – RSMAS blackbody temperature = -0.899 °C
(brackets indicate average over time interval shown).

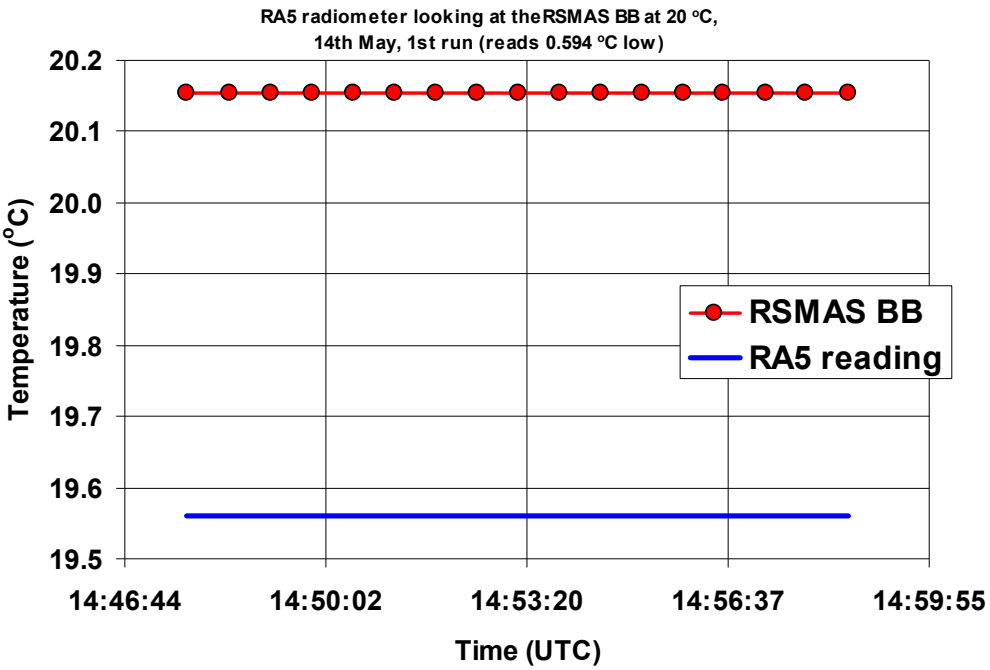

Figure 3.1.26: RA5 radiometer viewing the RSMAS blackbody at 20 °C, 1st run.
<Radiometer measurement> – RSMAS blackbody temperature = -0.594 °C
(brackets indicate average over time interval shown).

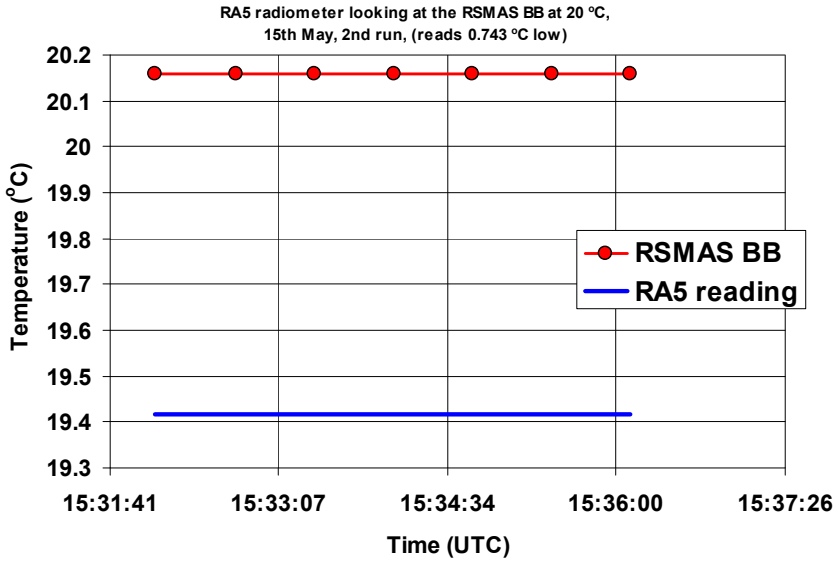

Figure 3.1.27: RA5 radiometer viewing the RSMAS blackbody at 20 °C, 2nd run.
<Radiometer measurement> – RSMAS blackbody temperature = -0.743 °C
(brackets indicate average over time interval shown).

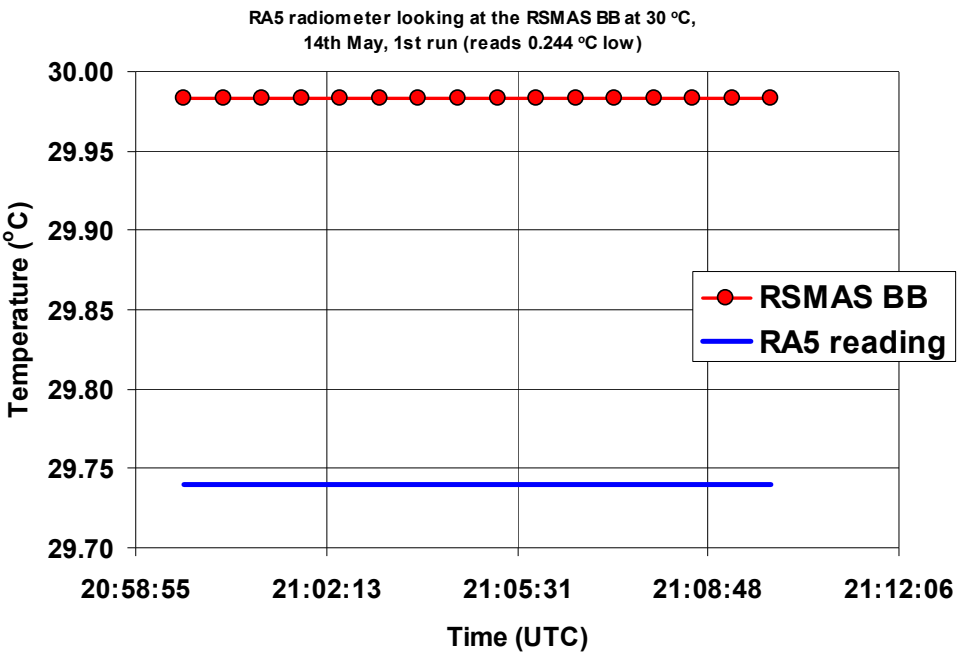

Figure 3.1.28: RA5 radiometer viewing the RSMAS blackbody at 30 °C, 1st run.
<Radiometer measurement> – RSMAS blackbody temperature = -0.244 °C
(brackets indicate average over time interval shown).

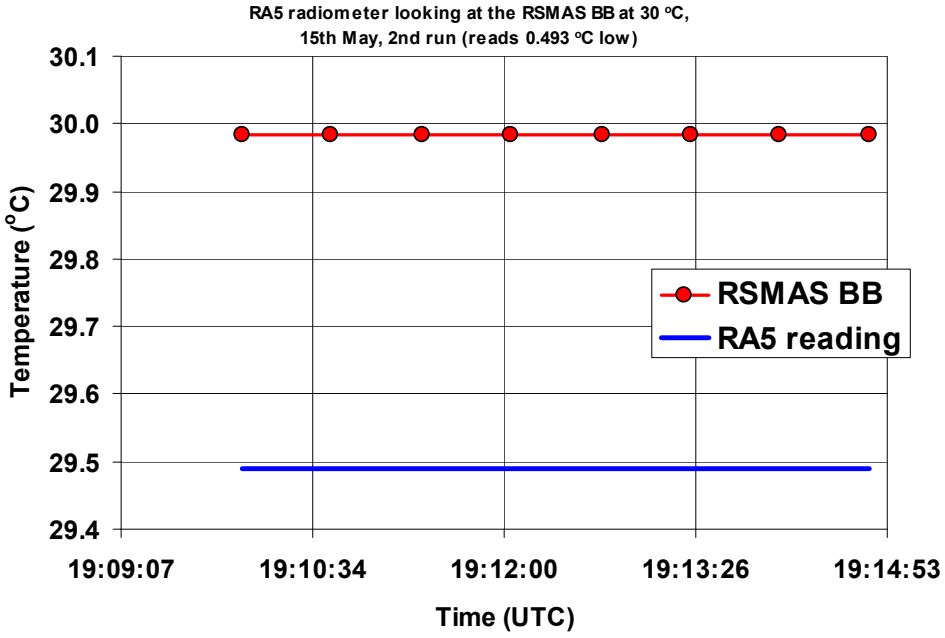

Figure 3.1.29: RA5 radiometer viewing the RSMAS blackbody at 30 °C, 2nd run.
<Radiometer measurement> – RSMAS blackbody temperature = -0.493 °C
(brackets indicate average over time interval shown).

3.1.3.1.10 RA5 radiometer viewing the NIST blackbody

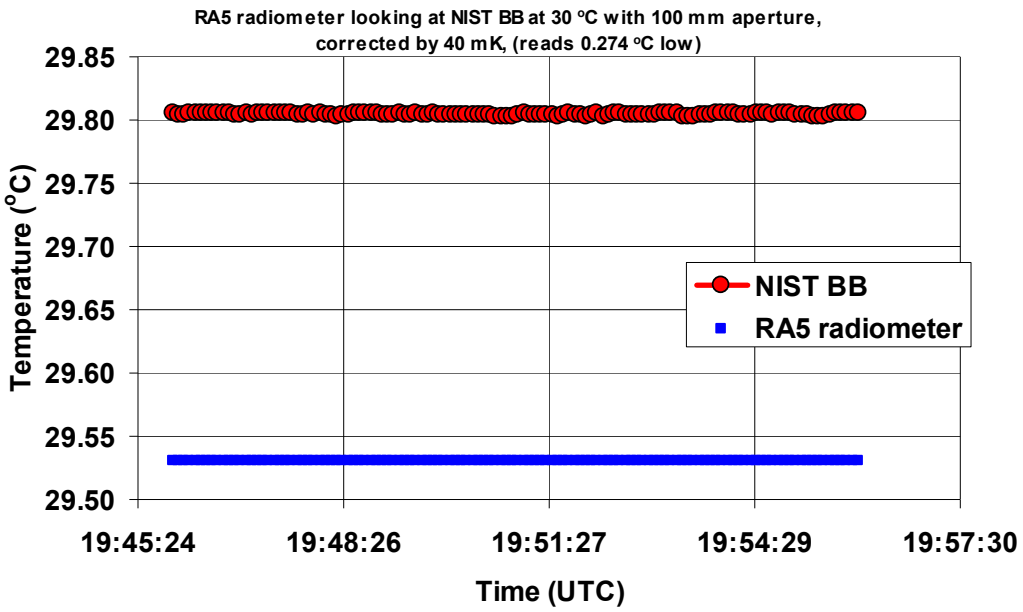

Figure 3.1.30: RA5 radiometer viewing the NIST blackbody at 30 °C.
<Radiometer measurement> – RSMAS blackbody temperature = -0.274 °C
(brackets indicate average over time interval shown).

3.1.3.1.11 Ocean surface temperature measurements using the CEAM radiometers.

Figure 3.1.31 shows the ocean surface temperature values measured by the CEAM RA1, RA2 and RA3 radiometers during the Miami Sea Surface Temperature (SST) comparison. Figure 3.1.32 shows the difference of the CEAM RA1, RA2 and RA3 ocean surface temperature measurements from the corresponding ISAR radiometer measurements.

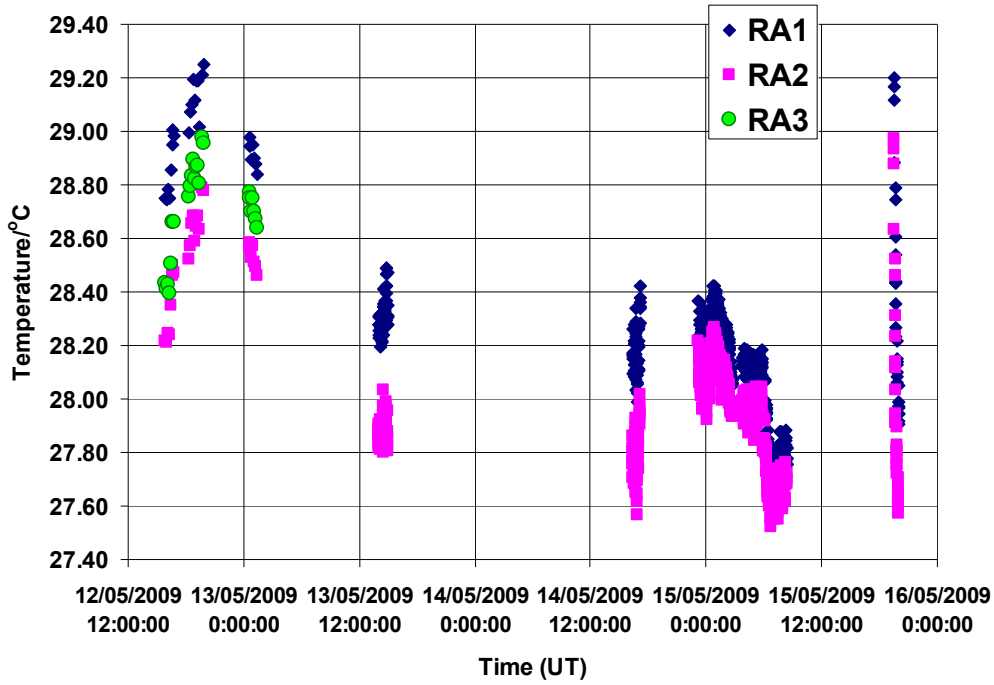

Figure 3.1.31: Ocean surface temperature measurements reported by CEAM using radiometers RA1, RA2 and RA3.

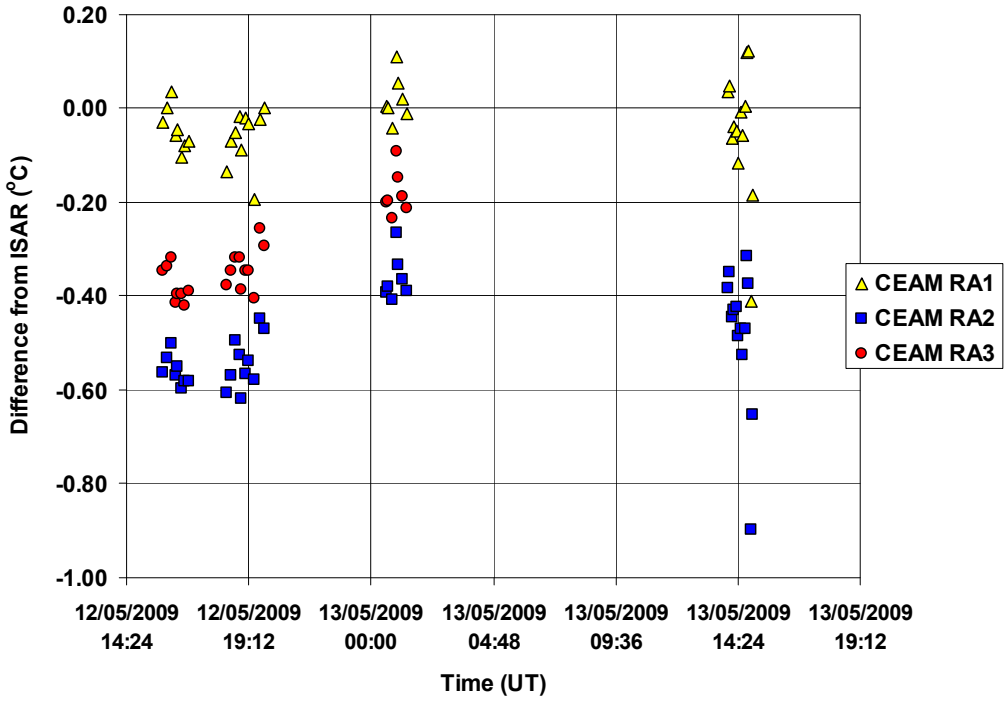

Figure 3.1.32: Difference of the CEAM RA1, RA2 and RA3 ocean surface temperature measurements from the corresponding ISAR radiometer measurements.

3.2 Department of Earth Physics and Thermodynamics (DEPT), University of Valencia

3.2.1 Contact information:

DEPT contact for the comparison: Dr. César Coll
Address: Dept. of Earth Physics and Thermodynamics, Faculty of Physics, University of Valencia, Dr. Moliner, 50. 46100 Burjassot, Spain.
Email: cesar.coll@uv.es

3.2.2 Radiometers used in the comparison

Make and type of Instrument: Radiometer CIMEL Electronique CE312-1 (two units). (http://www.cimel.fr/photo/radiometer_us.htm)

Outline technical description of instrument: Type of detector: thermopile. 4 spectral bands: B1 8 µm to14 µm, B2 11.5 µm to 12.5 µm, B3 10.5 µm to 11.5 µm, and B4 8.2 µm to 9.2 µm. Broad band: Germaniun window and zinc sulphide filters. Narrow bands: interference filters. Field of view: 10º. The instrument has a built-in radiance reference made of a concealable gold-coated mirror which enables comparison between the target radiance and the reference radiation from inside the detector cavity. The temperature of the detector is measured with a PRT, thus allowing compensation for the cavity radiation.

References:

1. Sicard, M., Spyak, P. R., Brogniez, G., Legrand, M., Abuhassan, N. K., Pietras, C., and Buis, J. P. (1999). Thermal infrared field radiometer for vicarious cross-calibration: characterization and comparisons with other field instruments. *Optical Engineering*, 38 (2), 345-356.

2. M. Legrand, C. Pietras, G. Brogniez, M. Haeffelin, N. K. Abuhassan and M. Sicard (2000). A high-accuracy multiwavelength radiometer for in situ measurements in the thermal infrared. Part I: characterization of the instrument, *J. Atmos. Ocean Techn.,* 17, 1203-1214.

Establishment or traceability route for primary calibration including date of last realisation and breakdown of uncertainty:

The radiometer has not undergone a traceable primary calibration. The spectral characterisation of the instrument can be found in references 1 and 2 above. The following error analysis is based on estimates, experience and laboratory measurements with a Landcal Blackbody Source P80P (April 6 and 7, 2009).

Type A

- Repeatability: Typical value of the standard deviation of 12 measurements at a fixed black body temperature without re-alignment of radiometer.

Unit 1	B1	B2	B3	B4	mean
K	0.01	0.07	0.04	0.12	0.07
%	0.003	0.02	0.01	0.04	0.02

Unit 2	B1	B2	B3	B4	mean
K	0.02	0.09	0.09	0.08	0.07
%	0.007	0.03	0.03	0.03	0.02

- Reproducibility: Typical value of difference between two runs of radiometer measurements at the same black body temperature including re-alignment.

Unit 1	B1	B2	B3	B4	mean
K	0.08	0.08	0.08	0.08	0.08
%	0.03	0.03	0.03	0.03	0.03

Unit 2	B1	B2	B3	B4	mean
K	0.21	0.07	0.04	0.09	0.10
%	0.07	0.02	0.01	0.03	0.03

Total Type A uncertainty (RSS):

Unit 1	B1	B2	B3	B4	mean
K	0.08	0.11	0.09	0.14	0.11
%	0.03	0.04	0.03	0.05	0.04

Unit 2	B1	B2	B3	B4	mean
K	0.21	0.11	0.10	0.12	0.14
%	0.07	0.04	0.03	0.04	0.05

Type B

- Linearity of radiometer: 0.2 K (Typical value for all bands according to reference 1).

- Primary calibration: Typical value of difference between radiometer brightness temperature and Landcal Blackbody Source P80P temperature (K).

	B1	B2	B3	B4	mean
Unit 1	0.4	0.6	0.2	0.4	0.4
Unit 2	0.5	0.5	0.4	0.5	0.5

- Drift since calibration: 0.0 K (as expected since very recent calibration measurements).

Total Type B uncertainty (RSS):

	B1	B2	B3	B4	mean
Unit 1	0.4	0.6	0.3	0.4	0.4
Unit 2	0.5	0.5	0.4	0.5	0.5

Type A + Type B uncertainty (RSS):

	B1	B2	B3	B4	mean
Unit 1	0.5	0.6	0.3	0.5	0.5
Unit 2	0.6	0.5	0.5	0.6	0.6

Operational methodology during measurement campaign:

Calibration measurements were performed in the laboratory following, as closely as possible, the procedures described in the Draft Protocol. The Landcal Blackbody Source P80P was set at four temperatures (278, 283, 293 and 303 K) in two different runs. Enough time was allowed for the black body to reach equilibrium at each temperature. Radiometers were aligned with the black body cavity, and placed at a distance so that the field of view was smaller than the cavity diameter. Standard processing (see references above) was applied to the radiometer readouts to calculate the equivalent brightness temperature. The four bands of the two CE312-1 instruments were used. The measured values reported above are typical values for all black body temperatures considered for each band of each radiometer unit. The mean values considering all bands of each radiometer unit are also given.

Radiometer usage (deployment)

Field measurements (hand held and tripod mounted) of land surface temperature and emissivity for validation of thermal infrared products from satellite sensors (Envisat/AATSR, Terra/MODIS and ASTER, Landsat/ETM+) over test sites in Spain. Laboratory measurements of soil emissivity.

Uncertainty of measurement

The following tables summarise the uncertainties determined/estimated for each radiometer.

CIMEL Electronique CE312-1 Radiometer – Unit 1

Parameter	Type A Uncertainty in Value / %	Type B Uncertainty in Value / (appropriate units)	Uncertainty in Brightness temperature K
Repeatability of measurement	0.02[(1)]		0.07[(1)]
Reproducibility of measurement	0.03[(2)]		0.08[(2)]
Linearity of radiometer		0.2 K[(3)]	0.2
Primary calibration		0.4 K[(4)]	0.4
Drift since calibration		-	-
RMS total	0.04 % 0.11 K	**0.4 K**	0.5

CIMEL Electronique CE312-1 Radiometer – Unit 2

Parameter	Type A Uncertainty in Value / %	Type B Uncertainty in Value / (appropriate units)	Uncertainty in Brightness temperature K
Repeatability of measurement	0.02[(1)]		0.07[(1)]
Reproducibility of measurement	0.03[(2)]		0.10[(2)]
Linearity of radiometer		0.2 K[(3)]	0.2
Primary calibration		0.5 K[(4)]	0.5
Drift since calibration		-	-
RMS total	0.05 % 0.14 K	**0.5 K**	0.6

(1) Typical value of the standard deviation of 12 measurements at fixed black body temperature without re-alignment of radiometer. Mean values for all bands are shown. Values are detailed for each band in Appendix B.
(2) Typical value of difference between two runs of radiometer measurements at the same black body temperature including re-alignment. Mean values for all bands are shown. Values are detailed for each band in Appendix B.

(3) From reference 1 (Sicard et al., 1999) in Appendix B.
(4) Typical value of difference between radiometer brightness temperature and Landcal Blackbody Source P80P temperature. Mean values for all bands are shown. Values are detailed for each band in Appendix B.

3.2.3 Results

The DEPT radiometers took part in the NPL blackbody comparison.

3.2.3.1 Comparison of CE312 unit-1 to the NPL variable temperature blackbody

Figures 3.2.1 to 3.2.6 show the output of the four channels of the DEPT CE-312 Unit 1 radiometer when it was viewing the NPL blackbody maintained at different temperatures. The same Figures also show the brightness temperature of the NPL blackbody as a function of time. The Tables below each Figure list the difference between the average temperature displayed by each radiometer channel and the corresponding avearge radiance temperature of the NPL variable temperature blackbody.

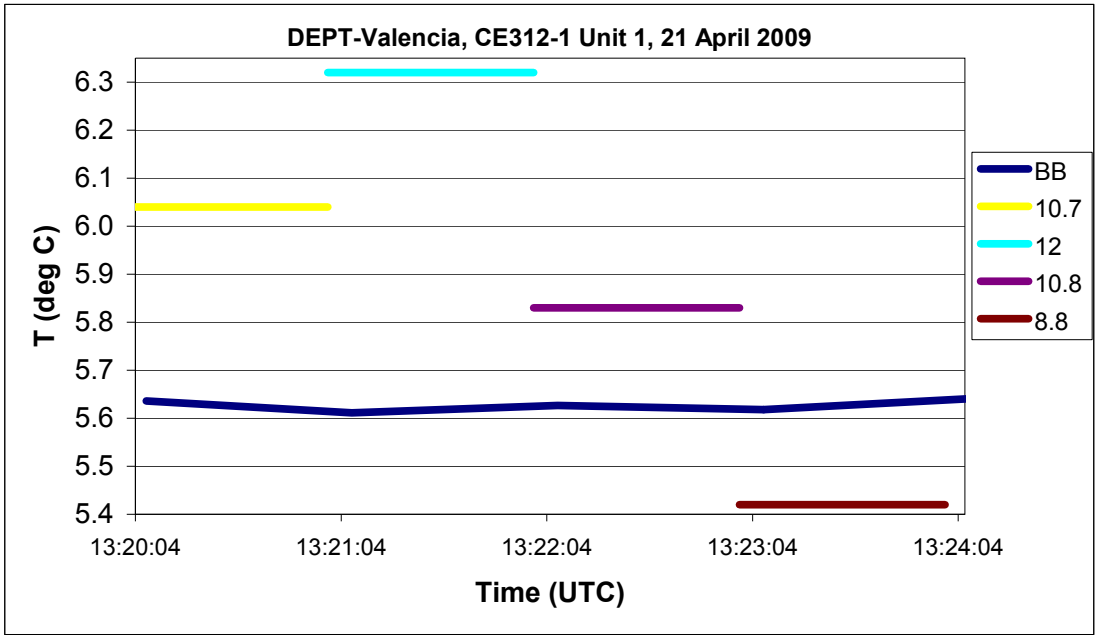

Figure 3.2.1: The DEPT CE-312 Unit 1 viewing the NPL blackbody at 5 °C.
The table below indicates the deviation of the different radiometer channels δT from the average blackbody temperature, over the measurement interval.

Channel (μm)	δT (deg C)
10.7	**0.416**
12.0	**0.701**
10.8	**0.208**
8.8	**-0.209**

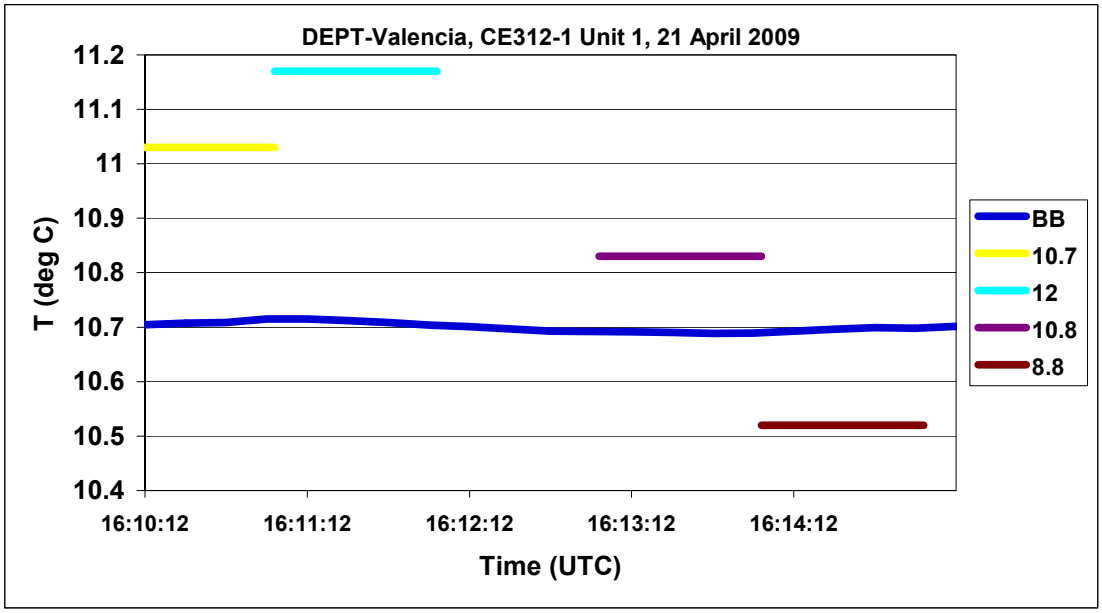

Figure 3.2.2: The DEPT CE312 unit 1 viewing the NPL blackbody at 10 ^{o}C, 1st measurement. The table below indicates the deviation of the different radiometer channels δT from the average blackbody temperature, over the measurement interval.

Channel (μm)	δT (deg C)
10.7	0.321
12.0	0.464
10.8	0.14
8.8	-0.179

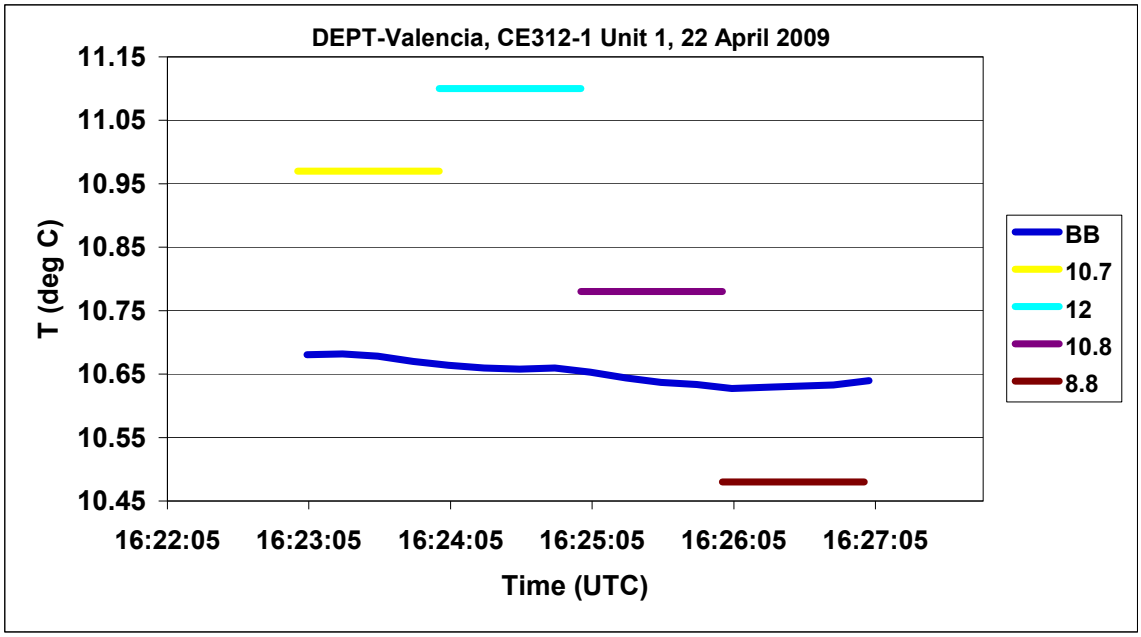

Figure 3.2.3: The DEPT CE312 unit 1 viewing the NPL blackbody at 10 °C, 2nd measurement. The table below indicates the deviation of the different radiometer channels δT from the average blackbody temperature, over the measurement interval.

Channel (μm)	δT (deg C)
10.7	0.292
12.0	0.442
10.8	0.145
8.8	-0.154

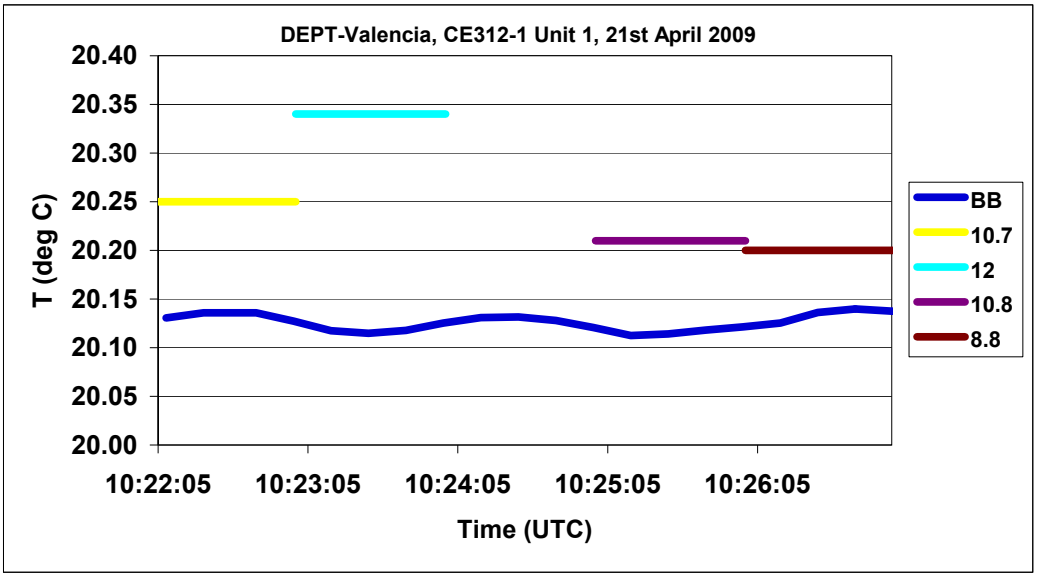

Figure 3.2.4: The DEPT CE312 unit 1 viewing the NPL blackbody at 20 °C, 1st measurement. The table below indicates the deviation of the different radiometer channels δT from the average blackbody temperature, over the measurement interval.

Channel (μm)	δT (deg C)
10.7	0.118
12.0	0.221
10.8	0.082
8.8	0.083

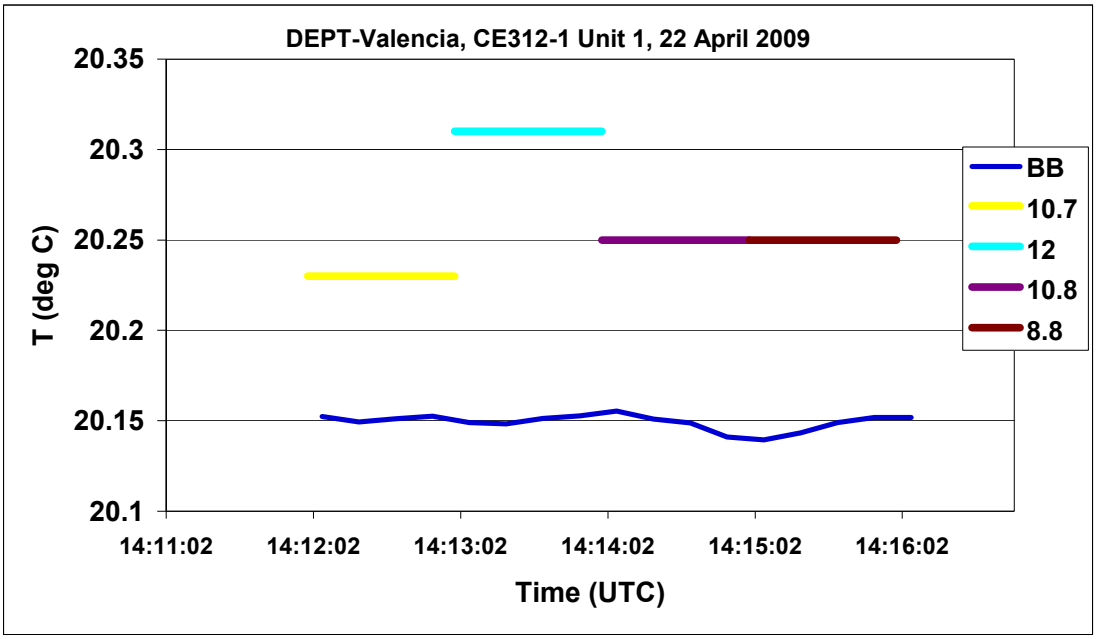

Figure 3.2.5: The DEPT CE312 unit 1 viewing the NPL blackbody at 20 °C, 2nd measurement. The table below indicates the deviation of the different radiometer channels δT from the average blackbody temperature, over the measurement interval.

Channel (μm)	δT (deg C)
10.7	0.079
12.0	0.160
10.8	0.101
8.8	0.104

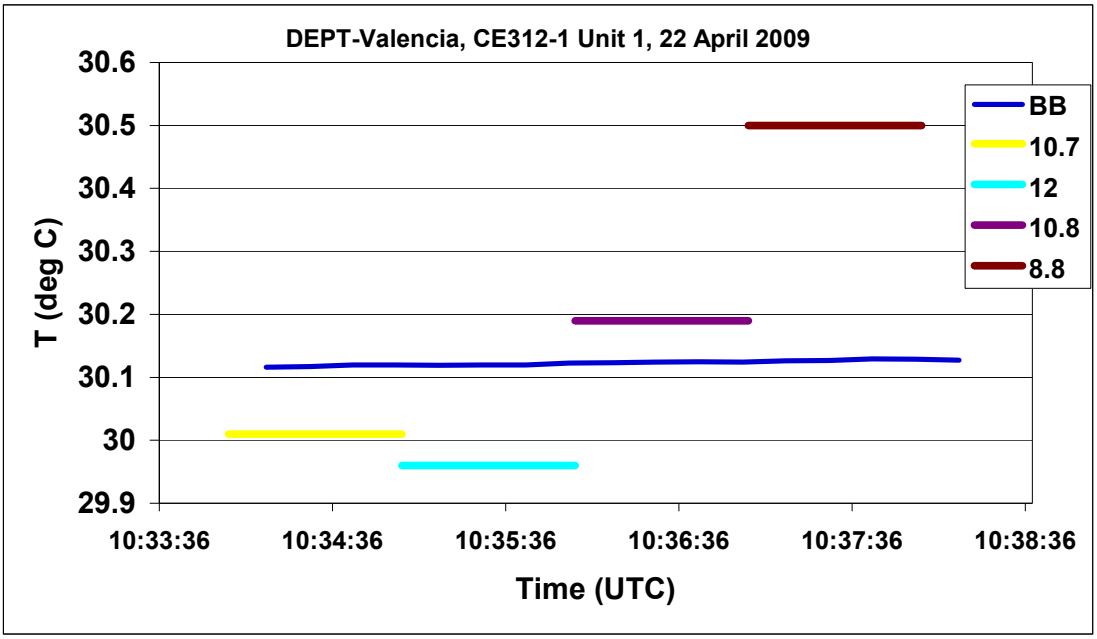

Figure 3.2.6: The DEPT CE312 unit 1 viewing the NPL blackbody at 30 °C. The table below indicates the deviation of the different radiometer channels δT from the average blackbody temperature, over the measurement interval.

Channel (μm)	δT (deg C)
10.7	-0.108
12.0	-0.160
10.8	0.066
8.8	0.372

3.2.3.2 Comparison of DEPT CE312 unit-2 viewing NPL blackbody

Figures 3.2.7 to 3.2.12 show the output of the four channels of the DEPT CE-312 Unit 2 radiometer when it was viewing the NPL variable temperature blackbody maintained at different temperatures. The same Figures also show the brightness temperature of the NPL blackbody as a function of time. The Tables below each Figure list the difference between the average temperature displayed by each channel and the corresponding value of the average radiance temperature of the NPL variable temperature blackbody.

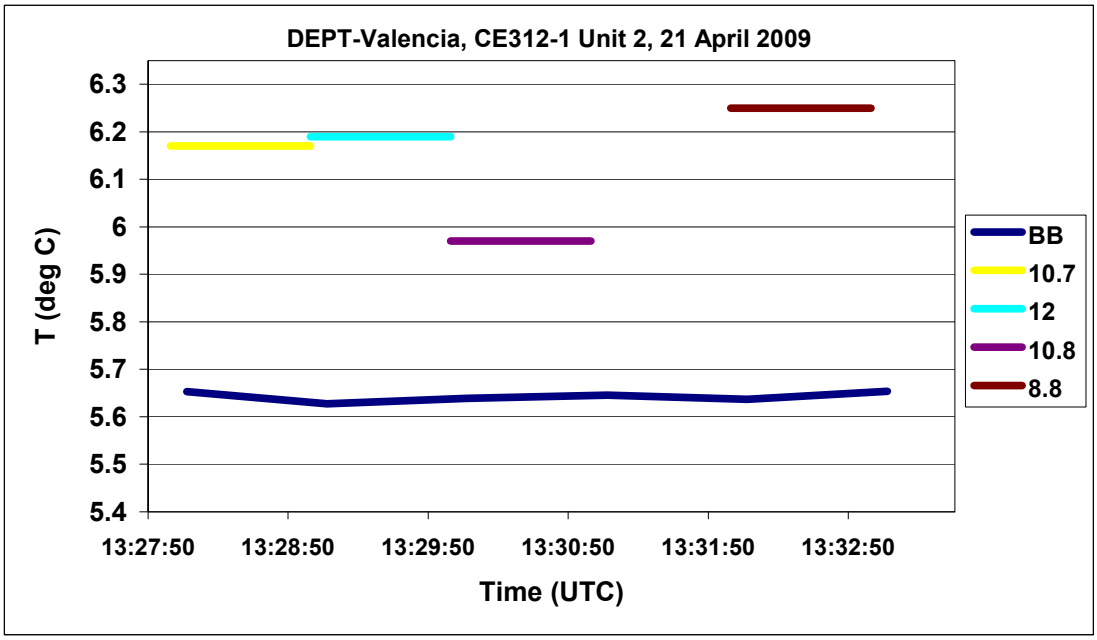

Figure 3.2.7: The DEPT CE-312 unit 2 viewing the NPL blackbody at 5 ^{o}C. The table below indicates the deviation of the different radiometer channels δT from the average blackbody temperature, over the measurement interval.

Channel (μm)	δT (deg C)
10.7	0.529
12.0	0.557
10.8	0.328
8.8	0.605

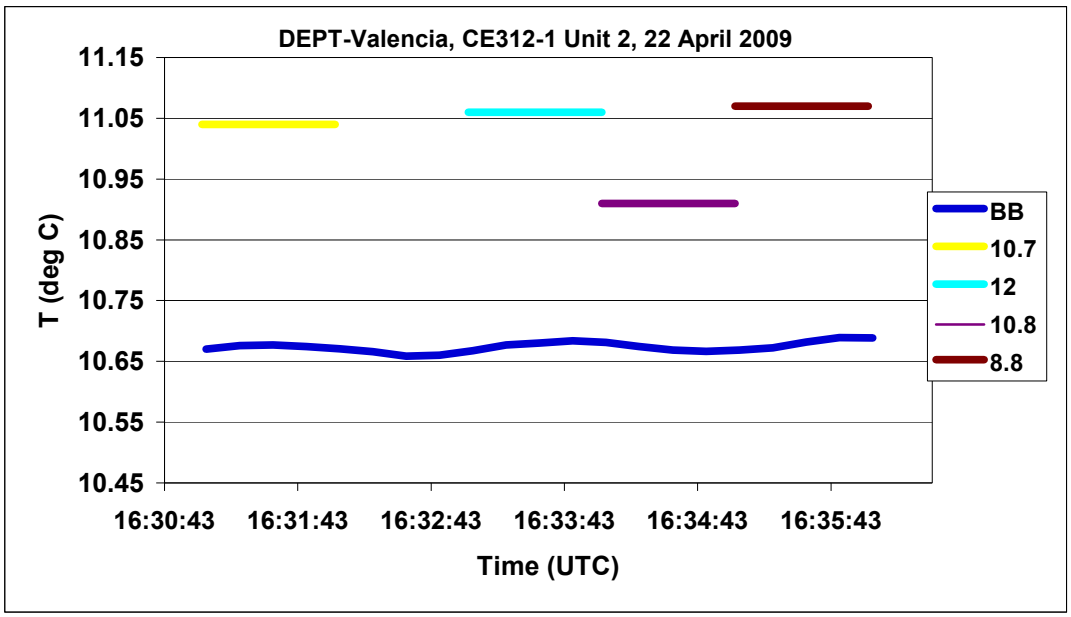

Figure 3.2.8: The DEPT CE-312 unit 2 viewing the NPL blackbody at 10 ^{o}C, 1st measurement. The table below indicates the deviation of the different radiometer channels δT from the average blackbody temperature, over the measurement interval.

Channel (μm)	δT (deg C)
10.7	0.423
12.0	0.467
10.8	0.289
8.8	0.514

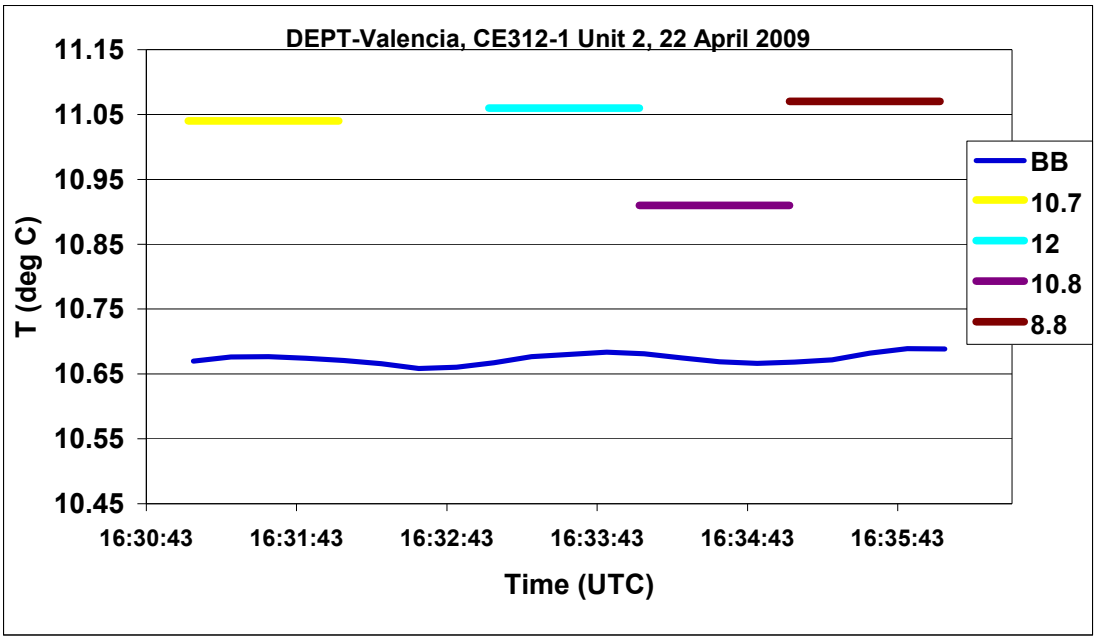

Figure 3.2.9: The DEPT CE-312 unit 2 viewing the NPL blackbody at 10 °C, 2nd measurement. The table below indicates the deviation of the different radiometer channels δT from the average blackbody temperature, over the measurement interval.

Channel (μm)	δT (deg C)
10.7	0.366
12.0	0.383
10.8	0.237
8.8	0.392

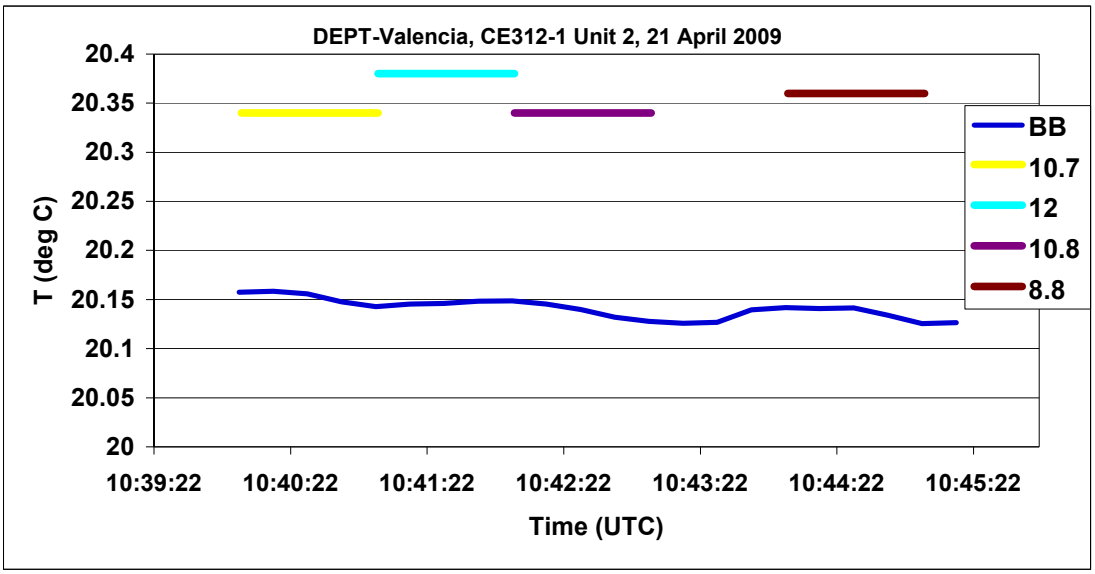

Figure 3.2.10: The DEPT CE-312 unit 2 viewing the NPL blackbody at 20 °C, 1st measurement. The table below indicates the deviation of the different radiometer channels δT from the average blackbody temperature, over the measurement interval.

Channel (μm)	δT (deg C)
10.7	0.189
12.0	0.233
10.8	0.204
8.8	0.225

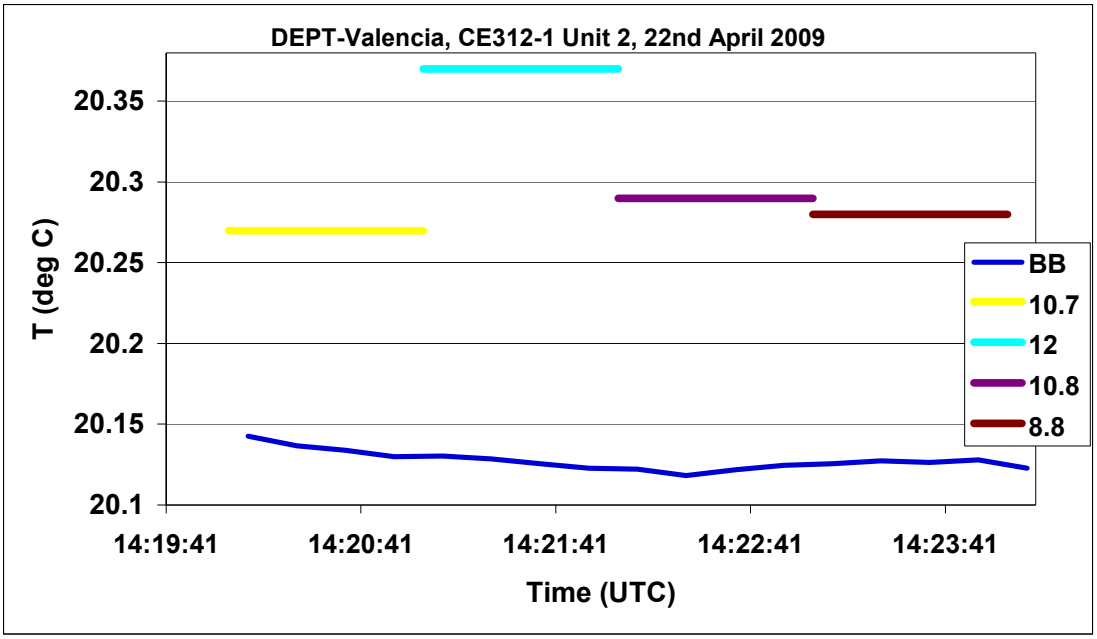

Figure 3.2.11: The DEPT CE-312 unit 2 viewing the NPL blackbody at 20°C, 2nd measurement. The table below indicates the deviation of the different radiometer channels δT from the average blackbody temperature, over the measurement interval.

Channel (μm)	δT (deg C)
10.7	0.134
12.0	0.243
10.8	0.168
8.8	0.153

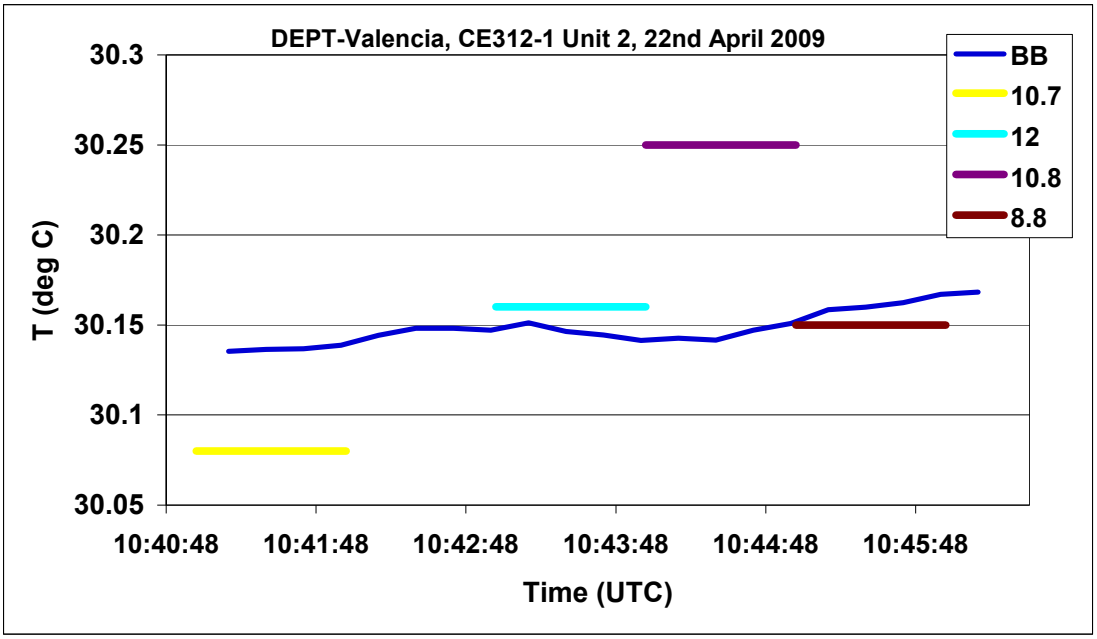

Figure 3.2.12: The DEPT CE312 unit 2 viewing the NPL blackbody at 30 °C. The table below indicates the deviation of the different radiometer channels δT from the average blackbody temperature, over the measurement interval.

Channel (μm)	δT (deg C)
10.7	-0.057
12.0	0.014
10.8	0.104
8.8	-0.012

3.3 Remote Sensing Institute, German Aerospace Centre (DLR)

3.3.1 Contact information

DLR contact for the comparison: Dr Willem Vreeling
Address: PO Box 1116, 82230 Wessling, Germany
EMAIL: WILLEM.VREELING@DLR.DE

3.3.2 Radiometer used in the comparison

Outline technical description of radiometer: D & P micro FTIR model 102
(http://www.dpinstruments.com/)

A small portable FTIR spectrometer operating over the spectral range 2 μm to 16 μm with a 4.8 degree FOV entrance optic.

In usage the instrument measures the full spectrum (nominally 6800 spectral channels) and then after correction for any calibration offsets to the spectrum, the measured brightness temperature is determined as a "best fit" to a Planckian radiator.

Establishment or traceability route for primary calibration including date of last realisation and breakdown of uncertainty: unknown

Uncertainty
The radiometer is stated to have an uncertainty of 0.2 K for Type B. Its Type A varied according to specific measurements in the laboratory; this was between 0.09 K and 0.17 K (depending on the temperature of black body being measured) and 0.1 K when viewing the ocean, although for two specific measurements of the ocean this was much larger at 2 K and 5.1 K.

3.3.3 Results

The DLR radiometer participated in the RSMAS blackbody and RSMAS ocean surface temperature comparisons.

3.3.3.1 Comparison of the DLR radiometer to the RSMAS blackbody

Figures 3.3.1 to 3.3.6 show the temperature values reported by the DLR radiometer when monitoring the RSMAS blackbody cavity. Also plotted in the same Figures are the corresponding values of the brightness temperature of the RSMAS blackbody cavity. Figure 3.3.7 shows the corresponding measurements when the same radiometer was viewing the NIST blackbody cavity. Figure 3.3.8 shows the difference between the DLR Ocean surface temperature measurements from the corresponding ISAR radiometer measurements.

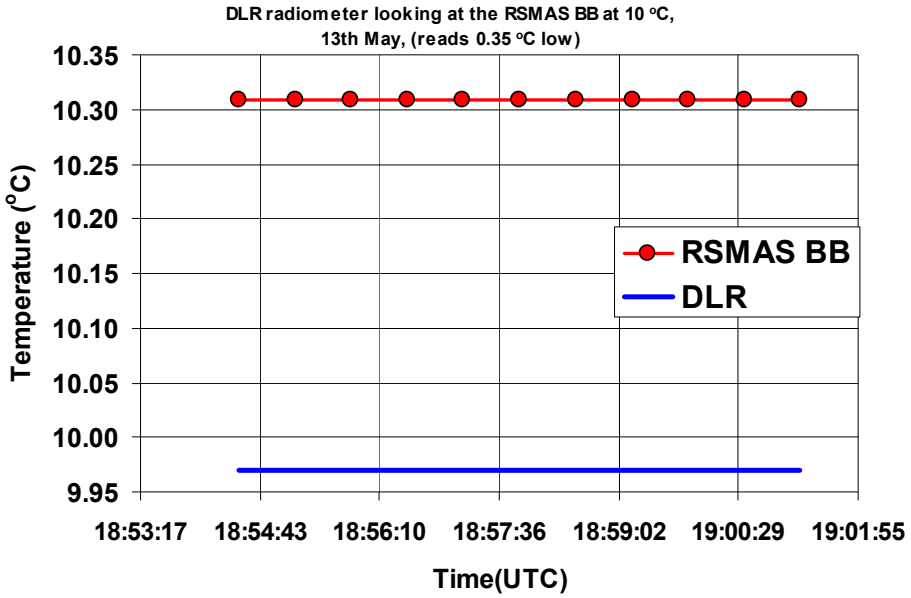

Figure 3.3.1: DLR radiometer viewing the RSMAS blackbody at 10 °C, 1st run.
<Radiometer measurement> – RSMAS blackbody temperature = -0.35 °C
(brackets indicate average over time interval shown).

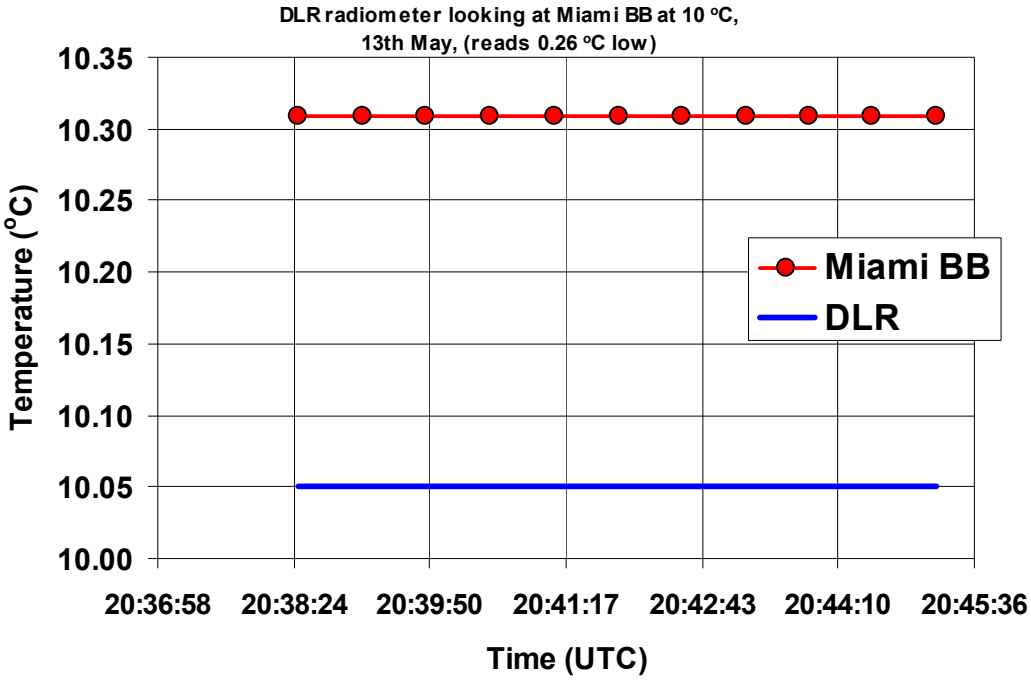

Figure 3.3.2: DLR radiometer viewing the RSMAS blackbody at 10 °C, 2nd run.
<Radiometer measurement> – RSMAS blackbody temperature = -0.26 °C
(brackets indicate average over time interval shown).

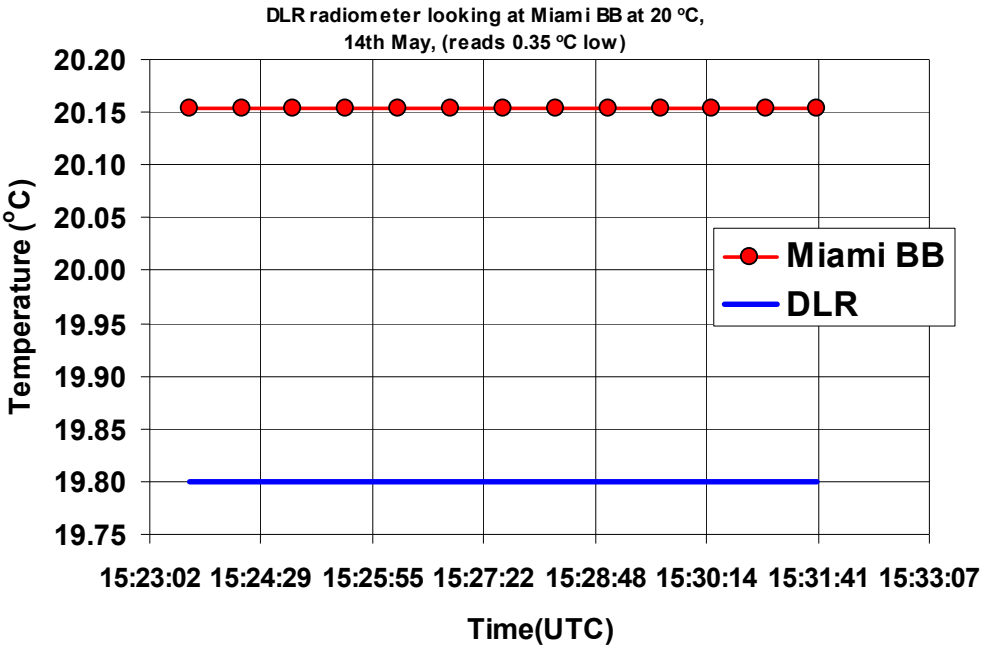

Figure 3.3.3: DLR radiometer viewing the RSMAS blackbody at 20 °C, 1st run.
<Radiometer measurement> – RSMAS blackbody temperature = -0.35 °C
(brackets indicate average over time interval shown).

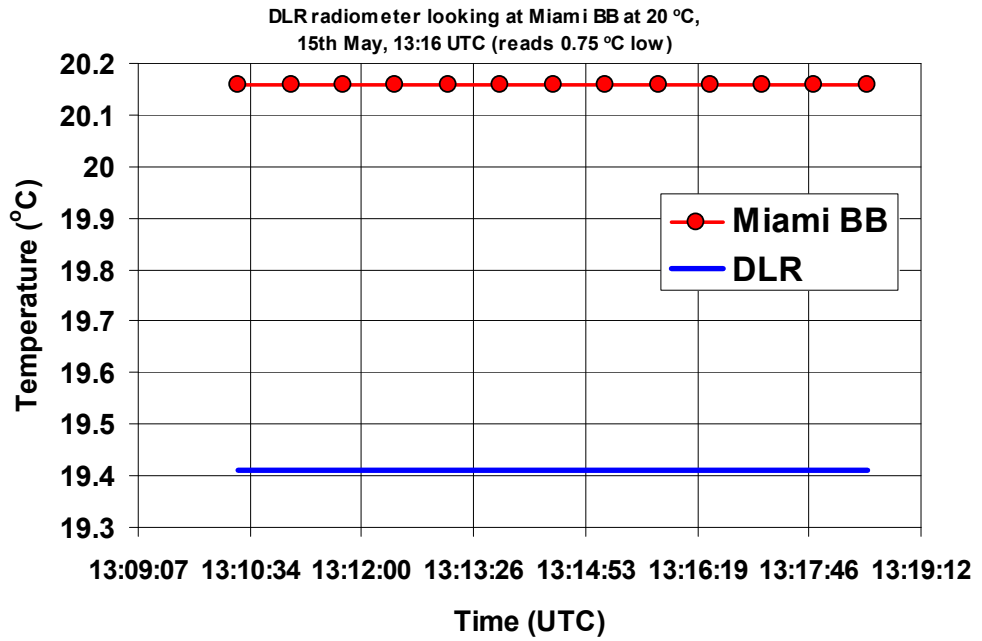

Figure 3.3.4: DLR radiometer viewing the RSMAS blackbody at 20 °C, 2nd run.
<Radiometer measurement> – RSMAS blackbody temperature = -0.75 °C
(brackets indicate average over time interval shown).

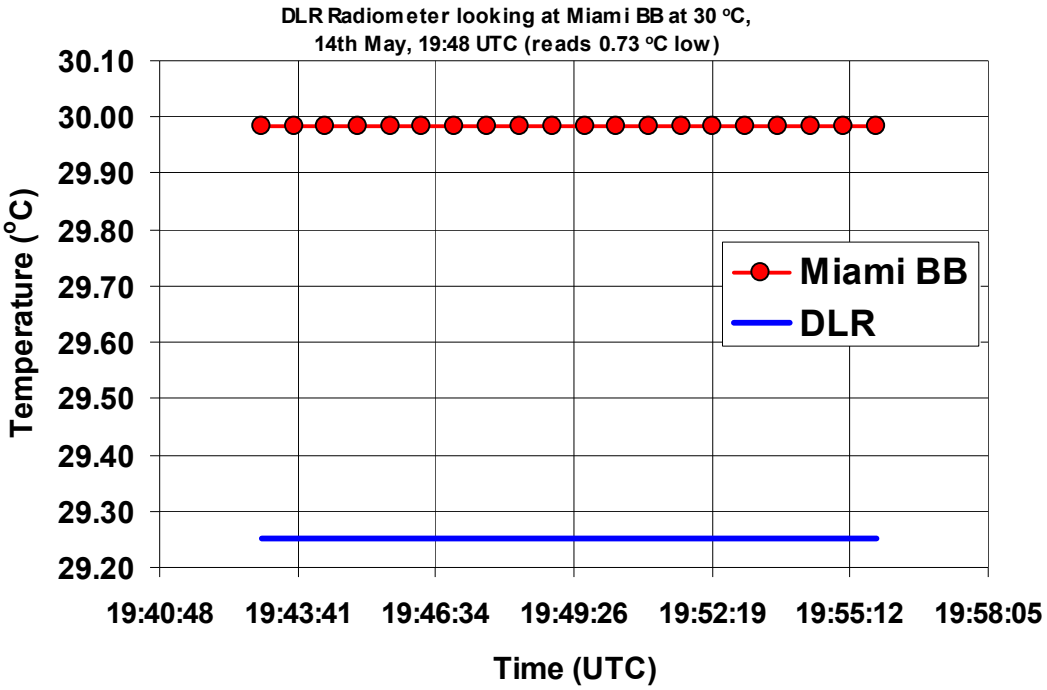

Figure 3.3.5: DLR radiometer viewing the RSMAS blackbody at 30 °C, 1st run.
<Radiometer measurement> – RSMAS blackbody temperature = -0.73 °C
(brackets indicate average over time interval shown).

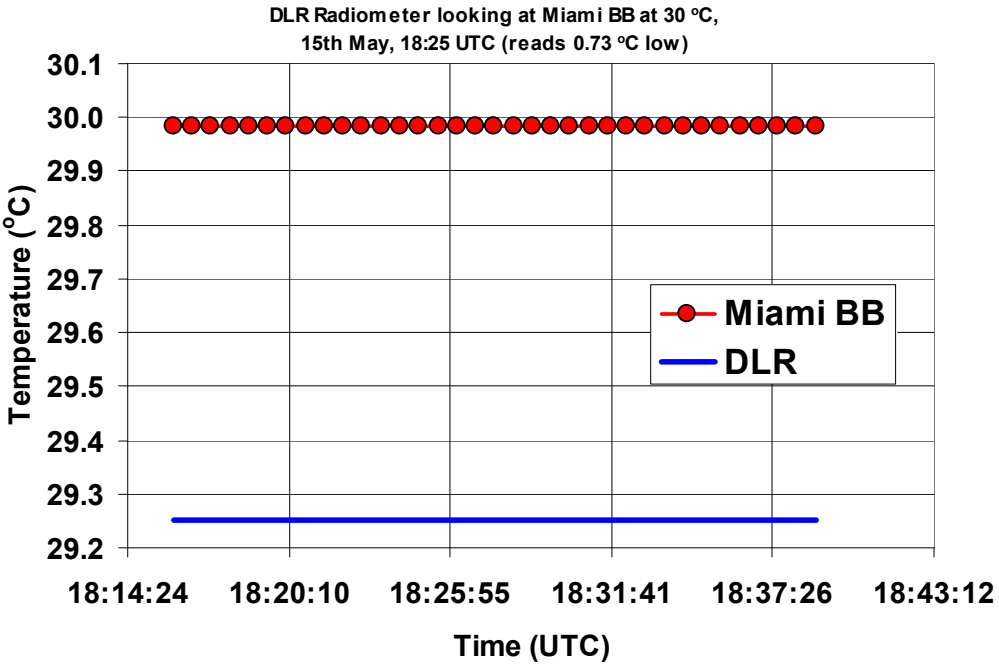

Figure 3.3.6: DLR radiometer viewing the RSMAS blackbody at 30 °C, 2nd run.
<Radiometer measurement> – RSMAS blackbody temperature = -0.73 °C
(brackets indicate average over time interval shown).

3.3.3.2 Comparison of the DLR radiometer to the NIST blackbody

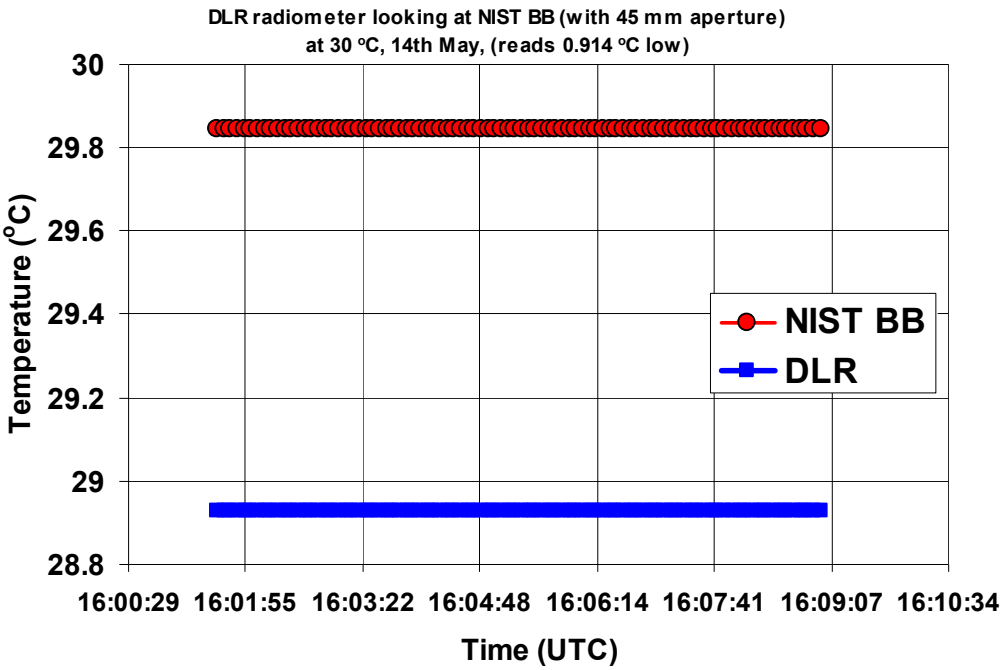

Figure 3.3.7: DLR radiometer output when directed at the NIST BB (with the 45 mm aperture). The output of the DLR radiometer is 0.914 °C lower than the average of the NIST BB temperature values.

3.3.3.3 DLR sea surface temperature measurements.

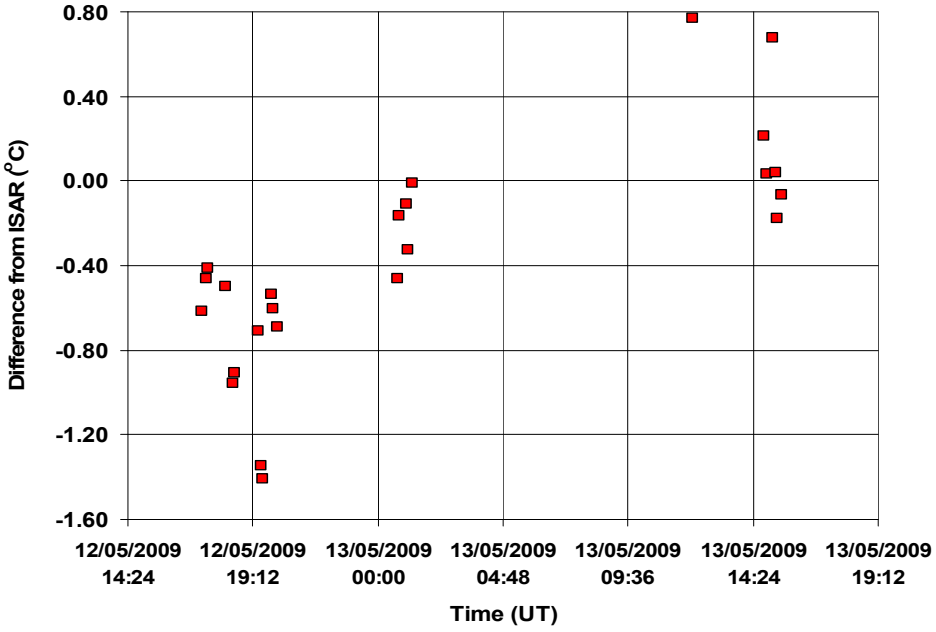

Figure 3.3.8: Difference of the DLR ocean temperature measurements from the corresponding ISAR radiometer SST measurements.

3.4 Grupo de Observacion de la Tierra Y la Atmosfera (GOTA), University of Laguna

3.4.1 Contact information

GOTA contact for the comparison: Dr Manuel Arbelo
Address: GOTA, Avda. Astrofisico FCO. Sanchez, Facultad de Fisica,
38206 La Laguna, Spain
Email: marbelo@ull.es

3.4.2 Radiometer used in the comparison

Outline technical description of instrument: CIMEL Electronique CE312-2. (http://www.cimel.fr/photo/radiometer_us.htm)

Type of detector: thermopile. 6 spectral bands: B1 8-13 μm, B2 11.0-11.7 μm, B3 10.3-11.0 μm, B4 8.9-9.3 μm, B5 8.5-8.9 μm, and B6 8.1-8.5 μm. Broad band: Germanium window and zinc sulphide filters. Narrow bands: interference filters. Field of view: 10º. The instrument has a built-in radiance reference made of a concealable gold-coated mirror which enables comparison between the target radiance and the reference radiation from inside the detector cavity. The temperature of the detector is measured with a PRT, thus allowing compensation for the cavity radiation.

References:

1. Sicard, M., Spyak, P. R., Brogniez, G., Legrand, M., Abuhassan, N. K., Pietras, C., and Buis, J. P. (1999). Thermal infrared field radiometer for vicarious cross-calibration: characterization and comparisons with other field instruments. *Optical Engineering*, 38 (2), 345-356.

2. M. Legrand, C. Pietras, G. Brogniez, M. Haeffelin, N. K. Abuhassan and M. Sicard (2000). A high-accuracy multiwavelength radiometer for in situ measurements in the thermal infrared. Part I: characterization of the instrument, *J. Atmos. Ocean Techn.,* 17, 1203-1214.

3.4.2.1 Establishment or traceability route for primary calibration including date of last realisation and breakdown of uncertainty:

The radiometer has undergone a traceable primary calibration. The spectral characterisation of the instrument can be found in references 1 and 2 above. The following error analysis is based on calibration with our traceable Landcal Blackbody Source P80P (April 6 and 7, 2009).

TYPE A

- Repeatability: typical value of the standard deviation of 10 measurements at fixed black body temperature without re-alignment of radiometer.

	B1	B2	B3	B4	B5	B6	MEAN
K	0.03	0.12	0.10	0.09	0.12	0.11	0.09
%	0.01	0.04	0.03	0.03	0.04	0.04	0.03

- Reproducibility: typical value of difference between two runs of radiometer measurements at the same black body temperature including re-alignment.

	B1	B2	B3	B4	B5	B6	MEAN
K	0.05	0.03	0.02	0.03	0.04	0.02	0.03
%	0.02	0.01	0.01	0.01	0.02	0.01	0.01

Total Type A uncertainty (RSS):

	B1	B2	B3	B4	B5	B6	MEAN
K	0.06	0.12	0.10	0.09	0.13	0.11	0.09
%	0.02	0.04	0.03	0.03	0.04	0.04	0.03

TYPE B

- Linearity of radiometer: within temperature range of 278-303 K.

	B1	B2	B3	B4	B5	B6	MEAN
K	0.07	0.10	0.10	0.07	0.11	0.08	0.09

- Primary calibration: typical value of difference between radiometer brightness temperature and Landcal Blackbody Source P80P temperature.

	B1	B2	B3	B4	B5	B6	MEAN
K	0.9	0.3	0.3	0.3	0.3	0.1	0.4

- Drift since calibration: 0.0 K (as expected since very recent calibration measurements).

Total Type B uncertainty (RSS):

	B1	B2	B3	B4	B5	B6	MEAN
K	0.9	0.3	0.3	0.3	0.3	0.2	0.4

TYPE A + TYPE B UNCERTAINTY (RSS): 0.4 K

Operational methodology during measurement campaign:

Calibration measurements were performed in the laboratory following, as close as possible, the procedures described in the Draft Protocol. The Landcal Blackbody Source P80P was set at four temperatures (278, 283, 293 and 303 K) in two different runs. Enough time was allowed for the black body to reach equilibrium at each temperature. Radiometers were aligned with the black body cavity, and placed at a distance so that the field of view was smaller than the cavity diameter. Standard processing (see references above) was applied to the radiometer readouts to calculate the equivalent brightness temperature. The six bands of the CE312-2 instrument were used.

Radiometer usage (deployment)

Field measurements (hand held and tripod mounted) of land surface temperature and emissivity for validation of thermal infrared products from satellite sensors (Terra/MODIS and ASTER) over test sites in Spain as well as laboratory measurements of soil emissivity.

Uncertainty of Measurement:
The following table provides a summary of the uncertainties evaluated for the radiometer

CIMEL Electronique CE312-2 Radiometer

Parameter	Type A Uncertainty in Value / %	Type B Uncertainty in Value / (appropriate units)	Uncertainty in Brightness temperature K
Repeatability of measurement	0.03[(1)]		0.09[(1)]
Reproducibility of measurement	0.01[(2)]		0.03[(2)]
Linearity of radiometer		0.1 K	0.1 K
Primary calibration		0.4 K[(3)]	0.4 K
Drift since calibration		-	-
RMS total	0.03 % 0.09 K	**0.4 K**	0.4 K

(1) Typical value of the standard deviation of 10 measurements at fixed black body temperature without re-alignment of radiometer.
(2) Typical value of difference between two runs of radiometer measurements at the same black body temperature including re-alignment.
(3) Typical value of difference between radiometer brightness temperature and Landcal Blackbody Source P80P temperature. Mean values for all bands are shown.

3.4.3 Results

The GOTA radiometer took part in the NPL blackbody, RSMAS blackbody and Miami ocean surface temperature comparisons.

3.4.3.1 Comparison of the CE312-2 radiometer to the NPL blackbody

Figures 3.4.1 to 3.4.6 show the temperature values measured by the different channels of the GOTA radiometer when monitoring the NPL blackbody cavity at different temperatures. Figures 3.4.7 to 3.2.11 show the temperature values measured by the different channels of the GOTA radiometer when monitoring the RSMAS blackbody cavity. Figure 3.2.12 shows the temperature values measured by the different channels of the GOTA radiometer when monitoring the NIST blackbody cavity temperature. The Tables below each Figure list the difference between the average temperature displayed by each radiometer channel and the average radiance temperature of the NPL variable temperature blackbody.

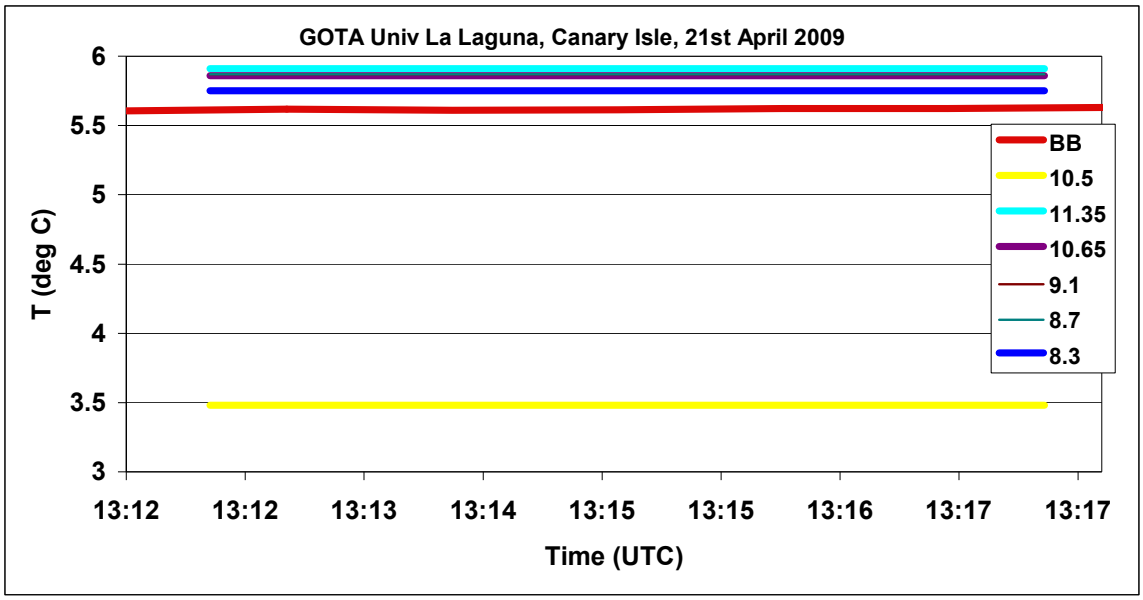

Figure 3.4.1: GOTA radiometer viewing the NPL blackbody at 5 °C.

The table below indicates the deviation of the different radiometer channels δT from the average blackbody temperature, over the measurement interval.

Channel (μm)	δT (deg C)
10.5	-2.137
11.35	0.293
10.65	0.243
9.1	0.253
8.7	0.253
8.3	0.133

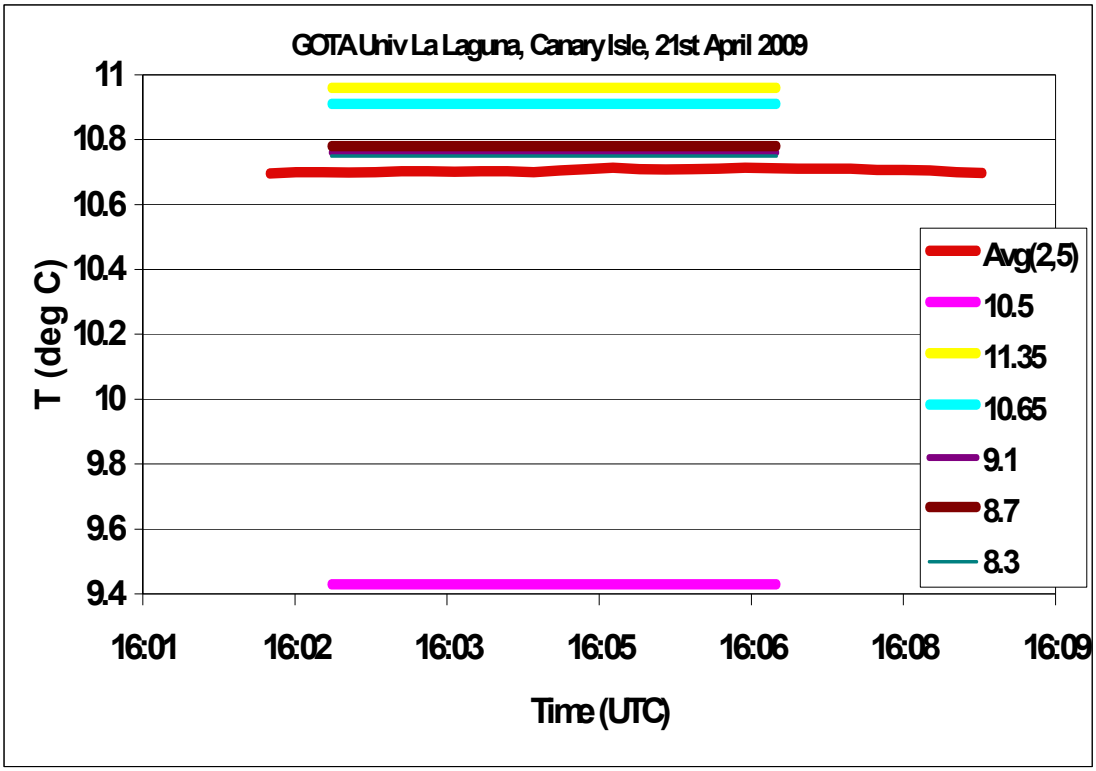

Figure 3.4.2: GOTA radiometer viewing the NPL blackbody at 10 ^{o}C, 1st run.
The table below indicates the deviation of the different radiometer channels δT from the average blackbody temperature, over the measurement interval.

Channel (μm)	δT (deg C)
10.5	-1.276
11.35	0.254
10.65	0.204
9.1	0.054
8.7	0.074
8.3	0.044

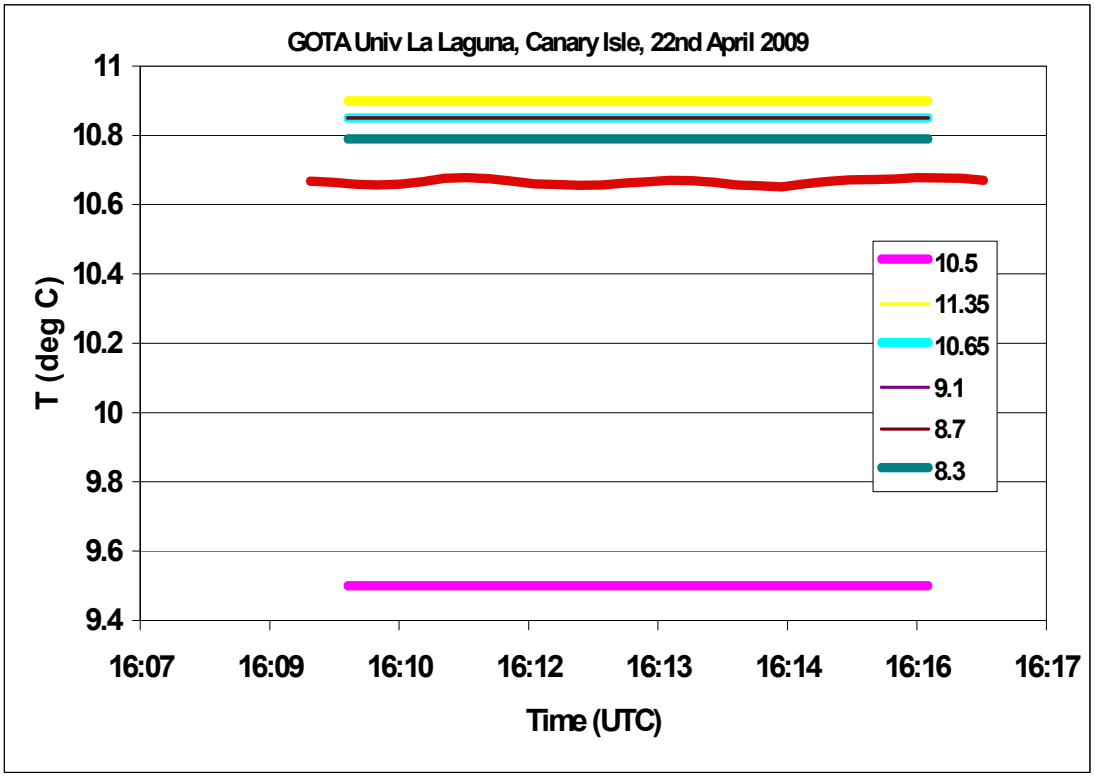

Figure 3.4.3: GOTA radiometer viewing the NPL blackbody at 10 °C, 2nd run.
The table below indicates the deviation of the different radiometer channels δT from the average blackbody temperature, over the measurement interval.

Channel (μm)	δT (deg C)
10.5	-1.165
11.35	0.235
10.65	0.185
9.1	0.185
8.7	0.185
8.3	0.125

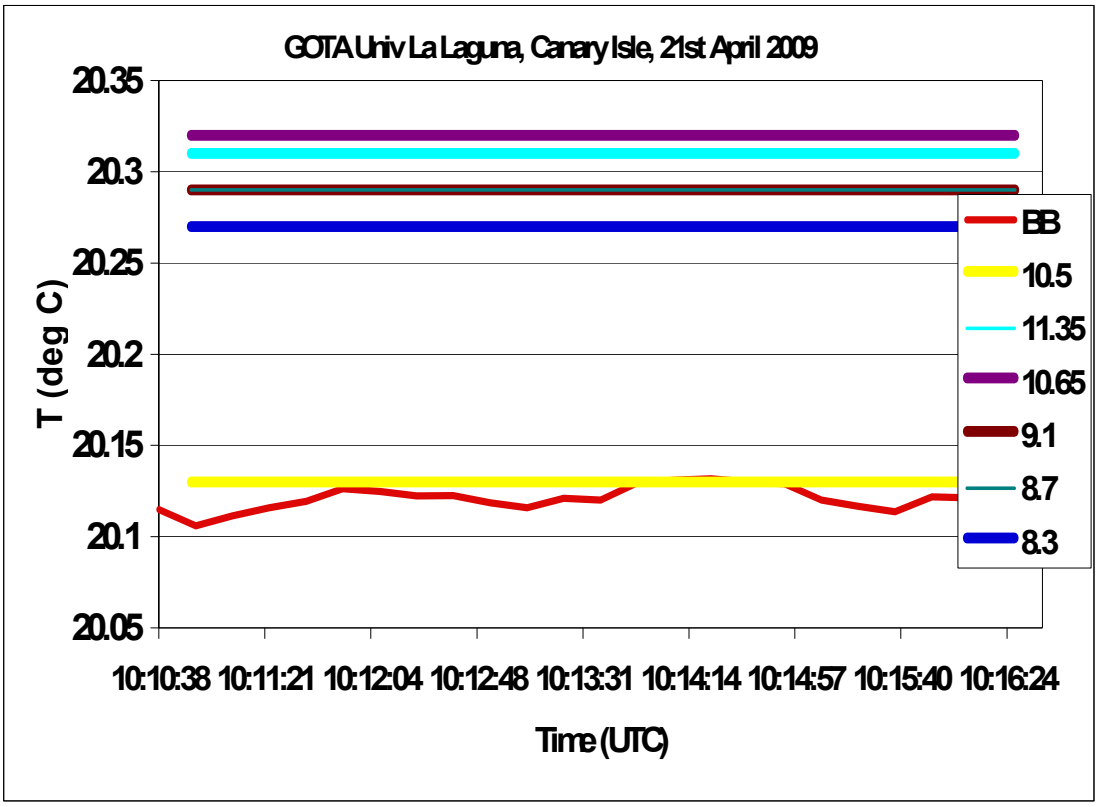

Figure 3.4.4: GOTA radiometer viewing the NPL blackbody at 20 °C, 1st run.
The table below indicates the deviation of the different radiometer channels δT from the average blackbody temperature, over the measurement interval.

Channel (μm)	δT (deg C)
10.5	0.009
11.35	0.189
10.65	0.199
9.1	0.169
8.7	0.169
8.3	0.149

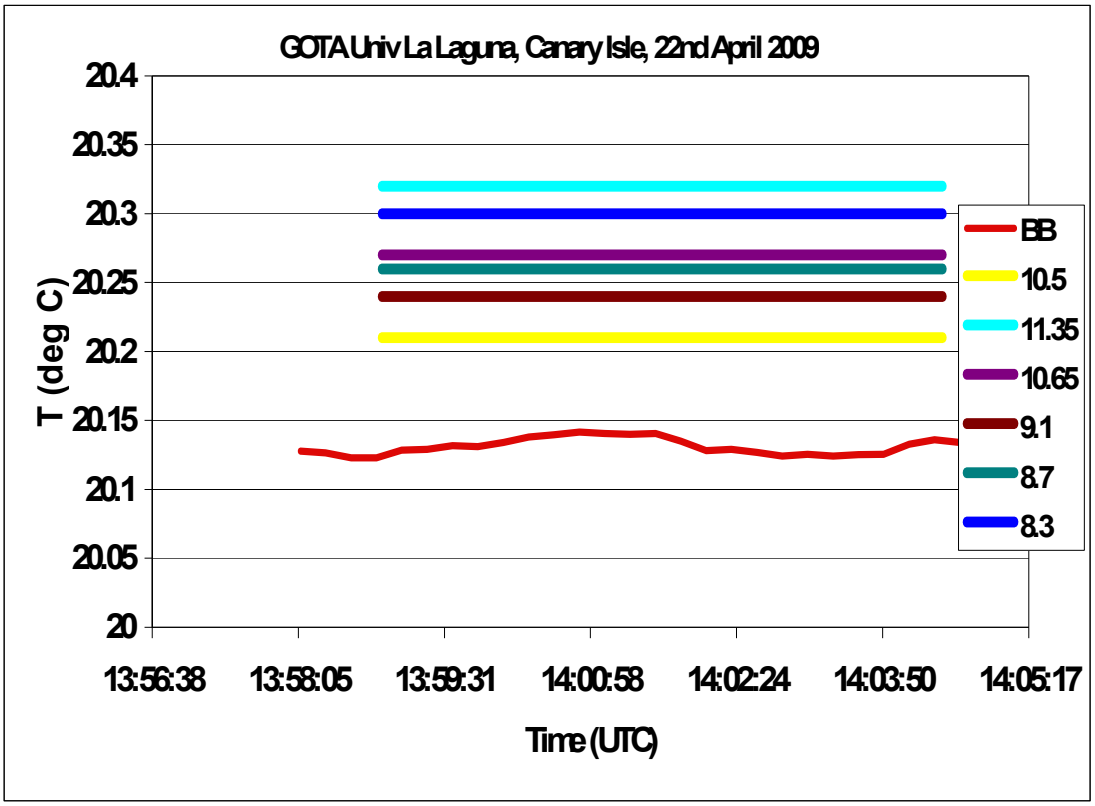

Figure 3.4.5: GOTA radiometer viewing the NPL blackbody at 20 °C, 2nd run.
The table below indicates the deviation of the different radiometer channels δT from the average blackbody temperature, over the measurement interval.

Channel (μm)	δT (deg C)
10.5	0.079
11.35	0.189
10.65	0.139
9.1	0.109
8.7	0.129
8.3	0.169

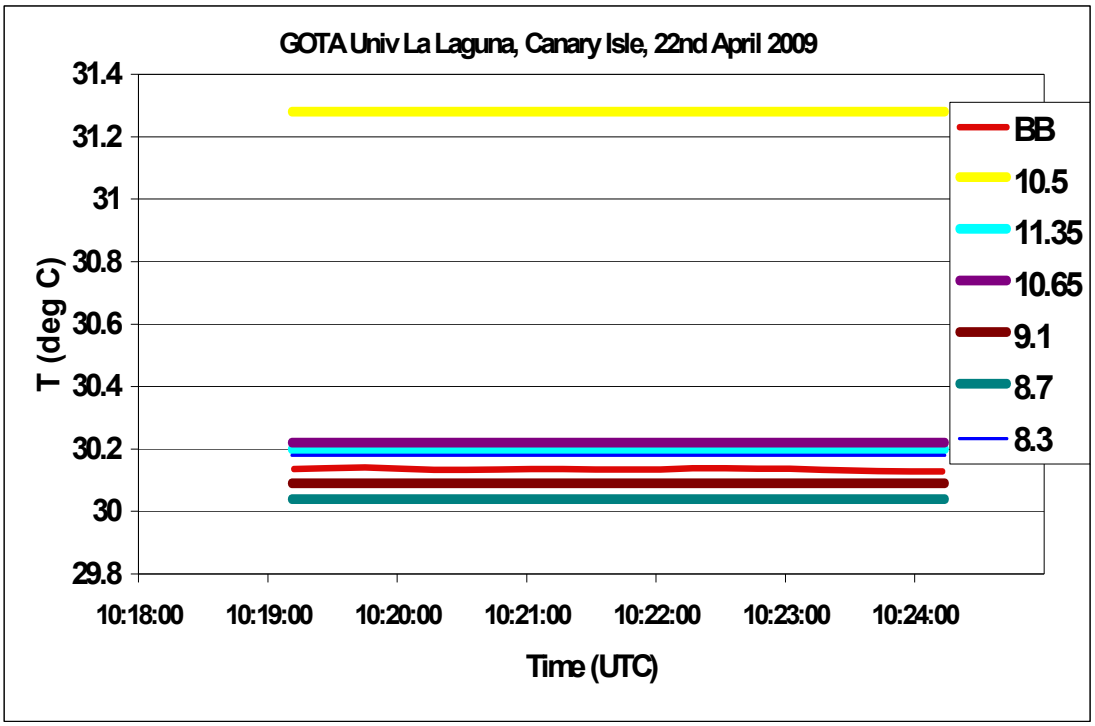

Figure 3.4.6: GOTA radiometer viewing the NPL blackbody at 30 °C. The table below indicates the deviation of the different radiometer channels δT from the average blackbody temperature, over the measurement interval.

Channel (μm)	δT (deg C)
10.5	1.147
11.35	0.067
10.65	0.087
9.1	-0.043
8.7	-0.093
8.3	0.047

3.4.3.2 Comparison to the RSMAS blackbody

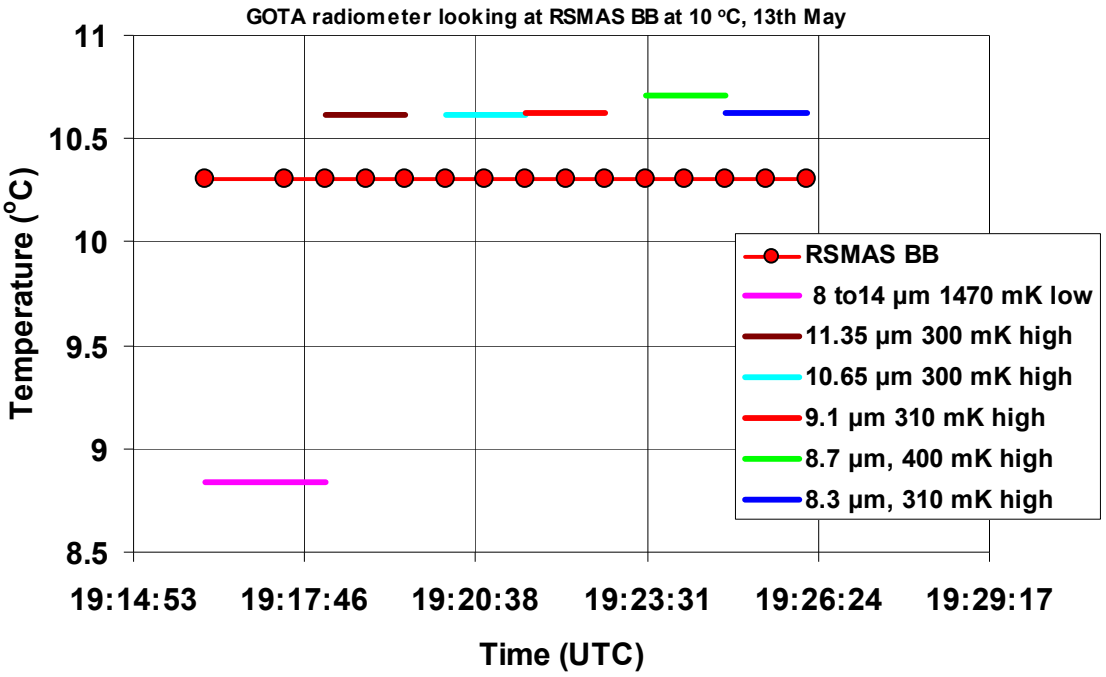

Figure 3.4.7: GOTA radiometer viewing the RSMAS blackbody at 10 °C.
The figure legend indicates the deviation of the different radiometer channels from the average blackbody temperature, over the measurement interval.

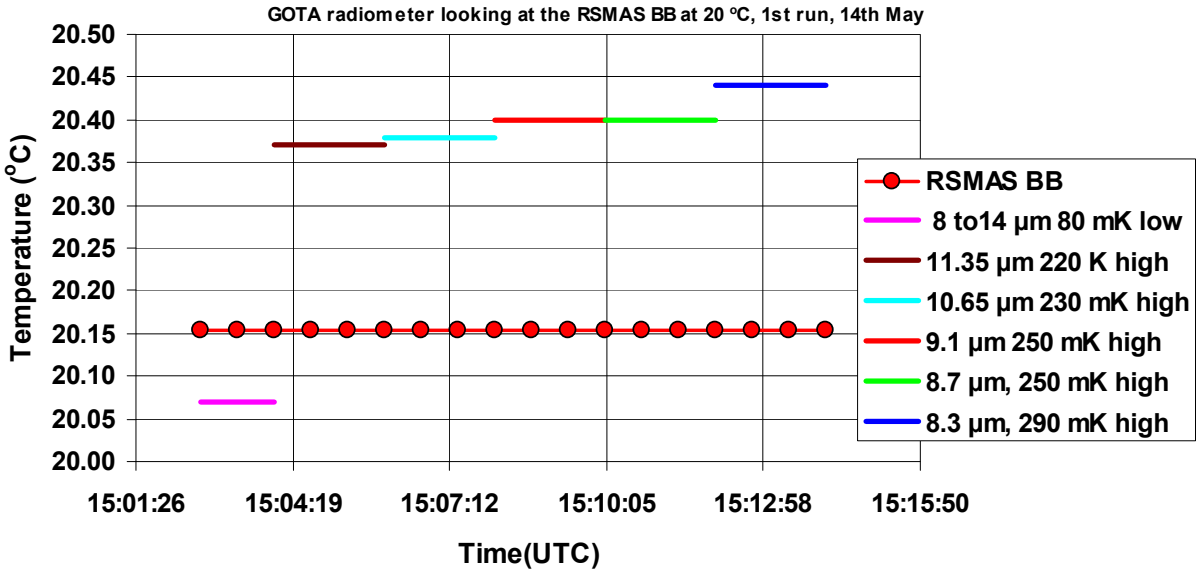

Figure 3.4.8: GOTA radiometer viewing the RSMAS blackbody at 20 °C, 1st run.
The figure legend indicates the deviation of the different radiometer channels from the average blackbody temperature, over the measurement interval.

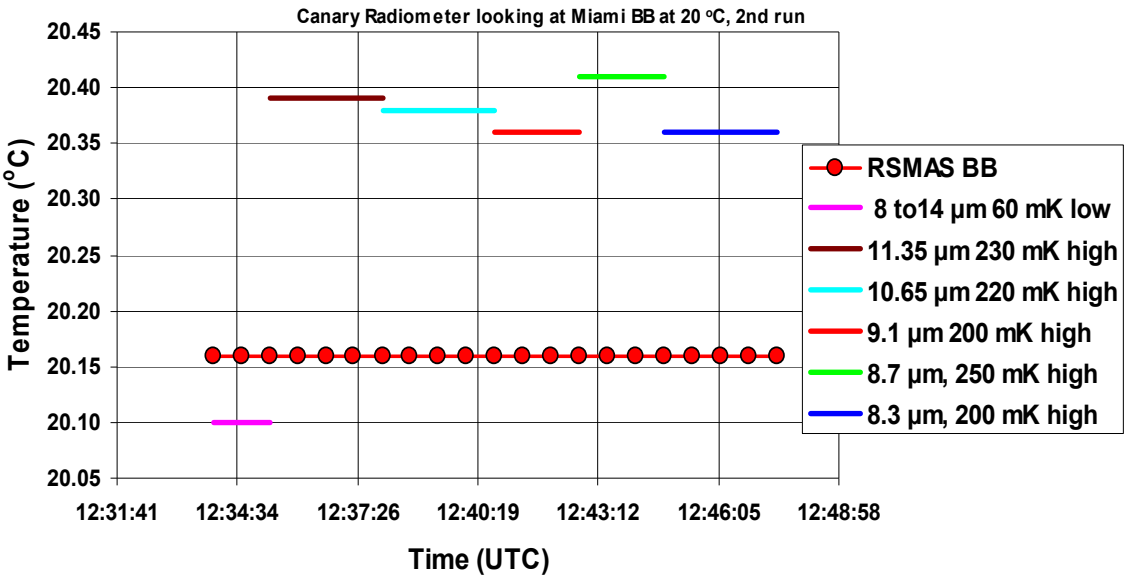

Figure 3.4.9: GOTA radiometer viewing the RSMAS blackbody at 20 °C, 2nd run.
The figure legend indicates the deviation of the different radiometer channels from the average blackbody temperature, over the measurement interval.

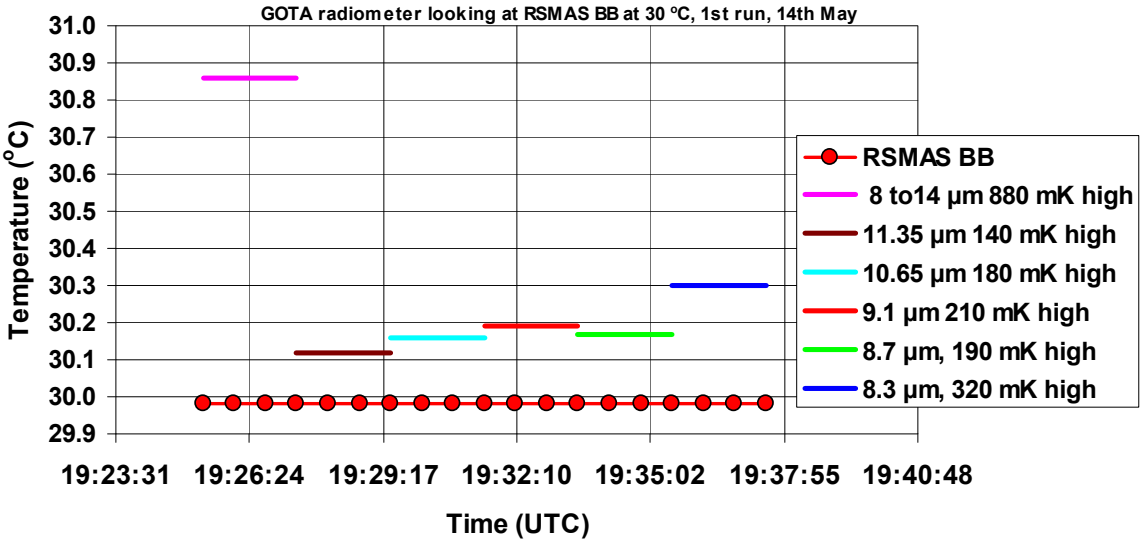

Figure 3.4.10: GOTA radiometer viewing the RSMAS blackbody at 30 °C, 1st run.
The figure legend indicates the deviation of the different radiometer channels from the average blackbody temperature, over the measurement interval.

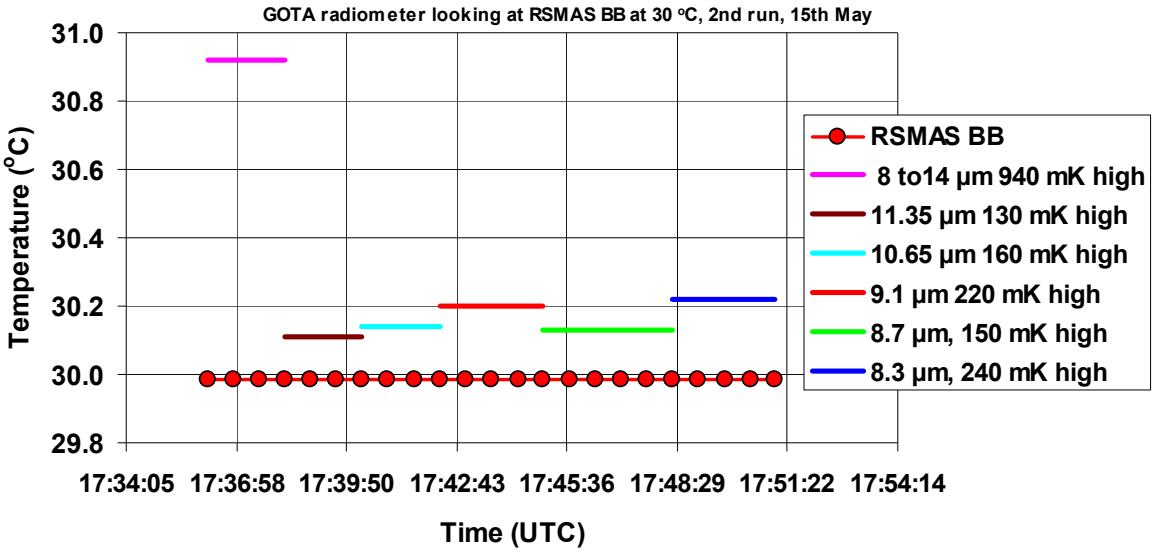

Figure 3.4.11: GOTA radiometer viewing the RSMAS blackbody at 30 °C, 2nd run.
The figure legend indicates the deviation of the different radiometer channels from the average blackbody temperature, over the measurement interval.

3.4.3.3 Comparison to the NIST reference blackbody

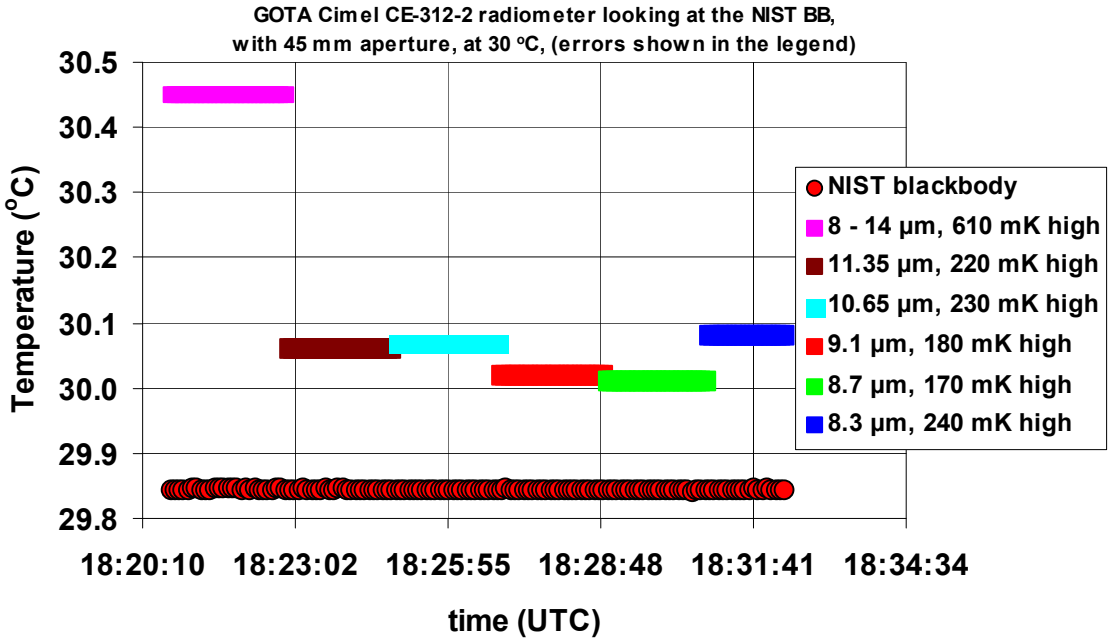

Figure 3.4.12: GOTA radiometer viewing the NIST blackbody at 30 °C, (blackbody with 45 mm diameter aperture). The figure legend indicates the deviation of the different radiometer channels from the average blackbody temperature, over the measurement interval.

3.4.3.4 Measurements of sea surface temperature.

Figure 3.4.13 shows the difference of the ocean surface temperature measurements completed by the different channels of the GOTA radiometer from the corresponding measurements completed by the ISAR radiometer.

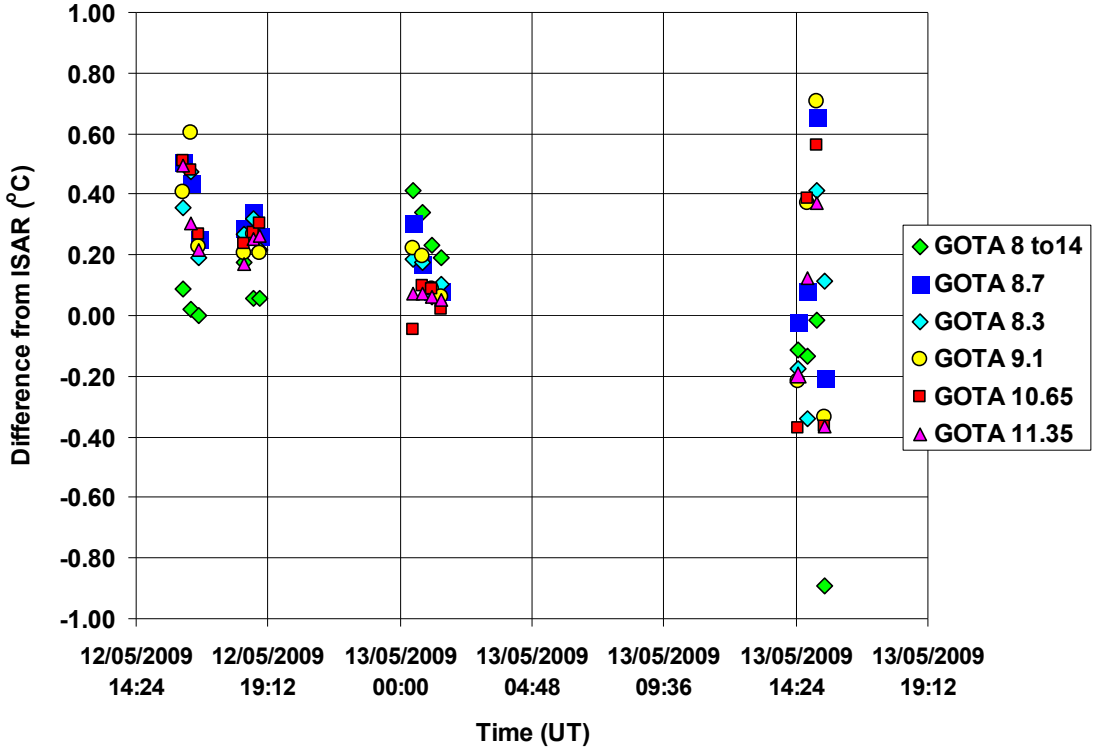

Figure 3.4.13: Difference of the ocean surface temperature measurements completed by the different channels of the GOTA radiometer from the corresponding measurements completed by the ISAR radiometer.

3.5 Imaging Processing Laboratory (IPL), University of Valencia

3.5.1 Contact information:

IPL contact for the comparison: Dr José Antonio Sobrino
Address: IPL, University of Valencia, P. O. Box 22085, 46071 Valencia, Spain.
Email: Sobrino@uv.es

3.5.2 Radiometers used for the comparison: CIMEL CE 312-2 radiometer

Radiometer Technical Characteristics

a) Radiometer type

i) CIMEL CE 312-2 Thermal radiometer
(http://www.cimel.fr/photo/radiometer_us.htm)

Bands	Bandwith	Effective Wavelength (µm)	Range (°C)	Accuracy (°C)	Field of View (°)
1	8.0 – 13.0	10.54	- 80 to 60	0.1	10
2	10.95 – 11.65	11.27			
3	10.25 – 10.95	11.66			
4	8.93 – 9.28	9.07			
5	8.48 – 8.64	8.64			
6	8.13 – 8.48	8.28			

b) Shape and Size

Shape: Cylinder
Height: 24 cm
Base: 8 cm
Thermal radiometer has a fixed metallic ring in the middle of the radiometer to be mounted in any tripod.
Minimum height of working depends of sample characteristics.

Methodology used in the measurements with the CIMEL radiometer

The CIMEL radiometer was used in mode "6flt1m", which means that one single measurement is made for the six filters (this single measurement for the six filters lasts around 30 seconds). This kind of measurement was repeated N times, with N=5 when the blackbody was set at 5ºC and N=7,8 when the blackbody was set at 20 and 30ºC.

Uncertainties

The following table summarises the uncertainties estimated for the IPL radiometer.

WAVELENGTH/µM	TYPE A	TYPE B
10.54	**0.05 K**	**0.4 K**
11.29	**0.12 K**	**0.3 K**
10.57	**0.10K**	**0.3 K**
9.15	**0.09 K**	**0.3 K**
8.69	**0.13 K**	**0.3 K**
8.44	**0.11 K**	**0.2 K**

3.5.3 Results

The IPL radiometer took part in the NPL blackbody comparison only. The first set of data provided by IPL corresponding to the 5 ^{o}C and 10 ^{o}C blackbody temperatures (referred to as the "uncorrected" data) included a mistake in the processing of the data. These data were subsequently corrected by IPL to rectify this error and the corrected data are included in this section as the "corrected" data.

Figure 3.5.1 shows the uncorrected output of the IPL radiometer when it was viewing the NPL blackbody at 5 ^{o}C. The table below this figure lists the deviation of the uncorrected output of the different radiometer channels δT from the average blackbody temperature, over the measurement interval. Figure 3.5.2 shows the corrected output of the IPL radiometer when it was viewing the NPL blackbody at 5 ^{o}C. The table below this figure lists the deviation of the corrected output of the different radiometer channels δT from the average blackbody temperature, over the measurement interval.

Figure 3.5.3 shows the uncorrected output of the IPL radiometer when it was viewing the NPL blackbody at 10 ^{o}C (1st measurement). The table below this figure lists the deviation of the uncorrected output of the different radiometer channels δT from the average blackbody temperature, over the measurement interval. Figure 3.5.4 shows the corrected output of the IPL radiometer when it was viewing the NPL blackbody at 10 ^{o}C (1st measurement). The table below this figure lists the deviation of the corrected output of the different radiometer channels δT from the average blackbody temperature, over the measurement interval.

Figure 3.5.5 shows the uncorrected output of the IPL radiometer when it was viewing the NPL blackbody at 10 ^{o}C (2nd measurement). The table below this figure lists the deviation of the uncorrected output of the different radiometer channels δT from the average blackbody temperature, over the measurement interval. Figure 3.5.6 shows the corrected output of the IPL radiometer when it was viewing the NPL blackbody at 10 ^{o}C (2nd measurement). The table below this figure lists the deviation of the corrected output of the different radiometer channels δT from the average blackbody temperature, over the measurement interval.

Figure 3.5.7 shows the output of the IPL radiometer when it was viewing the NPL blackbody at 20 ^{o}C (1st measurement). The table below this figure lists the deviation of the output of the different radiometer channels δT from the average blackbody temperature, over the measurement interval. Figure 3.5.8 shows the output of the IPL radiometer when it was viewing the NPL blackbody at 20 ^{o}C (2nd measurement). The table below this figure lists the deviation of the output of the different radiometer channels δT from the average blackbody temperature, over the measurement interval.

Figure 3.5.9 shows the output of the IPL radiometer when it was viewing the NPL blackbody at 30 ^{o}C (1st measurement). The table below this figure lists the deviation of the output of the different radiometer channels δT from the average blackbody temperature, over the measurement interval. Figure 3.5.10 shows the output of the IPL radiometer when it was viewing the NPL blackbody at 30 ^{o}C (2nd measurement). The table below this figure lists the deviation of the output of the different radiometer channels δT from the average blackbody temperature, over the measurement interval

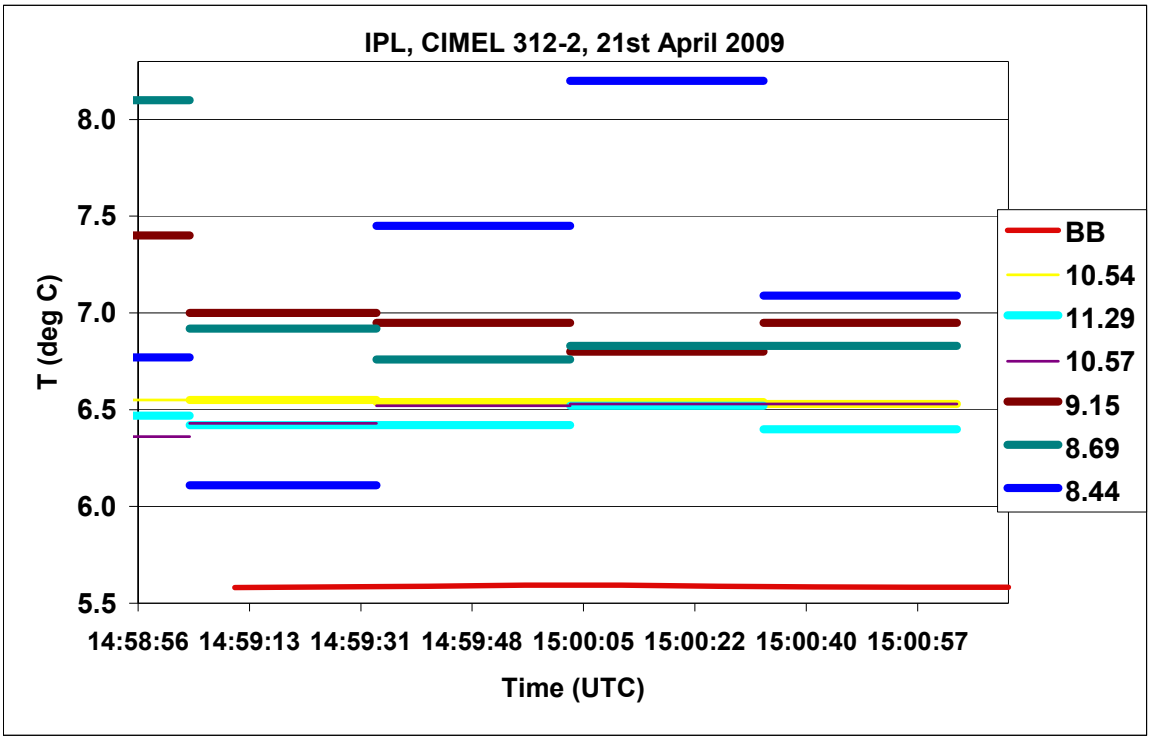

Figure 3.5.1: Plot of the uncorrected output of the IPL radiometer when it was viewing the NPL blackbody at 5 °C. The table below this figure lists the deviation of the uncorrected output of the different radiometer channels δT from the average blackbody temperature, over the measurement interval.

Channel (μm)	δT (deg C)
10.54	0.956
11.29	0.860
10.57	0.888
9.15	1.434
8.69	1.502
8.44	1.538

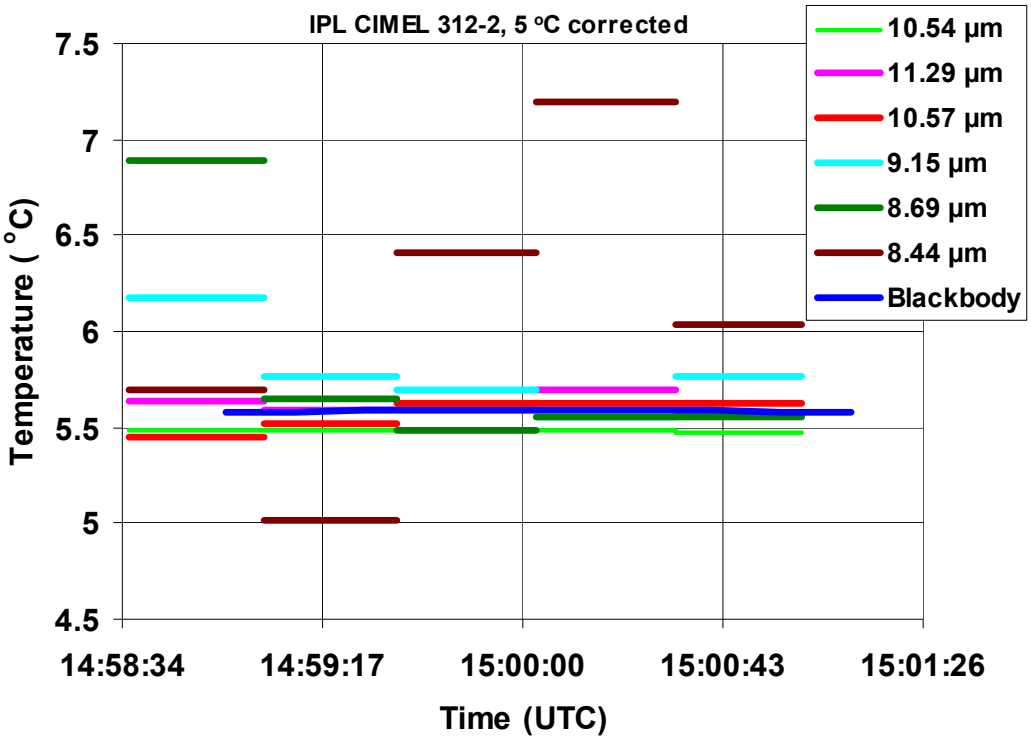

Figure 3.5.2: Plot of the corrected output of the IPL radiometer when it was viewing the NPL blackbody at 5 °C. The table below this figure lists the deviation of the corrected output of the different radiometer channels δT from the average blackbody temperature, over the measurement interval.

Channel (µm)	δT (deg C)
10.54	-0.104
11.29	0.03
10.57	-0.016
9.15	0.206
8.69	0.238
8.44	0.486

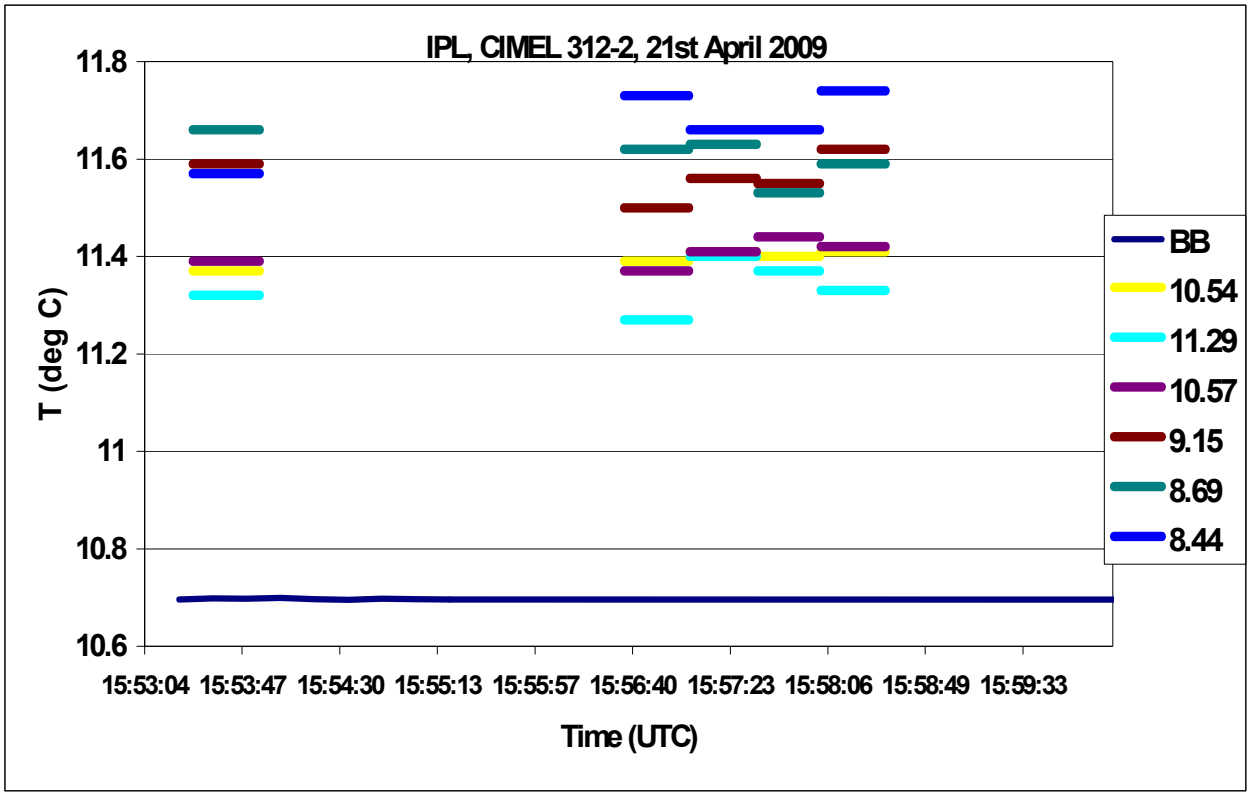

Figure 3.5.3: Plot of the uncorrected output of the IPL radiometer when it was viewing the NPL blackbody at 10 ^{o}C (1st measurement). The table below this figure lists the deviation of the uncorrected output of the different radiometer channels δT from the average blackbody temperature, over the measurement interval.

Channel (μm)	δT (deg C)
10.54	0.691
11.29	0.644
10.57	0.716
9.15	0.881
8.69	0.896
8.44	0.983

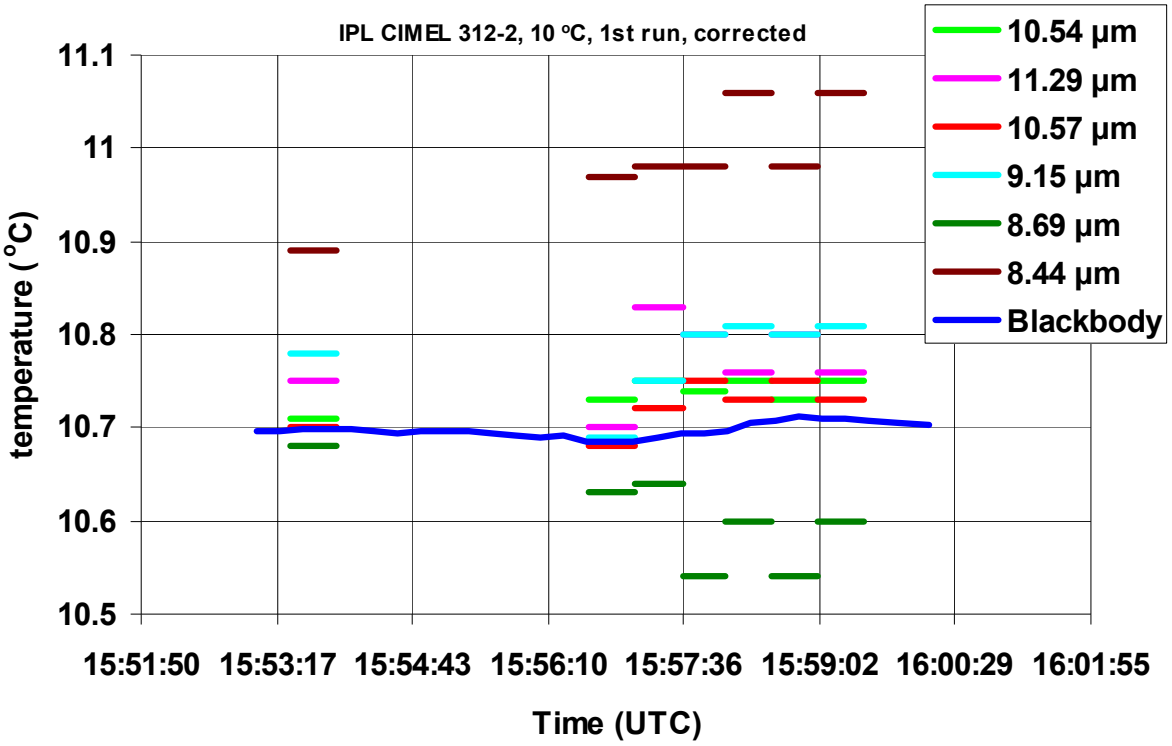

Figure 3.5.4: Plot of the corrected output of the IPL radiometer when it was viewing the NPL blackbody at 10 °C (1st measurement). The table below this figure lists the deviation of the corrected output of the different radiometer channels δT from the average blackbody temperature, over the measurement interval.

Channel (µm)	δT (deg C)
10.54	0.04
11.29	0.074
10.57	0.026
9.15	0.08
8.69	-0.093
8.44	0.291

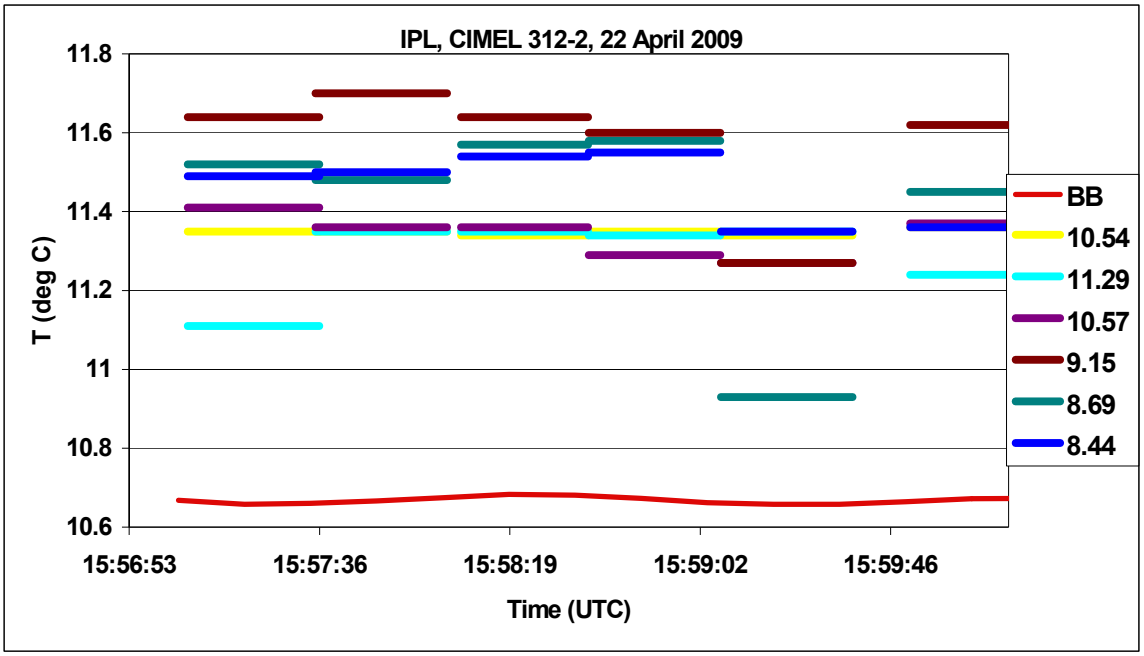

Figure 3.5.5: Plot of the uncorrected output of the IPL radiometer when it was viewing the NPL blackbody at 10 °C (2nd measurement). The table below this figure lists the deviation of the uncorrected output of the different radiometer channels δT from the average blackbody temperature, over the measurement interval.

Channel (μm)	δT (deg C)
10.54	0.683
11.29	0.633
10.57	0.655
9.15	0.934
8.69	0.773
8.44	0.809

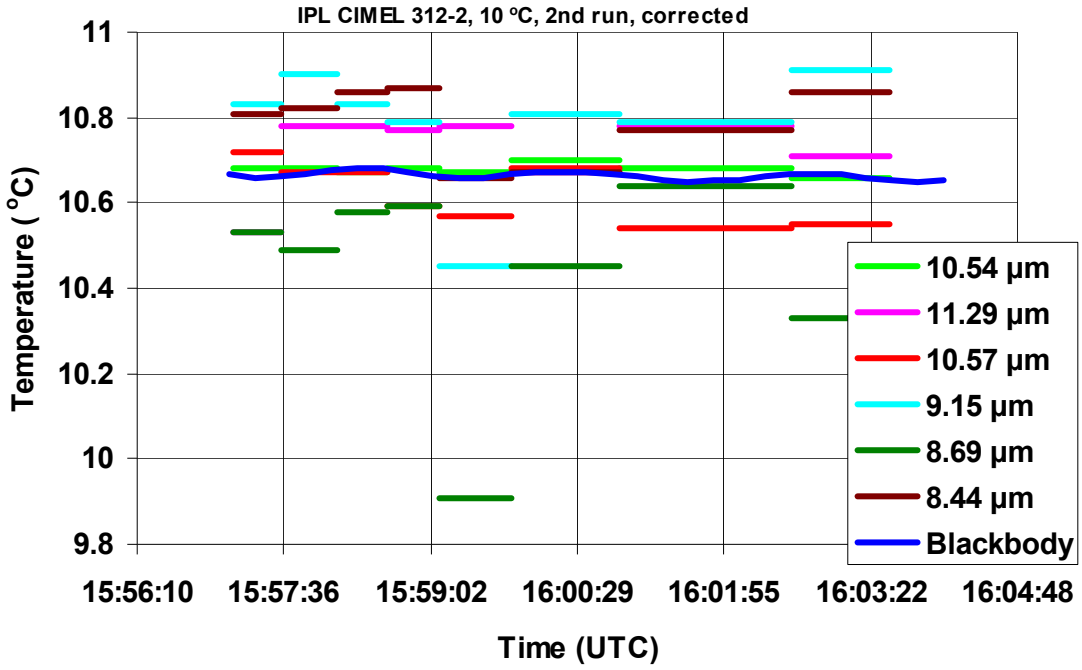

Figure 3.5.6: Plot of the corrected output of the IPL radiometer when it was viewing the NPL blackbody at 10 °C (2nd measurement). The table below this figure lists the deviation of the corrected output of the different radiometer channels δT from the average blackbody temperature, over the measurement interval.

Channel (µm)	δT (deg C)
10.54	0.014
11.29	0.062
10.57	-0.04
9.15	0.125
8.69	-0.223
8.44	0.127

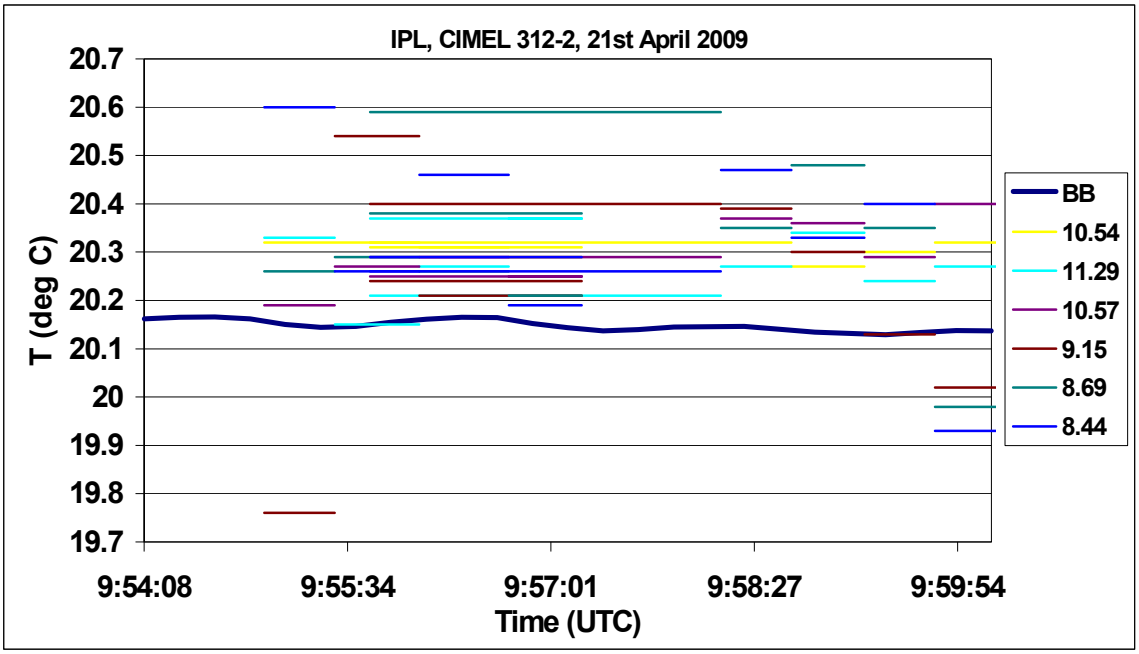

Figure 3.5.7: Plot of the output of the IPL radiometer when it was viewing the NPL blackbody at 20 ^{o}C (1st measurement). The table below this figure lists the deviation of the output of the different radiometer channels δT from the average blackbody temperature, over the measurement interval.

Channel (μm)	δT (deg C)
10.54	0.162
11.29	0.136
10.57	0.150
9.15	0.074
8.69	0.169
8.44	0.173

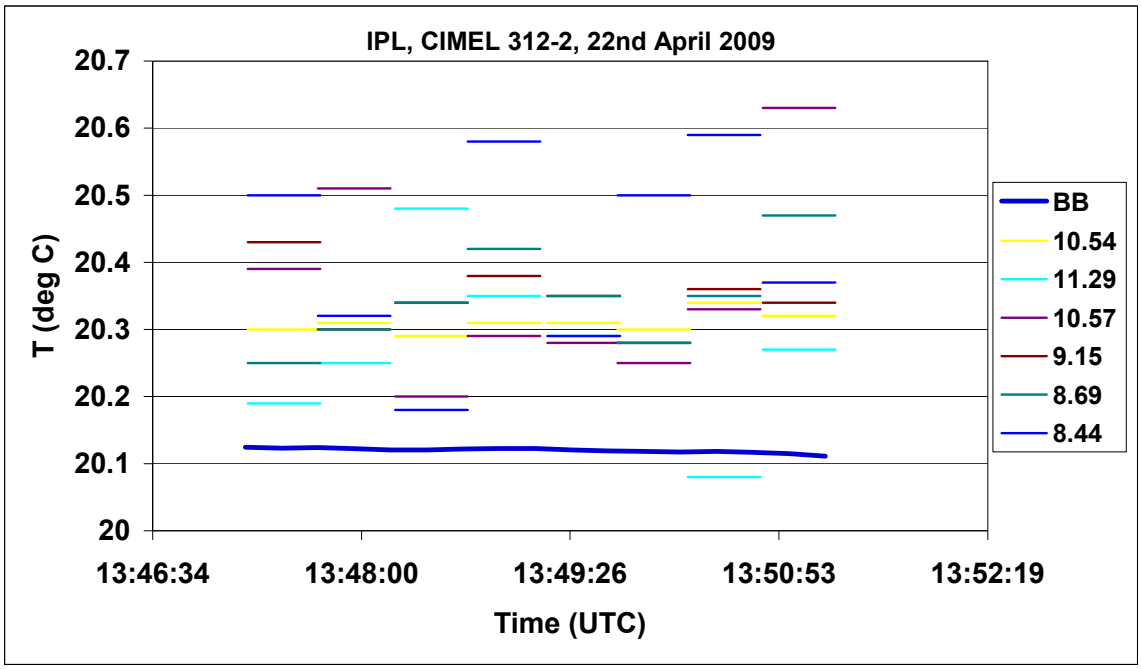

Figure 3.5.8: Plot of the output of the IPL radiometer when it was viewing the NPL blackbody at 20 ^{o}C (2nd measurement). The table below this figure lists the deviation of the output of the different radiometer channels δT from the average blackbody temperature, over the measurement interval.

Channel (μm)	δT (deg C)
10.54	0.190
11.29	0.154
10.57	0.240
9.15	0.228
8.69	0.225
8.44	0.296

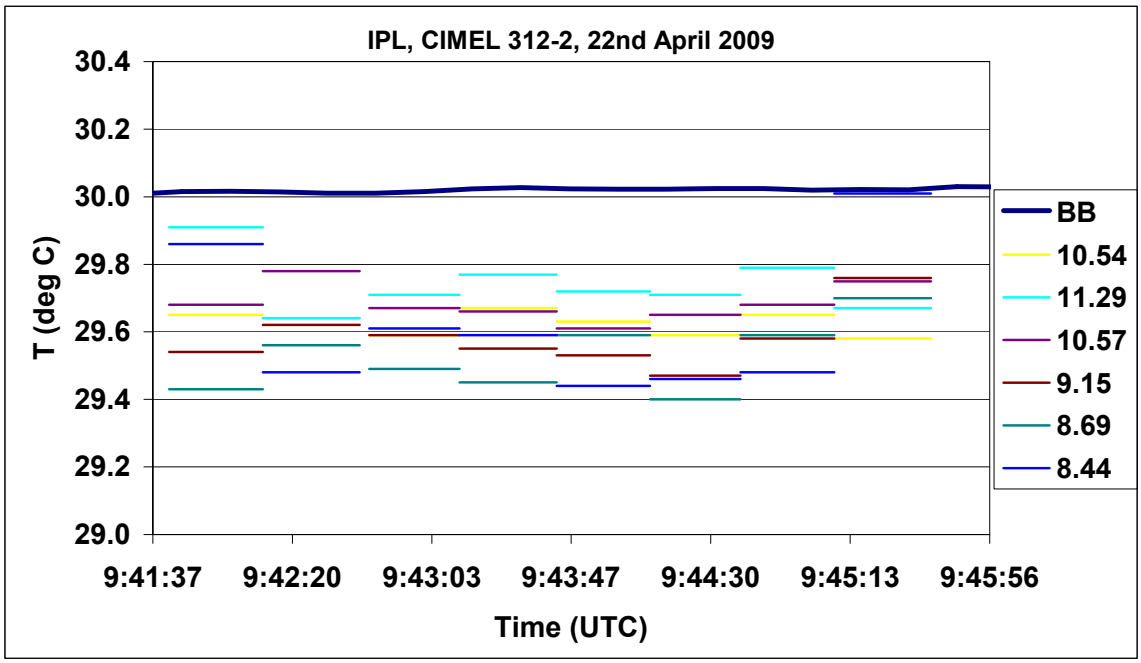

Figure 3.5.9: Plot of the output of the IPL radiometer when it was viewing the NPL blackbody at 30 ^{o}C (1st measurement). The table below this figure lists the deviation of the output of the different radiometer channels δT from the average blackbody temperature, over the measurement interval.

Channel (μm)	δT (deg C)
10.54	-0.393
11.29	-0.278
10.57	-0.333
9.15	-0.438
8.69	-0.492
8.44	-0.402

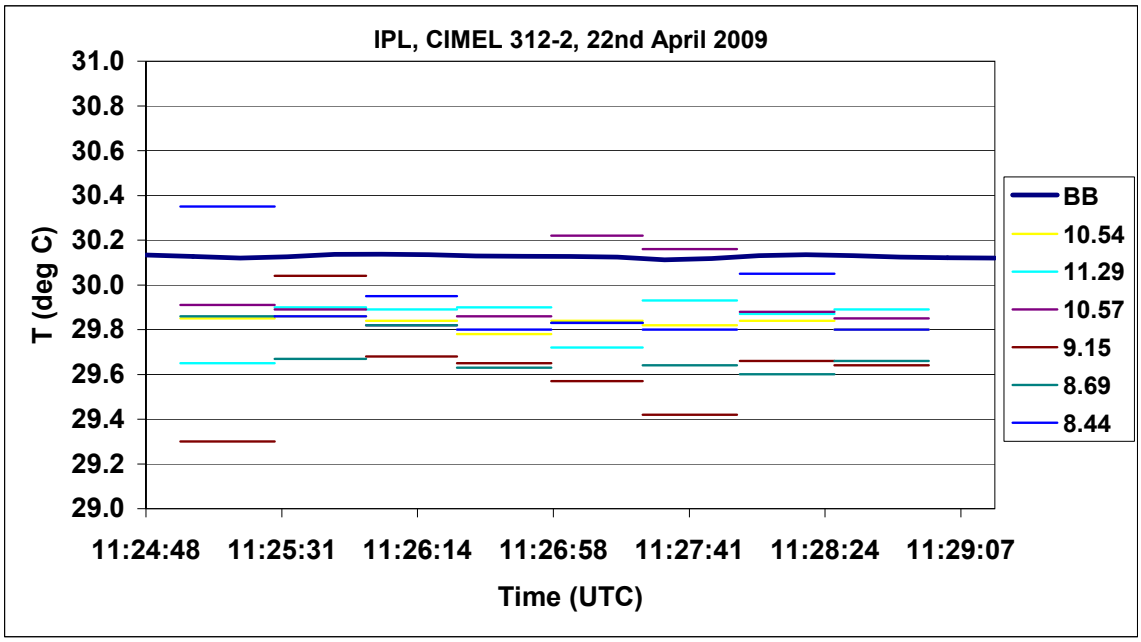

Figure 3.5.10: Plot of the output of the IPL radiometer when it was viewing the NPL blackbody at 30 ^{o}C (2nd measurement). The table below this figure lists the deviation of the output of the different radiometer channels δT from the average blackbody temperature, over the measurement interval.

Channel (μm)	δT (deg C)
10.54	-0.298
11.29	-0.283
10.57	-0.178
9.15	-0.507
8.69	-0.413
8.44	-0.197

3.6 Institute of Meteorology and Climate Research (IMK), Karlsruhe Institute of Technology (KIT)

3.6.1 Contact information

IMK contact for the comparison: Dr Frank-M. Göttsche
Address: Forschungszentrum Karlsruhe, Postfach 3640, 76021 Karlsruhe, Germany
Email: frank.goettsche@imk.fzk.de

3.6.2 Radiometer used in the comparison

Make and type of radiometer: Heitronics KT15.85 IIP, detector type A
(http://www.heitronics.de/fileadmin/content/Prospekte/KT15IIP_e_V510.pdf)

Outline technical description of instrument: Pyroelectric sensor (silicon) using chopped radiation method; internally referenced to PT-100.

FOV: 8.536°, spectral band: 9.6-11.5 micron, Temperature range: 248.15K - 473.15K

References:

1. Infrarot Strahlungspyrometer KT15 II, Bedienungsanleitung (User Manual), Doc 95582943, Heitronics Infrarot Messtechnik GmbH
2. www.heitronics.com

Establishment or traceability route for primary calibration including date of last realisation and breakdown of uncertainty:

Radiometers have undergone primary calibration by manufacturer. Re-calibration is performed once per year using a water bath BB (estimated accuracy: 0.2K).

Operational methodology during measurement campaign:

Alignment with hand-held inclinometer; sea surface emissivities from Niclos et al. (2005) depending on view angle. Simultaneous measurements of downwelling LW (sky) radiance at complimentary angle to account for reflected radiance. SST was calculated at KT15.85 centre wavelength (10.55 micron) for each scan (15s interval) and then averaged over 1min (4 scans) and over 10min (40 scans).

References:

1. Niclos, R., Valor, E., Caselles, V., Coll, C., and Sanchez, J.M. (2005). In situ angular measurements of thermal infrared sea surface emissivity—Validation of models. *Remote Sensing of Environment*, 94, 83-93.

Radiometer usage (deployment):

Permanent, long-term (5+ years) deployment at 4 field sites in Portugal, Namibia, and Senegal. The radiometers are used for validating satellite-derived land surface temperature products. At each station 3 to 4 KT15.85 IIP are in continuous operation.

Uncertainties
Radiometer Heitronics KT15.85 IIP , detector type A

Parameter	Type A Uncertainty in Value / %	Type B Uncertainty in Value / (appropriate units)	Uncertainty in Brightness temperature K
Repeatability of measurement	0.12K / 0.040%		0.12K
Reproducibility of measurement	0.06K / 0.020%		0.06K
Linearity of radiometer		0.10K	0.10K
Primary calibration		0.20K	0.20K
Drift since calibration		-	-
RMS total	0.13K / 0.045%	**0.22K**	0.26K

Uncertainty budget for the IR radiometer measurement of brightness temperature of a blackbody

Contribution	Standard Uncertainty Value (mK)	Comment	
Calibration of radiometer	200	external blackbody or if internal this should include reference to the calibration of the internal black body and in both cases the uncertainty of the ultimate reference blackbody to SI. This may be a thermometer and	
Linearity of radiometer	100	is the responsivity of the radiometer constant with illumination or signal levels. Most detectors deviate at high levels and any gain changes can also have an effect. This may to some extent be calibrated out but if there is any observed non-linearity interpolation needs to be applied with care.	
Drift since calibration	0	Calibration of most instruments will drift. This accounts for time between calibration (1)	Comment: internally linked to PRT
Measurement repeatability	120	variation (noise) in signal when measuring black body source in lab	
Reproducibility	60	variation in instrument reading for a constant source when re-aligned	
Size of source	0	uncertainty in any correction or if no correction due to differences in souce size between calibration source and measured or latter and infinite source	
Temperature sensitivity of radiometer	50	Most instruments have a sensitivity in their response due to ambient temperature	
electronics, shutters etc	0	If not accounted for elsewhere uncertainty in gain of amplifiers (lock-in etc) or stability of choppers should be considered	
Combined uncertainty	**265.52**		
Combined uncertainty (k=2)	**531.04**		

Uncertainty budget for the IR radiometer measurement of brightness temperature of Ocean

Contribution	Standard Uncertainty Value (mK)	Comment
Calibration of radiometer	200	This might be as calibrated to another external blackbody or if internal this should include reference to the calibration of the internal black body and in both cases the uncertainty of the ultimate reference blackbody to SI. This may be a thermometer and emissivity.

3.6.3 Results

The KIT radiometers took part in the NPL blackbody, RSMAS blackbody and Miami ocean temperature comparisons. Figures 3.6.1 to 3.6.5 show the temperature values reported by the KIT ground radiometer when monitoring the NPL blackbody cavity temperature. Figure 3.6.6 shows the temperature values reported by the KIT ground radiometer when monitoring the NPL gallium blackbody cavity temperature. Figures 3.6.7 to 3.6.11 show the temperature values reported by the KIT ground radiometer when monitoring the RSMAS blackbody cavity temperature. Figure 3.6.12 shows the temperature values reported by the KIT ground radiometer when monitoring the NIST blackbody cavity temperature. Figure 3.6.13 shows the temperature values reported by the KIT sky radiometer when monitoring the NIST blackbody cavity temperature. Figure 3.6.14 shows the ocean temperature values reported by the KIT ground radiometer, while Figure 3.6.15 shows the difference

of these values from the mean of the four continuously measuring radiometers. Figure 3.5.16 shows the difference of the KIT radiometer from the measurements reported by the ISAR radiometer.

3.6.3.1 Comparison of the KIT ground radiometer to the NPL blackbody

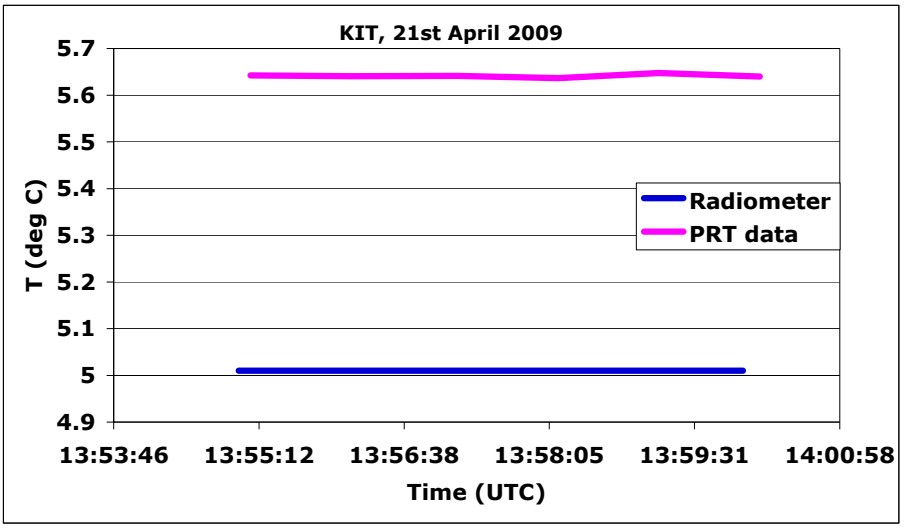

Figure 3.6.1: KIT ground radiometer viewing the NPL blackbody at 5 °C.
<Radiometer measurement> – <BB temperature> = -0.632 K
(brackets indicate average over time interval shown)

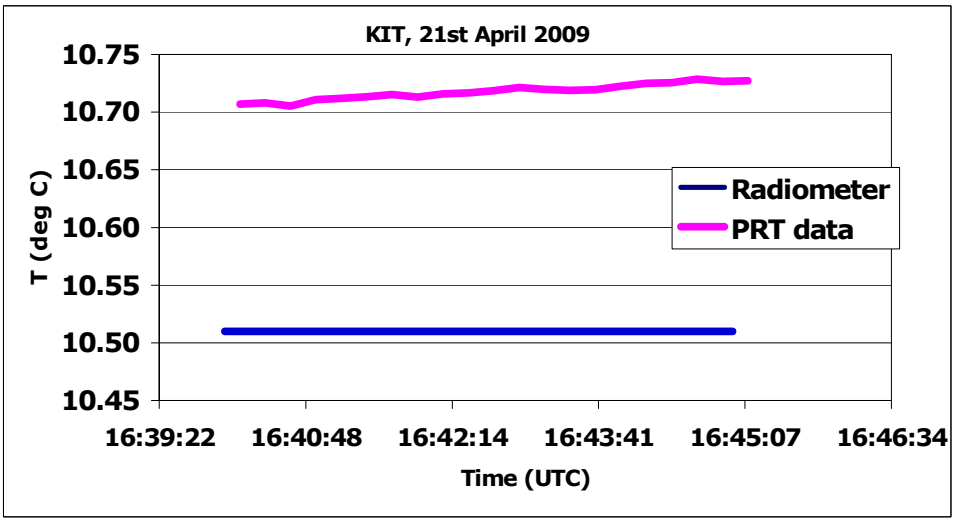

Figure 3.6.2: KIT ground radiometer viewing the NPL blackbody at 10 °C.
<Radiometer measurement> – <BB temperature> = -0.208 K
(brackets indicate average over time interval shown)

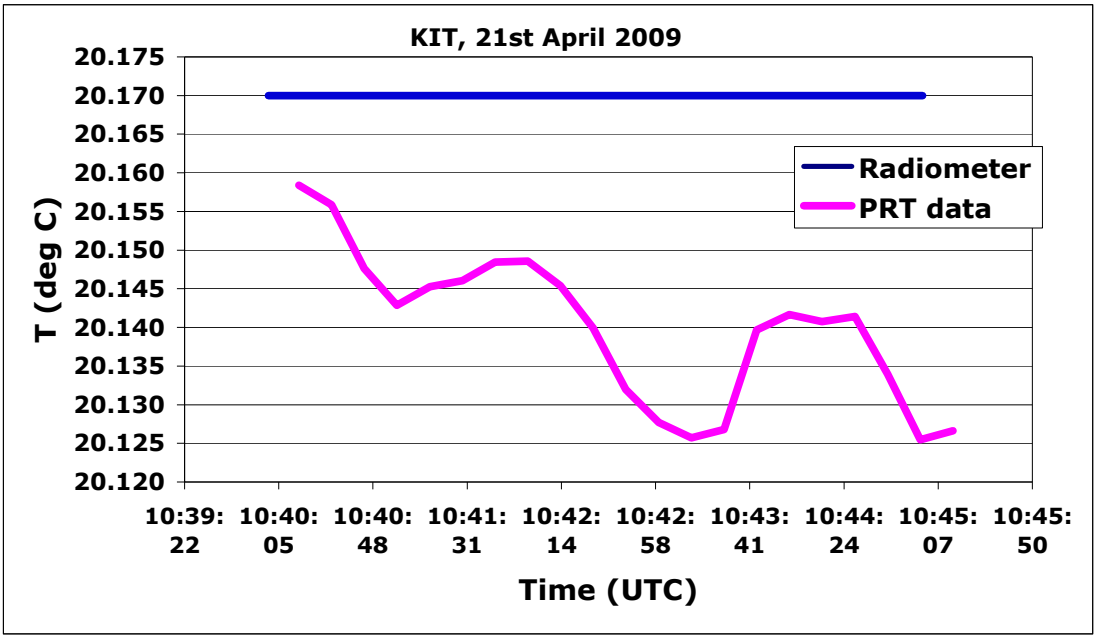

Figure 3.6.3: KIT ground radiometer viewing the NPL blackbody at 20 °C
1st measurement. <Radiometer measurement> – <BB temperature> = 0.030 K
(brackets indicate average over time interval shown)

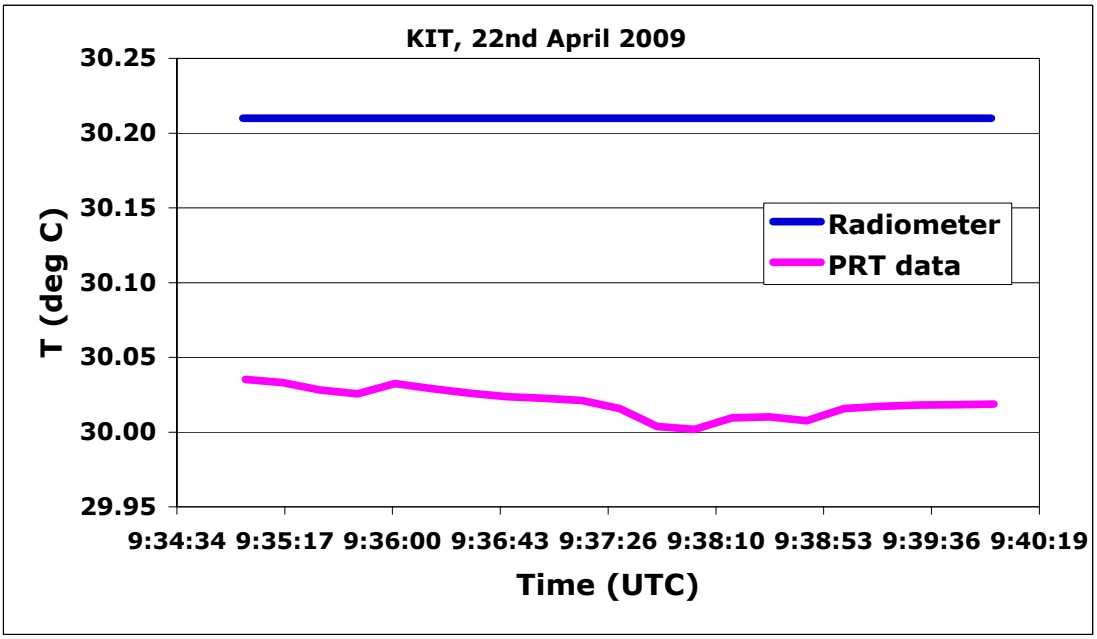

Figure 3.6.4: KIT ground radiometer viewing the NPL blackbody at 30 °C,
1st measurement. <Radiometer measurement> – <BB temperature> = 0.190 K
(brackets indicate average over time interval shown)

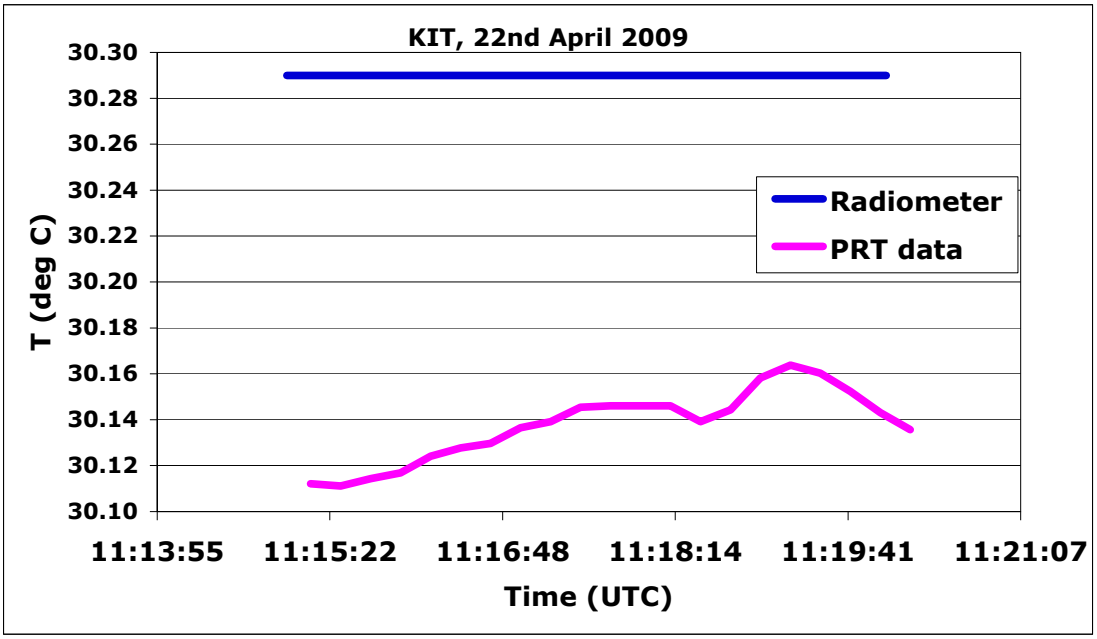

Figure 3.6.5: KIT ground radiometer viewing the NPL blackbody at 30 °C,
2nd measurement. <Radiometer measurement> – <BB temperature> = 0.152 K
(brackets indicate average over time interval shown)

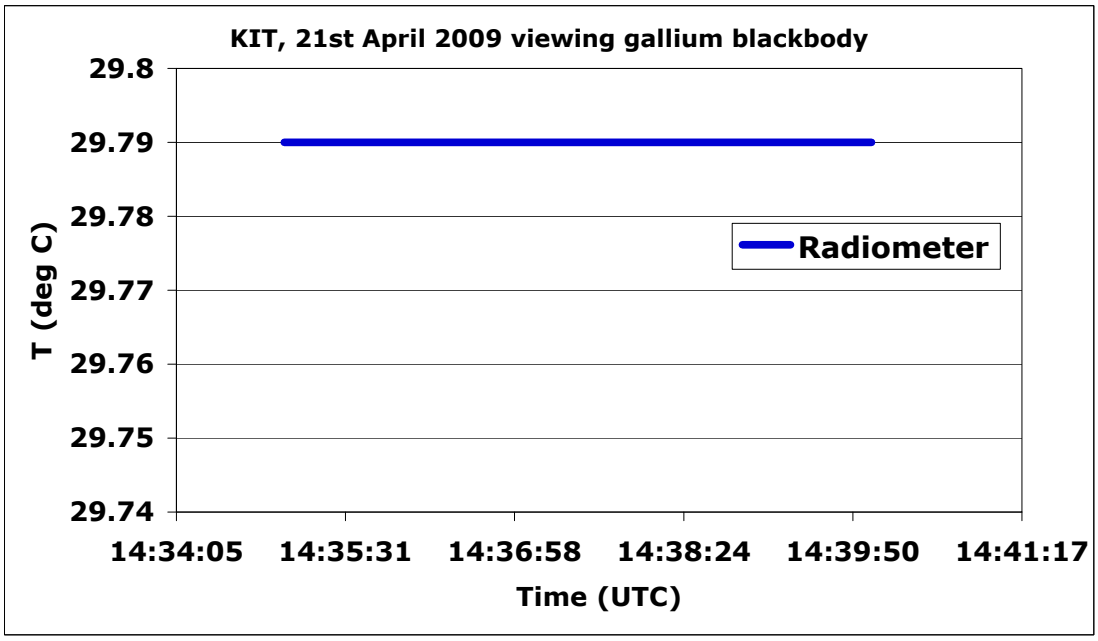

Fig 3.6.6: KIT ground radiometer viewing the NPL gallium blackbody.
Radiometer measurement> – Gallium melting temp. = 0.025 K
(brackets indicate average over time interval shown)

3.6.3.2 Comparison to the RSMAS blackbody

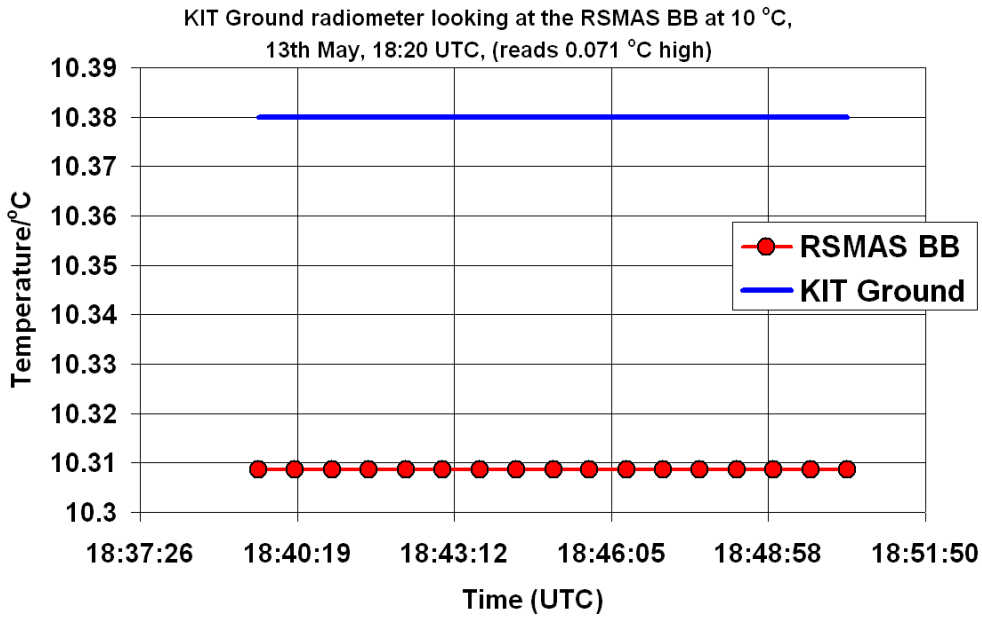

Figure 3.6.7: KIT ground radiometer viewing the RSMAS blackbody at 10 °C.
<Radiometer measurement> – <BB temperature> = 0.071 K
(brackets indicate average over time interval shown)

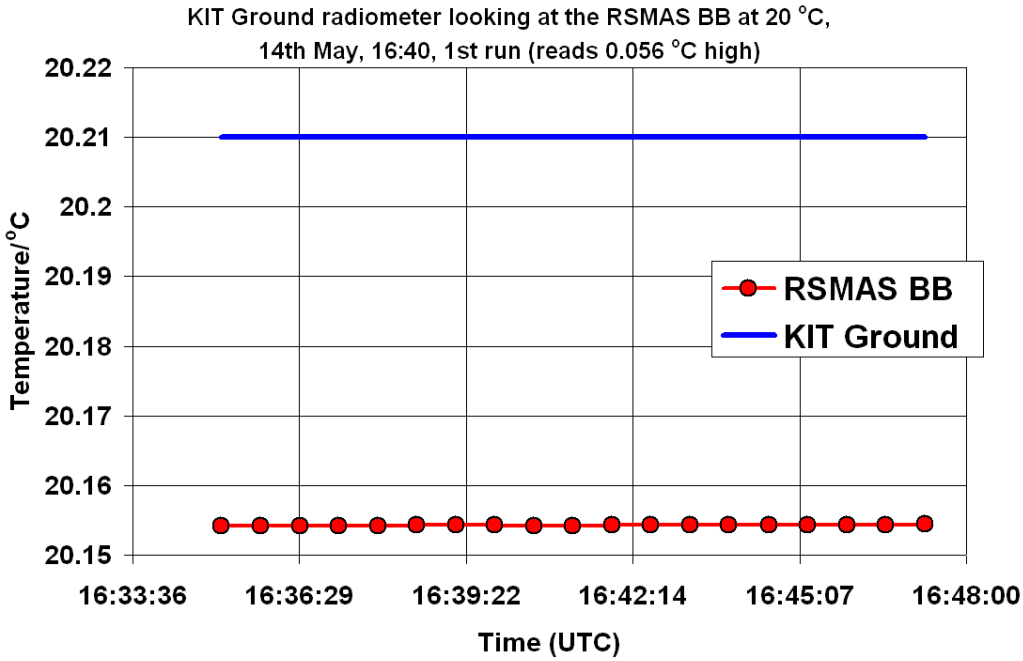

Figure 3.6.8: KIT ground radiometer viewing the RSMAS blackbody at 20 °C,
1st measurement. <Radiometer measurement> – <BB temperature> = 0.056 K
(brackets indicate average over time interval shown)

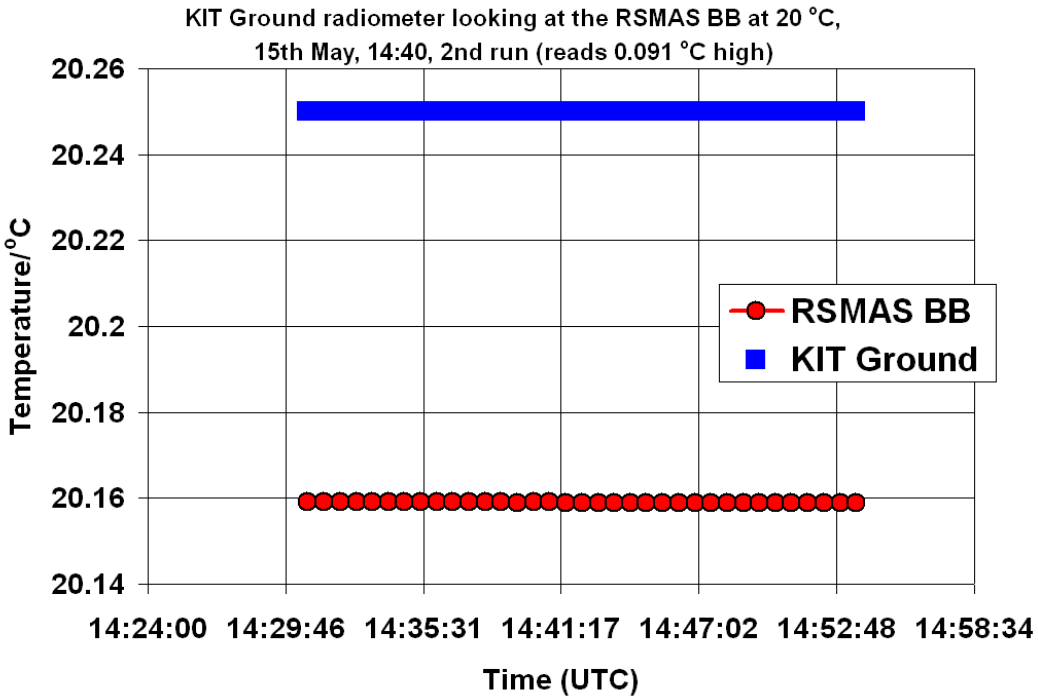

Figure 3.6.9: KIT ground radiometer viewing the RSMAS blackbody at 20 °C, 2nd measurement. <Radiometer measurement> – <BB temperature> = 0.091 K (brackets indicate average over time interval shown).

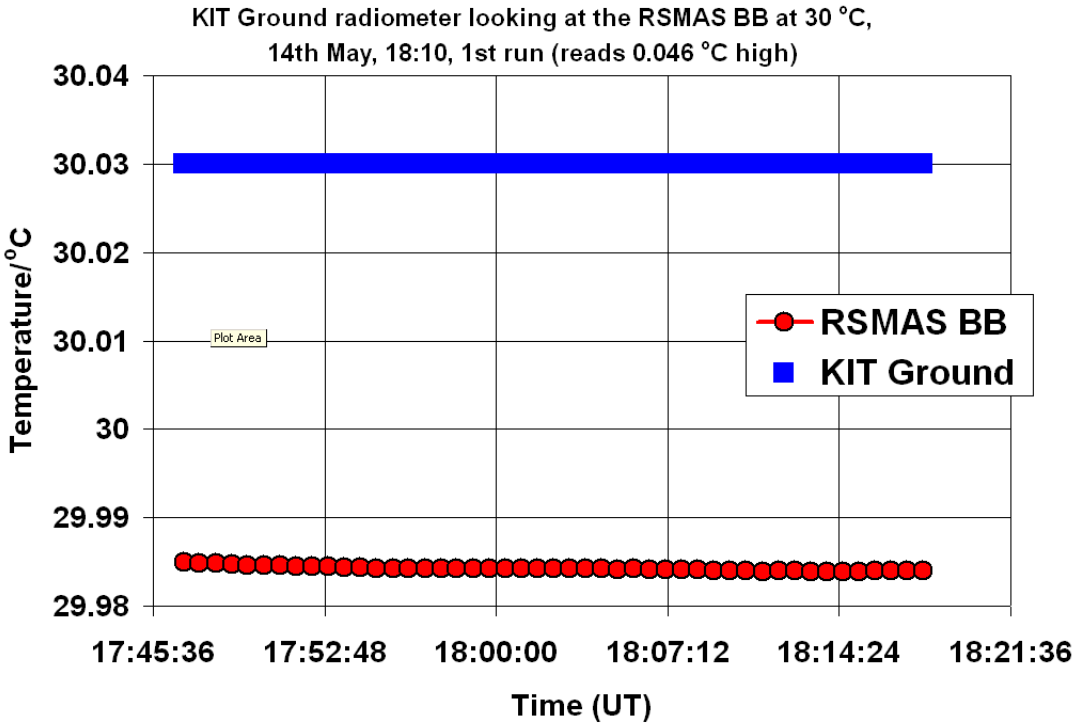

Figure 3.6.10: KIT ground radiometer viewing the RSMAS blackbody at 30 °C, 1st measurement. <Radiometer measurement> – <BB temperature> = 0.046 K (brackets indicate average over time interval shown).

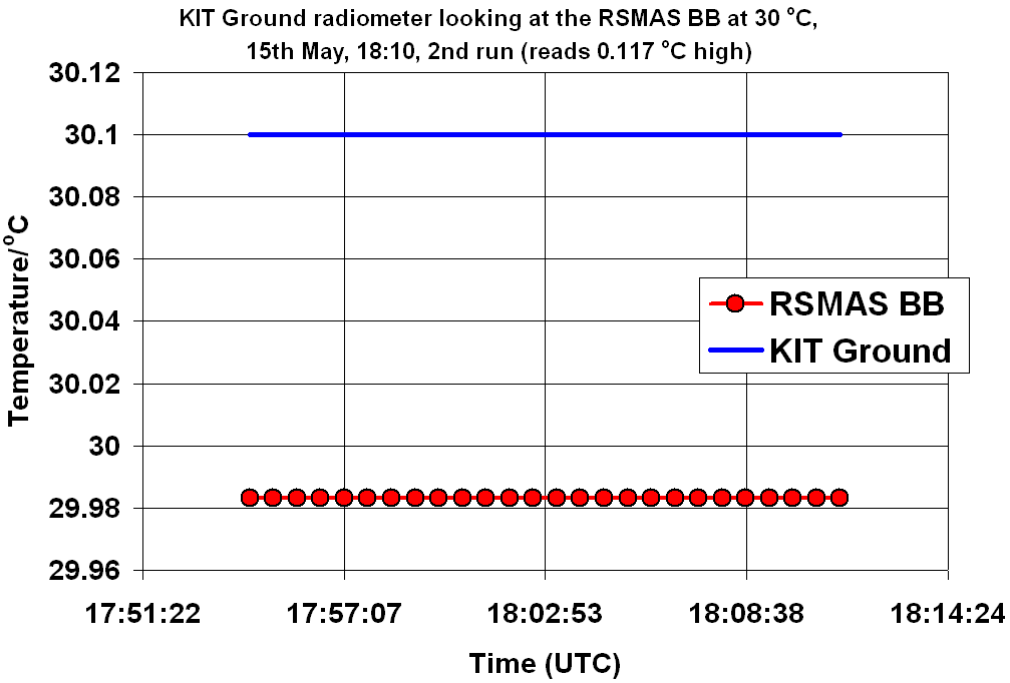

Figure 3.6.11: KIT ground radiometer viewing the RSMAS blackbody at 30 °C, 2nd measurement. <Radiometer measurement> – <BB temperature> = 0.117 K (brackets indicate average over time interval shown).

3.6.3.3 KIT ground radiometer viewing the NIST blackbody

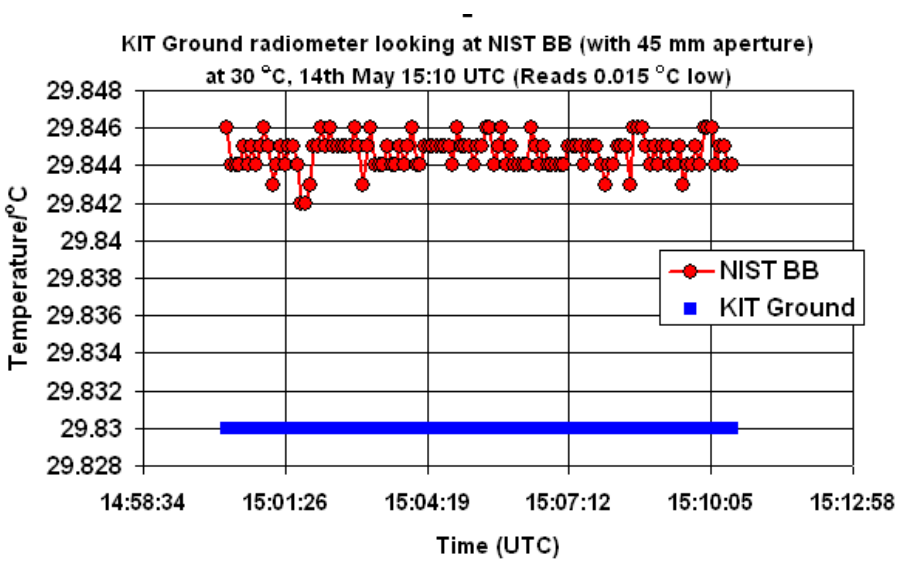

Figure 3.6.12: KIT Ground radiometer viewing the NIST blackbody at 30 °C. <Radiometer measurement> – <BB temperature> = -0.015 K (brackets indicate average over time interval shown)

3.6.3.4 KIT Sky radiometer viewing the NIST blackbody

Only one measurement was completed with the KIT Sky radiometer (at 30 °C). The temperature error read by the KIT Sky radiometer was 120 mK (radiometer reads "high").

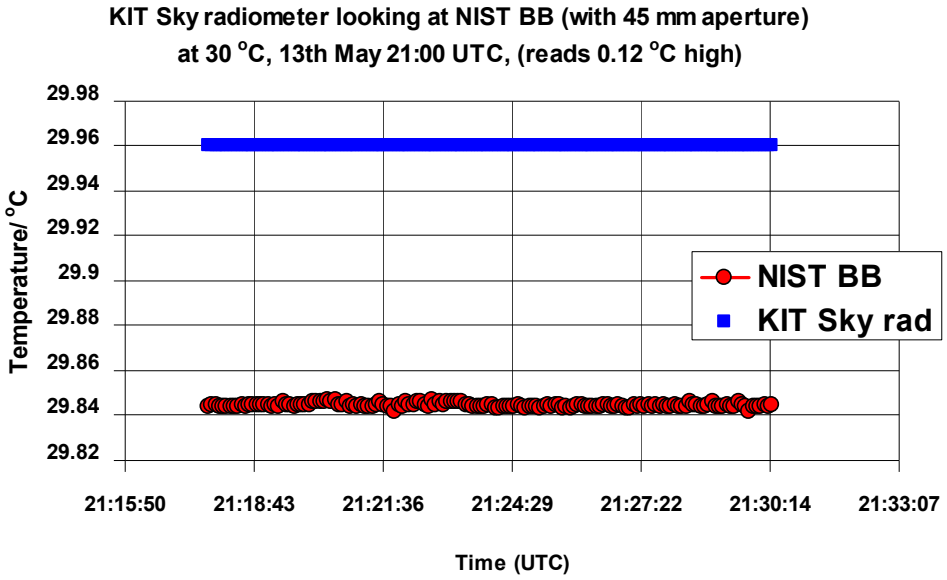

Figure 3.6.13: KIT Sky radiometer viewing the NIST blackbody at 30 °C.
<Radiometer measurement> – <BB temperature> = 0.12 K
(brackets indicate average over time interval shown)

3.6.3.5 Ocean surface temperature measurements using the KIT radiometer

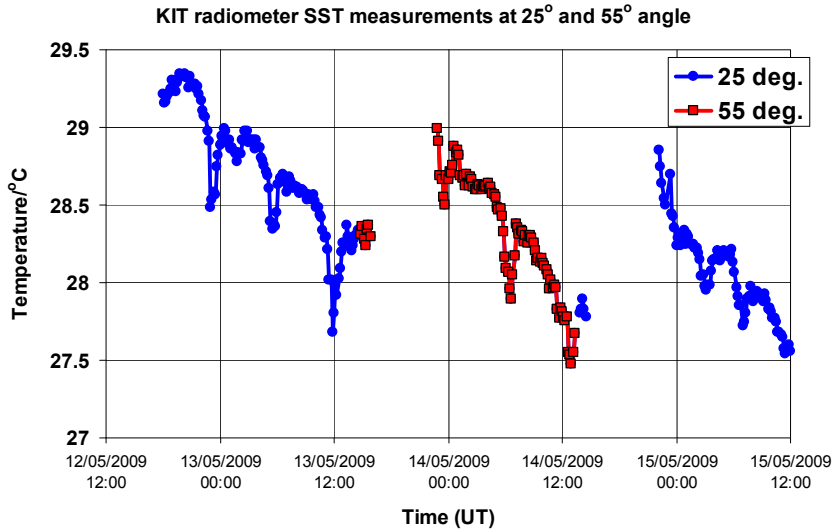

Figure 3.6.14: Ocean temperature measured by the KIT radiometer over the 12th May to 15th May period. Measurements were completed at two angles, 25° and 55°.

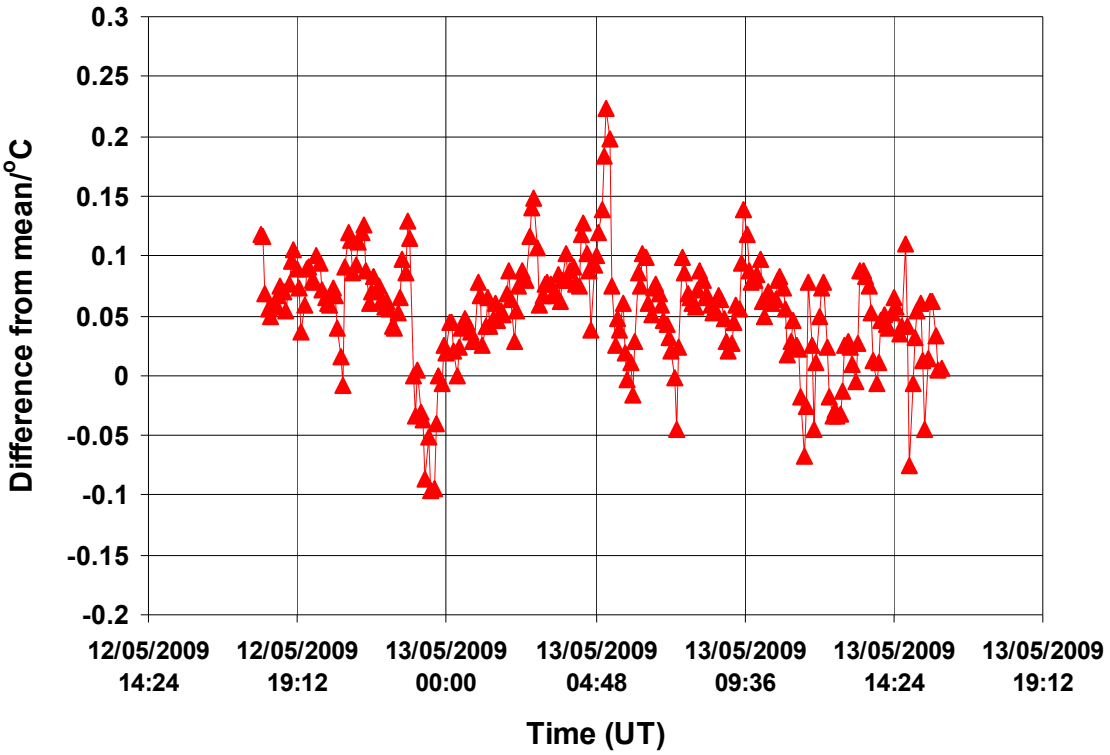

Figure 3.6.15: Difference in the ocean surface temperature readings of the KIT radiometer from the mean of the four continuously measuring radiometers (data only available over a limited time period).

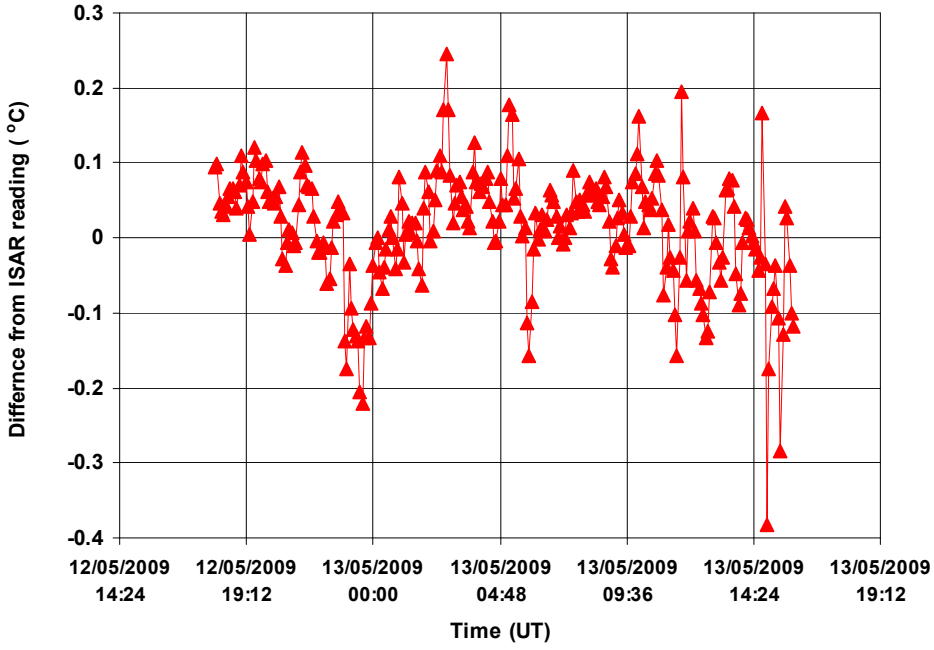

Figure 3.6.16: Difference in the ocean surface temperature readings of the KIT radiometer from the ISAR radiometer.

3.7 National Oceanography Centre (NOC), University of Southampton

3.7.1 Contact information:

NOC contact for the comparison: Dr Weinfrid Wimmer
Address: European Way, Southampton, SO19 9TX, UK
Email: W.wimmer@soton.ac.uk

3.7.2 Radiometer used in the comparison

Make and type of radiometer: Infrared Sea surface Autonomous Radiometer (ISAR). Further information on this radiometer can be found at: (http://www.isar.org.uk/).

Outline technical description of instrument: The instrument consists of a radiometer (Heitronics KT15 with spectral band: 9.6 μm to 10.5 μm) and two internal reference black bodies (one at ambient and one heated). Radiometer views the reference black bodies and the scene for each measurement.

Establishment or traceability route for primary calibration including date of last realisation and breakdown of uncertainty:

Radiometer is calibrated with reference to a CASOTS II (NOC) manufactured black body) a water bath controlled entity with a reference HART platinum resistance thermometer.

Uncertainty

The radiometer is stated to have an uncertainty of 0.1 K for both lab and ocean view, this is assumed to include both Type A and Type B components.

3.7.3 Results

The ISAR radiometer took part in the NPL blackbody, RSMAS blackbody and Miami ocean temperature comparisons. Figures 3.7.1 to 3.7.6 show the temperature values reported by the ISAR radiometer when monitoring the NPL blackbody cavity temperature. Figure 3.7.7 shows the temperature values reported by the ISAR radiometer when monitoring the NPL gallium blackbody cavity temperature. Figures 3.7.8 to 3.7.12 show the temperature values reported by the ISAR radiometer when monitoring the RSMAS blackbody cavity temperature. Figure 3.7.13 shows the temperature values reported by the ISAR radiometer when monitoring the NIST blackbody cavity temperature (with 45 mm diameter aperture). Figure 3.7.14 shows the temperature values reported by the ISAR radiometer when monitoring the NIST blackbody cavity temperature (with 100 mm diameter aperture). Figure 3.7.15 shows the Ocean temperature values reported by the ISAR radiometer, while Figure 3.7.15 shows the difference of these values from the mean of the four continuously measuring radiometers.

3.7.3.1 Comparison of the ISAR radiometer to the NPL blackbody.

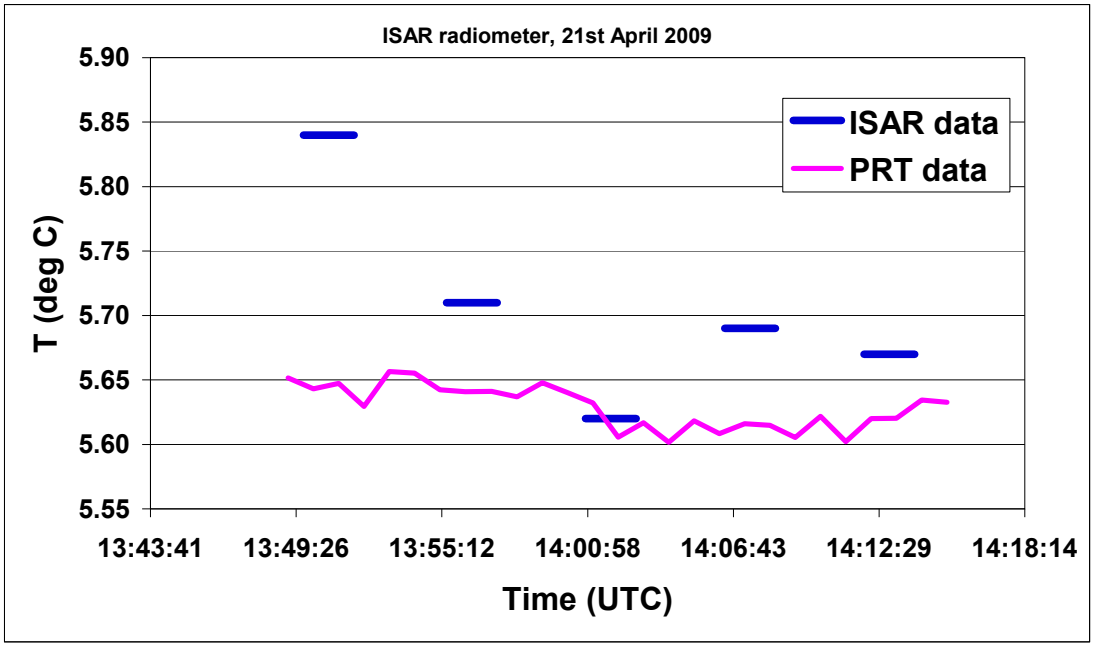

Figure 3.7.1: ISAR radiometer viewing the NPL blackbody at 5 °C (only measurement)
<Radiometer measurement> – <BB temperature> = 0.077 K
(brackets indicate average over time interval shown)

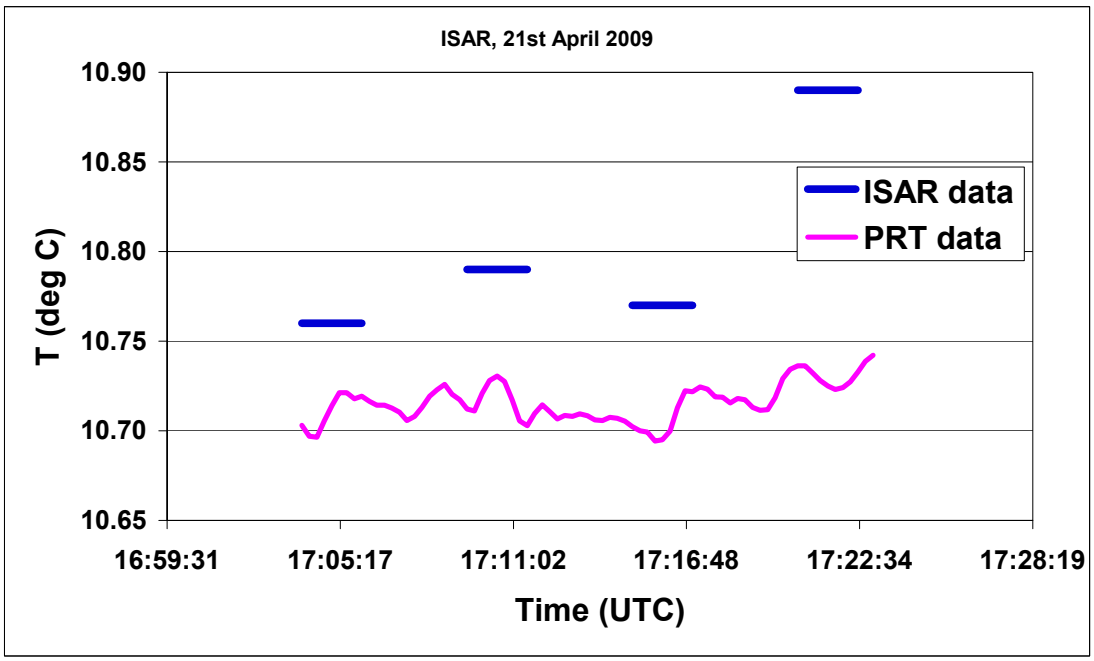

Figure 3.7.2: ISAR radiometer viewing the NPL blackbody at 10 °C, 1st measurement
<Radiometer measurement> – <BB temperature> = 0.087 K
(brackets indicate average over time interval shown)

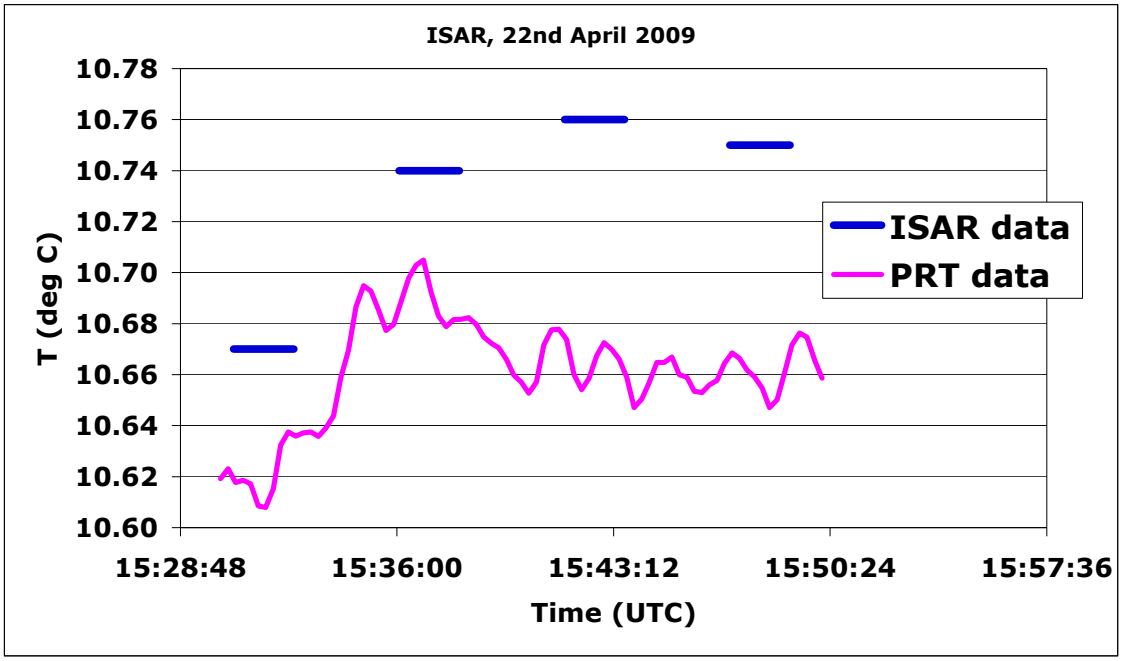

Figure 3.7.3: ISAR radiometer viewing the NPL blackbody at 10 °C, 2nd measurement
<Radiometer measurement> – <BB temperature> = 0.069 K
(brackets indicate average over time interval shown)

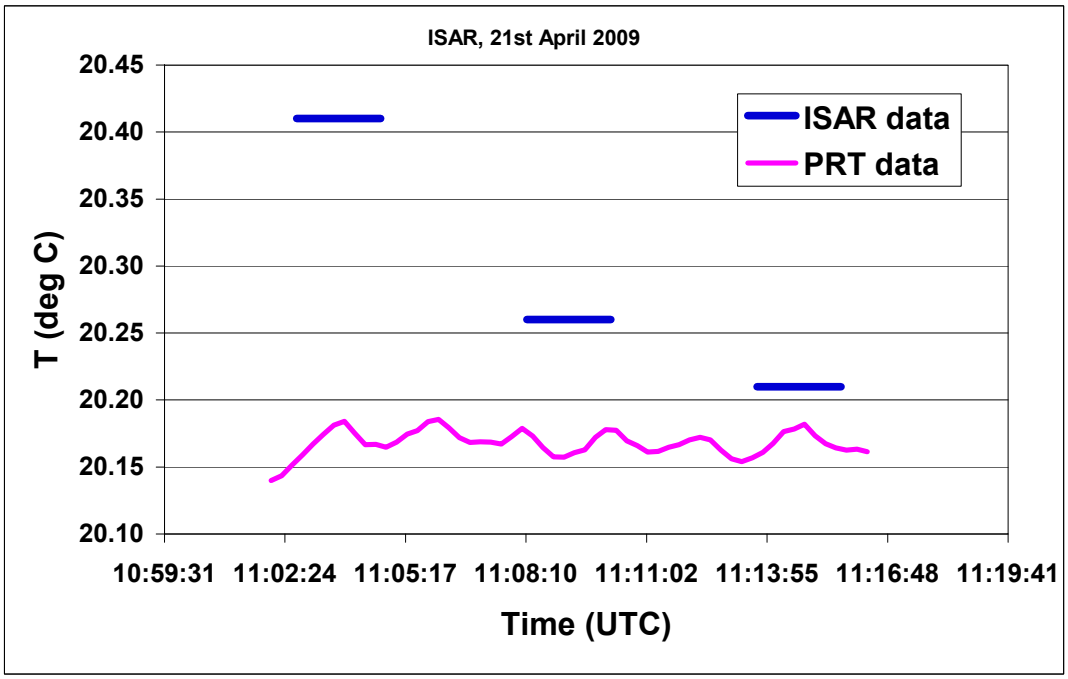

Figure 3.7.4: ISAR radiometer viewing the NPL blackbody at 20 °C, 1st measurement
<Radiometer measurement> – <BB temperature> = 0.126 K
(brackets indicate average over time interval shown)

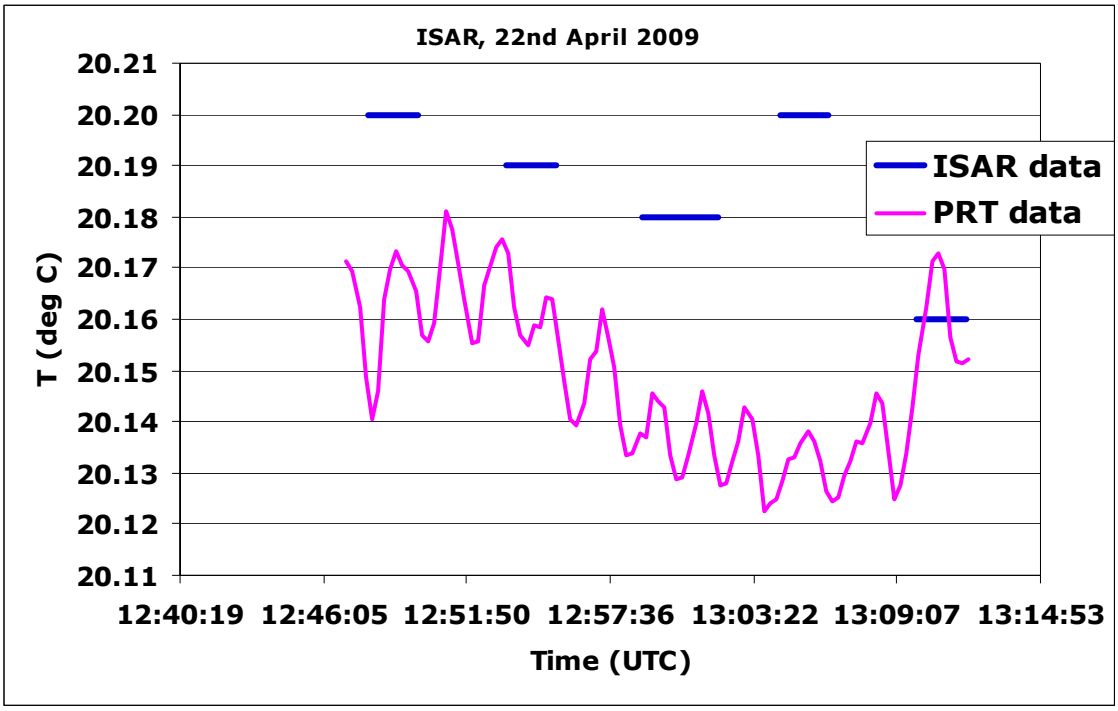

Figure 3.7.5: ISAR radiometer viewing the NPL blackbody at 20 °C, 2nd measurement
<Radiometer measurement> – <BB temperature> = 0.038 K
(brackets indicate average over time interval shown)

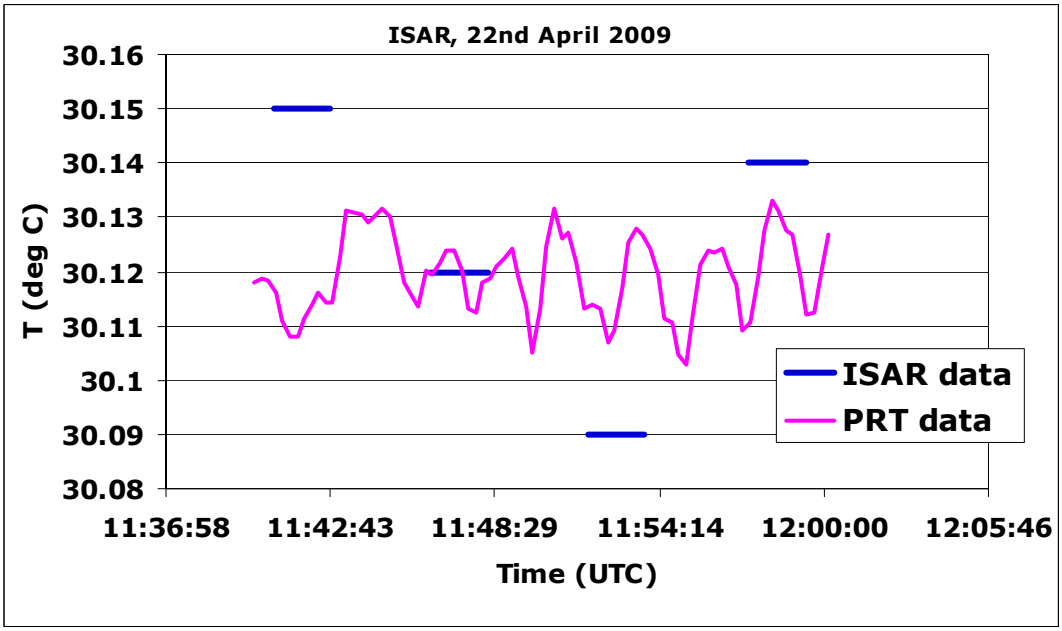

Figure 3.7.6: ISAR radiometer viewing the NPL blackbody at 30 °C
<Radiometer measurement> – <BB temperature> = 0.006 K
(brackets indicate average over time interval shown)

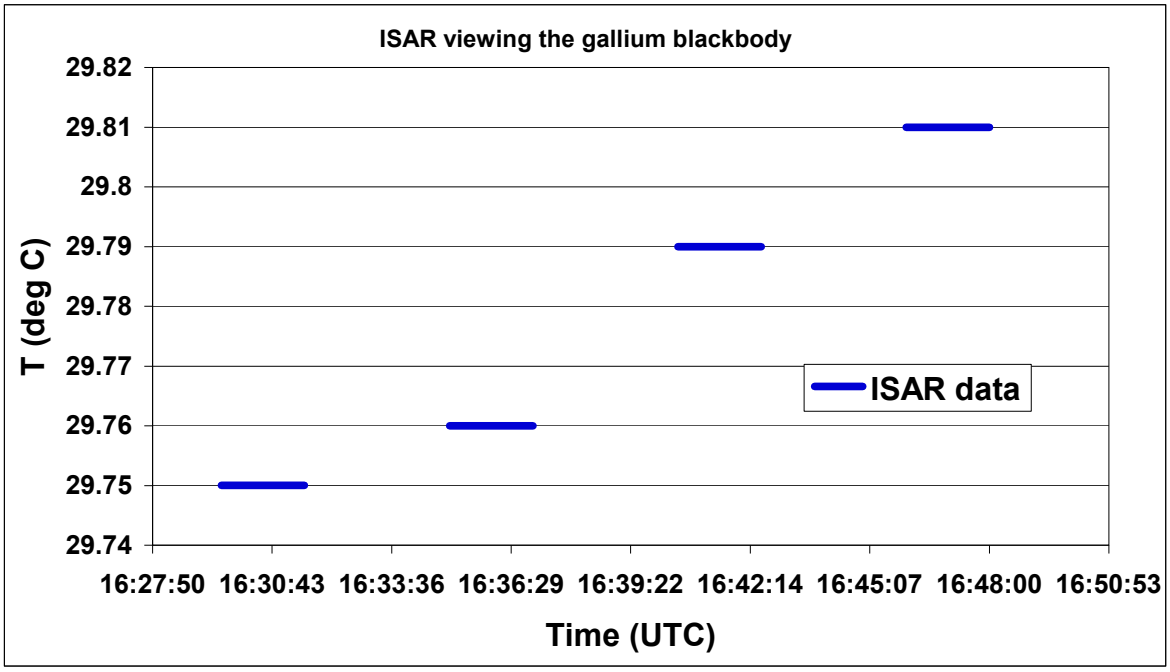

Figure 3.7.7: ISAR radiometer viewing the NPL gallium blackbody.
<Radiometer measurement> – gallium melting temp. = 0.013 K
(brackets indicate average over time interval shown).

3.7.3.2 Comparison to the RSMAS blackbody

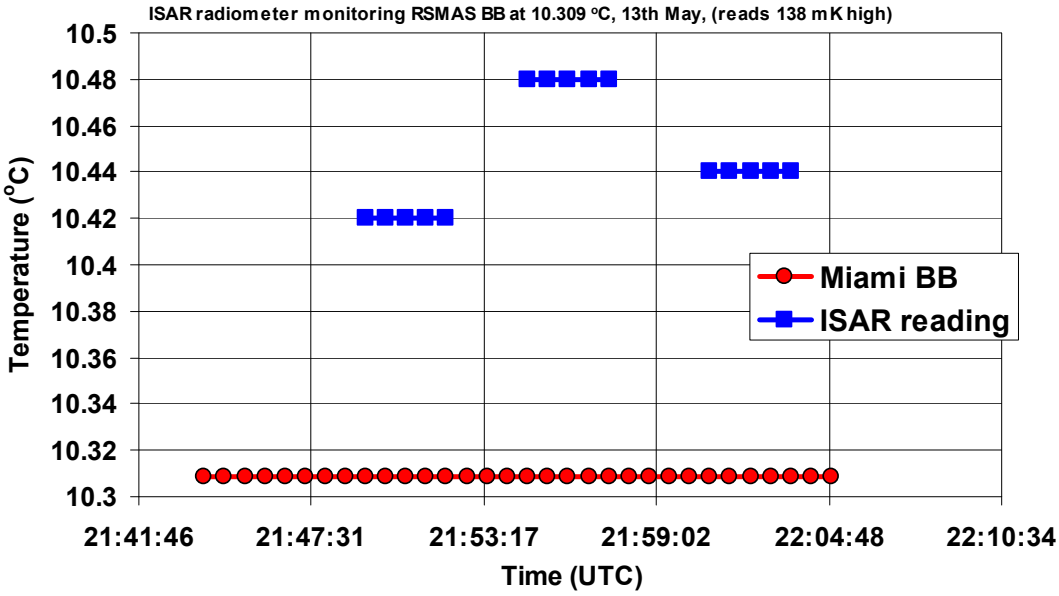

Figure 3.7.8: ISAR radiometer viewing the RSMAS blackbody at 10 °C,
1st measurement. <Radiometer measurement> – RSMAS blackbody temp. = 0.138 K
(brackets indicate average over time interval shown)

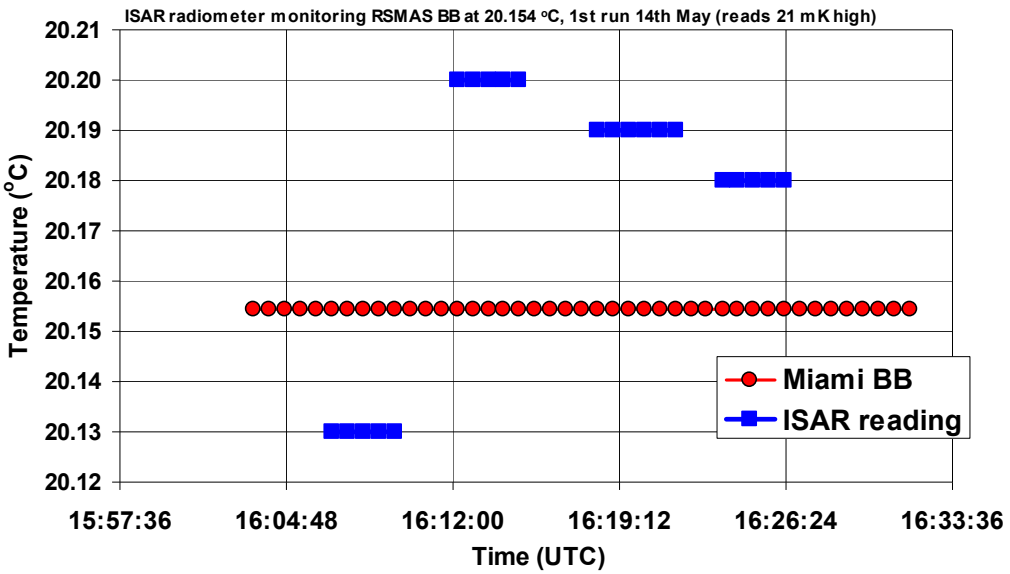

Figure 3.7.9: ISAR radiometer viewing the RSMAS blackbody at 20 °C,
1st measurement. <Radiometer measurement> – RSMAS blackbody temp. = 0.021 K
(brackets indicate average over time interval shown)

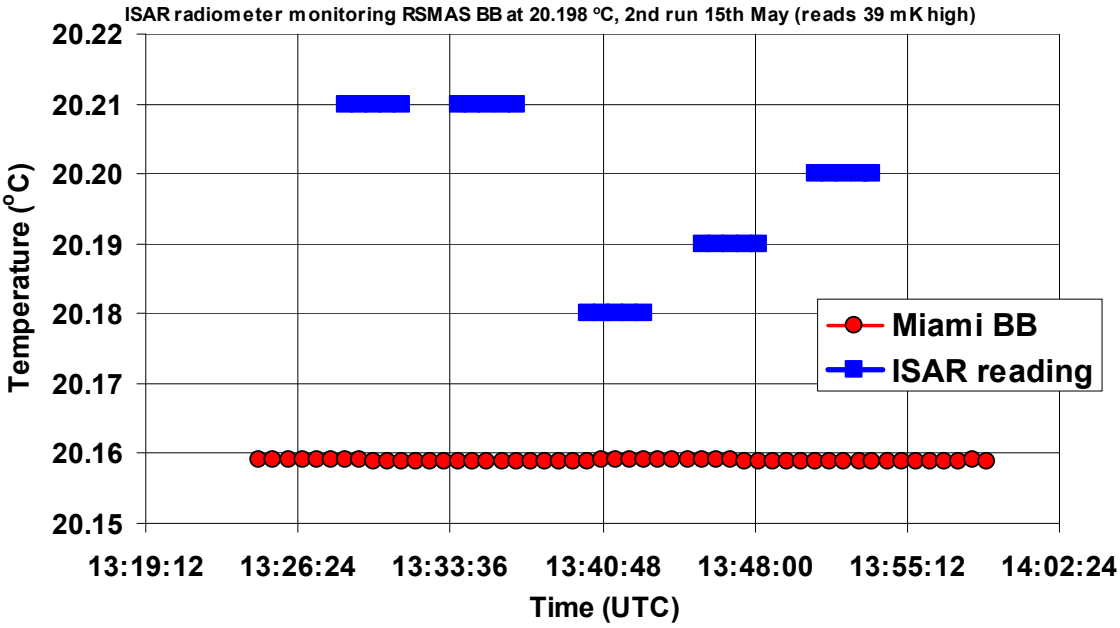

Figure 3.7.10: ISAR radiometer viewing the RSMAS blackbody at 20 °C
2nd measurement. <Radiometer measurement> – RSMAS blackbody temp. = 0.039 K
(brackets indicate average over time interval shown)

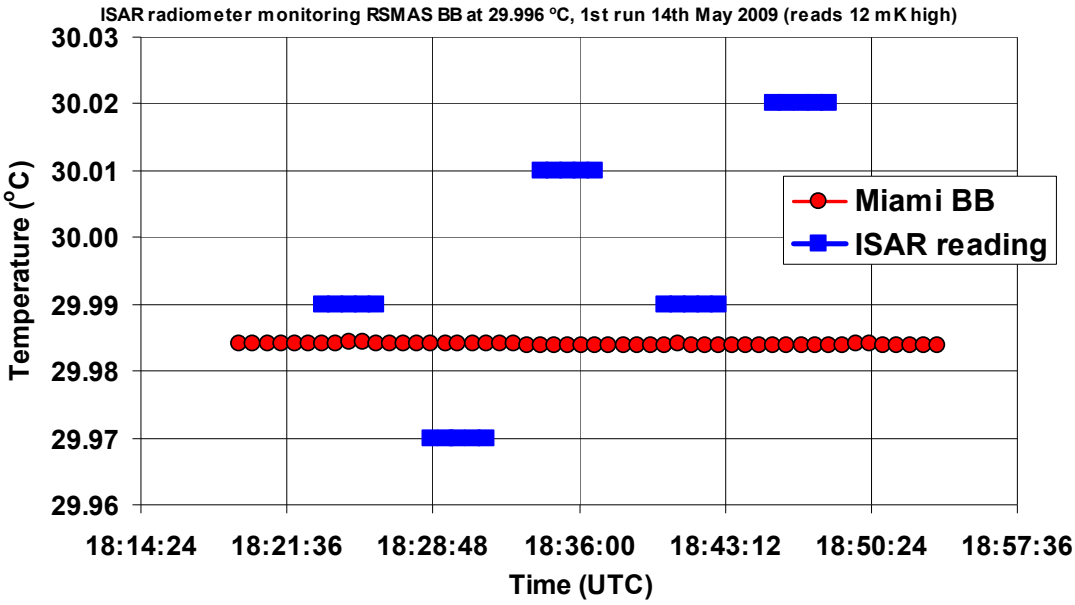

Figure 3.7.11: ISAR radiometer viewing the RSMAS blackbody at 30 °C,
1st measurement. <Radiometer measurement> – RSMAS blackbody temp. = 0.012 K
(brackets indicate average over time interval shown)

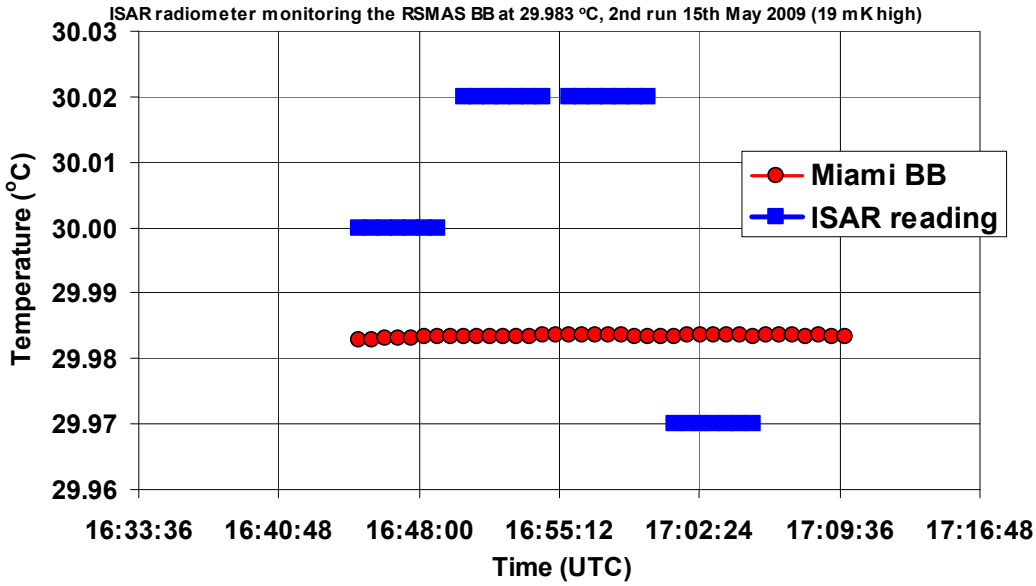

Figure 3.7.12: ISAR radiometer viewing the RSMAS blackbody at 30 °C,
2nd measurement. <Radiometer measurement> – RSMAS blackbody temp. = 0.019 K
(brackets indicate average over time interval shown)

3.7.3.3 Comparison to the NIST blackbody

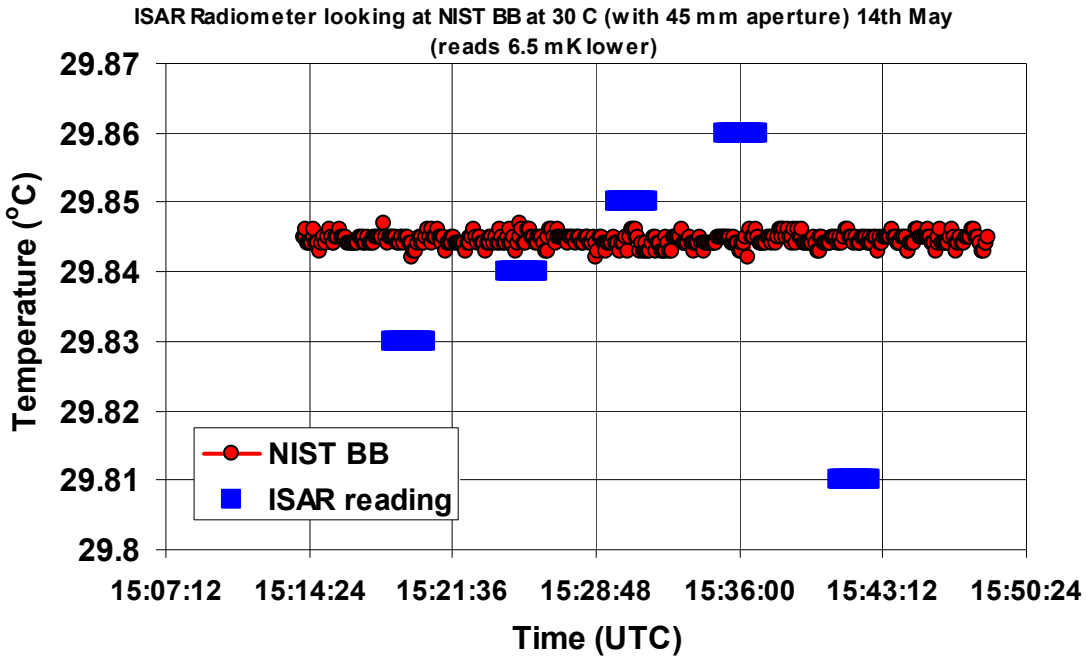

Figure 3.7.13: ISAR radiometer viewing the NIST blackbody at 30 °C, 45 mm aperture
<Radiometer measurement> – NIST blackbody temperature = -0.0065 K
(brackets indicate average over time interval shown)

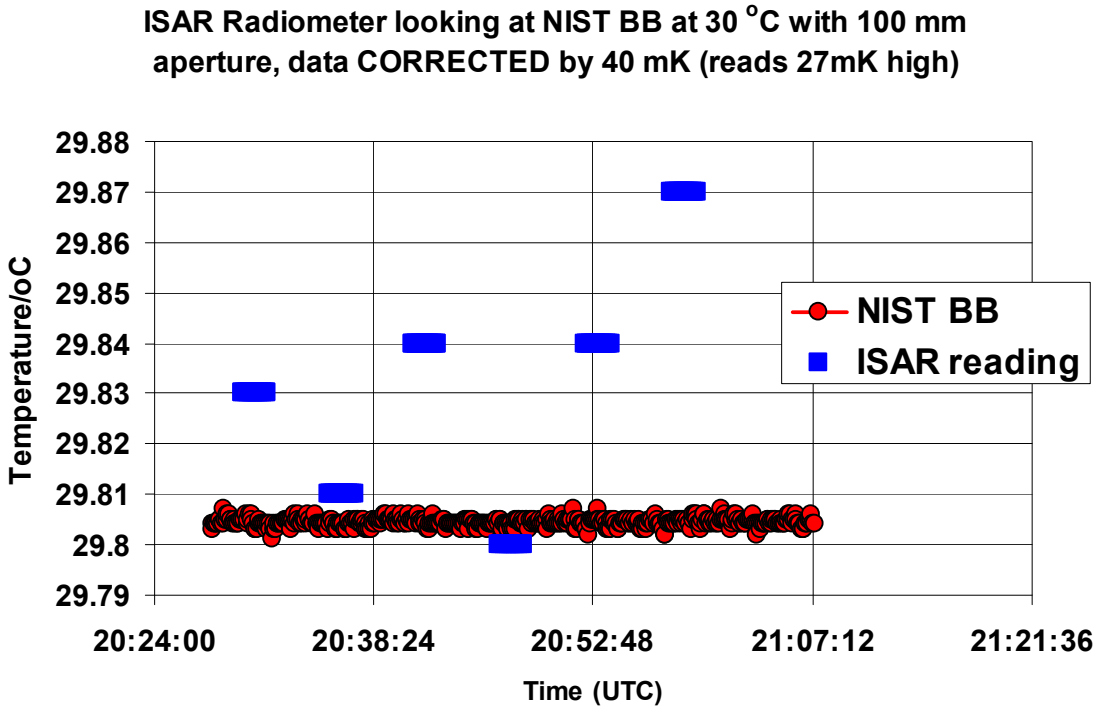

Figure 3.7.14: ISAR radiometer viewing the NIST blackbody at 30 °C,
100 mm aperture, <Radiometer measurement> – NIST blackbody temp = 0.027 K,
(brackets indicate average over time interval shown)

3.7.3.4 ISAR SST measurements

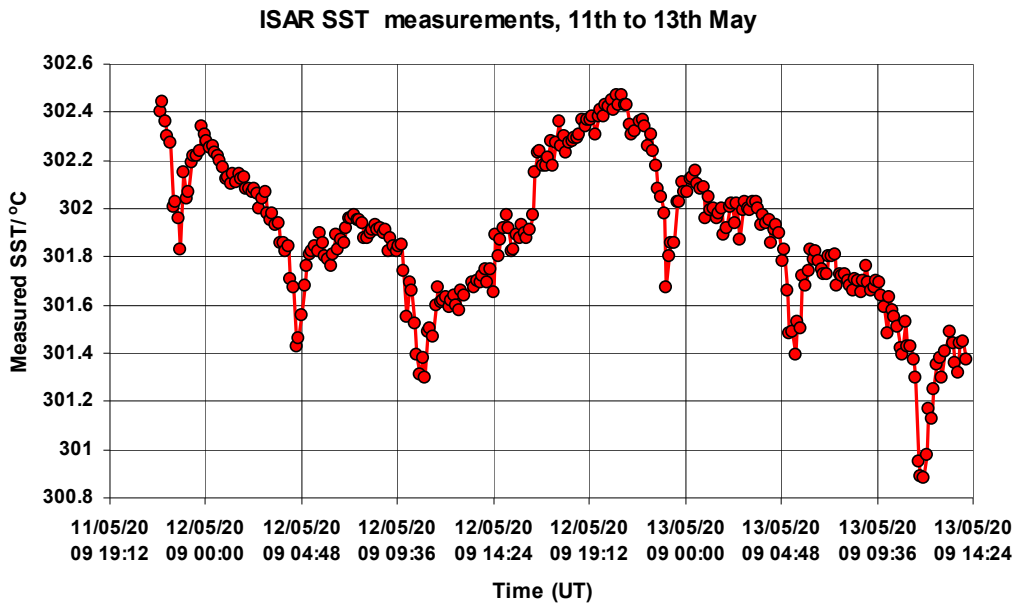

Figure 3.7.15: ISAR ocean surface temperature measurements recorded during the 11th to 13th May 2009 period

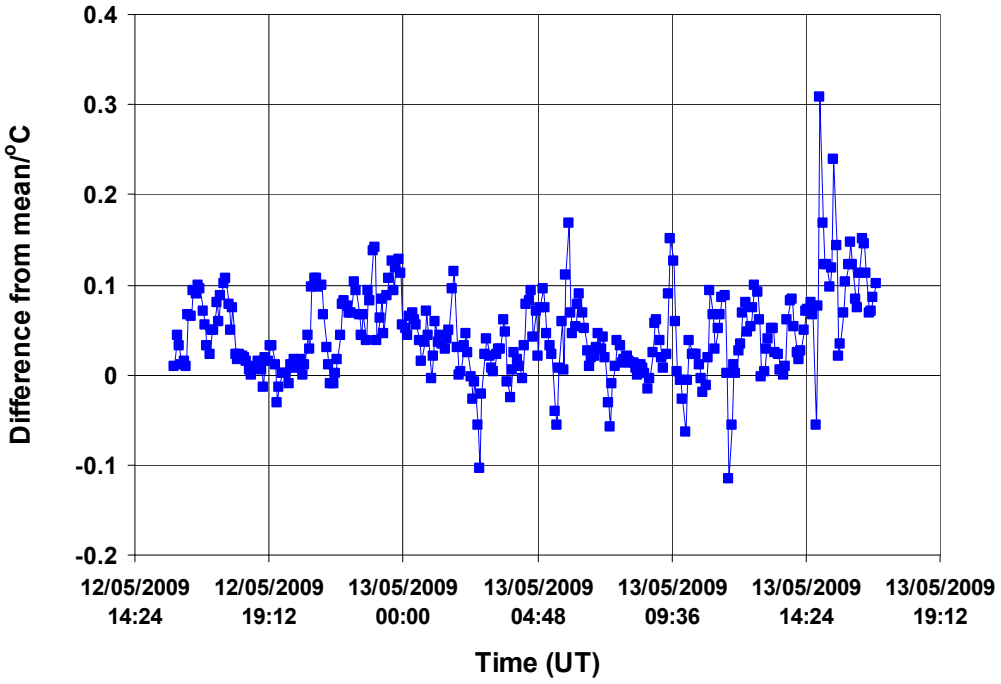

Figure 3.7.16: Difference in the ocean temperature measurements of the ISAR radiometer from the mean of the four continuously measuring radiometers (data only available over a limited time period).

3.8 Ocean Remote Sensing Institute, Ocean University of China (OUC)

3.8.1 Contact information

OUC contact for the comparison: Dr Lei Guan
Address: 5 Yushan Road, Qingdao, 266003, China
Email: leiguan@ouc.edu.cn

3.8.2 Radiometer used in the comparison

Infrared Sea surface Autonomous Radiometer (ISAR) **(http://www.isar.org.uk/)**

Outline technical description of instrument: The instrument consists of a radiometer (Heitronics KT15 with spectral band: 9.6-10.5 μm) and two internal reference black bodies (one at ambient and one heated). Radiometer views reference black bodies and scene for each measurement.

Establishment or traceability route for primary calibration including date of last realisation and breakdown of uncertainty: Traceable to manufacturer (i.e. NOC)

Uncertainty

The radiometer is stated to have an uncertainty of 0.1 K for both lab and ocean view, this is assumed to include both Type A and Type B components.

3.8.3 Results

The OUC (ISAR) radiometer took part in the NPL blackbody comparison.

3.8.3.1 Comparison to the NPL variable temperature blackbody

Figures 3.8.1 to 3.8.8 show the temperature readings of the OUC (ISAR) radiometer as a function of time, when it was monitoring the BPL blackbody cavity temperature. The same Figures also show the NPL blackbody cavity temperature as a function of time.

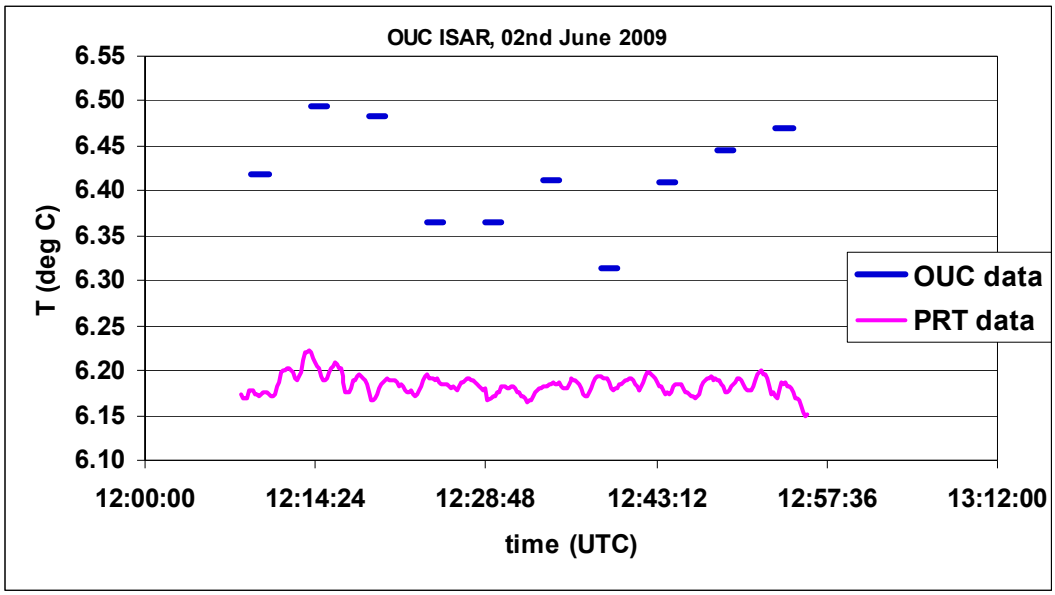

Figure 3.8.1: OUC ISAR radiometer viewing the NPL blackbody at 5 °C, 1st measurement. <Radiometer measurement> – <BB temperature> = 0.237 K (brackets indicate average over time interval shown)

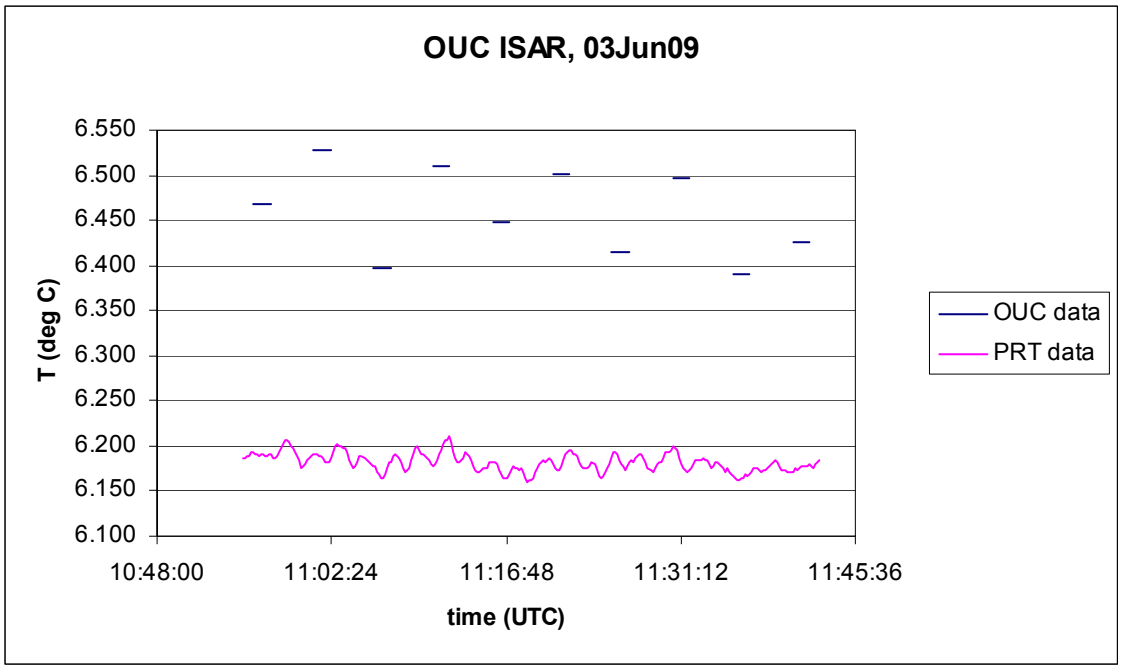

Figure 3.8.2: OUC ISAR radiometer viewing the NPL blackbody at 5 °C,
2nd measurement. <Radiometer measurement> – <BB temperature> = 0.279 K,
(brackets indicate average over time interval shown)

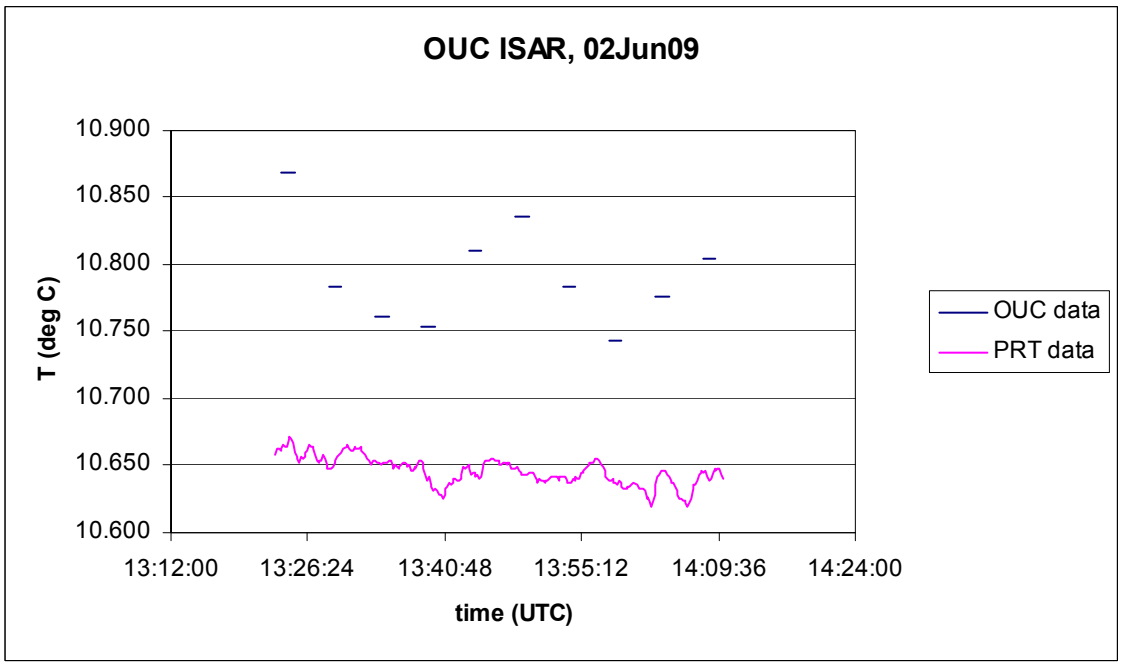

Figure 3.8.3: OUC ISAR radiometer viewing the NPL blackbody at 10 °C,
1st measurement, <Radiometer measurement> – <BB temperature> = 0.145 K
(brackets indicate average over time interval shown)

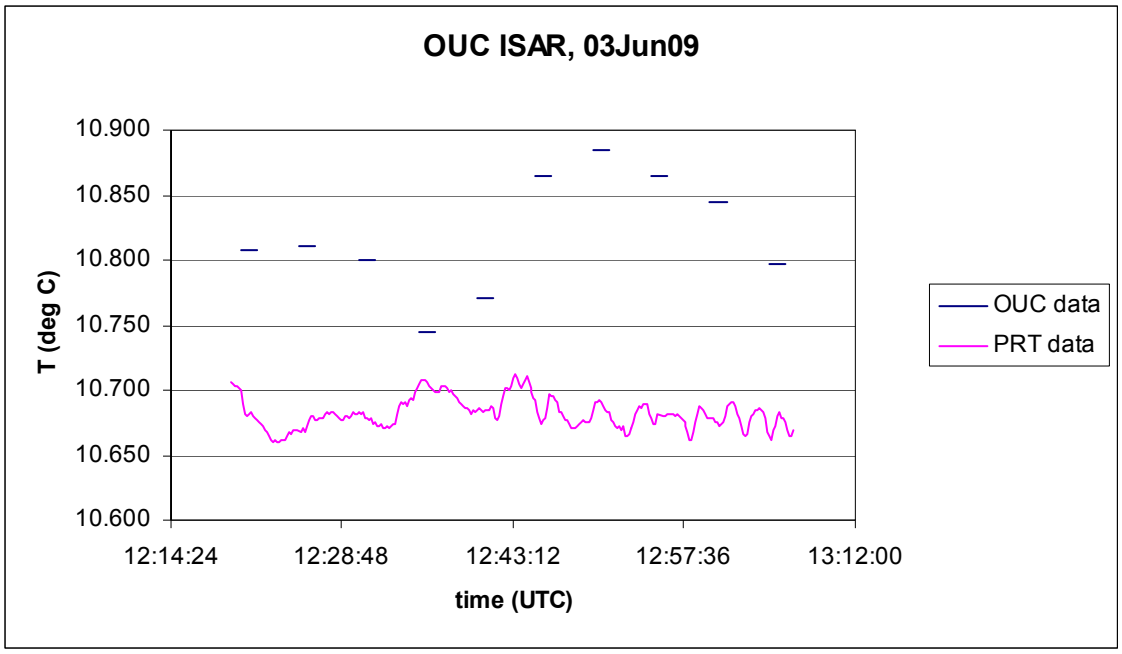

Figure 3.8.4: OUC ISAR radiometer viewing the NPL blackbody at 10 °C,
2nd measurement. <Radiometer measurement> – <BB temperature> = 0.136 K,
(brackets indicate average over time interval shown)

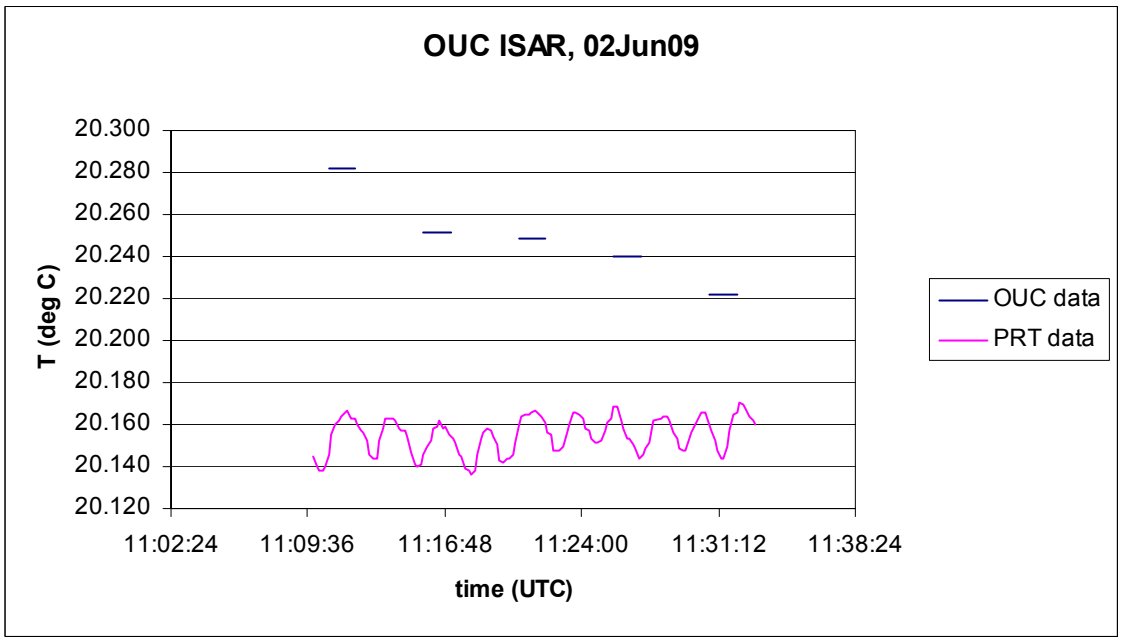

Figure 3.8.5: OUC ISAR radiometer viewing the NPL blackbody at 20 °C,
1st measurement, <Radiometer measurement> – <BB temperature> = 0.094 K,
(brackets indicate average over time interval shown)

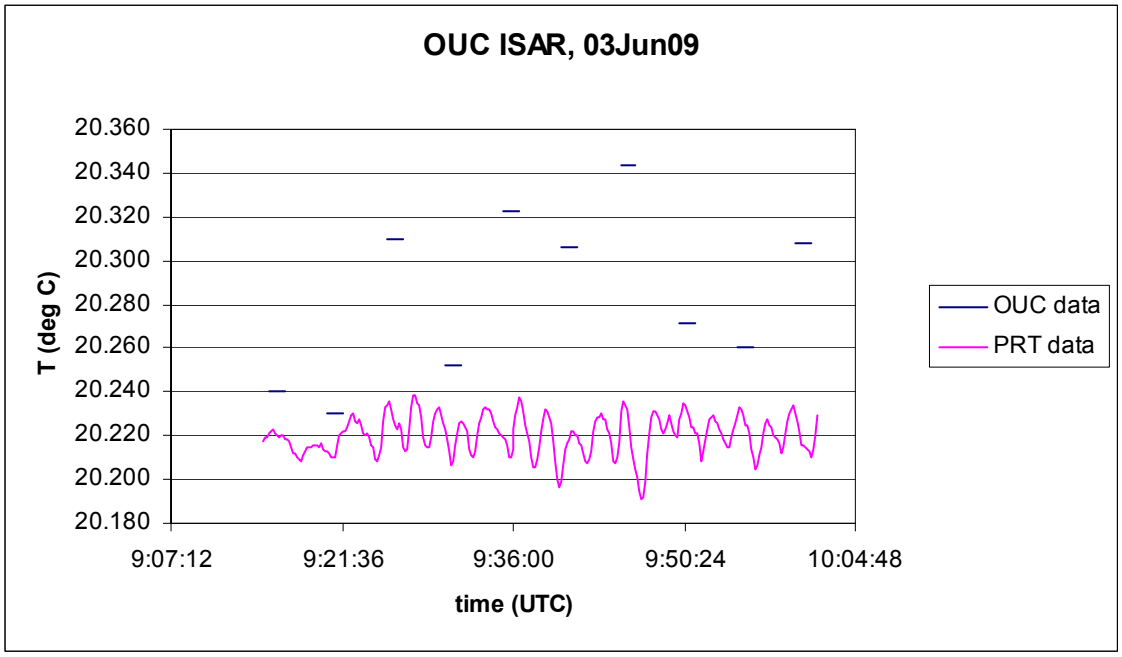

Figure 3.8.6: OUC ISAR radiometer viewing the NPL blackbody at 20 °C,
2nd measurement, <Radiometer measurement> – <BB temperature> = 0.064 K
(brackets indicate average over time interval shown)

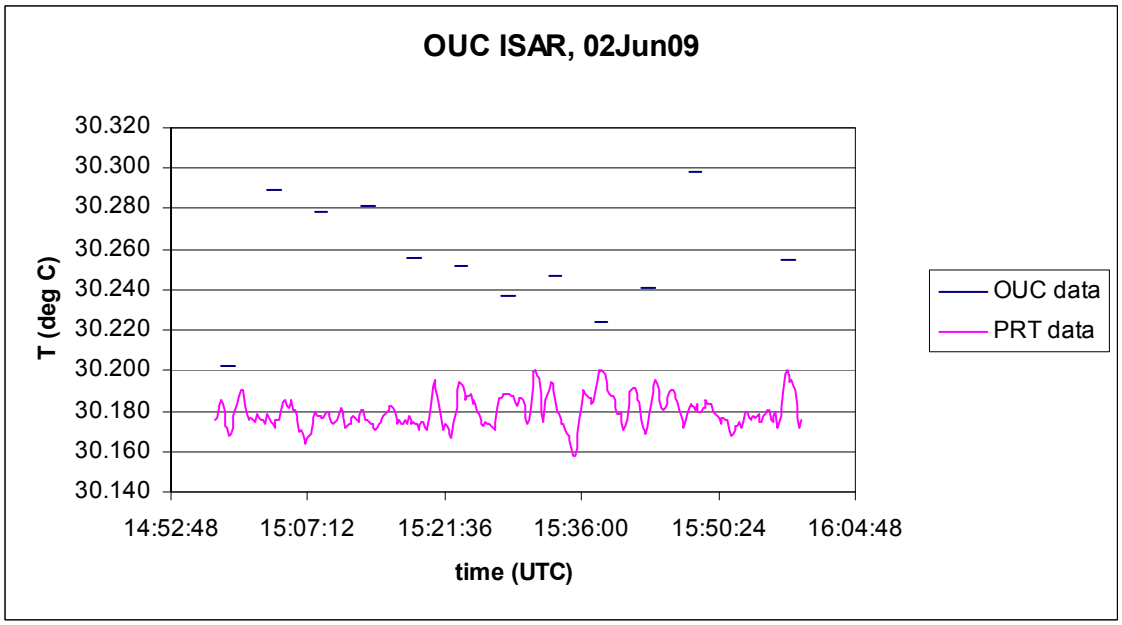

Figure 3.8.7: OUC ISAR radiometer viewing the NPL blackbody at 30 °C,
1st measurement, <Radiometer measurement> – <BB temperature> = 0.059 K,
(brackets indicate average over time interval shown)

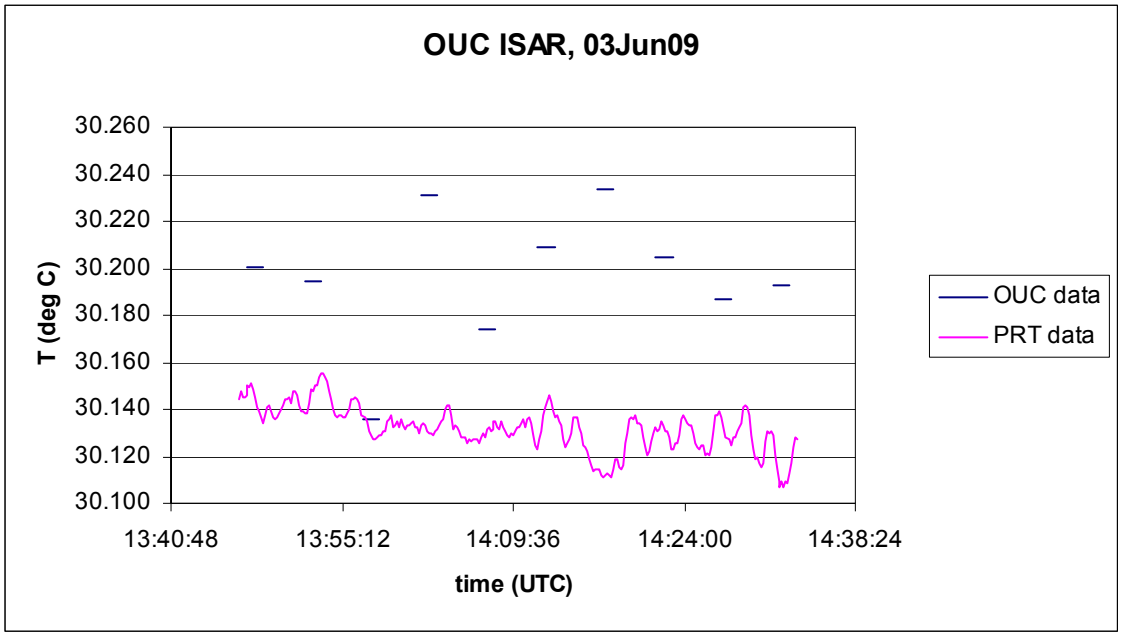

Figure 3.8.8: OUC ISAR radiometer viewing the NPL blackbody at 30 ^{o}C,
2nd measurement, <Radiometer measurement> – <BB temperature> = 0.048 K,
(brackets indicate average over time interval shown)

3.9 Rosenstiel School of Marine and Atmospheric Science (RSMAS) University of Miami

3.9.1 Contact information

RSMAS contact for the comparison: Profesor Peter Minnett
Address: 4600 Rickenbacker Causeway, Miami, FL 33149, USA.
Email: pminnett@rsmas.miami.edu

3.9.2 Radiometer used in the comparison

Make and type of radiometer: Marine-Atmosphere Emitted Radiance Interferometer (MAERI) (http://ams.allenpress.com/perlserv/?request=get-document&doi=10.1175%2F1520-0426(2001)018%3C0994:TMAERI%3E2.0.CO%3B2&ct=1).

Outline technical description of instrument: The instrument is an FT based radiometer designed and built by RSMAS and operating over the spectral range 3 μm to 18 μm with a FOV of 2.58 degrees. It operates with two internal calibration black bodies (one at ambient and the other ~60 °C) and views both nadir and azimuth as one measurement sequence.

Establishment or traceability route for primary calibration including date of last realisation and breakdown of uncertainty:

The thermometers measuring the internal reference black bodies are traceable to NIST with an uncertainty of 0.05 K

Uncertainty

The uncertainty quoted for MAERI is 0.05 K taken from above reference

3.9.3 Results

The MAERI radiometer took part in the Miami ocean surface temperature comparison. The first set of data provided by RSMAS (referred to as the uncorrected data) did not include the correction for the sea-water emissivity at 55^{o}. Given the importance of full transparency in the comparison this result is recorded and presented. However, after further review of the data it was later noticed that a key correction (sea water emissivity) which is normally applied had been omitted. Data referred to as the "corrected" data include the correction for the sea-water emissivity at 55^{o}. Figure 3.9.1 shows the uncorrected ocean surface temperature values reported by the MAERI radiometer. Figure 3.9.2 shows the difference of the uncorrected ocean surface temperature values reported by the MAERI radiometer from the mean of the four continuously monitoring radiometers. Figure 3.9.3 shows the difference of the corrected ocean surface temperature values reported by the MAERI radiometer from the mean of the four continuously monitoring radiometers. Figure 3.9.4 shows the difference of the corrected ocean surface temperature values reported by the MAERI radiometer from the corresponding values reported by the ISAR radiometer.

3.9.3.1 MAERI uncorrected ocean temperature measurements

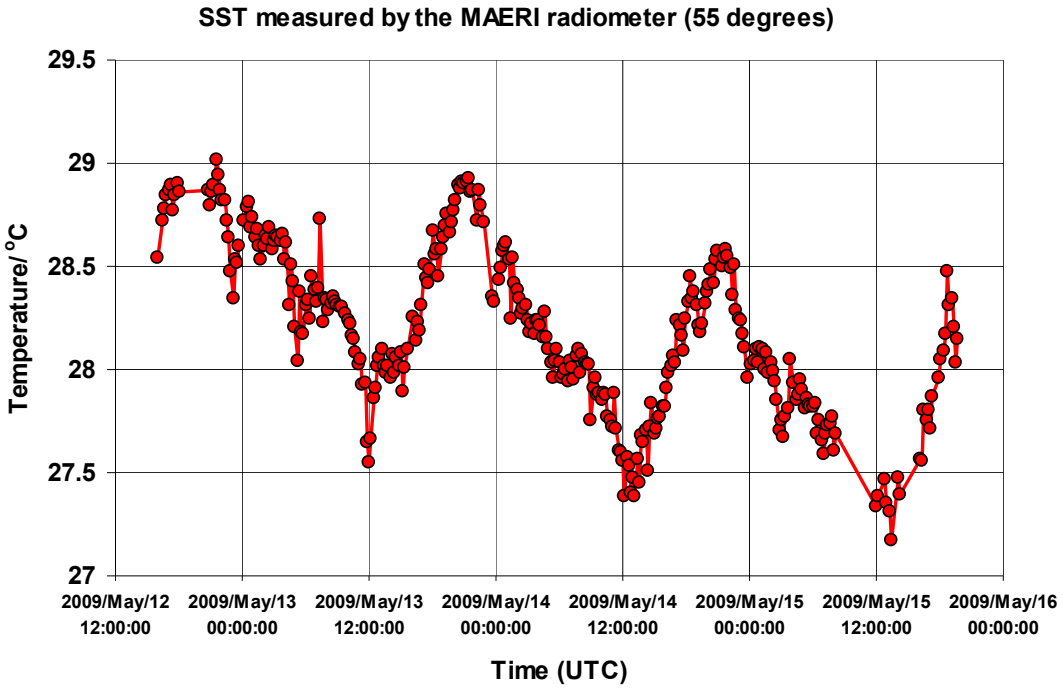

Figure 3.9.1: Uncorrected ocean surface temperature measurements completed by the MAERI radiometer over the 12th May to 15th May period. Measurements were completed at 55°.

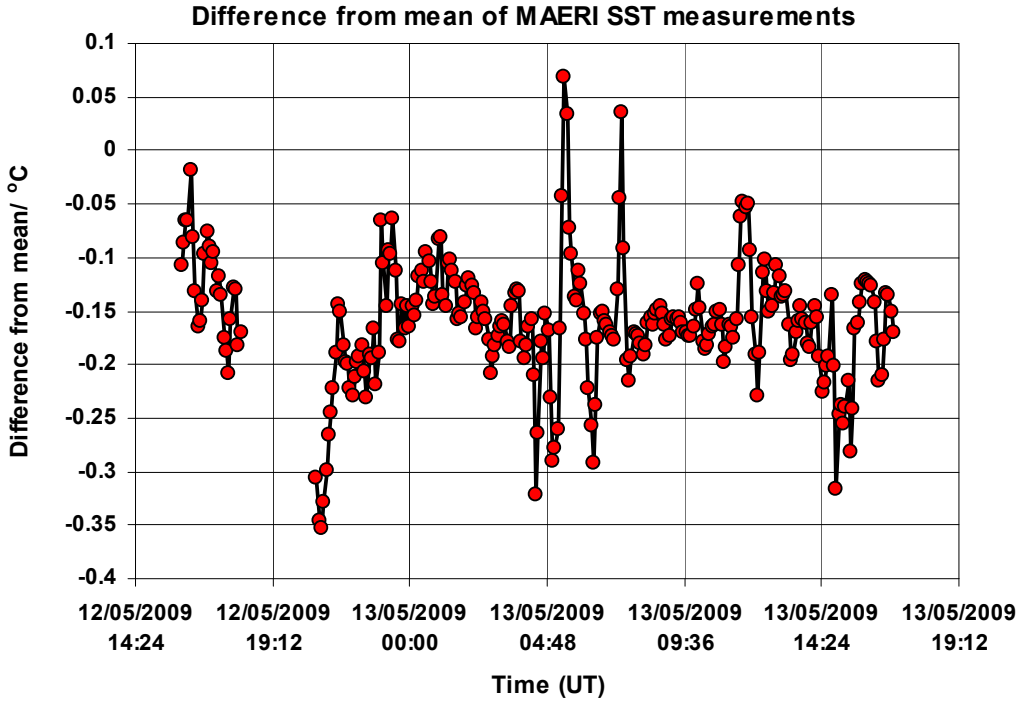

Figure 3.9.2: Difference of the uncorrected ocean surface temperature measurements completed by the MAERI radiometer from the mean of the four continuously measuring radiometers (data only available over a limited time period).

3.9.3.2 MAERI corrected ocean temperature measurements.

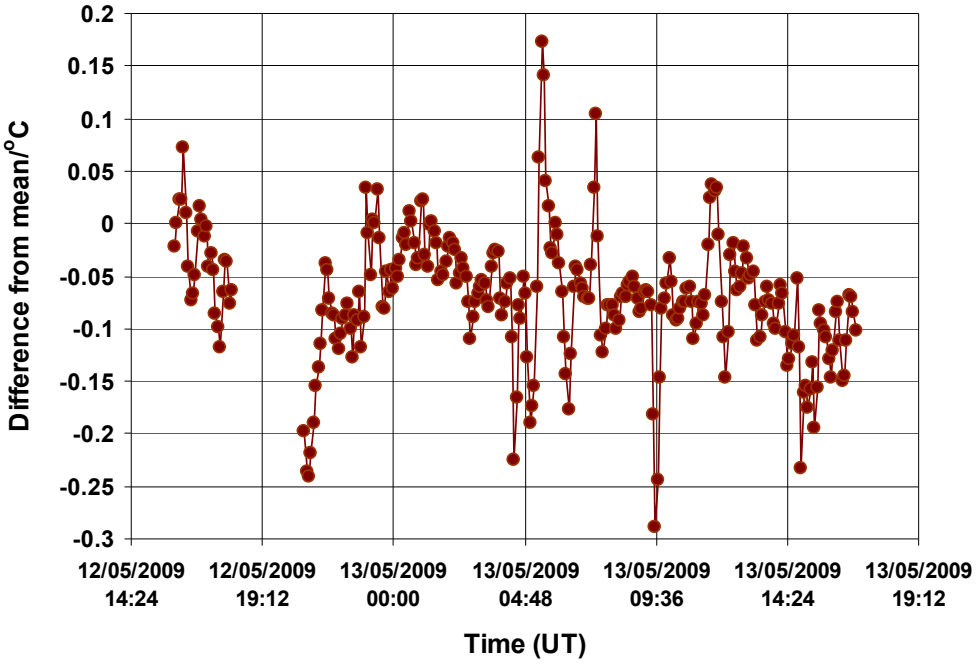

Figure 3.9.3: Difference in the corrected ocean surface temperature measurements of the MAERI radiometer from the mean of the four continuously measuring radiometers, (data only available over a limited time period).

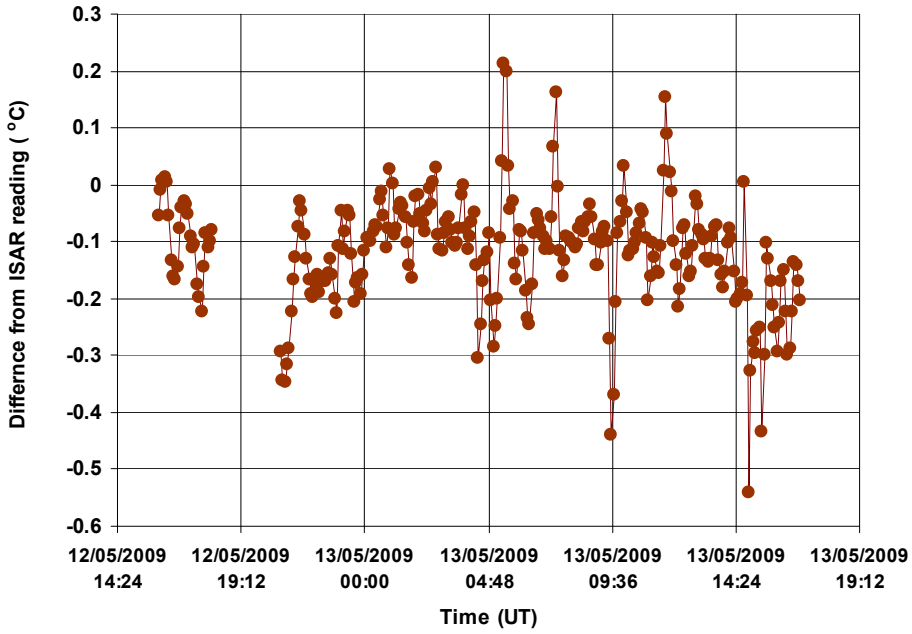

Figure 3.9.4: Difference in the corrected ocean surface temperature measurements of the MAERI radiometer from the corresponding ISAR radiometer measurements.

3.10 STFC Rutherford Appleton Laboratory (RAL)

3.10.1 Contact information

RAL contact for the comparison: Dr Tim Nightingale
Address: Chilton, Didcot, Oxon, OX11 0QX, UK
Email: tim.nightingale@stfc.ac.uk

3.10.2 Radiometer used in the comparison

Make and type of radiometer: Scanning Infrared Sea Surface Temperature Radiometer (SISTeR) manufactured by RAL. Further information on this radiometer can be found at: (http://www.atsr.rl.ac.uk/validation/sister/sis_inst/index.shtml)

Outline technical description of instrument: The instrument is a RAL manufactured pyroelectric spectrally filtered (selectable by wheel) based radiometer with two internal reference black bodies, one operating at ambient and the other heated ~10 K above ambient. During operation the radiometer views both the black bodies and the scene as a single measurement. In this comparison, a filter centred on 10.8 μm and an entrance FOV of 13 degrees was used.
Establishment or traceability route for primary calibration including date of last realisation and breakdown of uncertainty:
The SISTeR radiometer is calibrated traceable to a CASOTS Mk 1 external black body and its internal black body thermometers have been calibrated at Oxford University.

Uncertainty

Estimate of "bias" (Type B) **25 to 30 mK**

"the random noise on a single standard 0.8 s sample is about 30 mK – 35 mK at brightness temperatures near to ambient"

Type A **30 to 35 mK**

No difference indicated for ocean or lab measurements

3.10.3 Results

The SISTeR radiometer took part in the NPL blackbody, RSMAS blackbody and Miami ocean temperature comparisons. Figures 3.10.1 to 3.10.7 show the temperature values reported by SISTeR radiometer when monitoring the NPL blackbody cavity temperature. Figure 3.10.8 shows the temperature values reported by SISTeR radiometer when monitoring the NPL gallium blackbody cavity temperature. Figures 3.10.9 to 3.10.13 show the temperature values reported by the SISTeR radiometer when monitoring the RSMAS blackbody cavity temperature. Figure 3.10.14 shows the temperature values reported by SISTeR radiometer when monitoring the NIST blackbody cavity temperature when the diameter of the NIST blackbody aperture was set to 45 mm. Figure 3.10.15 shows the corresponding plot when the diameter of the NIST blackbody aperture was set to 100 mm. Figure 3.10.16 shows the ocean temperature values reported by SISTeR radiometer, while Figure 3.10.17 shows the difference of these values from the mean of the four continuously measuring radiometers. Finally, Figure 3.10.18 shows the difference of the ocean temperature values reported by SISTeR from the values reported by the ISAR radiometer.

3.10.3.1 Comparison to the NPL variable temperature blackbody

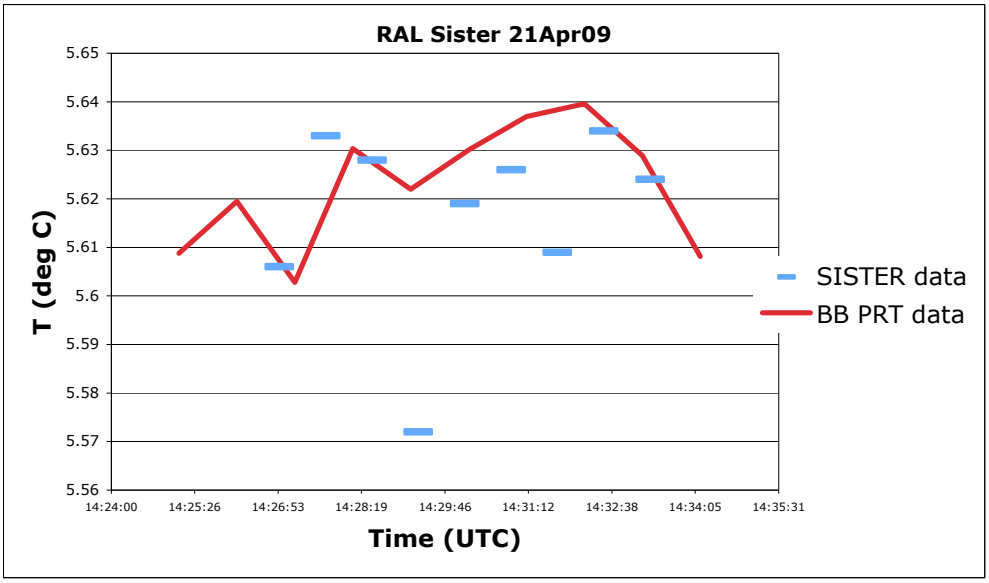

Figure 3.10.1: SISTeR radiometer viewing the NPL blackbody at 5 °C, 1st measurement
<Radiometer measurement> – <BB temperature> = -0.006 K
(brackets indicate average over time interval shown)

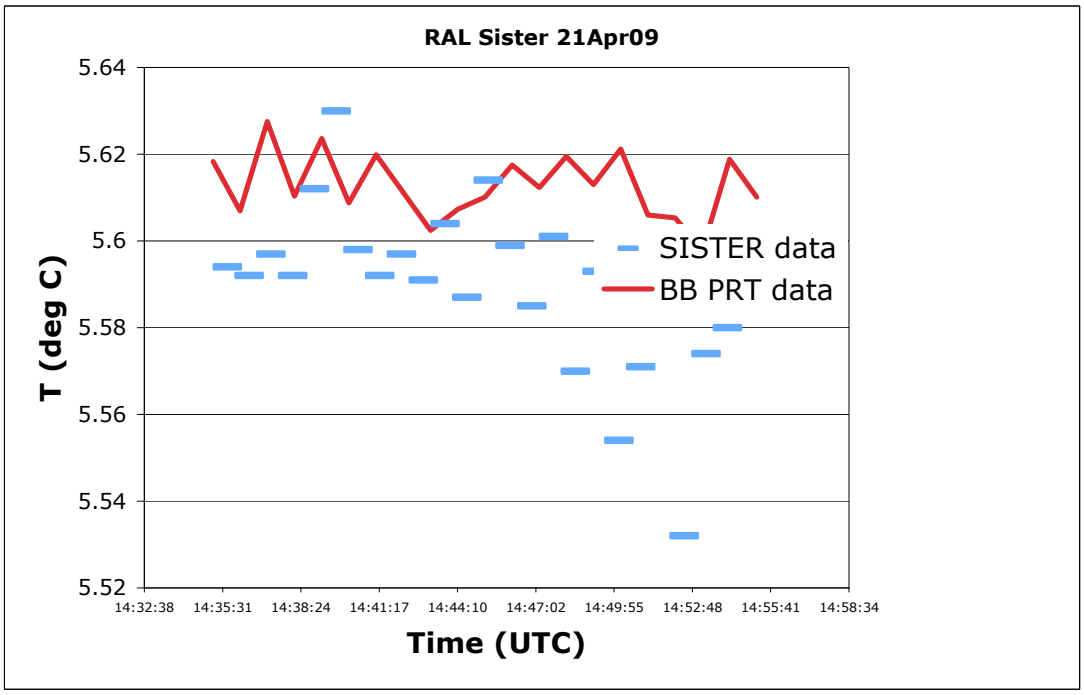

Figure 3.10.2: SISTeR radiometer viewing the NPL blackbody at 5 °C,
2nd measurement. <Radiometer measurement> – <BB temperature> = -0.023 K
(brackets indicate average over time interval shown)

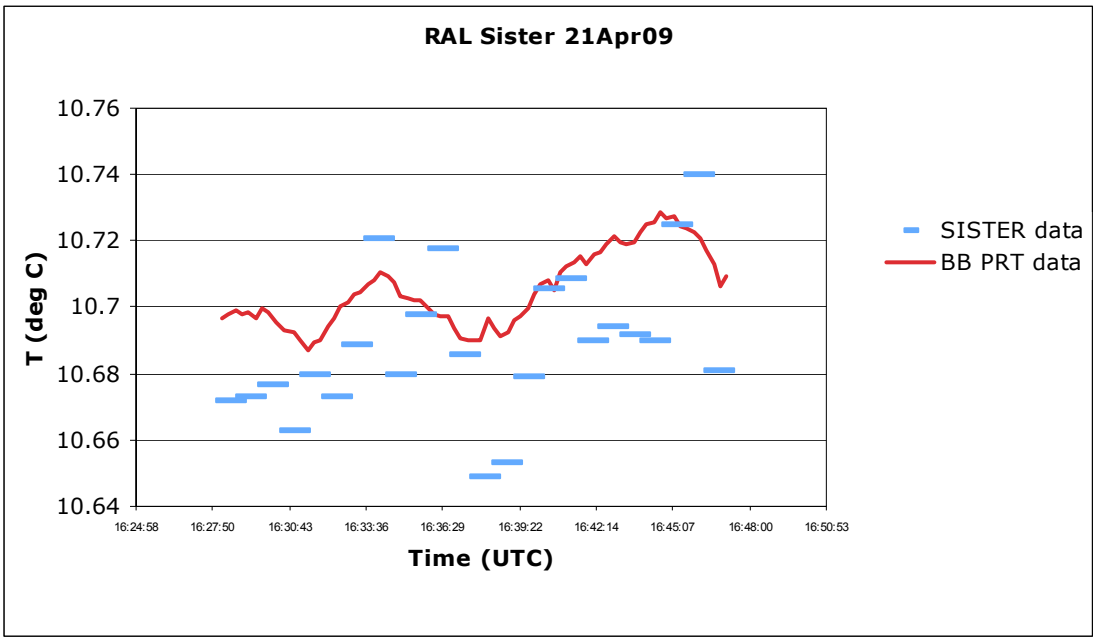

Figure 3.10.3: SISTeR radiometer viewing the NPL blackbody at 10 °C,
1st measurement. <Radiometer measurement> – <BB temperature> = -0.016 K,
(brackets indicate average over time interval shown)

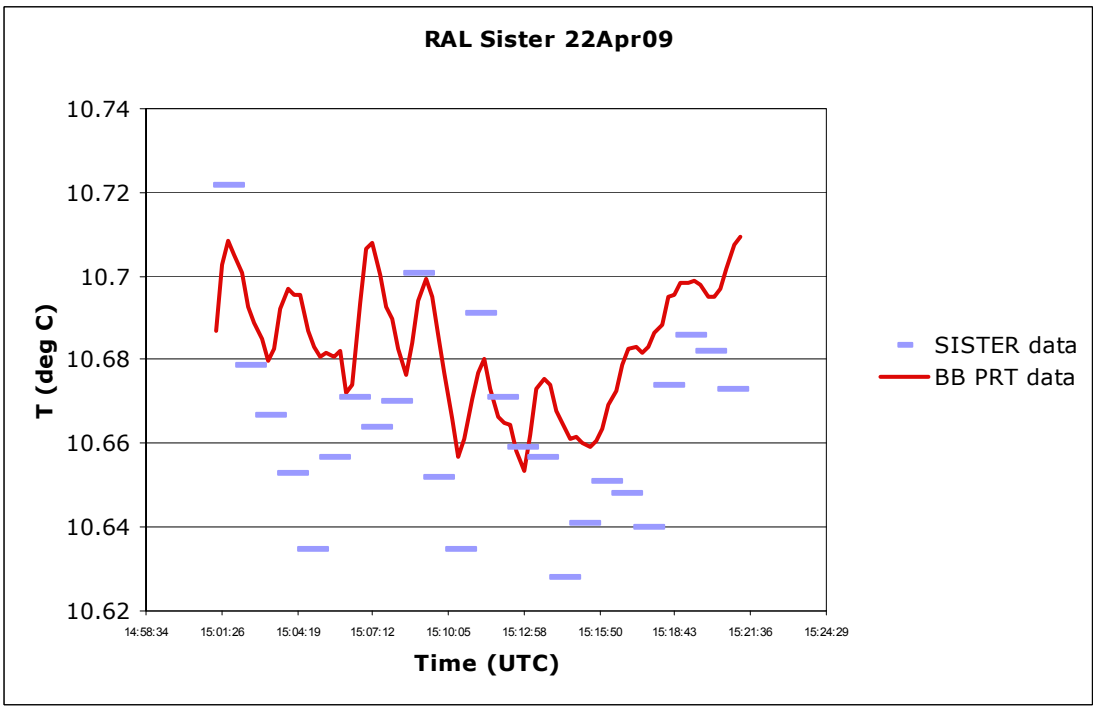

Figure 3.10.4: SISTeR radiometer viewing the NPL blackbody at 10 °C,
2nd measurement. <Radiometer measurement> – <BB temperature> = -0.019 K,
(brackets indicate average over time interval shown)

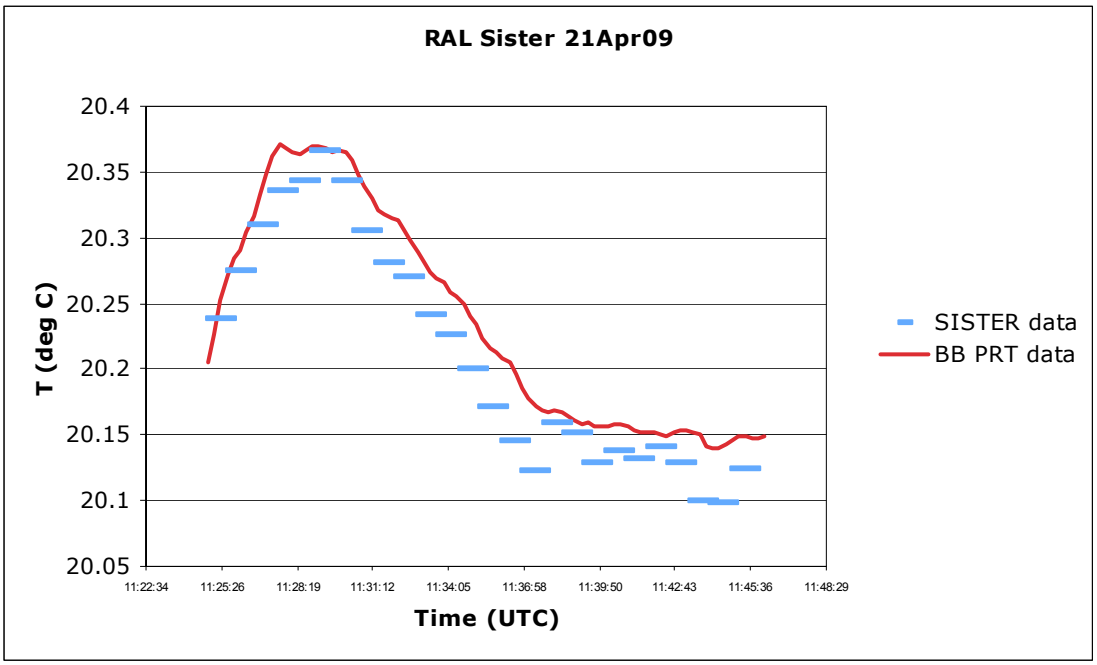

Figure 3.10.5: SISTeR radiometer viewing the NPL blackbody at 20 °C,
1st measurement. <Radiometer measurement> – <BB temperature> = -0.025 K,
(brackets indicate average over time interval shown)

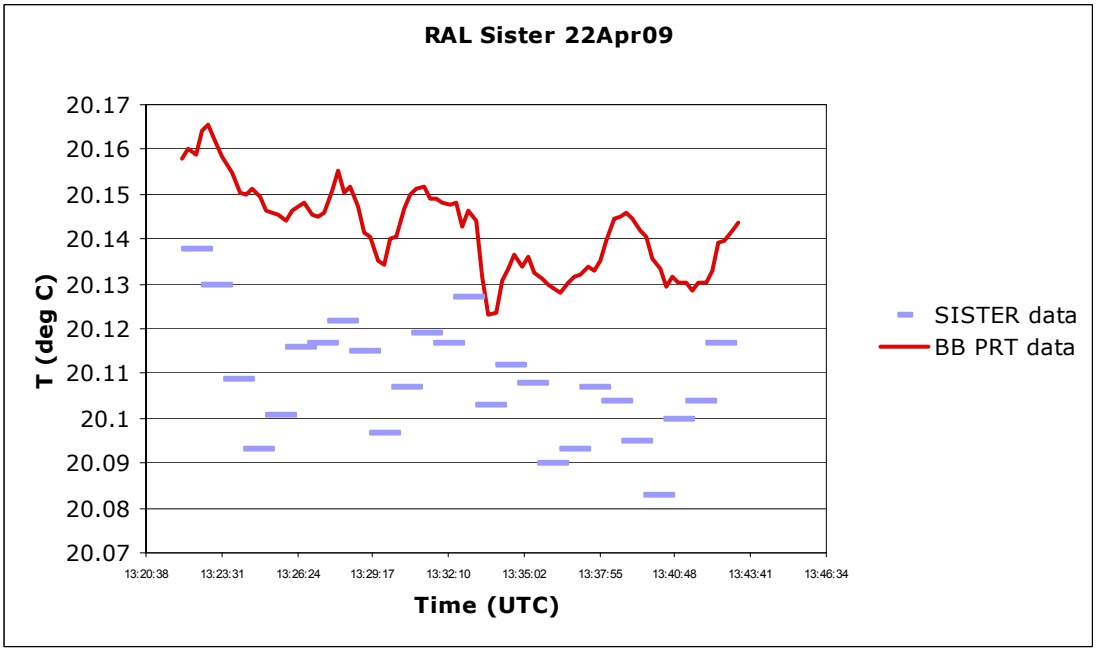

Figure 3.10.6: SISTeR radiometer viewing the NPL blackbody at 20 °C,
2nd measurement. <Radiometer measurement> – <BB temperature> = -0.033 K,
(brackets indicate average over time interval shown)

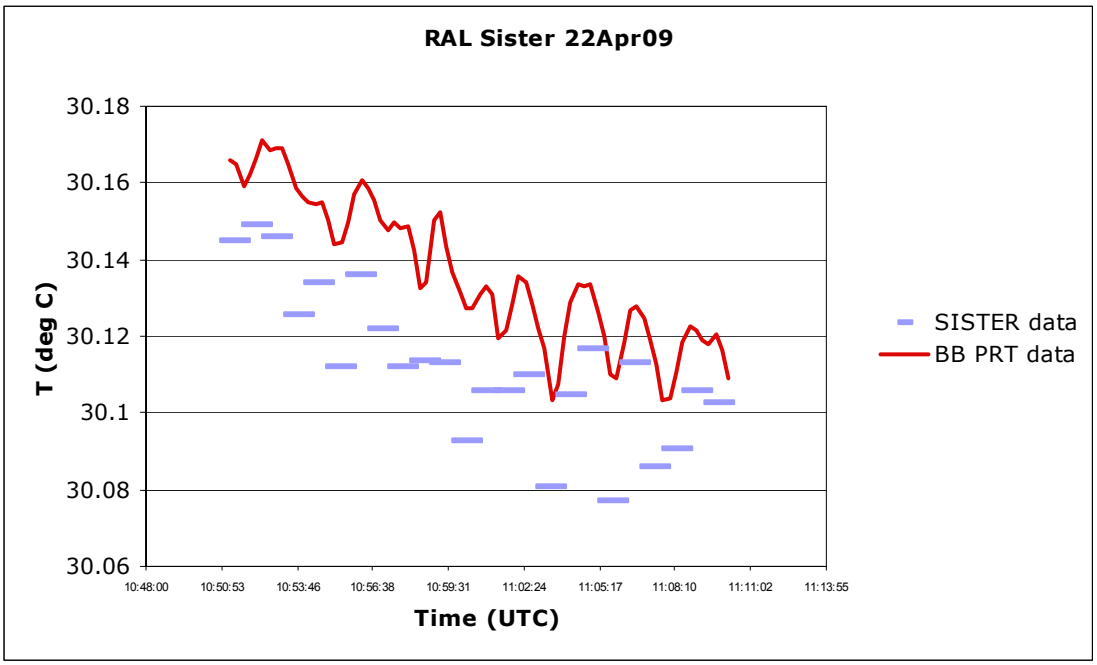

Figure 3.10.7: SISTeR radiometer viewing the NPL blackbody at 30 °C,
<Radiometer measurement> – <BB temperature> = -0.024 K,
(brackets indicate average over time interval shown)

3.10.3.2 Comparison to the NPL Gallium fixed point blackbody

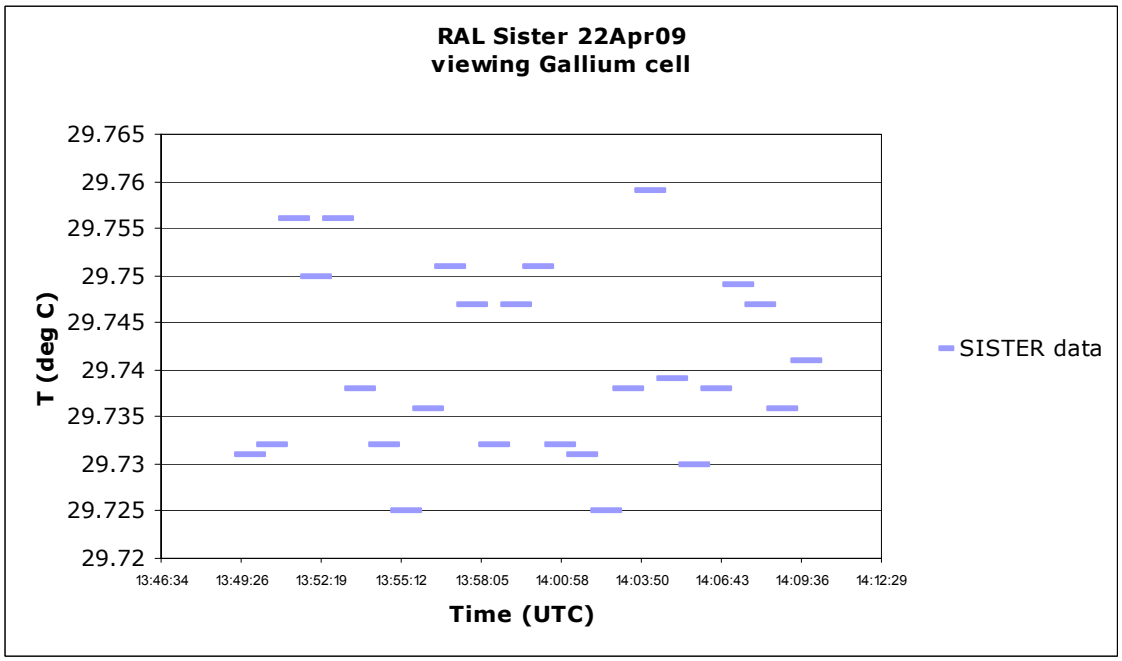

Figure 3.10.8: SISTeR radiometer viewing the gallium fixed point blackbody.
<Radiometer measurement> – gallium melting temperature = -0.024 K,
(brackets indicate average over time interval shown)

3.10.3.2 Comparison to the RSMAS blackbody

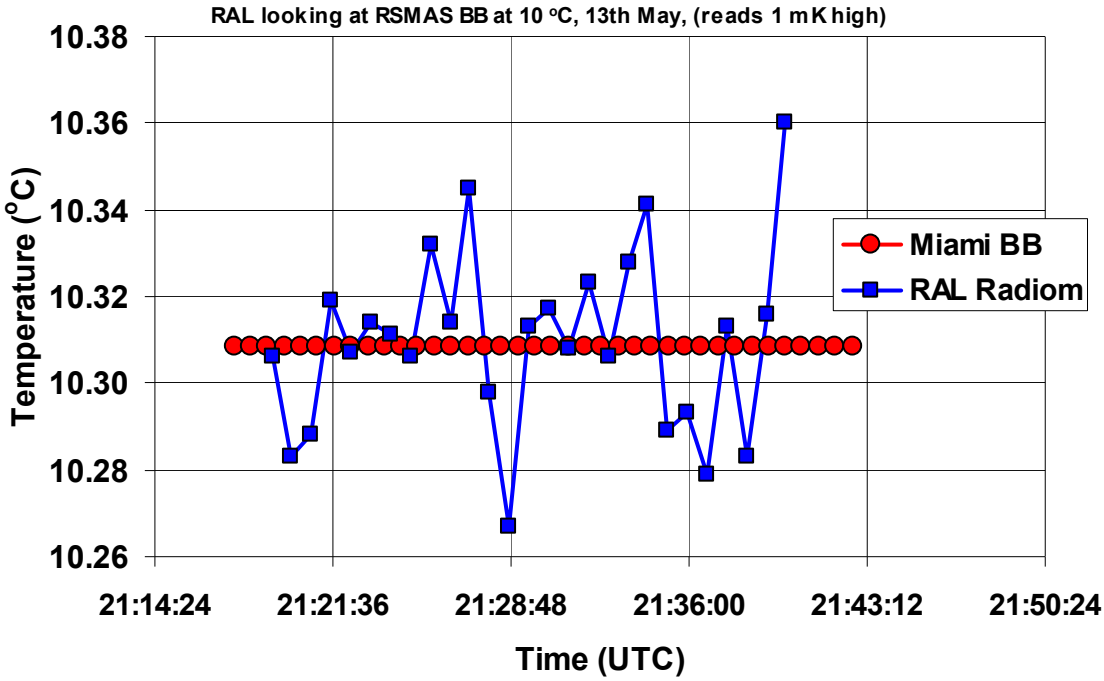

Figure 3.10.9: SISTeR radiometer viewing the RSMAS blackbody at 10 °C.
<Radiometer measurement> – <BB temperature> = 0.001 K,
(brackets indicate average over time interval shown)

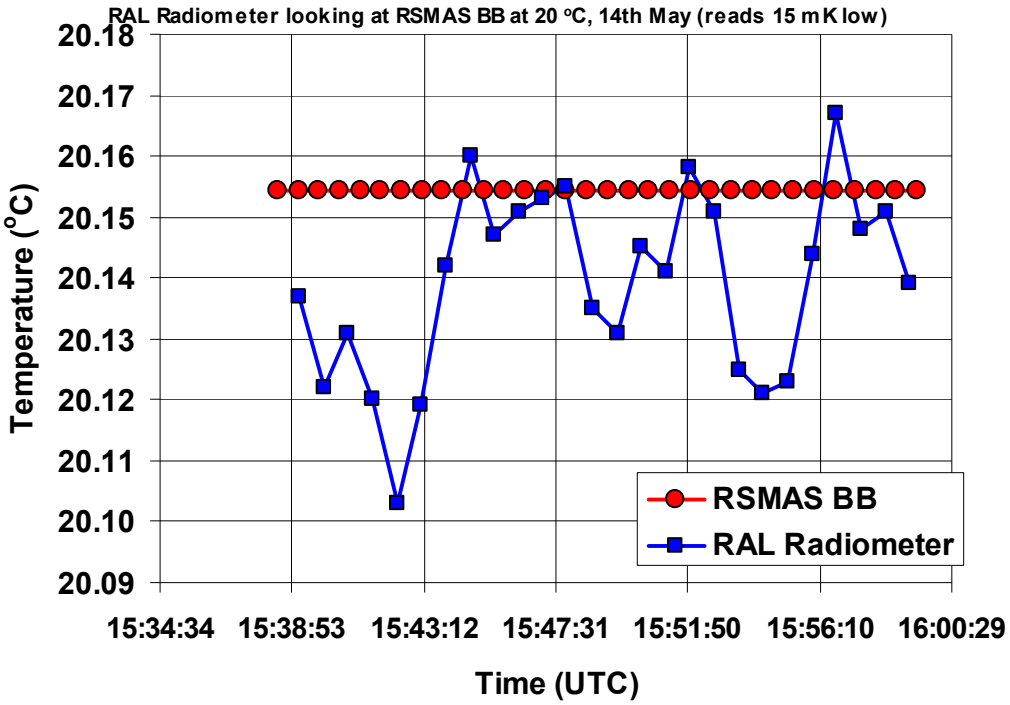

Figure 3.10.10: SISTeR radiometer viewing the RSMAS blackbody at 20 °C,
1st measurement. <Radiometer measurement> – <BB temperature> = -0.015 K
(brackets indicate average over time interval shown)

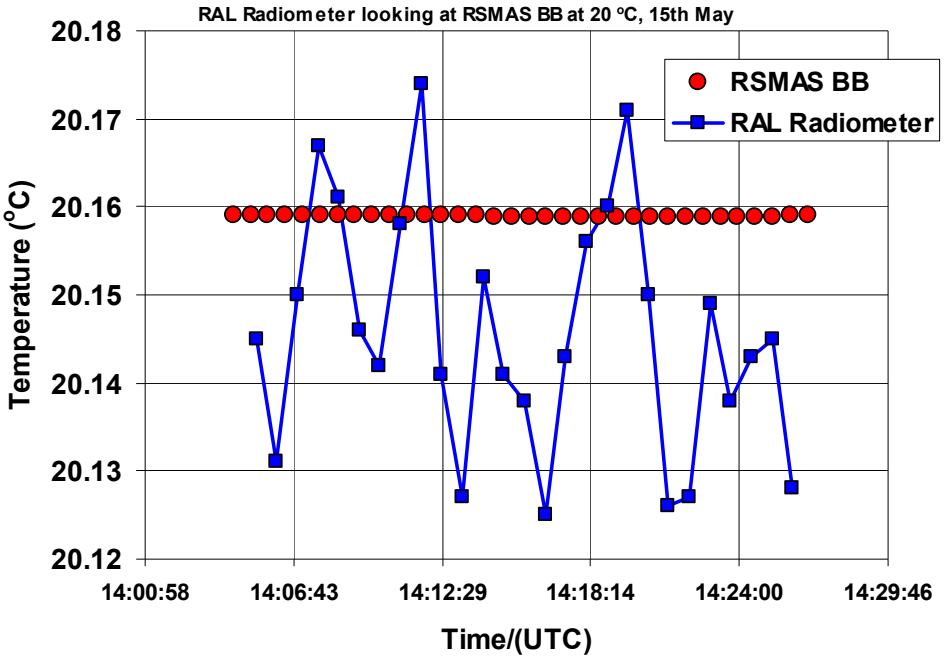

Figure 3.10.11: SISTeR radiometer viewing the RSMAS blackbody at 20 °C, 2nd measurement. <Radiometer measurement> – <BB temperature> = -0.013 K (brackets indicate average over time interval shown)

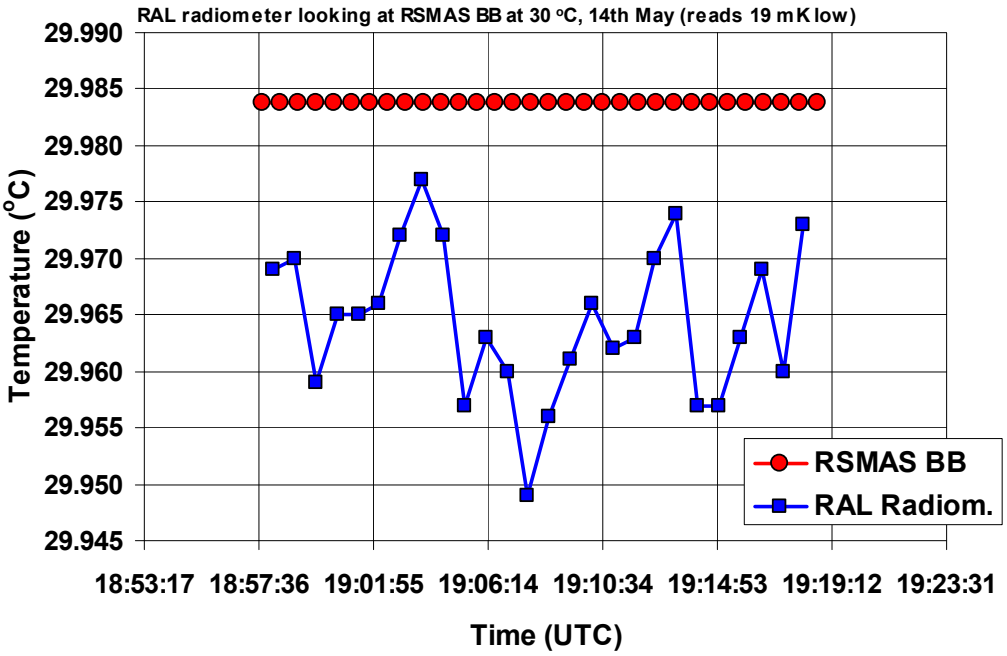

Figure 3.10.12: SISTeR radiometer viewing the RSMAS blackbody at 30 °C, 1st measurement. <Radiometer measurement> – <BB temperature> = -0.019 K (brackets indicate average over time interval shown)

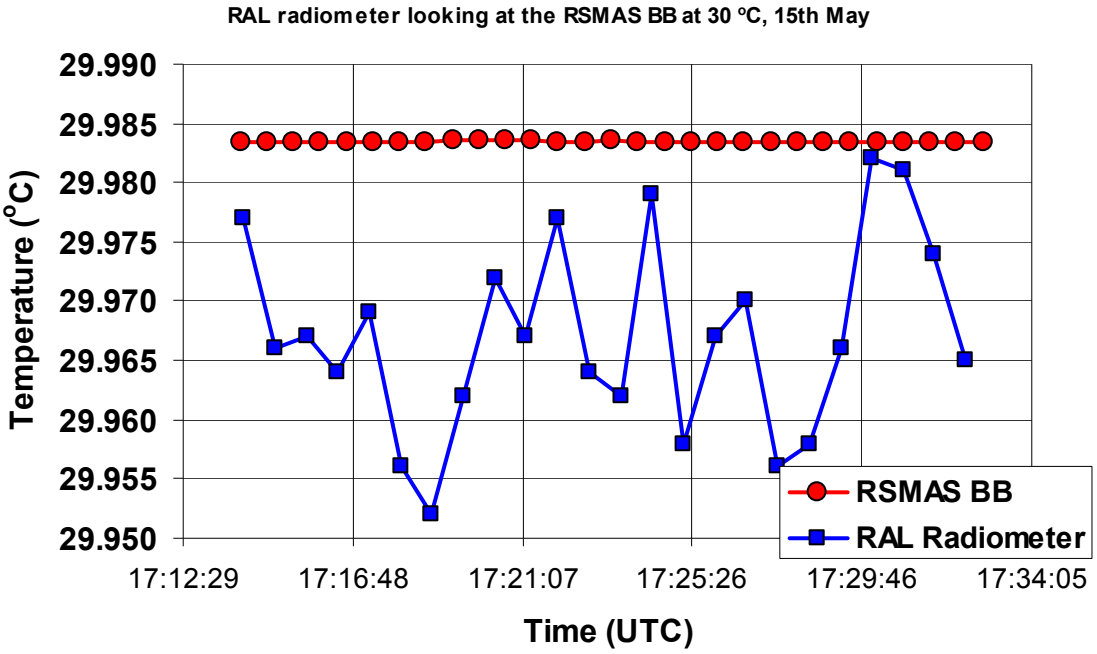

Figure 3.10.13: SISTeR radiometer viewing the RSMAS blackbody at 30 °C, 2nd measurement. <Radiometer measurement> – <BB temperature> = -0.015 K (brackets indicate average over time interval shown)

3.10.3.3 Comparison of the SISTeR radiometer to the NIST blackbody

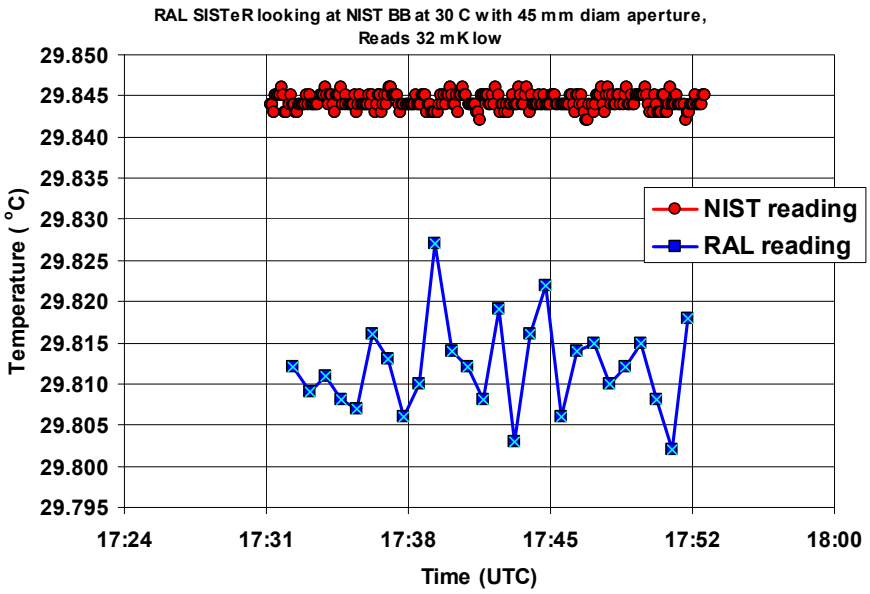

Figure 3.10.14: SISTeR radiometer viewing the NIST blackbody at 30 °C, (45 mm diameter aperture).
<Radiometer measurement> – <BB temperature> = -0.032 K

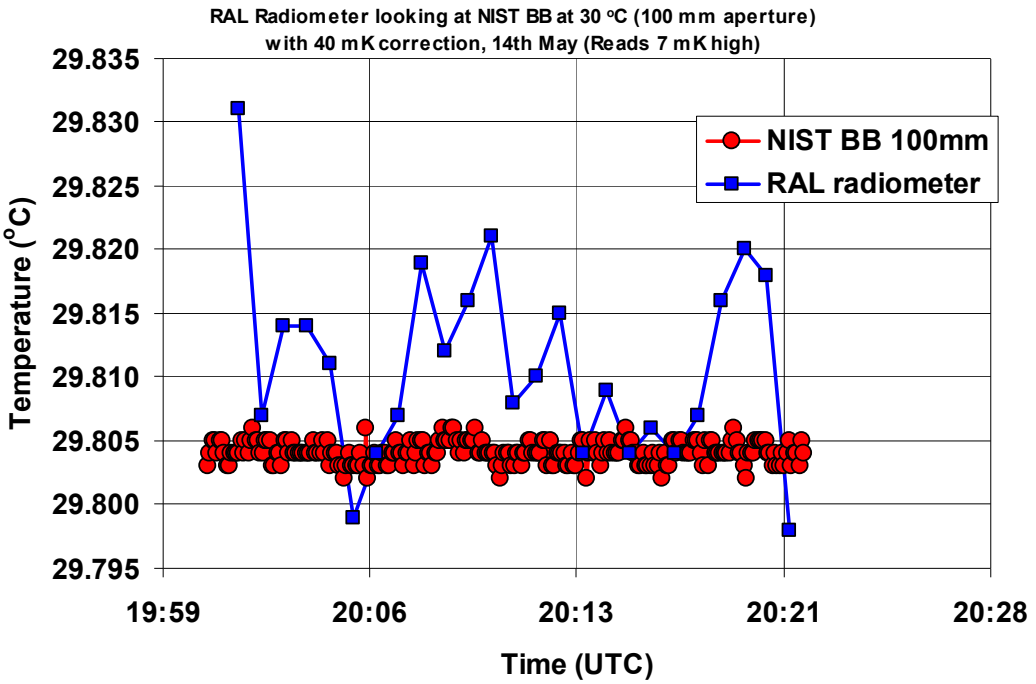

Figure 3.10.15: SISTeR radiometer viewing the NIST blackbody 30 °C,
(100 mm diameter aperture).
<Radiometer measurement> – <BB temperature> = 0.007 K

3.10.3.4SISTeR radiometer Ocean temperature measurements

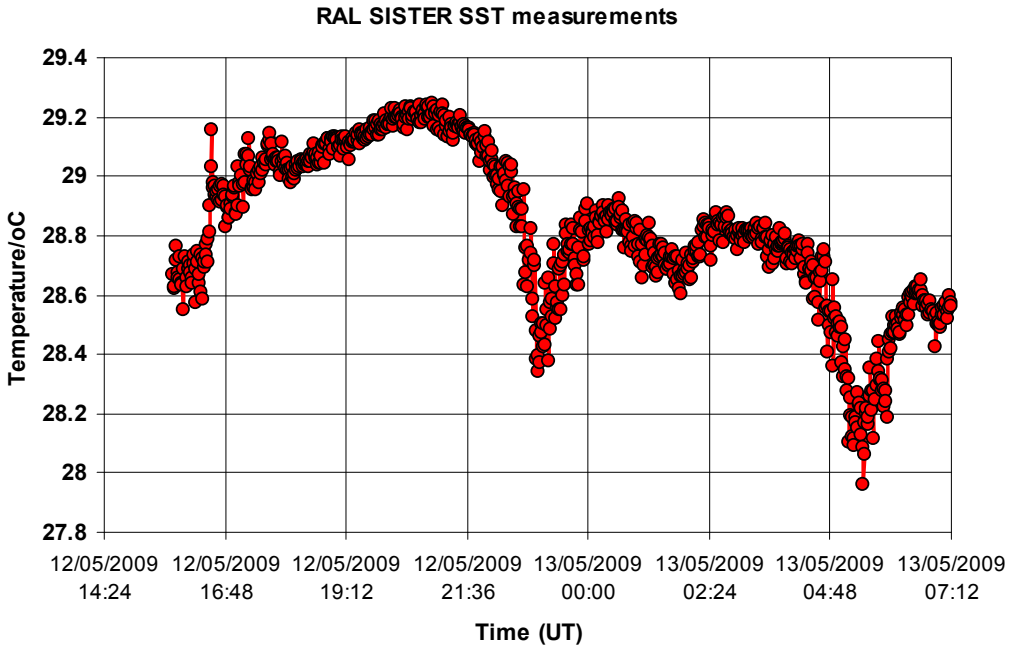

Figure 3.10.16: Ocean surface temperature measurements completed by the RAL SISTeR radiometer over the 12th May to 13th May period.

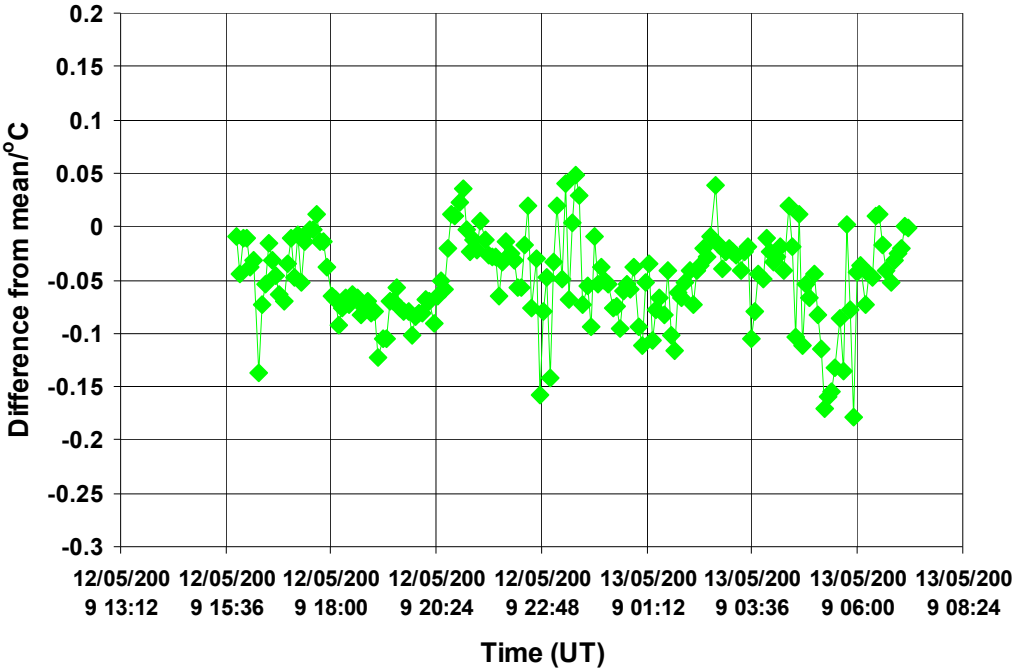

Figure 3.10.17: Difference in the ocean surface temperature measured by the RAL SISTeR radiometer from the mean of the four continuously measuring radiometers
(data only available over a limited time period).

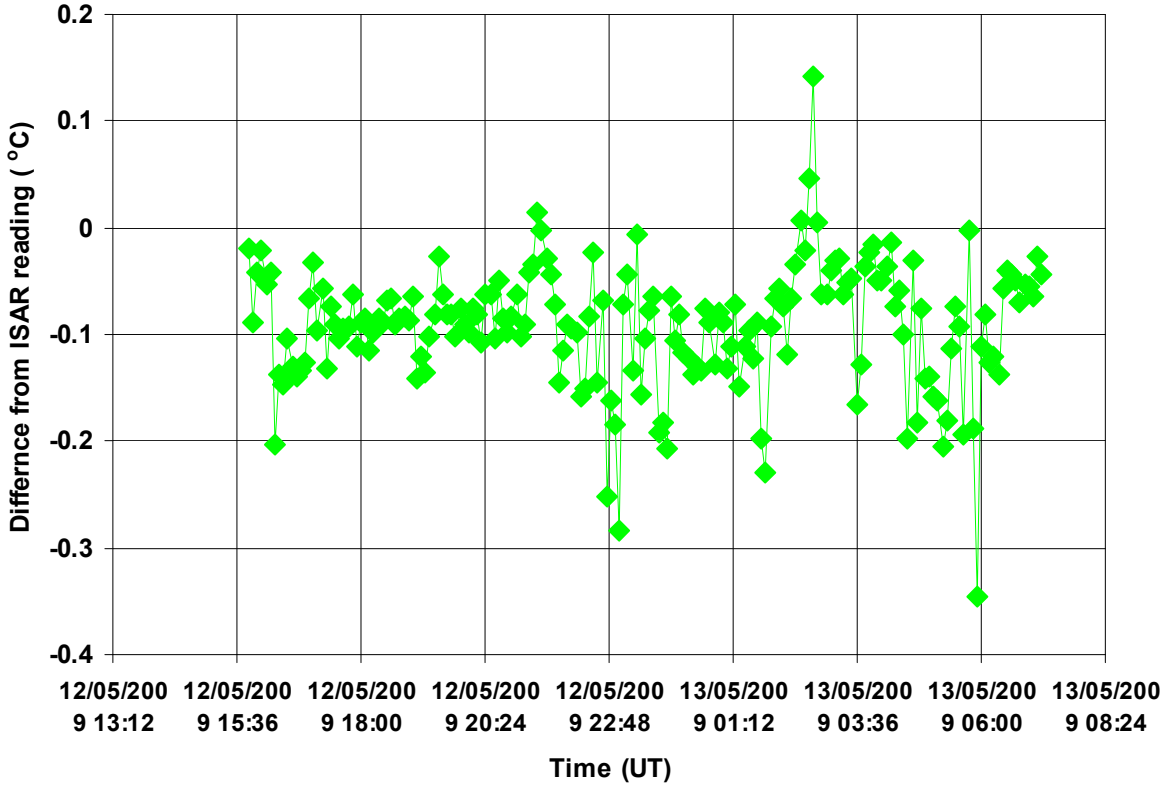

Figure 3.10.18: Difference in the ocean temperature measured by the RAL SISTeR radiometer from the corresponding values measured by the ISAR radiometer.

3.11 Summary of the results

This section provides a summary of the result provided by the participants of the CEOS IR comparison of brightness temperature of the reference (SI traceable) blackbodies completed at NPL and at the University of Miami in April and May 2009. It also provides a summary of the ocean surface temperature comparison completed at RSMAS.

3.11.1 Summary of the comparison of the radiometers to the reference blackbodies

The following set of Tables and Figures represent the measurements completed by participants in the laboratory against reference, SI traceable, black bodies. It is important to stress that the temperatures of the reference blackbodies were nominal and, of course, not necessarily perfectly stable. The plots shown in the Figures in this Section compare the measurements provided by the participating radiometers from the corresponding values of the temperature of the cavity of the reference black bodies. In some cases this may be a single set of data points taken on one day, in others it could be the mean of two days. The uncertainty bars represent the standard uncertainty (k=1) taken from the pre-draft. Uncertainty bars are provided whenever these were available.

Table 3.11.1 shows the difference of the measurements completed by participants on the NPL variable temperature blackbody from the blackbody temperature.

Table 3.11.1: Difference of the measurements completed by participants on the NPL variable temperature blackbody from the blackbody temperature.

	Set Temperature °C	NPL VTBB 1st measur. mK	NPL VTBB 2nd measur. mK
GOTA	30	1147	
8-14 µm	20	9	79
	10	-1276	-1165
	5	-2137	
GOTA	30	67	
11.35 µm	20	189	189
	10	254	235
	5	293	
GOTA	30	87	
10.65 µm	20	199	139
	10	204	185
	5	243	
GOTA	30	-43	
9.1 µm	20	169	109
	10	54	185
	5	253	
GOTA	30	-93	
8.7 µm	20	169	129
	10	74	185
	5	253	
Canary	30	47	
8.3 µm	20	149	169
	10	44	125
	5	133	
IPL	30	-393	-298
CE312-2	20	162	190
10.54 µm	10 (uncorrected)	691	683
	10 (corrected)	40	14
	5 (uncorrected)	956	
	5 (corrected)	-104	
IPL	30	-278	-283
CE312-2	20	136	154
11.29 µm	10 (uncorrected)	644	633
	10 (corrected)	74	62
	5 (uncorrected)	860	
	5 (corrected)	30	
IPL	30	-333	-178
CE312-2	20	150	240
10.57 µm	10 (uncorrected)	716	655
	10 (corrected)	26	-40
	5 (uncorrected)	888	
	5 (corrected)	-16	
IPL	30	-438	-507
CE312-2	20	74	228
9.15 µm	10 (uncorrected)	881	934
	10 (corrected)	80	125
	5 (uncorrected)	1434	
	5 (corrected)	206	
IPL	30	-492	-413
CE312-2	20	169	225
8.69 µm	10 (uncorrected)	896	773
	10 (corrected)	-93	-223
	5 (uncorrected)	1502	
	5 (corrected)	238	
IPL	30	-402	-197
CE312-2	20	173	296
8.44 µm	10 (uncorrected)	983	809
	10 (corrected)	291	127
	5 (uncorrected)	1538	
	5 (corrected)	486	

	Set Temperature °C	NPL VTBB 1st measur. mK	NPL VTBB 2nd measur. mK
Valencia DEPT	30	-108	
CE312-1-Unit 1	20	118	79
10.7 µm	10	321	292
	5	416	
Valencia DEPT	30	-160	
CE312-1-Unit 1	20	221	160
12 µm	10	464	442
	5	701	
Valencia DEPT	30	66	
CE312-1-Unit 1	20	82	101
10.8 µm	10	140	145
	5	208	
Valencia DEPT	30	372	
CE312-1-Unit 1	20	83	104
8.8 µm	10	-179	-154
	5	-209	
Valencia DEPT	30	-57	
CE312-1-Unit 2	20	189	134
10.7 µm	10	423	366
	5	529	
Valencia DEPT	30	14	
CE312-1-Unit 2	20	233	243
12 µm	10	467	383
	5	557	
Valencia DEPT	30	104	
CE312-1-Unit 2	20	204	168
10.8 µm	10	289	237
	5	328	
Valencia DEPT	30	-12	
CE312-1-Unit 2	20	225	153
8.8 µm	10	514	392
	5	605	
RAL	30	-24	
SISTER	20	-25	-33
	10	-16	-19
Southampton	30	6	
ISAR	20	126	28
	10	87	69
	5	77	
OUC	30	59	48
ISAR	20	94	64
	10	145	136
	5	237	279
KIT	30	190	152
Heidronics	20	30	
KT - 15	10	-208	
	5	-632	

Table 3.11.2 shows the difference of the measurements completed by participants on the RSMAS blackbody and NIST blackbody (with 45 mm diameter and 100 mm diameter apertures) from the blackbody temperatures.

Table 3.11.2: Difference of the measurements completed by participants on the RSMAS blackbody and NIST blackbody (with 45 mm diameter and 100 mm diameter apertures) from the blackbody temperatures.

	Set Temperature oC	MAERI BB 1st measurement mK	MAERI BB 2nd measurement mK	NIST BB 100 mm Apert. mK	NIST BB 45 mm Apert. mK
RAL	30	-19	-16	7	-32
SISTER	20	-15	-13		
	10	1			
Southampton	30	12	18	27	-7
ISAR	20	21	39		
	10	138			
KIT	30	46	117		
Ground	20	56	91		
radiometer	15	71			
DLR	30	-730	-730	-914	
radiometer	20	-350	-750		
	10	-350	-260		
CEAM	30	121	160	133	
RA1	20	-215	-276		
radiometer	10	-652			
CEAM	30	122	175	129	
RA2	20	-242	-290		
radiometer	10	-744			
CEAM	30	160	204	173	
RA3	20	-166	-183		
radiometer	10	-618			
CEAM	30	51	-144	60	
RA4	20	-309	-268		
radiometer	10	-232			
CEAM	30	-244	-493	-274	
RA5	20	-594	-743		
radiometer	10	-899			
GOTA-Canary	30	880	940		610
8 - 14 µm	20	-80	-60		
Channel	10	-1470			
GOTA-Canary	30	140	130		220
11.35 µm	20	220	230		
Channel	10	300			
GOTA-Canary	30	180	160		230
10.65 µm	20	230	220		
Channel	10	300			
GOTA-Canary	30	210	220		180
9.1 µm	20	250	200		
Channel	10	310			
GOTA-Canary	30	190	150		170
8.7 µm	20	250	250		
Channel	10	400			
GOTA-Canary	30	320	240		240
8.1 µm	20	290	200		
Channel	10	310			

Table 3.11.3 tabulates the differences in the readings of the radiometer which participated in both the NPL and Miami comparisons from the temperature of the NPL reference blackbody (columns 2, 3 and 4, yellow background) and from the RSMAS water bath blackbody (columns 5, 6 and 7, orange background). Table 3.11.3 also shows the difference of the differences of the reading of the radiometers and the reference blackbodies (columns 8, 9 and 10, green background). The difference of the differences are well within the combined uncertainty of the measurements, confirming the agreement of the NPL and RSMAS temperature scales.

Table 3.11.3: Radiometer "errors" when reading the NPL and RSMAS blackbodies. The difference in the corresponding "errors" are within the combined uncertainty of the measurements.

	NPL (mK)			RSMAS (mK)			RSMAS-NPL (mK)		
BB temp.	10 °C	20 °C	30 °C	10 °C	20 °C	30 °C	10 °C	20 °C	30 °C
Radiometer									
ISAR	78	82	6	138	30	15	60	-52	9
RAL	-18	-29	-24	1	-14	-18	19	15	7
KIT	-208	30	171	71	74	82	279	44	-90
8-14 µm	-1221	44	1147	-1470	-70	910	-250	-114	-237
11.35 µm	245	189	67	300	225	135	56	36	68
10.65 µm	195	169	87	300	225	170	106	56	83
9.1 µm	120	139	-43	310	225	215	191	86	258
8.7 µm	130	149	-93	400	250	170	271	101	263
8.3 µm	85	159	47	310	245	280	226	86	233

Figure 3.11.1 shows the plot of the mean of the differences of the all the radiometer readings from the temperature of the NPL variable temperature blackbody, maintained at a nominal temperature of 5 °C (this figure shows the uncorrected output of the IPL radiometer). Some of these points represent a single set of data points taken on one day, while some others represent the mean of two measurements completed on different days. The uncertainty bars represent the standard uncertainty (k=1) or (1 σ) of the radiometers provided by the participants. Appendix 1 shows the uncertainty budget associated with the cavity temperature of NPL reference blackbody, along with the corresponding standard uncertainty. Figure 3.11.2 shows the plot of the mean of the differences of the all the radiometer readings from the temperature of the NPL variable temperature blackbody, maintained at a nominal temperature of 5 °C (this figure shows the corrected output of the IPL radiometer).

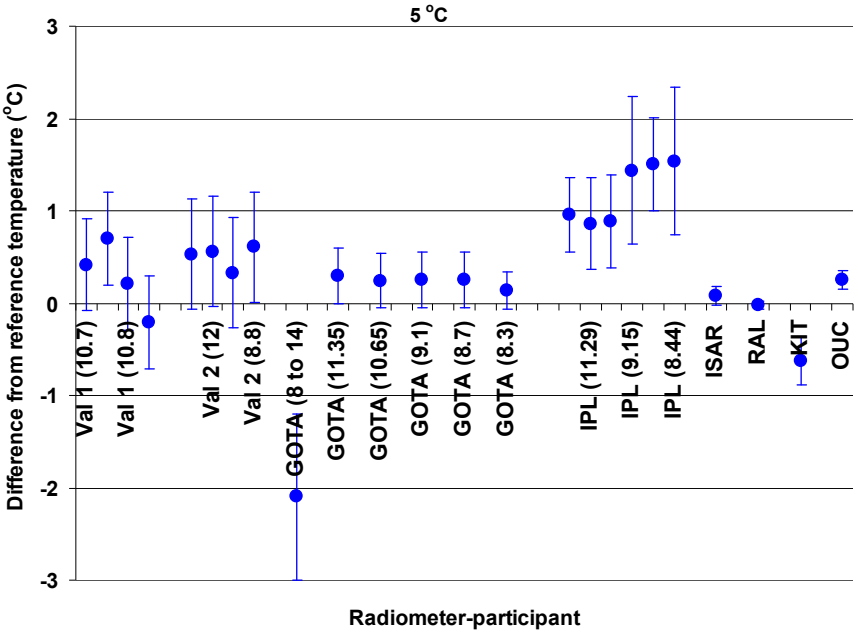

Figure 3.11.1: Plot of the mean of the differences of the radiometer readings from the temperature of the NPL variable temperature blackbody, maintained at a nominal temperature of 5 °C (this figure shows the uncorrected output of the IPL radiometer).

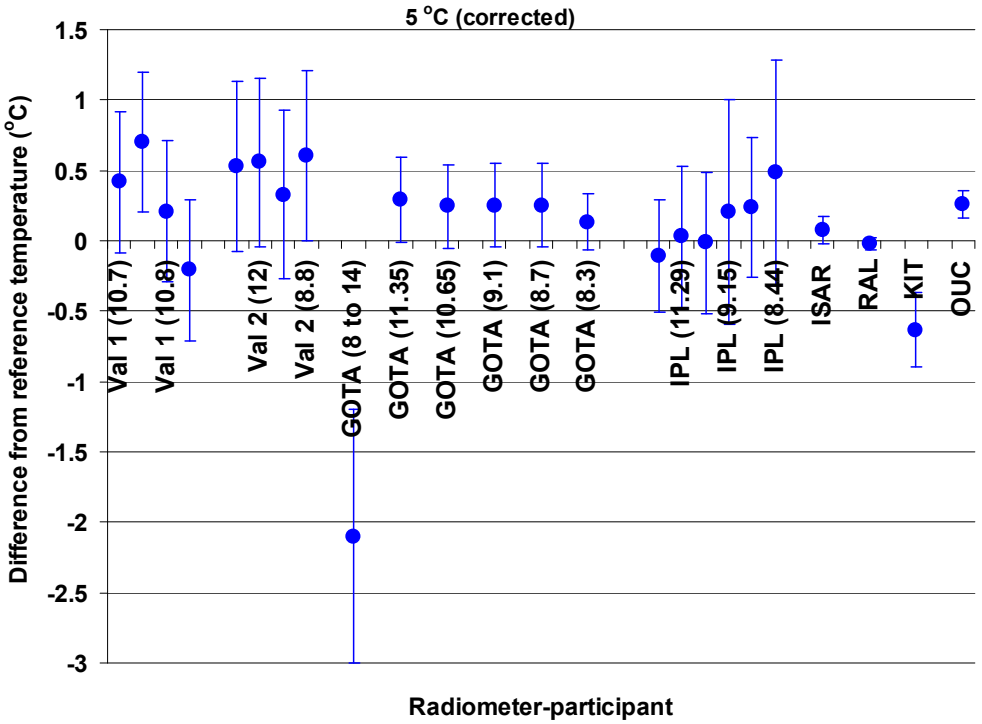

Figure 3.11.2: Plot of the mean of the differences of the radiometer readings from the temperature of the NPL variable temperature blackbody, maintained at a nominal temperature of 5 °C (this figure shows the corrected output of the IPL radiometer).

Figure 3.11.3 shows a plot of the mean of differences of the all the radiometer readings from the temperatures of the NPL variable temperature blackbody (blue circles) and the RSMAS water bath blackbody (red squares), both maintained at nominal temperatures of about 10 °C (this figure shows the uncorrected output of the IPL radiometer). Some of these points represent a single set of data points taken on one day, while some others represent the mean of two measurements completed on different days. The uncertainty bars represent the standard uncertainty (k=1) or (1 σ) of the radiometers provided by the participants. Appendix 1 shows the uncertainty budget associated with the cavity temperature of NPL reference blackbody. Appendix 2 lists the uncertainty (k=1) in the radiance temperature of the NIST water bath blackbody at different cavity temperatures. Figure 3.11.4 shows a plot of the mean of differences of the all the radiometer readings from the temperatures of the NPL variable temperature blackbody (blue circles) and the RSMAS water bath blackbody (red squares), both maintained at nominal temperatures of about 10 °C (this figure shows the corrected output of the IPL radiometer).

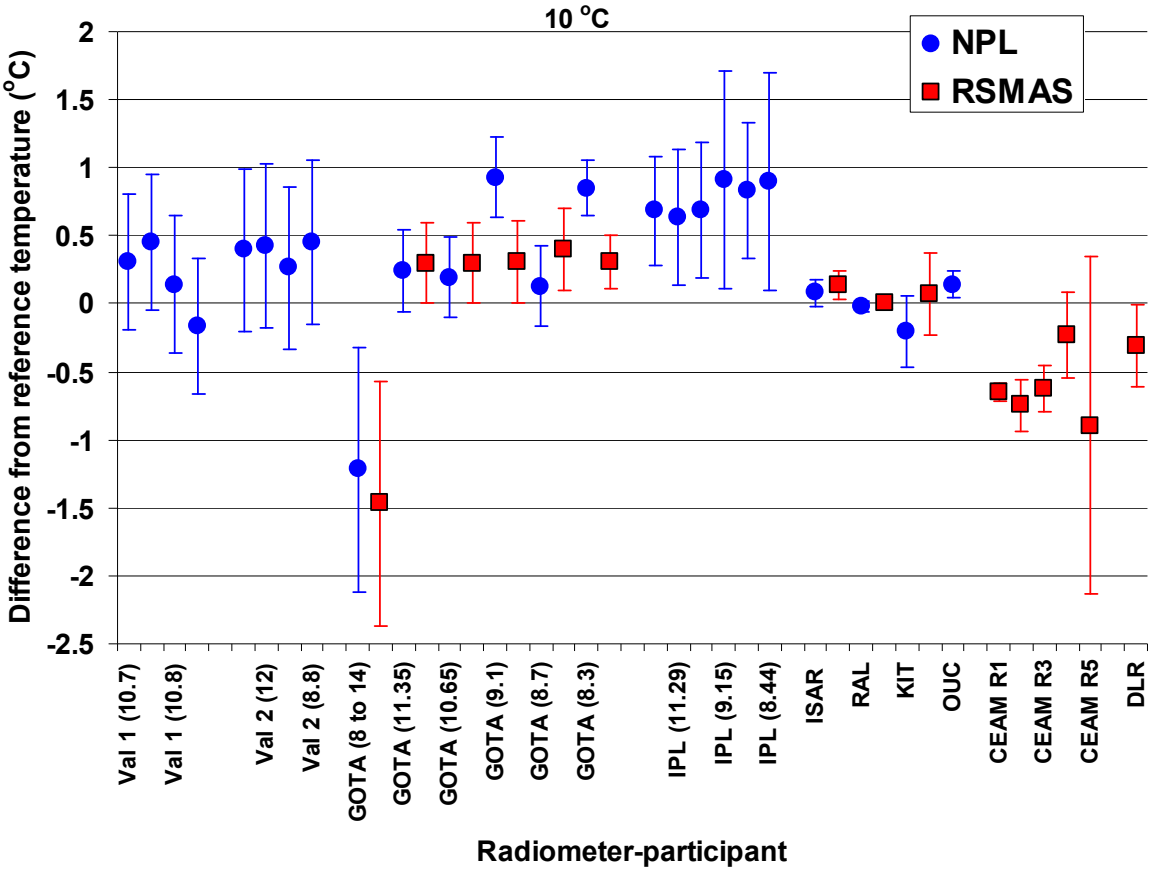

Figure 3.11.3: Plot of the mean of the differences of the radiometer readings from the temperature of the NPL variable temperature blackbody (blue circles), maintained at a nominal temperature of 10 °C. The red squares show the points corresponding to the RSMAS blackbody. This figure corresponds to the uncorrected values of the IPL radiometer.

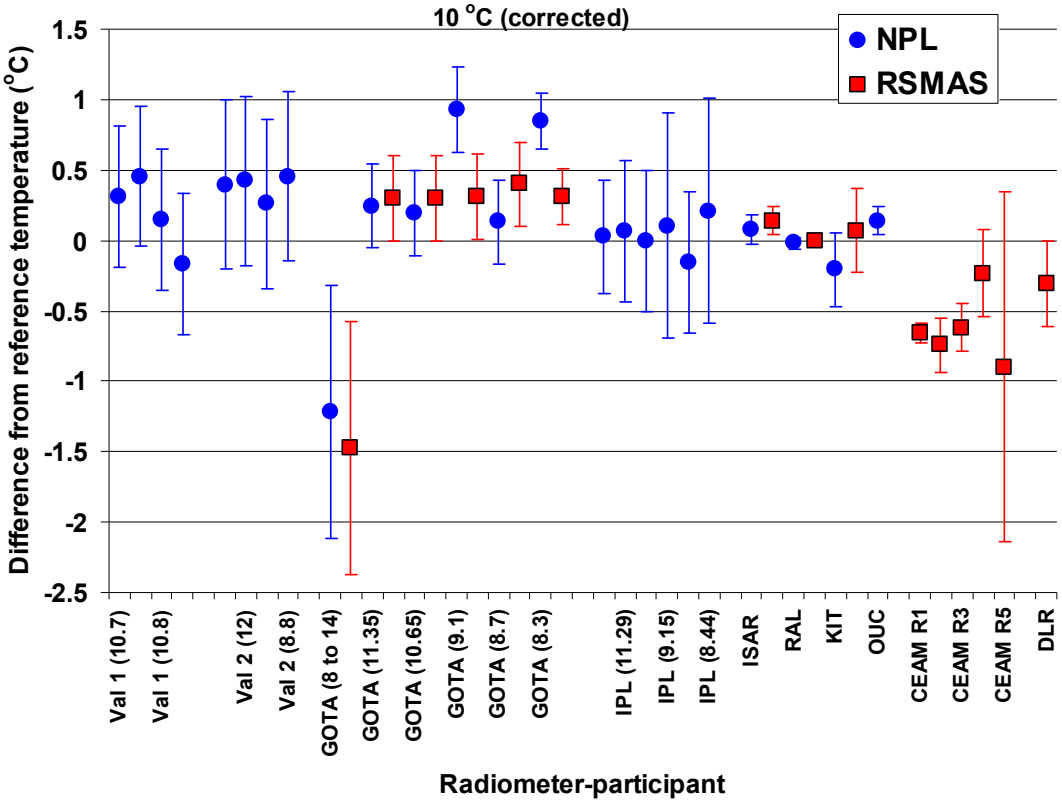

Figure 3.11.4: Plot of the mean of the differences of the radiometer readings from the temperature of the NPL variable temperature blackbody (blue circles), maintained at a nominal temperature of 10 °C. The red squares show the points corresponding to the RSMAS blackbody. This figure corresponds to the corrected values of the IPL radiometer.

Figure 3.11.5 shows a plot of the mean of differences of the all the radiometer readings from the temperatures of the NPL variable temperature blackbody (blue circles) and the RSMAS water bath blackbody (red squares), both maintained at nominal temperatures of about 20 °C. Some of these points represent a single set of data points taken on one day, while some others represent the mean of two measurements completed on different days. The uncertainty bars represent the standard uncertainty (k=1) or (1 σ) of the radiometers provided by the participants. Appendix 1 shows the uncertainty budget associated with the cavity temperature of NPL reference blackbody. Appendix 2 lists the uncertainty (k=1) in the radiance temperature of the NIST water bath blackbody at different cavity temperatures.

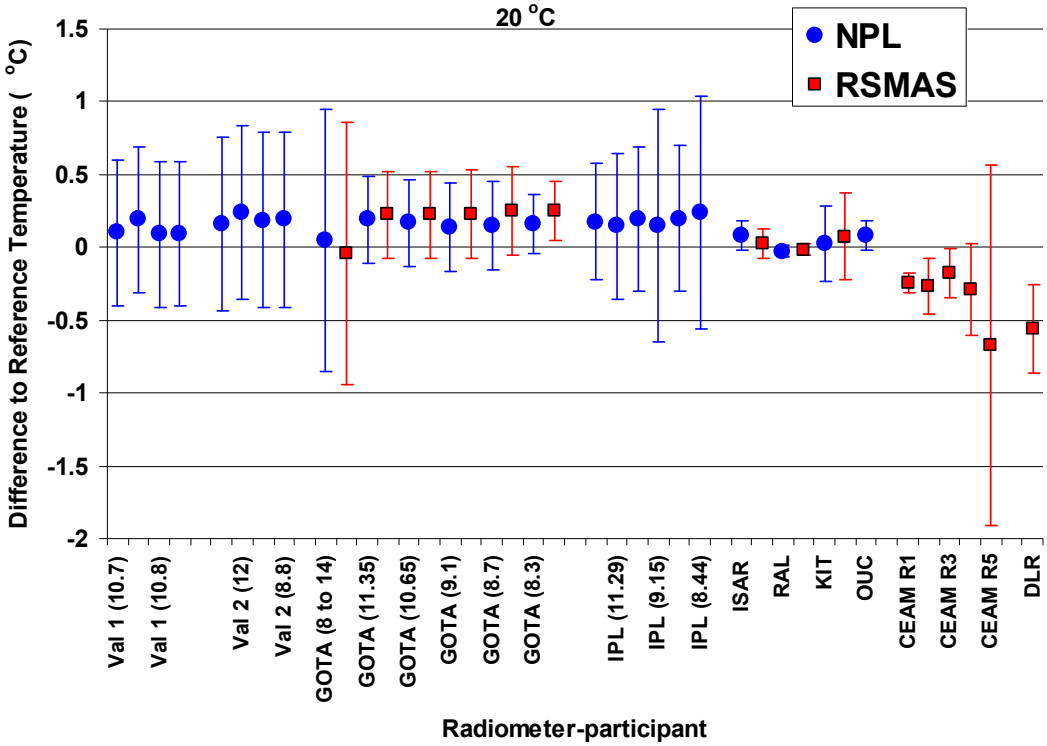

Figure 3.11.5: Plot of the mean of differences of the radiometer readings from the temperatures of the NPL (blue circles) and RSMAS (red squares) reference blackbodies, maintained at a nominal temperature of approximately 20 °C.

Figure 3.11.6 shows a plot of the mean of differences of the all the radiometer readings from the temperatures of the NPL variable temperature blackbody (blue circles) and the RSMAS water bath blackbody (red squares), both maintained at nominal temperatures of about 30 °C. Some of these points represent a single set of data points taken on one day, while some others represent the mean of two measurements completed on different days. The uncertainty bars represent the standard uncertainty (k=1) or (1 σ) of the radiometers provided by the participants. Appendix 1 shows the uncertainty budget associated with the cavity temperature of NPL reference blackbody. Appendix 2 lists the uncertainty (k=1) in the radiance temperature of the NIST water bath blackbody at different cavity temperatures.

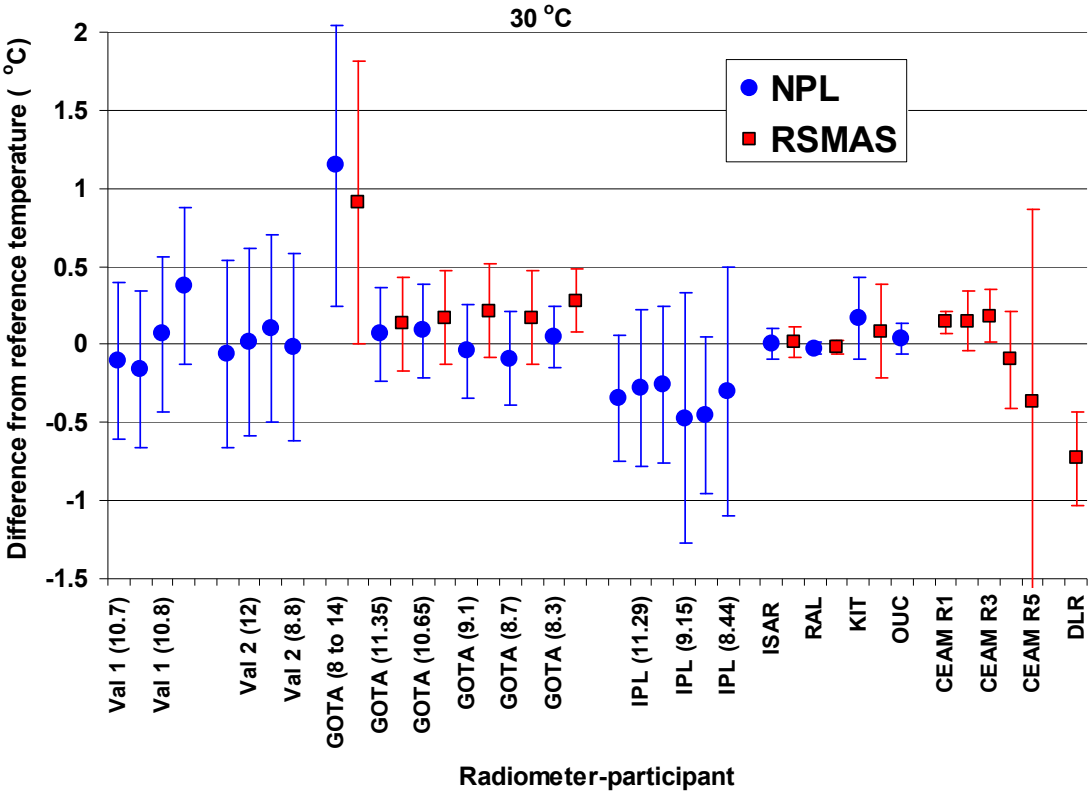

Figure 3.11.6: Plot of the mean of the differences of the radiometer readings from the temperature of the NPL (blue spots) and RSMAS (red spots) reference blackbodies, maintained at a nominal temperature of approximately 30 °C.

3.11.2 Ocean surface temperature measurements

Participants provided their measurements of the ocean surface temperature at different times. In order to be able to compare their measurements, a standard interpolation method was used to estimate the measurements of the different participants at 5 minute intervals.

Ocean surface temperature measurements should ideally be compared to a mean, determined from the measurements of the radiometers, weighted by their uncertainties. However, to do this requires a full breakdown of uncertainties so that the weights can be fully evaluated and agreed upon by participants in advance. This was not possible from the "pre-draft A" data for all radiometers. An alternative could be to take the simple mean of the radiometer measurements. However whilst this works when we have a complete data set of all radiometers, if some radiometers drop in and out of the mean by virtue of having made measurements or not, the mean value drifts. This makes it difficult to evaluate differences. In this Section, ocean surface temperature measurements are compared to the simple mean of the four continuously reading radiometers (MAERI, SISTeR, ISAR and KIT). Some steps are evident due to some radiometers not providing data over certain time periods.

Ocean surface temperature measurements are also plotted as the mean difference of all measured data compared to that of one nominally chosen radiometer. The radiometer chosen for this comparison is that of ISAR from the University of Southampton. The only reason for this choice is that this radiometer measured in a continuous mode for the period of the comparison and of all others operating in such a mode has the longest complete data set.

In reviewing the data, consideration was also made as to potential differences between night and day. With the possible exception of one participant there is no discernable difference between such measurements and so at this stage the summary is made as a mean of all measurements made between ~ 16:00 UT on May 12 and ~ 17:00 UT on May 13.

Figure 3.11.7 shows the ocean surface temperature measured by the four continuously reading radiometers from about 16:00 UT on May 12 to about 17:00 UT on May 13 before MAERI corrections were included to account for the water emissivity at 55°.

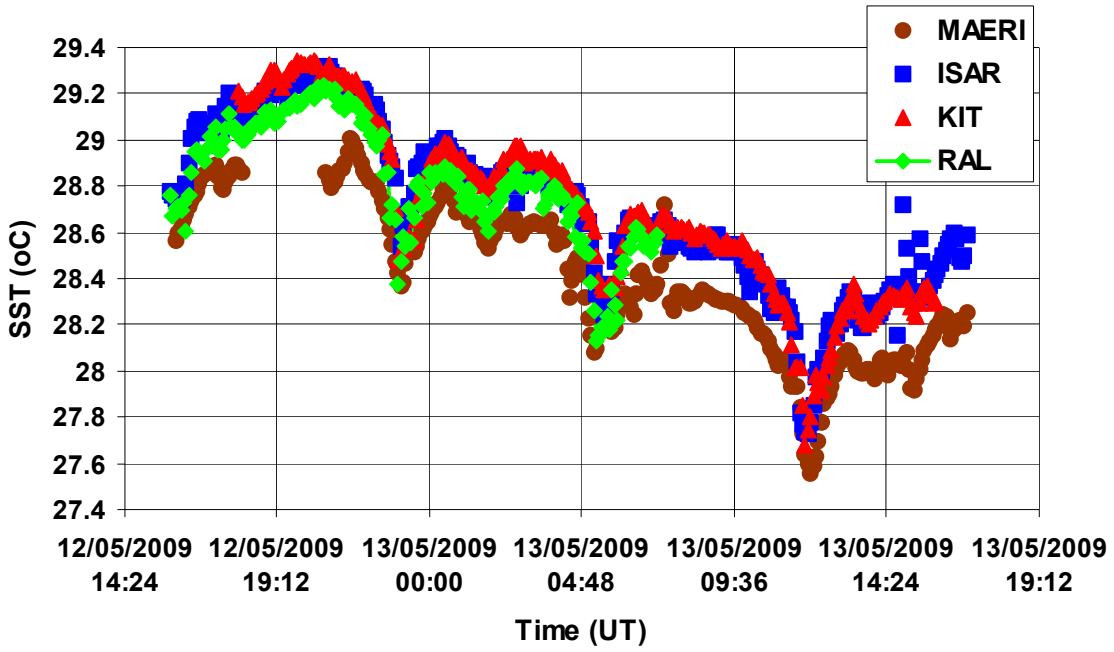

Figure 3.11.7: Ocean surface temperature measured by the four continuously reading radiometers from about 16:00 UT on May 12 to about 17:00 UT on May 13 before MAERI corrections were included to account for the water emissivity at 55°.

Figure 3.11.8 shows the ocean surface temperature measured by the four continuously reading radiometers from about 16:00 UT on May 12 to about 17:00 UT on May 13 after MAERI corrections were included to account for the water emissivity at 55°.

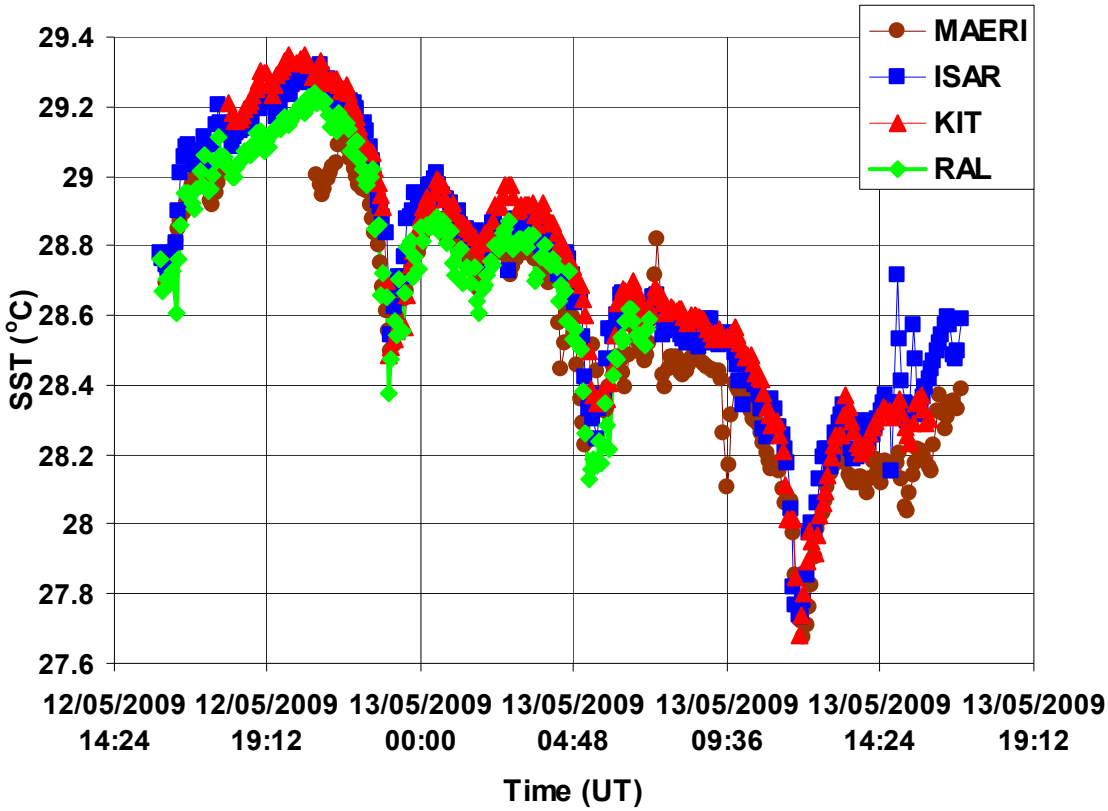

Figure 3.11.8: SST measured by the four continuously reading radiometers from about 16:00 UT on May 12 to about 17:00 UT on May 13 after MAERI corrections were included to account for the water emissivity at 55°.

Figure 3.11.9 shows the difference of each of the four continuously reading radiometers (MAERI, ISAR, KIT and RAL-SISTeR) from their mean. Figure 3.11.10 shows the difference of the three continuously reading radiometers (MAERI, KIT and RAL-SISTeR) from the ISAR radiometer measurements.

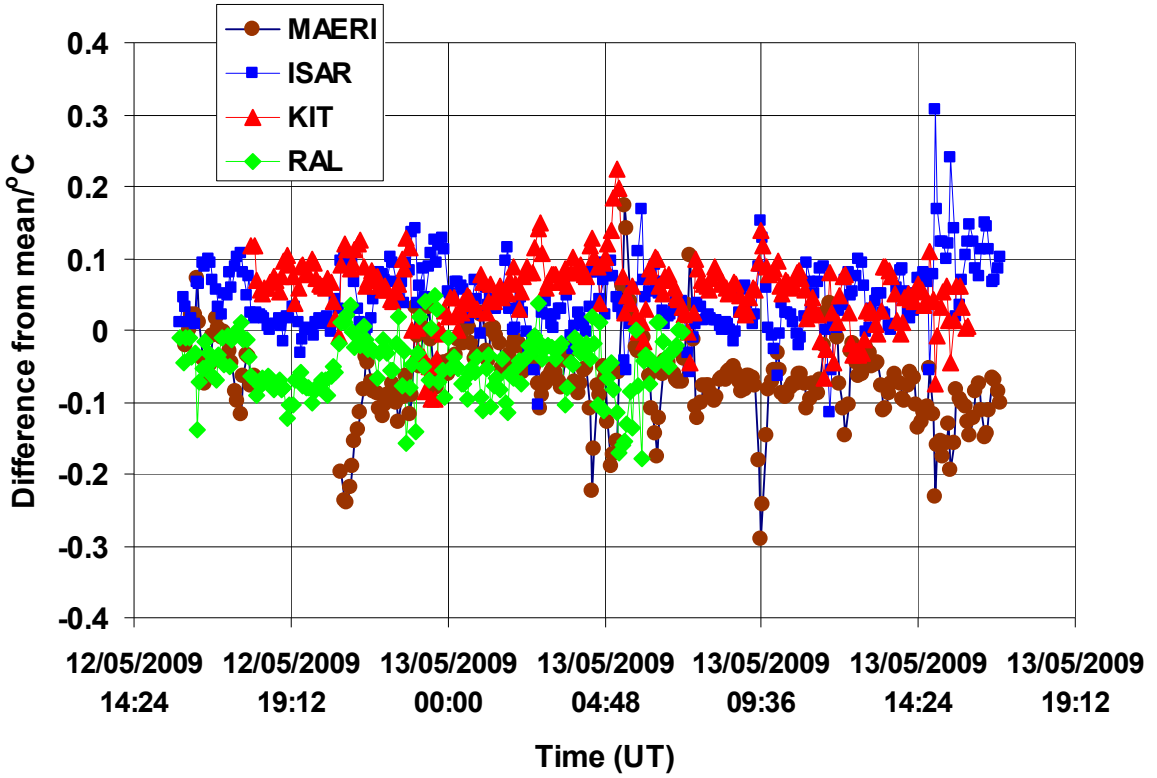

Figure 3.11.9: Difference of the four continuously reading radiometers (MAERI, ISAR, KIT and RAL-SISTeR) from their mean.

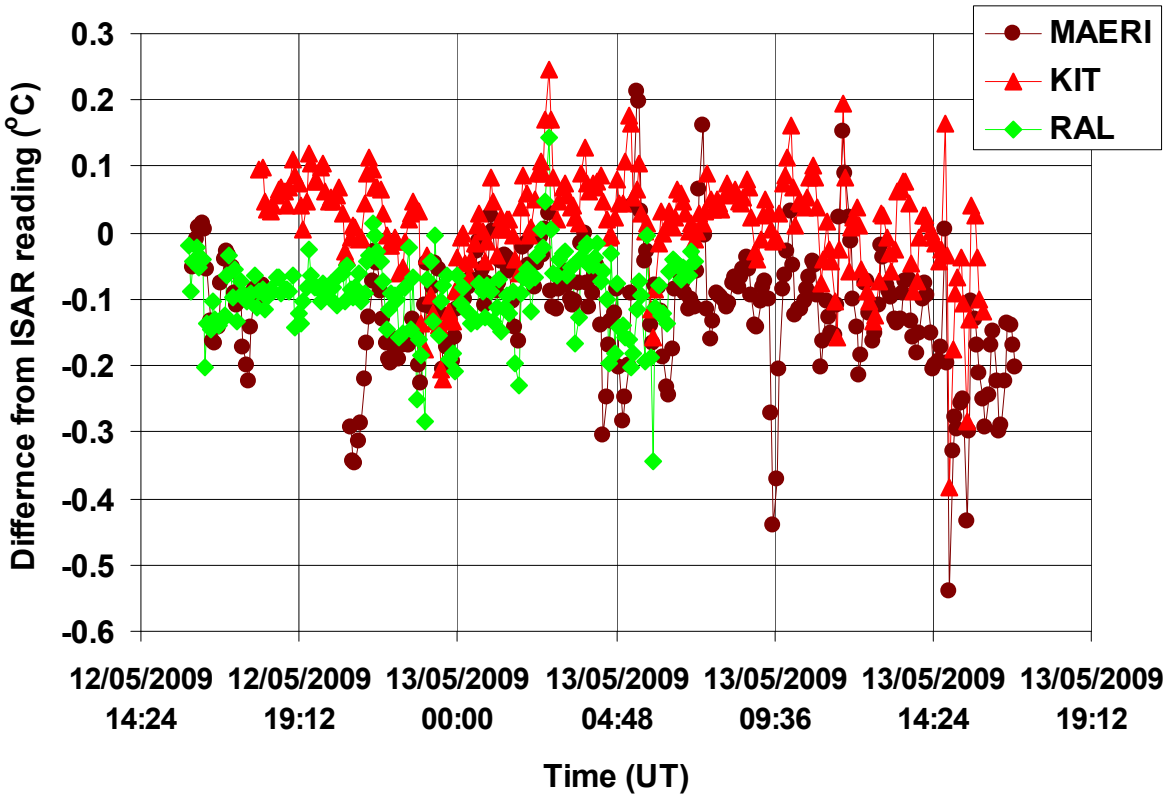

Figure 3.11.10: Difference of the three continuously reading radiometers (MAERI, KIT and RAL-SISTeR) from the ISAR radiometer measurements.

Figure 3.11.11 shows the ocean surface temperature measurements completed at Miami by the "manual" radiometers (GOTA, CEAM and DLR radiometers). The Figure includes the measurements completed with all the CEAM radiometers as well as all channels of the GOTA radiometer.

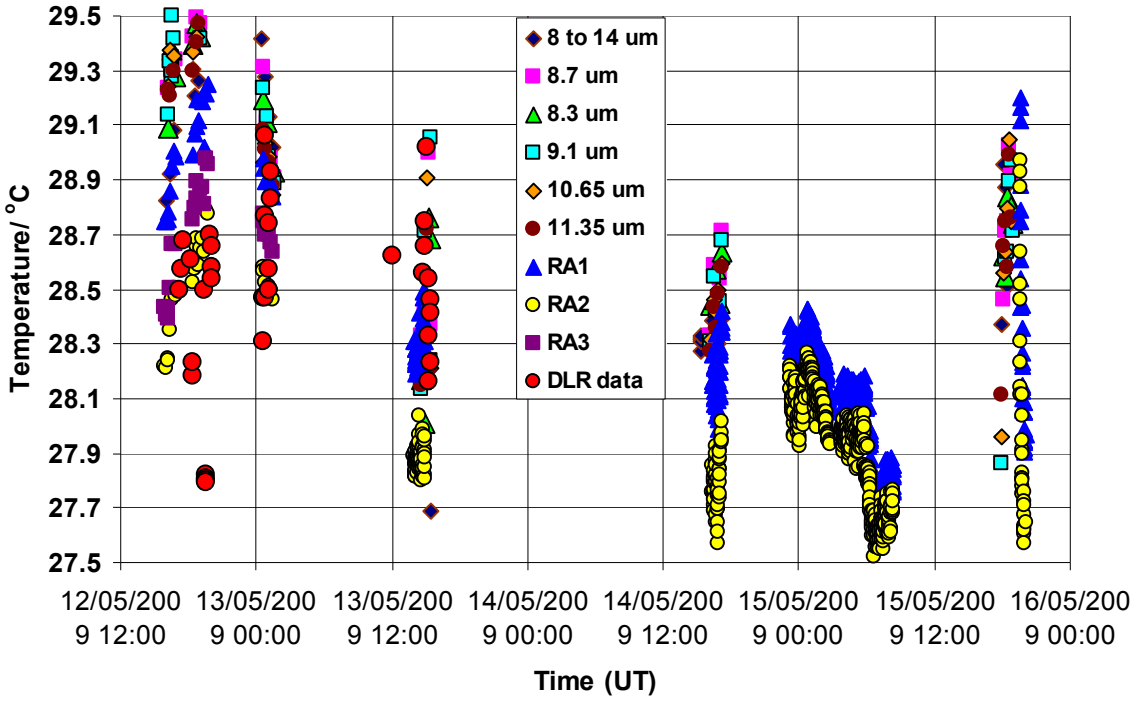

Figure 3.11.11: Ocean surface temperature measurements completed by the "manual" radiometers (GOTA, CEAM and DLR radiometers). The Figure includes the measurements completed by all the radiometer channels.

Figure 3.11.12 shows the difference of the ocean surface temperature measurements of all the radiometers which participated at Miami compared to the measurements completed by the ISAR radiometer.

Figure 3.11.13 shows the average of all measurements of the ocean surface temperature measured during the period from ~16:00 UT May 12 2009 to ~17:00 UT May 13 2009 referenced to the ISAR radiometer (i.e. $T_{rad} - T_{ISAR}$). The data points corresponding to NPL, NIST and RSMAS shown in Figure 3.11.13 represent differences of the ISAR radiometer to the laboratory-based measurements at 30 °C against each of the named blackbody references.

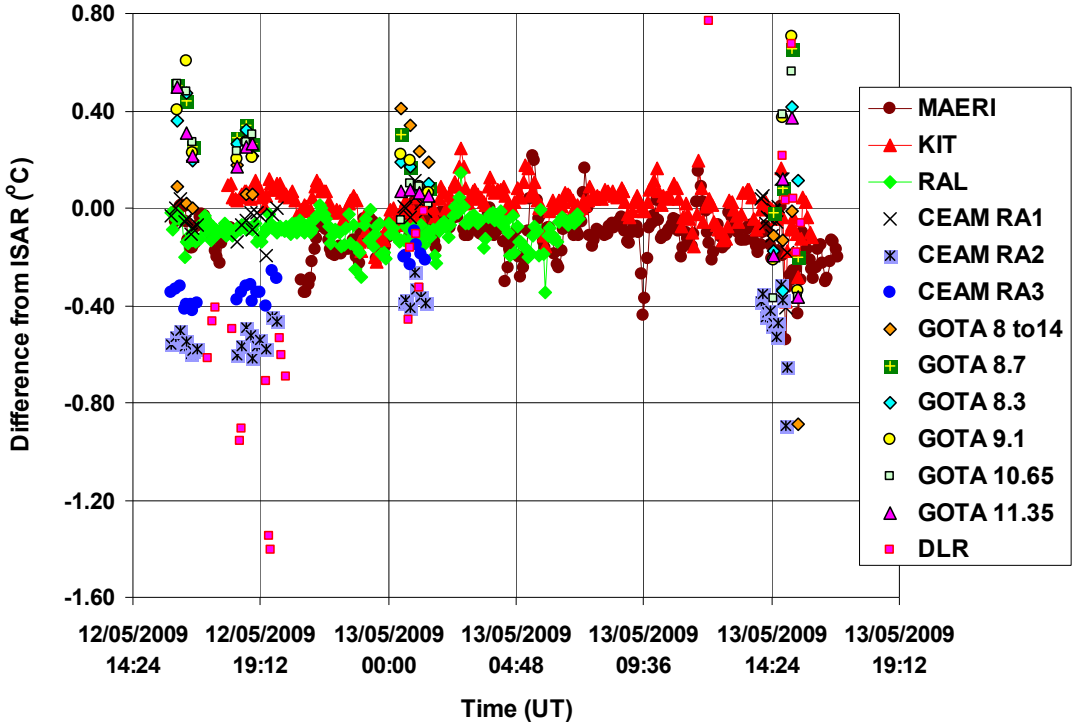

Figure 3.11.12: Difference of the ocean surface temperature measurements of all the radiometers which participated at Miami compared to the measurements completed by the ISAR radiometer.

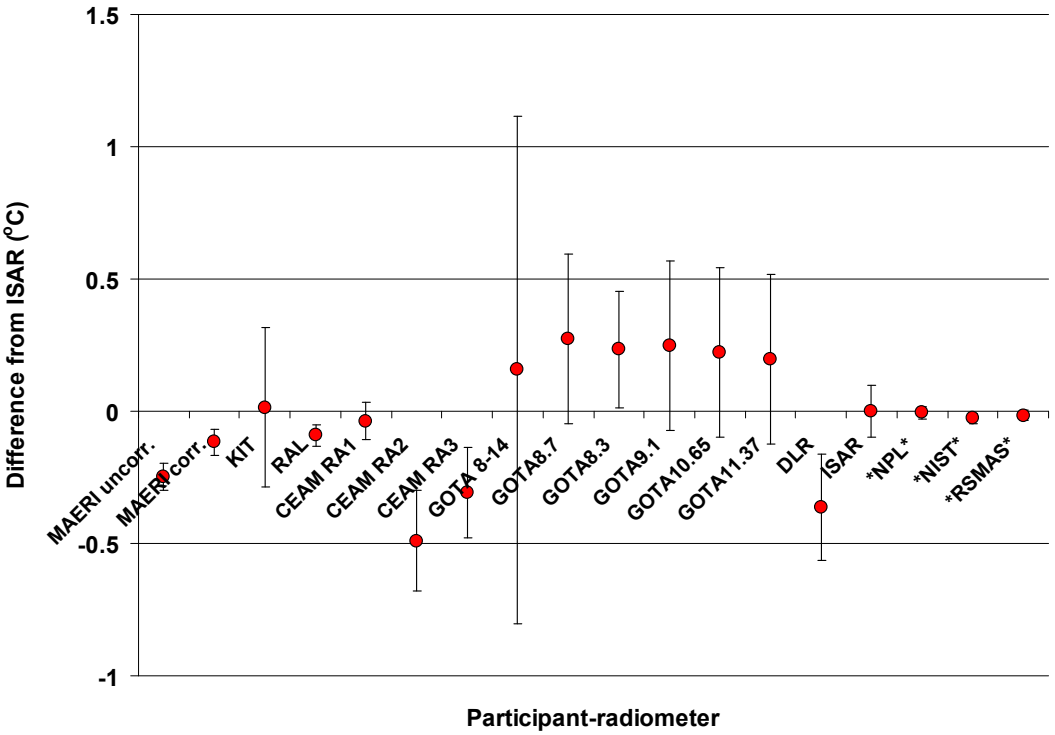

Figure 3.11.13: Difference of mean SST measurements as a difference to that of ISAR.

4. DISCUSSION

4.1 Water condensation at 10 °C

The comparison of the participants' radiometers at Miami using the RSMAS blackbody for blackbody temperatures below 20 °C was hindered by the high humidity which was present in the laboratory where the comparison was taking place. The Dew point in the laboratory was approximately 16 °C. When the RSMAS blackbody was set to 10 °C, condensation was clearly visible inside the RSMAS blackbody cavity. Some participants originally declined to take part in the measurement of the radiance temperature of the RSMAS blackbody at 10 °C because of the presence of the condensation, which (according to some participants) would "render their measurements (at 10 °C) meaningless". However, all participants agreed to complete measurements on the RSMAS blackbody when its temperature was set around 10 °C, after it was agreed that they could submit their data with a proviso that the data (at 10 °C) may be in error due to the water condensation in the RSMAS blackbody cavity. In the event, the "errors" of the data completed when the RSMAS blackbody was set at 10 °C were not significantly different to those corresponding to data acquired when the RSMAS blackbody was set at 20 °C and 30 °C.

4.2 Measurements of the SST at a number of angles to the nadir.

The intention was for all radiometers to measure the ocean surface temperature at more than one angle to the nadir. In particular the aim was to repeat the measurements at a minimum of two angles, 20° and at 55° to nadir. However, this proved to be impossible to accomplish because some of the radiometers could only measure at one angle only (e.g. MAERI could only measure at 55°). On the other hand, SISTeR and ISAR measure at lower angles but their operators were reluctant to measure at 55° (to the nadir) because of the dependence of the emissivity of the sea on angle of incidence. Finally, participants agreed to complete measurements (and submit the data) at a variety of angles provided they were allowed to include provisos/comments with their data that there may be errors/higher uncertainties for large angles of incidence. In the event, the shortage of time, combined with the poor reliability of some of the radiometers meant that very few radiometers actually attempted measurements at more than one angle to the nadir. Although measurements at multiple angles would have been useful to have, measurements at a single angle for each radiometer were considered sufficient as these radiometers *always* carry out ocean surface temperature measurements at a specific angle, and when they are deployed in the field (at sea) all measurements will be completed at that specific angle to the nadir.

5. REFERENCES

Barton, I. J., Minnett, P. J., Maillet K. A., Donlon, C. J., Hook, S. J., Jessup, A. T. and Nightingale, T.J., 2004, "The Miami 2001 infrared radiometer calibration and intercomparison: Part II Shipboard results", *Journal of Atmospheric and Oceanic Technology*, **21**, 268-283.

Fowler, J. B., 1995, "A third generation water bath based blackbody source", *J. Res. NIST*, **100**, 591-509.

Rice, J. P. and Johnson, B. C., 1998, "The NIST EOS thermal-infrared transfer radiometer", *Metrologia*, **35**, 505-409.

Rice, J. P., Butler, J. I., Johnson, B. C., Minnett, P. J., Maillet K. A., Nightingale, T. J, Hook, S. J., Abtahi, A., Donlon, and. Barton, I. J., 2004, "The Miami 2001 infrared radiometer calibration and intercomparison. Part I: Laboratory characterisation of blackbody targets", *Journal of Atmospheric and Oceanic Technology*, 21, 258-267.

Theocharous, E., Fox, N. P., Sapritsky, V. I., Mekhontsev, S. N. and Morozova, S. P., 1998, “Absolute measurements of black-body emitted radiance”, *Metrologia*, **35**, 549-554.

APPENDIX 1

NPL VARIABLE TEMPERATURE BLACKBODY (VTBB) UNCERTAINTY BUDGET AND MEASUREMENT TRACEABILITY

NEXTEL VELVET BLACK REFLECTANCE

The reflectance of Nextel Velvet black paint was measured for several witness samples at different times using the NPL hemispherical reflectance facility. The uncertainties on these measurements are at the ±0.5% level across the spectrum. [Note regarding the hemispherical reflectance facility: The potential for heating of the sample by the incident light has been identified as an unresolved problem with this facility. However this would lead to an *over* estimate of Nextel reflectance. Therefore the existing measurements can safely be used to determine an upper estimate of the cavity emissivity.]

CAVITY EMISSIVITY & AMBIENT REFLECTION

The effective emissivity of the cavity is determined using Monte Carlo ray tracing code developed for NPL by Virial Inc. This code has been validated by comparison to first principles calculations for several tractable cases. The uncertainty in this calculation depends on: (1) the Nextel reflectance uncertainty and (2) the BB temperature uniformity. A ±0.5% uncertainty in the Nextel reflectance leads to a cavity emissivity uncertainty of ±0.0002 for this cavity.

A cavity of emissivity ε will reflect $\rho = (1-\varepsilon)$ of ambient radiation. Therefore the correct way to deal with non-unity emissivity is to *subtract* $(1-\varepsilon)$ of the radiance emitted by an ideal blackbody at temperature T_{bb}, and to *add* $(1-\varepsilon)$ of the radiance emitted by a blackbody at temperature T_{amb}.

In the case of the NPL VTBB, there are two distinct "ambient" zones: (1) outside the steel flange and (2) between the copper aperture and the steel flange. The only section of the second zone seen by the BB rear plate is the steel flange itself. Therefore this zone makes two contributions to ambient radiation seen by the BB: (2a) thermal emission from the flange itself and (2b) reflection by the steel of emission from the blackbody. As the steel is smooth and fairly specular, reflection of any other ambient radiation is neglected. The contributions from 2a and 2b are coupled, since they each depend on the emissivity of stainless steel. Furthermore 2a depends on the steel temperature, which will always be between T_{bb} and T_{amb}.

The extreme values of the contribution from zone 2 are determined by calculating the contributions from the following combinations and using the smallest and largest to define the uncertainty range:

Case 1

- maximum steel temperature (either T_{bb} or T_{amb}, whichever is higher)
- maximum steel emissivity (0.5 assumed) → minimum reflectivity

Case 2

- maximum steel temperature
- minimum steel emissivity (0.3 assumed) → maximum reflectivity

Case 3

- minimum steel temperature
- minimum steel emissivity → maximum reflectivity

Case4

- minimum steel temperature
- maximum steel emissivity → minimum reflectivity

The above considerations allow the calculation of a net correction and its corresponding uncertainty. This correction must be calculated for each blackbody temperature, ambient temperature, and wavelength of interest. The radiometers participating in the CONTROLS comparison were mainly within the 8 μm to 12 μm range. Therefore the corrections introduced here are averages over this range.

These numbers are shown below.

T_{bb} (K)	Correction (K)	Uncertainty (K)
303	-0.016	0.005
293	0	0
283	-0.001	0.003
278	0.003	0.003

Uniformity

The spatial uniformity of the NPL VTBB operated at 303K was evaluated using the NPL AMBER radiometer (Theocharous et al., 1998). Measurements across a horizontal range of ±20 mm show that the rear plate of the blackbody is uniform to better than 5 mK.

Thermometry

Two small diameter industrial PRTs from Hart Scientific (model 5618B-6) measured the temperature of the rear plate of the BB. One was fully immersed in a hole drilled to tight tolerance in the copper plate such that the active element was at the centre of the plate. The other was immersed halfway. A 3rd uncalibrated PRT in a ceramic casing was suspended outside the BB aperture to monitor the temperature of the out-flowing nitrogen gas. The 4-wire resistance of the PRTs was measured by an Agilent 34970A DMM.

A comparison was made of the PRT resistance measured by the Agilent and a Senator resistance bridge, the latter calibrated to within 0.0001 ohms (equivalent to less than 0.3 mK for the PRTs) by an NPL standard resistor. The measurements (at 108 ohms) agreed to within 0.002%, much closer than the Agilent specification, which is 0.014% over 1 year.

Self-heating was tested by the Senator bridge. Close to R=100 Ohms, the temperature difference between readings using 0.5 mA and 2 mA is 0.00 87 K. However the current used by the Agilent (1 mA) is the same as the current used for the PRT calibration. Therefore no self-heating correction is required.

Conductive heat loss along the PRT steel cylindrical casing due to finite immersion depth must also be considered. For T_{bb} in the range used for the CONTROLS inter-comparison, the difference between the rear plate PRT readings was generally less than 20 mK at 30 deg C, and less than 10 mK at lower temperatures. Therefore using an average of the two PRT measurements and including an additional uncertainty equal to 10 mK is an adequate alternative to precise determination of conductive heat loss.

Cavity Thermal Gradient

The Monte Carlo emissivity code was used to calculate the uncertainty due to thermal gradients along the BB cylinder. The resulting uncertainty in BB emissivity is 0.05% per degree C at 300K, and 0.1% per degree C at 200K. In order to measure potential gradients for $T_{bb} \neq T_{amb}$ (T_{bb}=10 deg C in this case), a flat-ended surface measurement thermometer was placed on flat sections of stainless steel Swagelok flange nuts at the ethanol inlet and outlet ports. No gradient was measured to within the resolution of the thermometer (0.1 K), which suggests an upper limit of 0.005% radiance uncertainty at 300 K. A gradient of 0.5 K was assumed here as an upper bound. The resultant emissivity uncertainty of 0.025% is equivalent to 15 mK for wavelengths between 8 μm and 12 μm.

Thermal gradient across paint due to convective heat transfer

The nitrogen gas purging the VTBB interior is nominally at the same temperature as the copper body of the blackbody. If the gas is at a different temperature, however, then convective heat transfer can occur. In order to estimate the magnitude of this effect, a simple model was used in which the Nextel paint layer exchanges energy with both the copper body and the purge gas. (For this model, values of Nextel thickness and thermal conductivity reported by Quinn & Martin, and a value of heat transfer coefficient valid for weak forced convection were used.) The temperature of the gas was taken to be the value recorded by the 3rd PRT suspended just outside the BB. The results lead to the following uncertainty contributions: 0.005 K at T_{bb}=303 K, 0.002 K at T_{bb}=293 K, and 0.0027 K at T_{bb}=273 K.

AMBER radiometer characterisation of the VTBB

Traceability of the NPL VTBB to SI stems from this measurement. Two components are critical. Firstly AMBER directly measures the spectral radiances of the VTBB and a reference blackbody at a fixed point on the ITS-90 scale (i.e. the gallium melting point). Secondly the AMBER filter radiometer calibration is traceable to the NPL primary spectral responsivity scale, and this calibration (and its associated uncertainties) is used to convert the BB temperature measurement to spectral radiance. Comparison of the measured and calculated spectral radiances thus provides a traceable calibration of the NPL VTBB.

The uncertainty components associated with this measurement are:

- uncertainty in the radiance temperature of the reference blackbody: 23 mK (k=1)
- numerical integration of BB spectral radiance over AMBER responsivity. This is insignificant for T_{bb} close to the gallium point.

The figure below shows a comparison between the spectral radiance of the VTBB at 4.7 µm as measured by AMBER and as calculated from the PRT temperatures. The difference between the AMBER reading and the average calculated from the two PRT readings is less 10 mK, which is well within the gallium blackbody uncertainty.

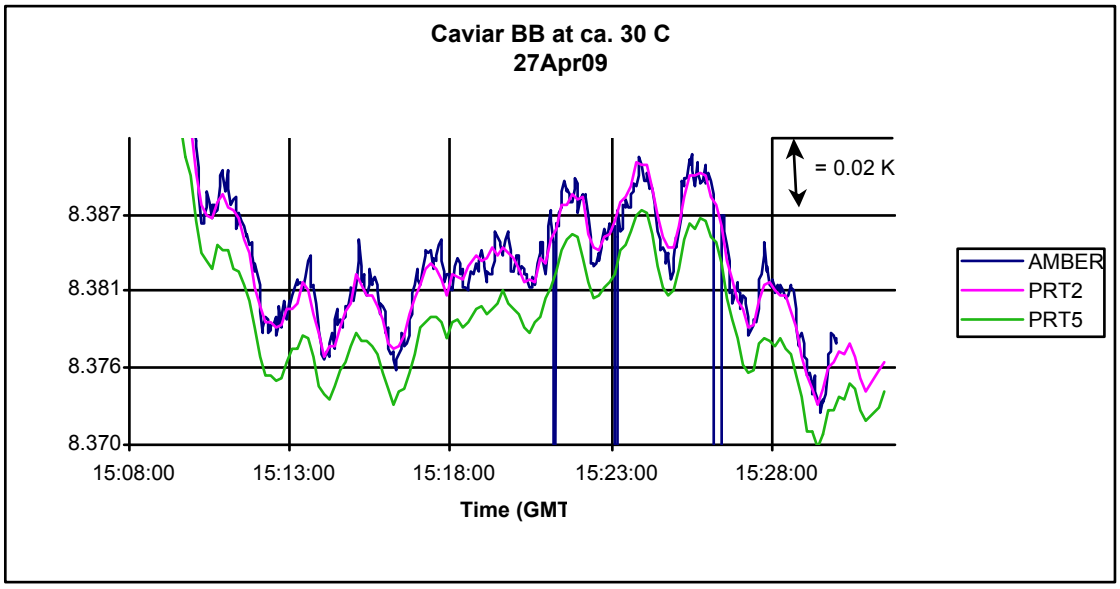

Figure A1: Spectral radiance of the VTBB at 4.7 µm as measured by AMBER and as calculated from the temperatures indicated by the two PRTs.

TABLE A1-1: NPL VTBB UNCERTAINTY BUDGET FOR CONTROLS

	comment	condition	Uncert.	units	divisor	T deg C (k=1)
Nextel reflectance	taken into account in "Emissivity & Reflection of ambient"		0.5%	reflectance		
Emissivity & Reflection of ambient	accounts for uncertainty in emissivity modelling	blackbody @ 303 K	0.005	deg C	1.73	0.003
	use highest value	blackbody @ 293 K	0	deg C		
		blackbody @ 283 K	0.002	deg C		
		blackbody @ 278 K	0.002	deg C		
uniformity		303 K	0.01	deg C	1.73	0.006
PRT calibration			0.012	deg C	2	0.006
PRT measurement by Agilent DMM	tested by comparison to calibrated Senator		0.014	%	2	0.018
Conductive heat loss along PRT stem	accounted for by "Difference between PRTs"					
Difference between PRTs	typically <20mK @ 30degC, <10mK between 5 & 20degC		0.01	deg C	1	0.010
Gradient across paint due to convective heat tansfer	assume coefficient = 25	303 K	0.0045	deg C	1.73	0.003
Temp gradient along cylinder	0.05% per deg C gradient; assume 0.5 deg gradient		0.015	deg C	1.73	0.009
	0.025% equivalent to 15 mK between 8 and 12 microns					
		Comb. Stand Unc (deg C) k=1				0.024

Appendix 2

List of the uncertainty values (k=1) of the NIST water bath blackbody at different cavity temperatures.

NIST Water Bath Blackbody
Uncertainty Table[a]
(ε = 0.9997 with uncertainty (k=1) of 0.0003 with No aperture)

Temperature Setting (K)	ΔT (mK)	Uncertainty (k=1) (mK)
278	+0.9	5.3
283	+0.5	4.9
293	0.0	3.7
303	-0.5	3.5
313	-1.1	3.8
323	-1.7	4.9
333	-2.4	6.1
343	-3.2	7.0
353	-4.0	7.3
363	-4.9	7.8

[a] Fowler, J. B., 1995: A third generation water bath based blackbody source, *J. Res. NIST*, **100,** 591-599